ISSN 0250-7625

IIASA REPORTS

International Institute for Applied Systems Analysis

Volume 2 Number 1 July-September 1980

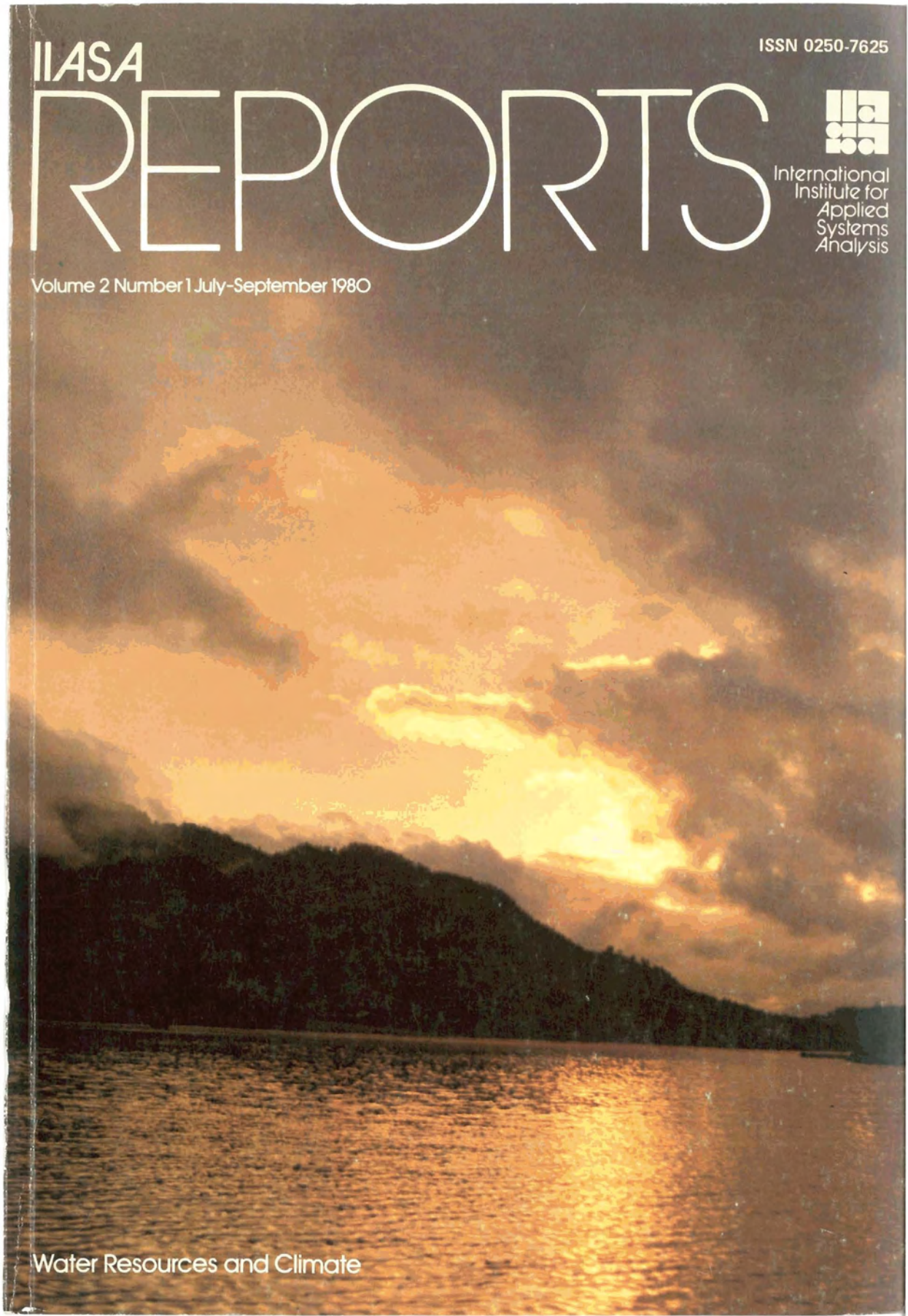

Water Resources and Climate

IIASA
REPORTS

Volume 2 (1980)

Cover

Cover Photograph: An evening view of Wiessensee in Kärnten, Austria, by Robert A. Duis, IIASA.

International Standard Serial Number 0250-7625

IIASA REPORTS

A JOURNAL OF INTERNATIONAL APPLIED SYSTEMS ANALYSIS

VOLUME 2 (1980)

WATER RESOURCES AND CLIMATE

INTERNATIONAL INSTITUTE FOR APPLIED SYSTEMS ANALYSIS
Laxenburg, Austria

FOREWORD

This issue of *IIASA Reports* is devoted to water-resource management and global climatic change. The three papers that appear here represent an important – but nonetheless limited – segment of the range of IIASA's research activities in these areas.

Two of them deal with important problems in regional water-resource management.

The first, by Young, Okada, and Hashimoto, studies alternative cost-allocation methods for regional water-supply systems. It investigates the performance of alternative methods of allocating cost against a set of criteria by which potential participants in a regional project might judge the fairness of the cost allocated to them. They show that most of the commonly proposed cost-allocation methods fail to meet one or more of these criteria. They also show that some concepts developed recently concerning the solution of cooperative games can be applied to the cost-allocation problem and can satisfy the criteria for fair division they adopt. Since their preferred method would be difficult to implement, work is continuing at IIASA in search of solutions to some of the practical implementation problems that Young, Okada, and Hashimoto have identified.

The second paper, by Gouevsky, Maidment, and Sikorski, describes an analysis of water demands in a large agroindustrial complex in the northeastern part of Bulgaria. The objective was to analyze the factors that influence agricultural water demands and associated agricultural production, taking into account the major goal of the regional complex, which is to maximize the total net benefit from crop and livestock production within the limited available regional resources. To pursue this objective, the analysts formulated and solved a linear programming model describing the agricultural system of the region, including critical inputs such as land, water, seed, fertilizers, chemicals, labor, machinery, fuel, and capital investment.

The results of the work provide useful information for the planning process. They show, for example, that the ultimate economical level of irrigation development (i.e., the level that maximizes net benefits) would provide irrigation for 70 percent of the arable land in the region. They also show where in the region irrigation investments should be made.

In contrast to these two analyses of regional problems, the paper by Flohn examines a potentially critical global environmental problem: climatic change. There is a widely recognized need to

elaborate plausible patterns of change that would accompany a global climatic warming, such as might arise from large increases in atmospheric carbon dioxide levels. There are two general approaches to deriving scenarios of future climate: one uses numerical modeling with general circulation models, and the other uses past warm periods as analogues of the future.

Flohn's paper brings these two approaches together. It uses model results to estimate the future evolution of temperature based on various growth rates of CO_2 and the compounding effects of other trace gases. While there is general agreement among models on many of the results for a high CO_2 world, they offer very little spatial detail. Thus, Flohn turns to the rich data base of paleoclimatology to see if possible future warming has been paralleled by past warm phases during the long historical evolution of climate. For example, he finds that, during the Medieval warm phase of about 1000 years ago, the global average temperature was about 1 °C warmer than today, corresponding to an increase in CO_2 concentration of about 50 percent. The Eem Interglacial era, 120 000 years ago, when the global average temperature was about 2 °C warmer, corresponds roughly to a doubling of CO_2, and the period of the ice-free Arctic ocean, more than two million years ago, when the temperature was about 4 °C warmer, corresponds roughly to a tripling of CO_2.

Flohn examines these past climates as bases for possible global warming scenarios. Among the more interesting findings is evidence that, during the much warmer era of two million years ago, there was a long stable period when an Antarctic ice dome of today's height coexisted with an open Arctic ocean, with temperate or boreal forests extending to latitudes 81–83 °N, interspersed only with some local mountain glaciers and no indication of tundra or permafrost. The implications of the hemispheric asymmetry of one heavily glaciated pole and one ice-free pole are that there would be drastic shifts of climatic belts. While it should be stressed that past climatic fluctuations were probably not caused by changes in amounts of atmospheric CO_2 and that the scenarios presented here only become relevant if very high rates of fossil-fuel use continue a century and more into the future, Flohn's paper is a step toward understanding plausible patterns of long-term climatic change.

Robert Anderson
Deputy Chairman
Resources and Environment Area

COST ALLOCATION IN WATER RESOURCES DEVELOPMENT – A CASE STUDY OF SWEDEN

H.P. Young
N. Okada
T. Hashimoto

PREFACE

The investigation of water resource systems has been an important part of resources- and environment-related research at IIASA since its inception. As demand for water increases relative to supply, the intensity and efficiency of water resources management must be improved. This in turn requires an increase in the degree of detail and sophistication of the analysis. The economic, social, and environmental impacts of various water resource development options are evaluated with the aid of mathematical modeling techniques, to generate inputs for planning, design, and operational decisions.

During 1978 it was decided to attempt an integration of the results of our studies on water demand with water supply considerations. This new task was named "Regional Water Management" (Task 1, Resources and Environment Area).

This paper considers the application of systems analysis to water management problems in Western Skåne, Sweden. These problems concern the allocation of limited supplies of water and related land resources for several mutually conflicting purposes, e.g., municipal, industrial, agricultural, and recreational water use.

This paper is part of a collaborative study on water resources in Western Skåne, Sweden, between the Swedish Environmental Protection Board, the University of Lund, and IIASA, and concerns a joint municipal water supply project. The viability of the project depends on the number of municipalities taking part. This paper is concerned with the methodological problems involved in allocating the costs of the joint project to provide incentives for the municipalities to participate.

1. INTRODUCTION

A central problem in planning the provision of goods or services by a public enterprise is how to determine a "fair" or "just" allocation of joint costs. This problem is particularly acute in the development of a common water resource like a multipurpose reservoir, where the greater cost-effectiveness of larger facilities means that the sum of the marginal costs* of each participant may be much less than the total cost of the project. The literature on water resources contains a variety of proposals for dealing with this kind of problem, some of which anticipate ideas (like the core) later developed in game theory (Ransmeier 1942; see also Loughlin 1977, Heaney 1979, and Straffin and Heaney 1980).

The methods most commonly used in current water resource planning practice are (i) to allocate costs in proportion to some single numerical criterion like use, population, or level of benefit; or (ii) to allocate certain costs (e.g., marginal costs) directly, and divide the remainder on the basis of some scheme similar to (i). Chief among the methods of the second type is the so-called *separable costs–remaining benefits* (SCRB) method, which is used for multipurpose reservoir projects in the United States (Inter-Agency Committee on Water Resources 1958, Eckstein 1958) and in other countries. This method will be treated in more detail in Section 6.

The same type of problem has also been extensively treated in the economics literature on public utility pricing. An approach commonly advocated here is *Ramsey pricing* (Ramsey 1927), which is based on the idea of setting prices to maximize some criterion of economic efficiency, like consumer surplus, subject to a breakeven constraint (Baumol and Bradford 1970). This approach relies on having extensive information about the demand for the goods and services over a range of consumption levels – information that is often not available in

*The marginal cost of including a participant is defined as the difference between the estimated cost of the joint project *excluding* him and the estimated cost of the joint project *including* him.

practice, especially for a resource, like water, in which established markets may not even exist. Ramsey pricing is also less suitable for planning long-term investments, where future demand can only be estimated.

A third strand in the literature comes from the theory of cooperative games, which provides various normative approaches to the problem of allocating joint costs (and benefits) among users by taking the strategic possibilities into account. Among the most commonly used of these game theory concepts are the *Shapley value* and the *nucleolus*. The application of these ideas to water resource projects is increasing; for a sample of the recent literature see Loehman and Whinston (1974), Suzuki and Nakayama (1976), Bogardi and Szidarovsky (1976), Okada (1977), and Loehman *et al.* (1979). Methods from the theory of cooperative games are particularly well-suited to contexts like water resources development in which the basic decision is often whether or not to supply a potential class of users at some targeted level, the implicit assumption being that this level is close to the optimal scale of development. The advantage is that the analysis is not made to depend on precise estimations of future demand curves, but only on "point" estimates of benefits. The disadvantage is that even such point estimates are often unreliable; moreover, it is implicitly assumed in the analysis that the optimal scale of development is known – which ultimately presumes that demands as well as costs are known. It has recently been shown that these shortcomings may be overcome by designing an appropriate noncooperative game, which reveals both consumer demands and the optimal scale of development, and at the same time allocates costs in a manner consistent with principles of cooperative equity (Young 1980).

The complexity of the cost allocation problem has led some authors to conclude that there is no economically justifiable way to allocate joint costs (see Ransmeier 1942, Thomas 1974). Nevertheless, in practice, the costs of a project must usually be allocated in some way among the beneficiaries. The purpose of this paper is to compare the merits of traditional methods of allocating costs with several well-known, and other lesser-known, methods from cooperative game theory. The analysis consists of two parts. First, we discuss certain established principles of "fairness" by which the different methods can be judged. Second, we compare the solutions given by each method for an actual example: a cost sharing problem among a group of municipalities in Sweden who wish to develop a joint municipal water supply. The object of this analysis is not to provide a strict axiomatic characterization of methods, but rather to explore their behavior in practice. Our conclusion is that, of the traditional approaches, proportional allocation according to a single numerical criterion may be preferable to the more complicated SCRB method, provided that the proportionality criterion seems fair and the accuracy of the values is not open to dispute. The SCRB method is shown to be seriously flawed in that it is not monotonic in total costs – that is, an *increase* in total costs may result in some participants having to pay less than before; this is due to the *ad hoc* way in which marginal costs are introduced. The game theory methods require more information and are more complicated; moreover, one of the best-known of these methods, the nucleolus, is also

not monotonic in total costs. By contrast, a lesser-known variation of the nucleolus, the *proportional nucleolus*, passes most of the tests of fairness considered here and would appear to merit serious consideration for cost allocation in water resources development.

2 JOINT COST FUNCTIONS

Consider three neighboring municipalities A, B, and C, who can supply themselves with municipal water either by building separate facilities or by building a joint water supply facility. We suppose that the joint facility is cheaper to construct than the separate projects due to economies of scale. The quantity of water to be supplied to each municipality is assumed given. The problem is then how to divide the costs among them.

Figure 1 shows the population of each municipality, the amounts of water to be supplied, and the cost of building separate facilities. Table1 gives water use per capita and the unit cost of supplying water in each municipality.

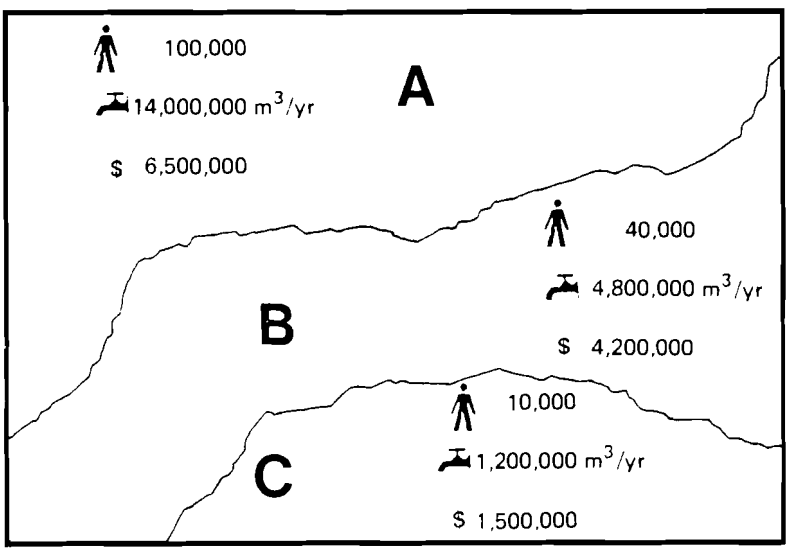

FIGURE 1 Three hypothetical municipalities A, B, and C, their populations, water demands, and the cost of building separate facilities.

Table 2 shows the costs of supplying the target amounts for different combinations. All possibilities are considered: A and B build a joint facility and C goes alone; B and C cooperate and A goes alone, and so on.

TABLE 1 Annual rates of water use and unit costs of supplying water in three hypothetical municipalities.

Municipality	Use per capita (m^3)	Unit cost ($/m^3$)
A	140	0.46
B	120	0.88
C	120	1.25

TABLE 2 Annual costs of water supply under various combinations.

Combination	Cost breakdown ($ X 10^6)	Total cost ($ X 10^6)
A + B + C	6.5 + 4.2 + 1.5	12.2
A + {B,C}	6.5 + 5.3	11.8
{A,B} + C	10.3 + 1.5	11.8
{A,C}[a] + B	8.0 + 4.2	12.2
{A,B,C}	10.6	10.6

[a] {A,C} = A + C = 8.0.

The cost figures show that building a facility to serve all three communities will be 1.6 million dollars cheaper than if three separate facilities were built. However, A and B together can also realize savings of $400,000 without including C; similarly, B and C can save $400,000 without including A. A and C, being geographically separated by B, cannot do any better by building a joint facility than they could by building separate facilities. The most cost-effective way of supplying water would be to build a joint facility serving all three communities.

More generally, let $\{1,2,...,n\} = N$ represent a group of prospective participants in a cooperative venture to provide a product or service to members of the group. The cost of serving a subgroup S, denoted by $c(S)$, is found by considering the *least-cost alternative* of providing the same service, either jointly or singly, to the members of S independently of how the others are served. The *joint cost function* $c(S)$ so defined must be *subadditive*, i.e., must satisfy $c(S) + c(T) \geqslant c(S \cup T)$ for any two nonoverlapping groups S and T, because the ways of serving S together with T include the possibility of serving S alone and T alone. Thus, in the above example, municipalities A and C would find it quite costly to build a single joint facility because of their geographical separation; hence the least-cost alternative would be to build one facility for A and another for C.

If the cost of serving any group of users is simply the sum of the costs of serving them singly, then the cost allocation problem is trivial. The more interesting, and more typical, case arises when the cost of serving several users by some joint facility is *less* than the sum of serving them singly, that is $c(N) < \Sigma_N\, c(i)$. The *cost savings* that would result from cooperating in a coalition S instead of going alone are

$$v(S) = \sum_S c(i) - c(S) \geqslant 0$$

The function v is called the *cost savings game*. To illustrate the different situations that can arise, suppose that the cost of serving a group S depends only on the number of members of S, and that the cost savings are greatest for larger groups due to economies of scale. One possibility is that the cost savings increase at a greater rate with each additional participant, as shown in Figure 2. Another, and

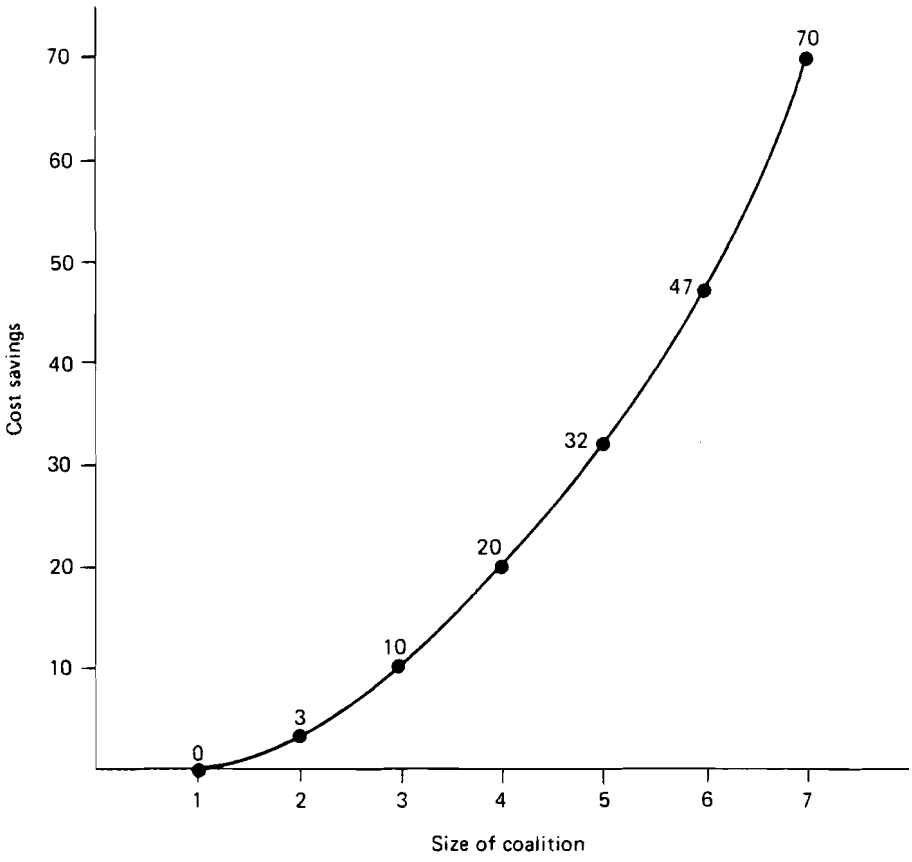

FIGURE 2 The cost savings of a joint project as a function of the size of the coalition: the rate of increase rises with each additional participant.

perhaps more typical, situation is that the rate of increase first rises, then falls, as shown in Figure 3.

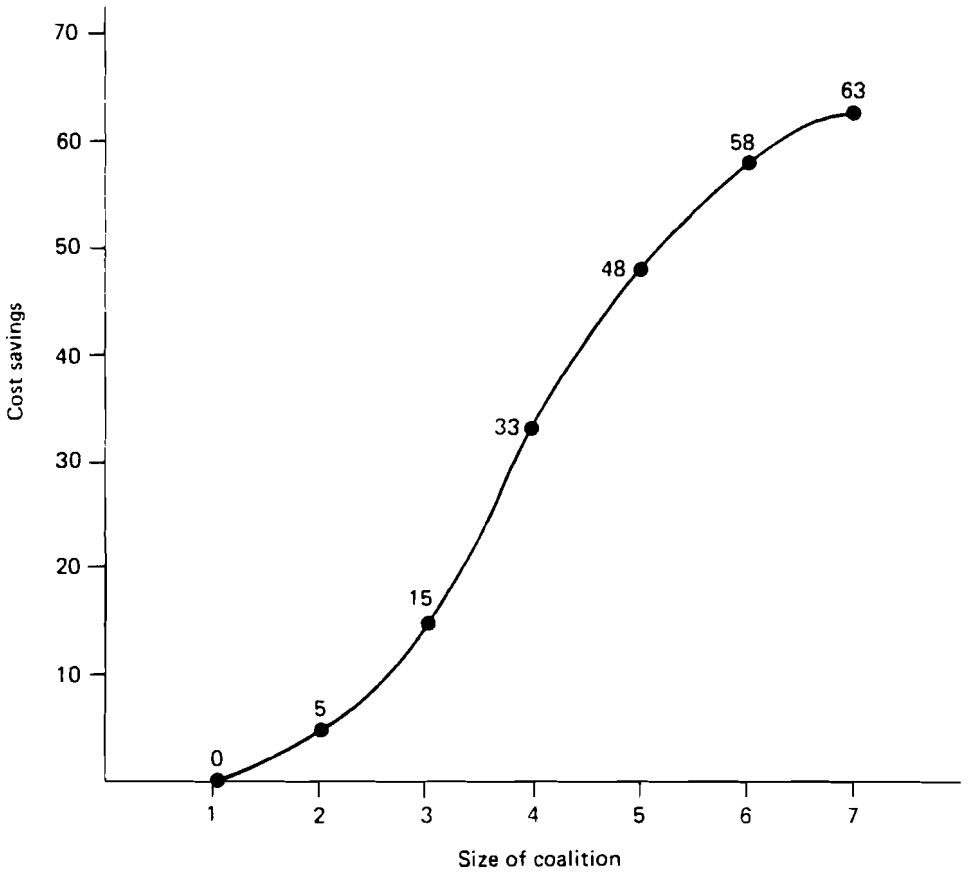

FIGURE 3 The cost savings of a joint project as a function of the size of the coalition: the rate of increase first rises, then falls.

It is found that justifying a "fair" allocation of costs is considerably more difficult in the latter case than in the former.

3 PRINCIPLES OF EQUITY: THE CORE

"Equity" can have a wide range of meanings. When considering what it means for a cost allocation to be equitable, it is first helpful to ask ourselves *why* it should be equitable. The answer: to encourage the agreement or cooperation of

those who pay the costs. Thus a reasonable test of the equity of a method is to see whether the participants agree in principle to the proposed allocation of costs.

In practice, one of the most common ways of achieving agreement on the distribution of costs is simply to allocate the costs in proportion to a criterion which stands for benefits received, such as use of facilities, number of users, or indeed, the benefits themselves – if they can be reliably estimated. *Ersatz* measures of benefits may actually be the more persuasive simply because their magnitudes are less open to dispute. This is the case in the municipal cost sharing problem discussed in Section 7. Here the costs to be shared relate to long-term investments, and future demand is conjectural at best, so the populations of the municipalities have been used as the basis for allocation.

One difficulty with allocating costs in this way is that it may conflict with some participants' perceptions of self-interest, and hence may not provide sufficient incentive for cooperation. In the municipality example above, an allocation of costs according to populations would result in the shares (in millions of dollars):

$$\text{A} \qquad \frac{100}{150}(10.6) = 7.067$$

$$\text{B} \qquad \frac{40}{150}(10.6) = 2.827$$

$$\text{C} \qquad \frac{10}{150}(10.6) = 0.707$$

However, municipality A would find it hard to accept such an allocation, since it could provide the same amount of water on its own for only \$6.5 million.

An allocation made on the basis of use gives even worse results for A (in millions of dollars):

$$\text{A} \qquad \frac{14}{20}(10.6) = 7.420$$

$$\text{B} \qquad \frac{4.8}{20}(10.6) = 2.544$$

$$\text{C} \qquad \frac{1.2}{20}(10.6) = 0.636$$

The difficulty with "proportional" allocation methods is that they ignore one of the fundamentals of the problem – the *alternative costs* embodied in the joint cost function $c(S)$. It is a minimum requirement of a fair allocation that it be *individually rational*: no user should pay more in the joint venture than he would have to pay on his own. This principle was stated by Ransmeier (1942) for the Tennessee Valley Authority projects, and is well established in the literature (von Neumann and Morgenstern 1944). It is a fundamental concept of

fairness since it constitutes the minimum incentive for an individual to join. To be individually rational, the costs y allocated to A, B, and C in the above example must satisfy $y_A \leq 6.5$, $y_B \leq 4.2$, $y_C \leq 1.5$, where $y_A + y_B + y_C = \$10.6$ million.

The same argument can be applied to groups of participants as well as to individuals and indeed was so stated by Ransmeier (1942). Consider, for example, neighboring municipalities A and B: they can build a joint facility for \$10.3 million, so it would certainly be unfair to allocate them more than \$10.3 million in total costs. Not only would it be unfair, but also, if cooperation is voluntary, there is a risk of A and B backing out if they have an allocation $y_A + y_B > 10.3$, since they can do better as a pair. The condition that no group pay more than its alternative cost is the principle of *group rationality*. Since a group may consist of a single participant, group rationality implies individual rationality. Figure 4 shows the set of all (nonnegative) allocations of \$10.6 million among A, B, and C, the shaded area being the subset of allocations satisfying group rationality.

In the general case, where there are n independent users $\{1,2,...,n\} = N$ and alternative costs are given by the function $c(S)$, the condition for group rationality for a cost allocation $y = (y_1, y_2, ..., y_n)$, $\sum_N y_i = c(N)$, is that

$$\sum_S y_i \leq c(S) \qquad \text{for all } S \subset N \tag{1}$$

A second principle with firm roots in the economics and project evaluation literature is that no participant should be charged less than the *marginal cost* (sometimes called the separable cost) of including him in the project (Federal Inter-Agency River Basin Committee 1950, Inter-Agency Committee on Water Resources 1958, Water Resources Council 1962). For example, it costs \$10.6 million to serve A, B, and C but only \$8.0 million to serve A and C. Therefore the marginal (or separable) cost of serving B is $\$10.6 - \$8.0 = \$2.6$ million, so it seems only fair that B should pay at least this amount. This concept is called *individual marginal cost coverage*. The marginal costs for A, B, and C are \$5.3, 2.6, and 0.3 million, respectively.

There is an obvious extension of this idea to groups. For example, the marginal cost of including the group {A,B} is $\$10.6 - \$1.5 = \$9.1$ million. The principle of *marginal cost coverage* states that every group of users should be charged at least the additional cost of serving them. This is only fair, since if $y_A + y_B < 9.1$, then C would be subsidizing A and B.

The idea of finding prices in which users do not subsidize each other in the use of a given public service or facility is also well-known in the theory of regulated public utilities (Faulhaber 1975, Zajac 1978).

Stated in general terms, the *marginality principle* is that a cost allocation y should satisfy

$$\sum_S y_i \geq c(N) - c(N - S) \qquad \text{for all } S \subset N \tag{2}$$

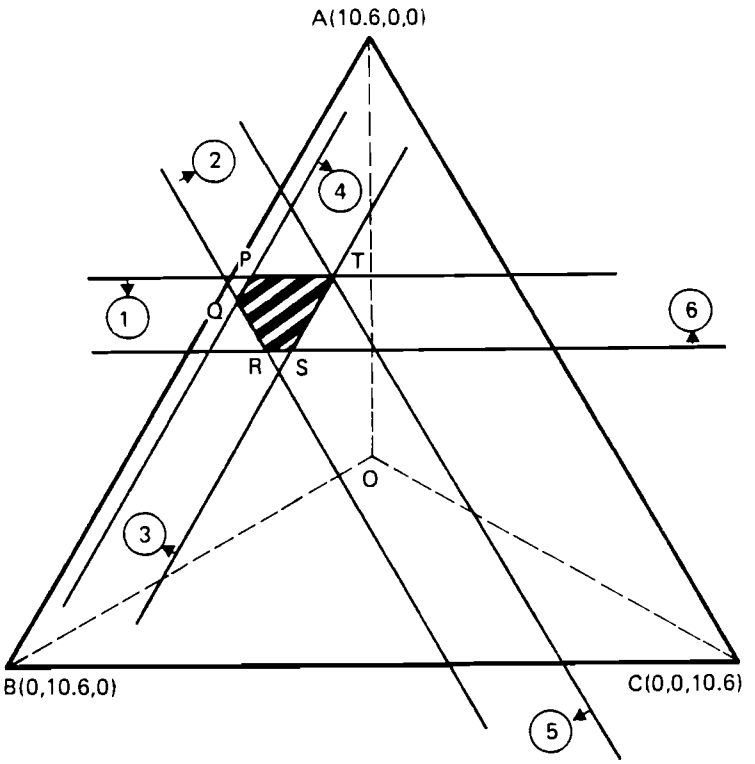

Constraints

(1) $y_A \leqslant 6.5$
(2) $y_B \leqslant 4.2$
(3) $y_C \leqslant 1.5$
(4) $y_A + y_B \leqslant 10.3$ [$\Rightarrow y_C \geqslant 0.3$ from (7)]
(5) $y_A + y_C \leqslant 8.0$ [$\Rightarrow y_B \geqslant 2.6$ from (7)]
(6) $y_B + y_C \leqslant 5.3$ [$\Rightarrow y_A \geqslant 5.3$ from (7)]
(7) $y_A + y_B + y_C = 10.6$

Vertices

P (6.5,3.8,0.3)
Q (6.1,4.2,0.3)
R (5.3,4.2,1.1)
S (5.3,3.8,1.5)
T (6.5,2.6,1.5)

FIGURE 4 Allocations of \$10.6 million among A, B, and C. The shaded area is the subset satisfying group rationality.

The argument for group rationality is based on strategic considerations, i.e., providing sufficient incentive for potential users to cooperate, whereas marginality can be viewed as a general concept of fairness that can be applied even if cooperation is mandated. However, an inspection of these two ideas reveals that they are in fact equivalent, given that all costs must be allocated, i.e., that $\Sigma_N\, y_i = c(N)$.

In game theory it is customary to interpret the two equivalent conditions (1) and (2) in terms of the cost savings game v.

Any *allocation* y of costs implies a corresponding *imputation* x of savings: if y_i is the cost assessed for i then the amount i saves by cooperating rather than going alone, x_i, is given by $y_i = c(i) - x_i$. In terms of v, the condition of individual rationality says that $x_i \geqslant 0$ for every participant i; group rationality says that

$$\begin{aligned} &\sum_S x_i \geqslant v(S) \qquad \text{for all } S \subset N \\ &\sum_N x_i = v(N) \end{aligned} \tag{3}$$

The set of all vectors x satisfying (3) is called the *core* of the game v.

In our example the core is the set of solutions to the following inequalities:

$$\begin{aligned} x &\geqslant 0 \\ x_A + x_B &\geqslant v(A,B) = (6.5 + 4.2) - 10.3 = 0.4 \\ x_A + x_C &\geqslant v(A,C) = (6.5 + 1.5) - 8.0 = 0.0 \\ x_B + x_C &\geqslant v(B,C) = (4.2 + 1.5) - 5.3 = 0.4 \\ x_A + x_B + x_C &= v(A,B,C) = (6.5 + 4.2 + 1.5) - 10.3 = 1.6 \end{aligned} \tag{4}$$

The shape of the core can be seen from the corresponding cost allocations in Figure 4.

The core provides a guideline for cost allocation by narrowing down the class of acceptable imputations, but it does not usually identify a unique answer. However, there is always the unfortunate possibility that there may be *no* core imputations; that is, no cost allocations that are either group rational or satisfy marginality. That this can happen in perfectly reasonable situations may be seen from the example of Figure 3. Here there are increasing returns to scale, but the rate of increase first rises, then falls. The minimum savings that can be realized by all seven users together is 63, but no matter how these savings are distributed, some group of five will receive at most 45, even though they could save more (48) as a subcoalition.

In such an example, a quick test to see whether the core is empty is to draw a line from the origin to the point corresponding to the total number of users; this line segment must lie above the savings curve for the core to be nonempty

(Shapley and Shubik 1973). In more complicated examples the feasibility of condition (3) can be checked using linear programming. In the three-municipality example, the core is small; if the total cost c(A,B,C) had happened to be \$12.0 million instead of \$10.6 million the core would have been empty.

Thus, core imputations are not bound to exist; however, the greater the economies of scale, the more likely a core is to be present. Moreover, when core imputations exist, they are typically not unique.

4 METHODS EXTENDING THE CORE

One approach to resolving the twin difficulties of nonexistence and nonuniqueness has been to look for some natural way of strengthening (or relaxing) the inequalities defining the core. This is one of the most common approaches in game theory literature. Three such methods will be discussed here: the least core and its specialization, the nucleolus; and two variations, the weak least core and weak nucleolus, and the proportional least core and proportional nucleolus.

4.1 The Least Core and Nucleolus

If the core of the cost savings game v is empty, the best alternatives of some subgroups are very good – in a certain sense "too" good – relative to the best alternative of the whole group. Hence we might consider imposing a tax on all proper subgroups as a way of encouraging the whole group to stick together. The least core is found by imposing the smallest uniform tax ϵ such that if all coalitions other than the whole group pay this tax, then a core imputation exists. Thus we require the least ϵ for which there exists an imputation x satisfying:

$$\begin{aligned} &\sum_S x_i \geqslant v(S) - \epsilon \qquad \text{for all } S \subset N \\ &\sum_N x_i = v(N) \end{aligned} \tag{5}$$

The *least core* is the set of all imputations x satisfying (5) for this least ϵ (Shapley and Shubik 1973). The corresponding allocations of costs are found by letting $y_i = c(i) - x_i$ for all i. Because of our assumptions about v, it can be shown that the result is always individually rational, i.e., that $x \geqslant 0$.

Suppose, on the other hand, that the cost savings game v already has a core, and it is necessary to find a unique solution. One way of narrowing down the choice is to imagine subsidizing all coalitions other than the whole group by a uniform amount ϵ. This amounts to solving (5) for smallest ϵ and allowing ϵ to go negative.

Computing the least core involves solving a linear program. For the three-municipality example, this program (in millions of dollars) is:

$$\min \epsilon$$

subject to

$$\begin{aligned} x_A \geq -\epsilon,\ x_B \geq -\epsilon, x_C \geq -\epsilon \\ x_A + x_B \geq 0.4 - \epsilon \\ x_A + x_C \geq -\epsilon \\ x_B + x_C \geq 0.4 - \epsilon \\ x_A + x_B + x_C = 1.6 \end{aligned} \tag{6}$$

The solution is $\epsilon = -0.533$, $x_A = x_B = x_C = 0.533$, and the corresponding unique cost allocation is $y_A = 5.967$, $y_B = 3.667$, and $y_C = 0.967$.

In some cases the linear program (5) may have several solutions. If so, the following "tie-breaking" device may be used:

For any imputation $\boldsymbol{x} = (x_1, x_2, ..., x_n)$ and coalition S, define the *excess* of S to be $v(S) - \Sigma_S x_i$. Let $e_1(\boldsymbol{x})$ be the largest excess of any coalition relative to $\boldsymbol{x}$, $e_2(\boldsymbol{x})$ the second largest excess, $e_3(\boldsymbol{x})$ the next, and so on. The least core is the set X_1 of all $\boldsymbol{x}$ that minimize $e_1(\boldsymbol{x})$. Let X_2 be the set of all $\boldsymbol{x}$ in X_1 that minimize $e_2(\boldsymbol{x})$, X_3 the set of all $\boldsymbol{x}$ in X_2 that minimize $e_3(\boldsymbol{x})$, and so on. This process eventually leads to an X_k consisting of a single computation $\bar{\boldsymbol{x}}$, called the *nucleolus* (Maschler *et al.* 1979, Schmeidler 1969).

4.2 The Weak Least Core and Weak Nucleolus

Suppose that a minimum uniform tax is imposed on any *individual user* who takes some course of action other than joining the whole group. Thus we find the least ϵ for which there is a solution $\boldsymbol{x}$ to the system:

$$\begin{aligned} &\sum_S x_i \geq v(S) - \epsilon|S| \qquad \text{for all } S \subset N \\ &\sum_N x_i = v(N) \end{aligned} \tag{7}$$

The set of all corresponding imputations $\boldsymbol{x}$ is the *weak least core.** For the above example, the weak least core is calculated by solving the linear program (in millions of dollars):

$$\min \epsilon$$

*For arbitrary ϵ the set of all solutions to (7) has been called the "weak ϵ-core" (Shapley and Shubik 1973); hence the designation "weak least core" in this case.

subject to

$$\begin{aligned} x_A \geqslant -\epsilon, x_B \geqslant -\epsilon, x_C \geqslant -\epsilon \\ x_A + x_B \geqslant 0.4 - 2\epsilon \\ x_A + x_C \geqslant -2\epsilon \\ x_B + x_C \geqslant 0.4 - 2\epsilon \\ x_A + x_B + x_C = 1.6 \end{aligned} \tag{8}$$

The unique solution is $\epsilon = -0.4$, $x_A = 0.4, x_B = 0.8, x_C = 0.4$, and the corresponding allocation of costs is $y_A = 6.1, y_B = 3.4$, and $y_C = 1.1$.

A choice between multiple solutions can be made as in the computation of the nucleolus by defining the excess of S to be $[v(S) - \Sigma_S x_i]/|S|$. We call the result the *weak nucleolus.* This method, while superficially similar to the least core, turns out to have an important property not shared by the least core; however, it also suffers from additional drawbacks (see Section 8).*

4.3 *The Proportional Least Core and Proportional Nucleolus*

Another variation on this theme is to modify the core by imposing a minimum tax (or subsidy) on all coalitions in proportion to their cost. Thus we postulate a tax rate t and solve the system

$$\min t$$

subject to

$$\begin{aligned} \sum_S x_i \geqslant (1 - t)v(S) \qquad \text{for all } S \subset N \\ \sum_N x_i = v(N) \end{aligned} \tag{9}$$

A minimum t exists provided $v(S) > 0$ for some $S \neq N$. A choice between multiple solutions can be made as in the computation of the nucleolus by defining the excess of a coalition S to be $[v(S) - \Sigma_S x_i]/v(S)$. [If $v(S) = 0$ we adopt the convention that $a/0 > b/0$ if $a > b$.]

For the above example the linear program (9) becomes

*One of these is that it may not be individually rational when the core is empty. This difficulty may be overcome by requiring that $x \geqslant 0$, a concept studied by Grotte under the name "normalized nucleolus" (Grotte 1970, 1976). We prefer not to use this designation because there are other natural ways of normalizing (see Section 4.3).

$$\min t$$

subject to

$$x \geqslant 0$$

$$x_A + x_B \geqslant 0.4(1 - t)$$

$$x_A + x_C \geqslant 0$$

$$x_B + x_C \geqslant 0.4(1 - t)$$

$$x_A + x_B + x_C = 1.6$$

The unique solution is $t = -3, x_A = 0, x_B = 1.6, x_C = 0$, and the corresponding cost allocation is $y_A = 6.5, y_B = 2.6$, and $y_C = 1.5$.

In other words, all of the savings in costs are allocated to B. The explanation for this is that B has effective veto power: neither A nor C can do any better than going alone without forming a coalition that includes B. For other solution concepts related to the core see Charnes *et al.* (1978), Maschler *et al.* (1979), and Heaney (1979).

5 THE SHAPLEY VALUE

The Shapley value for n players is given by the formula

$$y_i = \sum_{s=1}^{n} \frac{(s-1)!(n-s)!}{n!} \sum_{\substack{S : i \in S \\ |S| = s}} [c(S) - c(S - i)] \tag{10}$$

This is one of the earliest methods of allocation to be based on a consistent set of postulates about how an allocation should be made (Shapley 1953). All players are assumed to "sign up" in some particular order. If a group S has already signed up and i was the last member of the group to arrive, his *marginal cost contribution* to S is $c(S) - c(S - i)$. The Shapley value is i's average marginal contribution if all orders for signing up are assumed to be equally likely.

The Shapley values for municipalities A, B, and C are calculated in Table 3. The first column shows the six possible orders for signing up; the next three columns show the marginal contribution of each municipality.

TABLE 3 The Shapley values for municipalities A, B, and C.

	Marginal contribution ($ X 10^6)		
Order of signing	A	B	C
ABC	6.5	3.8	0.3
ACB	6.5	2.6	1.5
BAC	6.1	4.2	0.3
BCA	5.3	4.2	1.1
CAB	6.5	2.6	1.5
CBA	5.3	3.8	1.5
Total	36.2	21.2	6.2
Shapley value[a]	6.033	3.533	1.033

[a]The Shapley value is calculated by dividing the sum of the possible marginal contributions for each municipality (Total) by the number of possible orders of signing (6).

6 THE SEPARABLE COSTS–REMAINING BENEFITS (SCRB) METHOD

The last method to be considered here is one commonly used in practice for allocating the costs of multipurpose water development projects. The SCRB method is based on the simple and appealing idea that joint costs should be allocated, more or less, in proportion to the willingness of the user to pay. The "more or less" element is introduced because the proportional allocation is only performed after first assigning to each user his marginal (or separable) cost, and then taking as the criterion of proportionality each user's willingness to pay *minus* the marginal cost already allocated.

Specifically, let $b(i)$ be the benefit to user i and $c(i)$ his alternative cost. Evidently i would not be willing to pay more than $\min\{b(i),c(i)\}$ (sometimes called his justifiable expenditure) to participate in the joint project. The marginal cost of including i is $c'(i) = c(N) - c(N-i)$, which is less than or equal to $c(i)$ because the cost function is subadditive. In the SCRB nomenclature, i's "remaining benefit" $r(i)$ is his willingness to pay minus his marginal cost: $r(i) = \min\{b(i),c(i)\} - c'(i)$. Note that if $r(i) < 0$, then $c'(i) > b(i)$ and user i should not be included in the project. Therefore we can assume that all remaining benefits $r(i)$ are nonnegative. The remaining costs are $c(N) - \Sigma_N\, c'(j)$ and are allocated in proportion to the remaining benefits:

$$y_i = c'(i) + [r(i)/\underset{N}{\Sigma}\, r_j][c(N) - \underset{N}{\Sigma}\, c'(j)] \tag{11}$$

Using the marginal costs given in Section 3, the remaining benefits (in millions of dollars) for A, B, and C are calculated to be:

$$r(\mathrm{A}) = 6.5 - 5.3 = 1.2$$

$$r(\mathrm{B}) = 4.2 - 2.6 = 1.6$$

$$r(\mathrm{C}) = 1.5 - 0.3 = 1.2$$

$$\text{Total} = 4.0$$

The nonseparable costs are $10.6 - (5.3 + 2.6 + 0.3) = 2.4$, so the SCRB allocation (in millions of dollars) is:

$$y_{\mathrm{A}} = 5.3 + \frac{1.2}{4.0}(2.4) = 6.02$$

$$y_{\mathrm{B}} = 2.6 + \frac{1.6}{4.0}(2.4) = 3.56$$

$$y_{\mathrm{C}} = 0.3 + \frac{1.2}{4.0}(2.4) = 1.02$$

Variations of the SCRB method include proposals for allocating the nonseparable costs in proportion to some criterion such as use, priority of use, or population (James and Lee 1971). The difficulty with the SCRB method is that the simple underlying idea of allocating costs in proportion to benefits is lost by the *ad hoc* introduction of marginal costs; this leads to some strange results, as will be shown in Section 8.

7 A CASE STUDY OF SWEDEN

The area studied consists of 18 municipalities in the Skåne region of southern Sweden (Figure 5). At present, most of the municipal water supply is drawn from three sources: local groundwater, and two separate pipeline systems which distribute water from two lakes, Vombsjön and Ringsjön.

As early as the 1940s, certain municipalities in the area realized that local water sources might not be sufficient to meet future demand, and turned their attention to off-site sources. An association called the Sydvatten Company* was formed by several of them to plan the long-term water supply for the region. In the late 1960s, this group started to design a major project for obtaining water from a lake outside the region (Lake Bolmen) via an 80-km tunnel.
has recently been under reconsideration as the actual increase in water demand over the past decade has turned out to be short of the original forecasts.

*South Water Company.

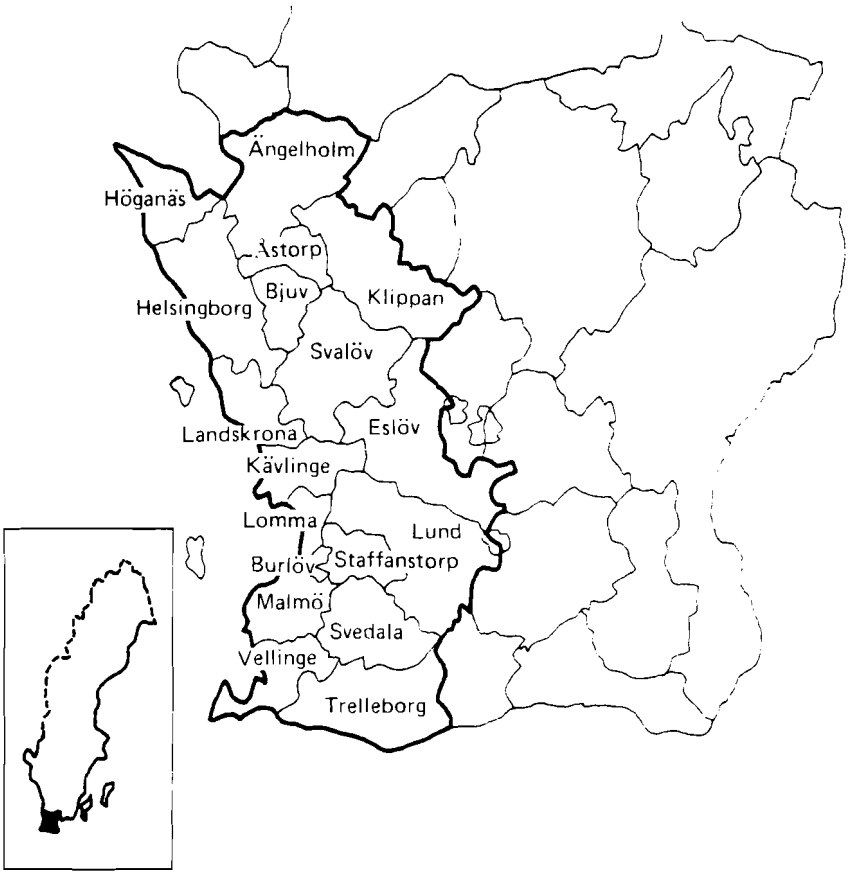

FIGURE 5 The region studied in Skåne, Sweden, and its division into municipalities.

The viability of the project depends on the number of additional municipalities that can be induced to participate in the project. This, in turn, depends on how much these municipalities will be obliged to pay for participation, bearing in mind the availability and costs of developing their own on-site resources. Moreover, there have been several unforeseen developments since the initiation of the project (e.g., greatly escalated costs, more optimistic estimates of local resources, and lower rates of demand growth), and these have brought the present population-based cost allocation procedure into question.

The basic concepts and methods developed in the preceding sections can be illustrated by applying them to the Swedish case over the decade 1970–1980, since data and forecasts for this period are readily available. The Sydvatten tunnel project mentioned earlier is not expected to have any impact on water

supply until the late 1980s, and so only conventional alternatives can be considered for meeting incremental demands over the period studied (e.g., extending the capacity of the pipeline system and increasing the use of local groundwater sources where feasible). The base year was taken to be 1970, and a water supply system was designed to satisfy the municipal "requirements" for 1980 as they were forecast in 1970. The different cost allocation methods described above were then applied to the system to examine the relative positions of the different municipalities. The results help clarify the way in which the different methods work, and why some of them may be preferable to others in practice.

7.1 Identifying Independent Actors

The first problem in defining the cost function is to identify the independent actors in the system. To develop the costs for each of the $2^{18} - 1 = 262{,}143$ possible groupings of the 18 municipalities would be impractical and unrealistic. In practice, the municipalities fall into natural groups based on past associations, geographical location, existing water transmission systems, and hydrological and geographical features determining the natural routes for water transmission networks.

A careful study of these conditions led to the grouping of the 18 municipalities into six independent units as shown in Figure 6. Group H, for example, consists of those municipalities which were already connected by the Ringsjön water supply system in 1970, together with the municipality of Svalöv, which would be located in the middle of the main transmission route. These groups are treated as single actors in the following analysis of alternative costs. Once a cost allocation for the groups has been determined, a further allocation of costs among the municipalities within each group could be made using a similar approach; however, this may not give the same result as if all municipalities were treated separately. The 1970 populations and forecast incremental water demands of each group are shown in Table 4.

7.2 Ambiguities in Defining the Cost Function: Direct Costs

In practice, ambiguities in defining the cost function arise due to the problem of *direct costs,* that is, costs that would be incurred by a given municipality no matter what course of action is pursued. For example, local water distribution systems are required within municipalities whether the water is supplied jointly or separately. The cost associated with municipal distribution systems may therefore be regarded as a direct cost. In principle, these costs could be excluded from the cost function on the grounds that they can be allocated independently. However, in practice, the borderline between direct and indirect costs is not always clear. In some municipalities, for instance, the water delivered by the regional

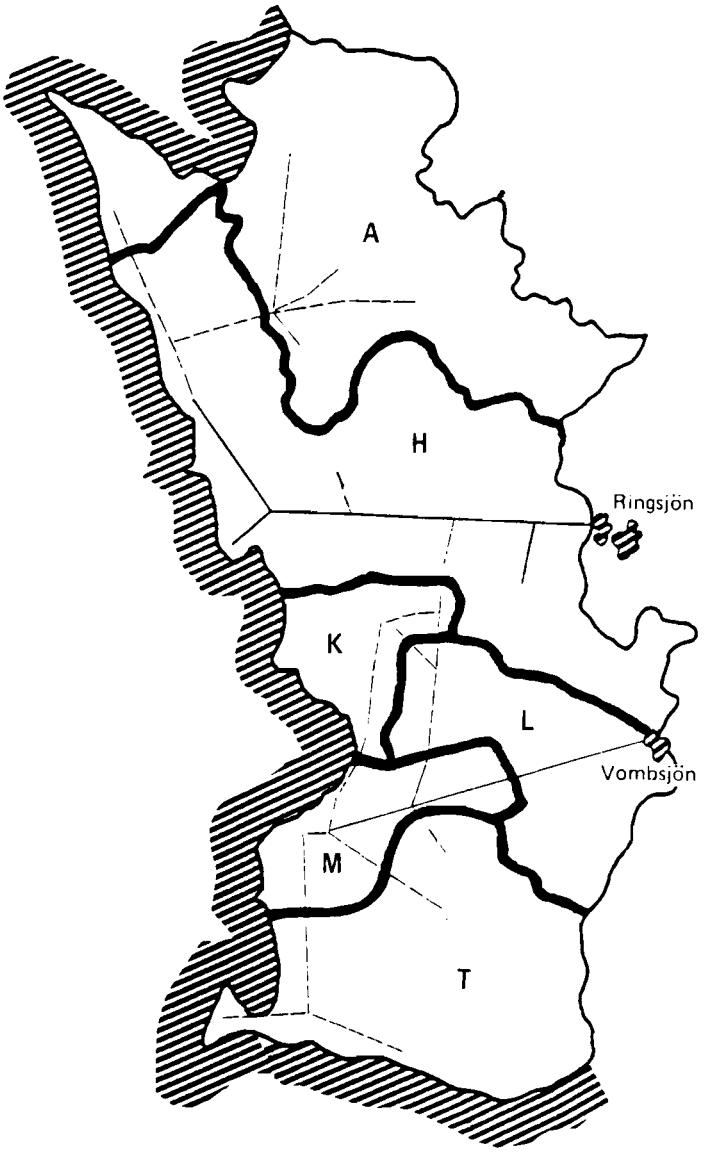

Group	*Municipalities in the group*
A	Ängelholm, Höganäs, Klippan, Åstorp, Bjuv
H	Helsingborg, Landskrona, Svalöv, Eslöv
K	Kävlinge, Lomma
L	Lund
M	Malmö, Burlöv, Staffanstorp
T	Trelleborg, Vellinge, Svedala

Boundaries of each group
Existing water network
Projected water network

FIGURE 6 The grouping of the 18 municipalities into six units, and the existing and projected water transmission networks.

TABLE 4 Populations and incremental water demands of the six municipal groups.

Group	Population ($\times 10^3$)	Incremental water demand ($\times 10^6$ m^3/yr)
A	85.0	6.72
H	176.3	8.23
K	26.8	3.75
L	69.0	3.53
M	287.3	14.64
T	59.5	6.21
Total	703.9	43.08

supply network must first be pumped up to a reservoir before distribution within the municipality; the facilities required for pumping depend on the pressure at the end of the transmission network. Thus the costs of these distribution facilities may *not* be independent of the method by which the water is supplied. The definition of the cost function naturally depends on the fraction of these costs treated as direct costs.

Since the definition of the cost function is always somewhat arbitrary in practice, it is desirable to choose a cost allocation method that is insensitive to the inclusion of direct costs. One of the difficulties with the SCRB method is that in some cases it is sensitive to the inclusion of direct costs. None of the game theory methods considered here suffers from this drawback.

7.3 Calculating the Cost Function

The water supply system includes two lakes (Vombsjön and Ringsjön), one major groundwater aquifer (Alnarp), and other minor on-site sources. The possible routes of a water transmission network (based on a preliminary analysis) are also shown in Figure 6.

To avoid inconsistencies in defining the cost function, it was assumed for the purpose of this study that the pressure at each demand point does not depend on the method by which the water is transmitted to that point. Thus the cost of distributing the water within each municipality does not depend on the arrangement by which the water is supplied, so this element can be treated as a direct cost and excluded from the cost function. The water delivered to each municipality was assumed to be of the same quality. The water was treated to bring it up to this level at the source, and the cost of treatment was included in the cost function.

Cost functions for transmitting and treating water were based on the formulas given in Appendix A. Using these functions, the total costs $c(S)$ associated with the least-cost combination of alternative supply sources were estimated for each coalition S. The results are shown in Table 5; commas signify that the least-cost option of that coalition is to break up into the subcoalitions indicated. The unit costs (per million cubic meters per year) are: A, 3.27; H, 2.08; K, 2.91; L, 4.50; M, 1.42; T, 3.51.

TABLE 5 Total costs (Skr $\times 10^6$) for various joint supply systems.

Group	Total cost	Group	Total cost	Group	Total cost
A	21.95	AHK	40.74	AHKL	48.95
H	17.08	AHL	43.22	AHKM	60.25
K	10.91	AH,M	55.50	AHK,T	62.72
L	15.88	AH,T	56.67	AHL,M	64.03
M	20.81	A,K,L	48.74	AHL,T	65.20
T	21.98	A,KM	53.40	AH,MT	74.10
		A,K,T	54.84	A,K,LM	63.96
AH	34.69	A,LM	53.05	A,K,L,T	70.72
A,K	32.86	A,L,T	59.81	A,K,MT	72.27
A,L	37.83	A,MT	61.36	A,LMT	73.41
A,M	42.76	HKL	27.26	HKL,M	48.07
A,T	43.93	HKM	42.55	HKL,T	49.24
HK	22.96	HK,T	44.94	HKMT	59.35
HL	25.00	HL,M	45.81	HLMT	64.41
H,M	37.89	HL,T	46.98	KLMT	56.61
H,T	39.06	H,MT	56.49	AHKL,T	70.93
K,L	26.79	K,LM	42.01	AHKLM	69.76
KM	31.45	K,L,T	48.77	AHKMT	77.42
K,T	32.89	K,MT	50.32	AHLMT	83.00
LM	31.10	LMT	51.46	AKLMT	73.97
L,T	37.86			HKLMT	66.46
MT	39.41				
				AHKLMT	83.82

The cost function reveals the relative strength of the different actors, which depends on factors such as the cost and availability of local resources, and access to the resources of others. For example, L finds that the unit cost of going alone is high; though it is located close to the major regional sources (Ringsjön and Vombsjön), it owns neither. Hence it has a strong incentive to participate in a joint scheme with the owners of the two sources, H and M. H and M have the lowest unit costs because they own the two systems, but they can reduce their

unit costs even further by including other municipalities in a joint scheme, due to economies of scale. However, the system owned by H (Ringsjön) has a greater excess capacity than that owned by M (Vombsjön). Hence the incremental cost of other municipalities joining in a coalition with M is higher than the incremental cost of joining with H. The effect is that H has more to offer its partners in a coalition than does M, and this will be reflected in the final cost allocation.

8 COMPARISON OF METHODS

Using the cost function developed above, we now compare the cost allocations of the different methods described in the preceding sections. We assume that all groups participate in a joint scheme at a total cost of Skr 83.82 million. The results obtained from the two proportional allocation schemes based on demand and population and from the SCRB method are shown in Table 6, as are the Shapley value, the nucleolus, the weak nucleolus, and the proportional nucleolus. The cost shares allocated to each group by the seven methods are illustrated in Figure 7 for ease of comparison.

TABLE 6 Cost allocations of Skr 83.82 million by seven methods.

	Cost allocations (Skr X 10^6)						
Allocation method	A	H	K	L	M	T	Total
Proportional to population	10.13	21.00	3.19	8.22	34.22	7.07	83.82
Proportional to demand	13.07	16.01	7.30	6.87	28.48	12.08	83.82
SCRB	19.54	13.28	5.62	10.90	16.66	17.82	83.82
Shapley value	20.01	10.71	6.61	10.37	16.94	19.18	83.82
Nucleolus	20.35	12.06	5.00	8.61	18.32	19.49	83.82
Weak nucleolus	20.03	12.52	3.94	9.07	18.54	19.71	83.82
Proportional nucleolus	20.36	12.46	3.52	8.67	18.82	19.99	83.82

Note that the "proportional" allocations differ markedly from the others. A comparison of the proportional allocations with the costs of going alone (Table 7) reveals that these methods would charge some participants in the joint project more than they would have had to pay on their own. Allocation by demand penalizes M for participating, while allocation by population penalizes both H and M.

This failure to satisfy the requirement of individual rationality is based on the fact that proportional methods do not take into account crucial differences among the participants in their access to sources of supply. The proportional procedures work against H and M, which have large populations, and favor the

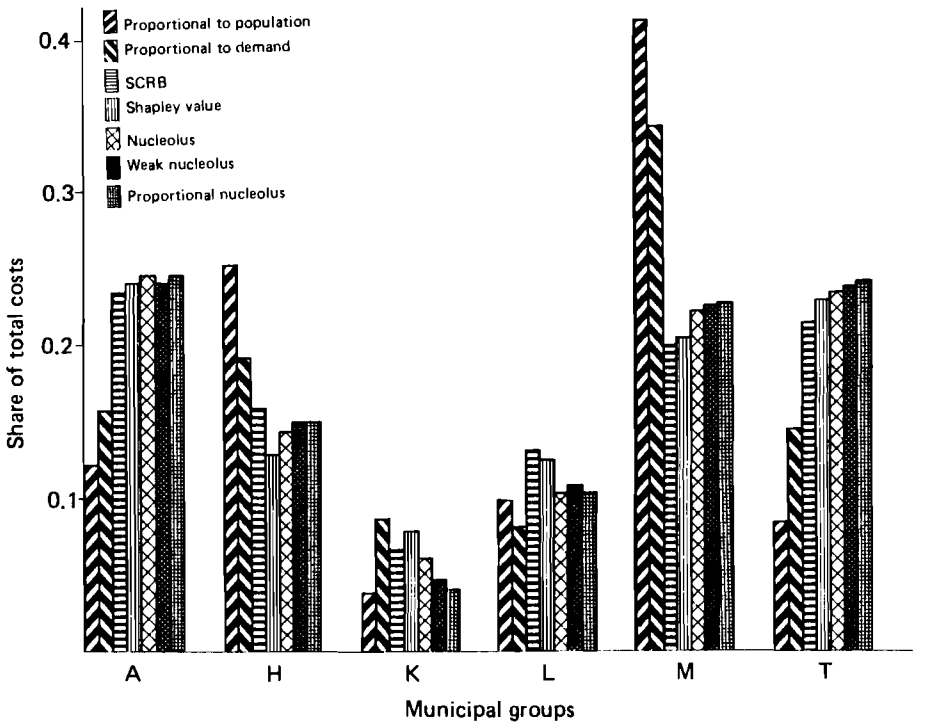

FIGURE 7 The shares of the total cost allocated to each group by the seven methods studied.

TABLE 7 Individual and marginal costs (Skr $\times 10^6$) for each group in the Swedish case study.

	A	H	K	L	M	T
Individual alternative costs	21.95	17.08	10.91	15.88	20.81	21.98
Marginal costs	17.36	9.85	0.82	6.40	12.89	14.06

outlying regions A and T. The inclusion of A and T is relatively costly, despite their smaller populations, because they are both remote from the major sources of supply. This fact is reflected in their high marginal costs (Table 7). Though A and T should be charged at least the marginal cost of including them, both proportional methods fail to do so. This is one serious disadvantage of the proportional allocation methods.

More seemingly reasonable than the proportional schemes, but actually almost as ill-behaved, is the SCRB method. This method is individually rational only if the alternative costs are less than the corresponding benefits (as assumed in the present case); otherwise this may not be so. It also may not satisfy group

rationality. For example, the three adjacent municipal groups H, K, and L can provide municipal water for themselves at a cost of Skr 27.26 million, but the SCRB method would assess them a total of Skr 29.80 million if they all shared in a regional facility. It would not be in the interest of H, K, and L to participate on the basis of such an assessment, because they are then, in effect, being forced to subsidize the other participants. Since there exist assessments in which no coalition subsidizes any other, such an allocation could be considered inequitable.

That the SCRB method suffers from this defect is not surprising, since it considers only the marginal costs of including individual participants, not the marginal costs of coalitions. In this case, the marginal cost of including both M *and* T is much higher than the sum of their individual marginal costs, since if one is already being served the *additional* expense of serving the other (or individual marginal cost) is low. Thus, while it is not necessary to estimate all cost elements in order to calculate the SCRB allocation, this short-cut has a price: it may result in a less equitable final distribution.

By contrast, a calculation of the Shapley value requires the alternative costs for all possible subsets. Unfortunately, however, this allocation also fails the group rationality and marginality tests. In particular, the Shapley value assesses the coalition HKL at Skr 430,000 more than its alternative cost.

Since group rationality and marginal cost coverage seem to be essential from the standpoint of equity, as well as to provide sufficient incentives for cooperation, the remaining three methods – the nucleolus, weak nucleolus, and proportional nucleolus – are potentially more desirable than those discussed above, as they always produce a core imputation if one exists. Is there any basis for preferring one method to another?

A general point raised in the early study by Ransmeier (1942) is that a method should be able to *adapt* to changing conditions. The need for adaptability is evident in the fact that, typically, total project costs are not known precisely until after the project has been completed. Since the cost allocation method is usually agreed upon before the project has been started, it must specify how different levels of total costs should be allocated. Such an agreement will initially be based on some best estimate of the costs of alternatives, but once an agreement has been reached the alternatives must be abandoned. It is therefore sufficient that a method specify how different levels of total costs should be allocated for fixed levels of alternative costs.

An elementary requirement of any such method is that if total costs increase then no participant will be charged less; conversely, if total costs decrease, no participant will be required to pay more. This property is called *monotonicity* (Megiddo 1974), and is fundamental in problems of fair division (see, for example, Huntington 1928, Balinski and Young 1974, 1975, 1977, 1979a, 1979b). Several of the methods considered so far do not possess this fundamental property. As an example, suppose that the total cost of the Swedish project involved an overrun of Skr 4 million, bringing the total to Skr 87.82 million (see Table 8).

TABLE 8 Comparison of the allocations under increased cost with the initial allocations (Skr X 10^6).

	Cost allocation (Skr X 10^6)						
Allocation method	A	H	K	L	M	T	Total
Proportional to population	10.61	22.00	3.35	8.62	35.86	7.40	87.82
	10.13	21.00	3.19	8.22	34.22	7.07	83.82
Proportional to demand	13.70	16.78	7.64	7.20	29.84	12.66	87.82
	13.07	16.01	7.30	6.87	28.48	12.08	83.82
SCRB	21.42	14.19	5.46	10.97	17.31	18.47	87.82
	19.54	13.28	5.62	10.90	16.66	17.82	83.82
Shapley value	20.67	11.38	7.29	11.03	17.60	19.84	87.82
	20.01	10.71	6.61	10.37	16.94	19.18	83.82
Nucleolus	20.76	13.25	4.51	9.80	19.16	20.33	87.82
	20.35	12.06	5.00	8.61	18.32	19.49	83.82
Weak nucleolus	20.70	13.19	4.61	9.74	19.21	20.38	87.82
	20.03	12.52	3.94	9.07	18.54	19.71	83.82
Proportional nucleolus	20.61	13.20	4.72	9.84	19.14	20.31	87.82
	20.36	12.46	3.52	8.67	18.82	19.99	83.82

This situation could arise if the method used for supplying the whole coalition involved components that would not be cost-effective in any smaller coalition, for example, the large fixed costs required for an interbasin transfer project. In fact a project of this nature is currently under construction in Sweden, and the costs are already substantially more than predicted.

Comparing the new allocations with the old (Table 8), we notice that the nucleolus requires K to pay *less* even though the total cost of the project has increased. Similarly, the SCRB method allocates K Skr 160,000 less when costs increase. This nonmonotonic behavior suggests that the nucleolus and SCRB methods may not be reasonable cost allocation procedures.

On the other hand, it is clear that methods which allocate costs in proportion to some single criterion, like population or use, must be monotonic. This is also the case for the Shapley value, the weak nucleolus, and the proportional nucleolus. For the Shapley value and weak nucleolus, any change in total costs is distributed equally among the actors (see Appendix B).* However, this particular way of dividing changes in costs is questionable. Why should all participants

*The nonmonotonicity of the nucleolus was first pointed out by Megiddo (1974).

have to share unforeseen joint expenses equally, when their shares in the enterprise are very different? Using the weak nucleolus, for example, it is quite possible that a tiny participant, who contributes essentially no costs (or savings) to any coalition would still have to contribute as much to defray a cost overrun as would his giant neighbors. This kind of behavior seems unacceptable.*

Perhaps the fairest way of measuring the participants' shares in the enterprise is not by their costs (most of which they might well have incurred acting alone), but rather by the amounts that they save by virtue of taking part in the enterprise as opposed to going alone. A reasonable scheme would be to divide any unforeseen costs in proportion to the benefits enjoyed. This is precisely the way in which the proportional nucleolus works (see Appendix B).

9 SUMMARY

Given the practical need to allocate the costs of a joint water resource facility among the different users, it is necessary to choose rationally among the many different methods of allocation available. Using a definite computational procedure itself provides some semblance of rationality. However, the justification of a method does not lie in the computational procedure employed, but in its behavior in practice. Thus it is necessary to compare the different methods on the basis of principle. The literature on cost allocation suggests a number of such principles, including: simplicity, reasonable information requirements, adaptability (which includes monotonicity in costs), insensitivity to direct costs, individual and group rationality, and marginal cost coverage.

Seven different approaches have been selected for comparison from among the various methods discussed in the project evaluation and game theory literature, and their performance evaluated by application to an actual municipal cost allocation problem in Sweden. One of the methods used most widely for multipurpose projects, the SCRB method, suffers from a number of disadvantages, including nonmonotonicity in costs, failure to satisfy group rationality (and individual rationality in some cases), as well as failure to cover marginal costs for groups. The underlying SCRB idea of allocating costs in proportion to benefits is attractive; the difficulties seem to arise from the *ad hoc* introduction of marginal costs. A more sophisticated game theory method, the Shapley value, is monotonic and satisfies individual rationality, but, as shown by the Swedish example, may not satisfy group rationality when it is possible to do so.

Three of the remaining methods – the nucleolus, weak nucleolus, and proportional nucleolus – always satisfy group rationality and marginal cost coverage when it is possible to do so. However, the nucleolus seems unsatisfactory because it is not monotonic in costs. The weak nucleolus and proportional

*The fact that a "dummy player" (i.e., one who contributes zero additional costs to any coalition) can be assessed positive costs by the weak nucleolus was first pointed out by Reinhard Selten.

nucleolus are both monotonic, but the latter allocates changes in costs in a manner more consistent with the benefits that the participants reap from the enterprise. Hence, of all game theory methods considered here, the proportional nucleolus appears to be the most attractive.

The game theory methods all suffer from the disadvantages that they are fairly complicated and require detailed information on costs. All of the methods except for the simplest proportional allocation schemes rely on information about demands and the optimal scale of development – information which in practice may be unreliable or nonexistent. This is particularly true for long-term investment projects such as the Swedish case discussed above. It is therefore not surprising to find that a simple scheme based on allocating costs in proportion to the population was eventually chosen, since insufficient information was available to adopt a more equitable approach.

APPENDIX A: COST OF WATER SUPPLY NETWORK

This section describes the procedure used to determine the capital costs of pipes and pumps necessary to supply the required amounts of water to the demand points shown in Table A1. The distances between points (in parentheses) and

TABLE A1 Incremental water demand for all municipalities in the study area for the period 1970–1980.[a]

Municipality	Incremental water demand ($\times 10^6$ m^3/yr)	Municipality	Incremental water demand ($\times 10^6$ m^3/yr)
Ängelholm	2.65	Lund	3.53
Höganäs	1.48	Malmö	10.66
Klippan	0.60	Burlöv	1.67
Åstorp	0.63	Staffanstorp	2.30
Bjuv	1.36	Trelleborg	1.26
Helsingborg	4.60	Vellinge[b]	2.30
Landskrona	1.80	Räng[b]	0.57
Svalöv	0.50	Skanör[b]	0.25
Eslöv	1.32	Svedala[b]	1.10
Kävlinge	2.74	Bara[b]	0.73
Lomma	1.01		

[a] Taken from Sydvatten, Prognos 73.
[b] Bara is included in the municipality of Svedala; Vellinge, Räng, and Skanör constitute a single municipality.

their elevations are shown in Figure A1. It is assumed that the pressure at each demand point does not depend on the arrangement by which the water is

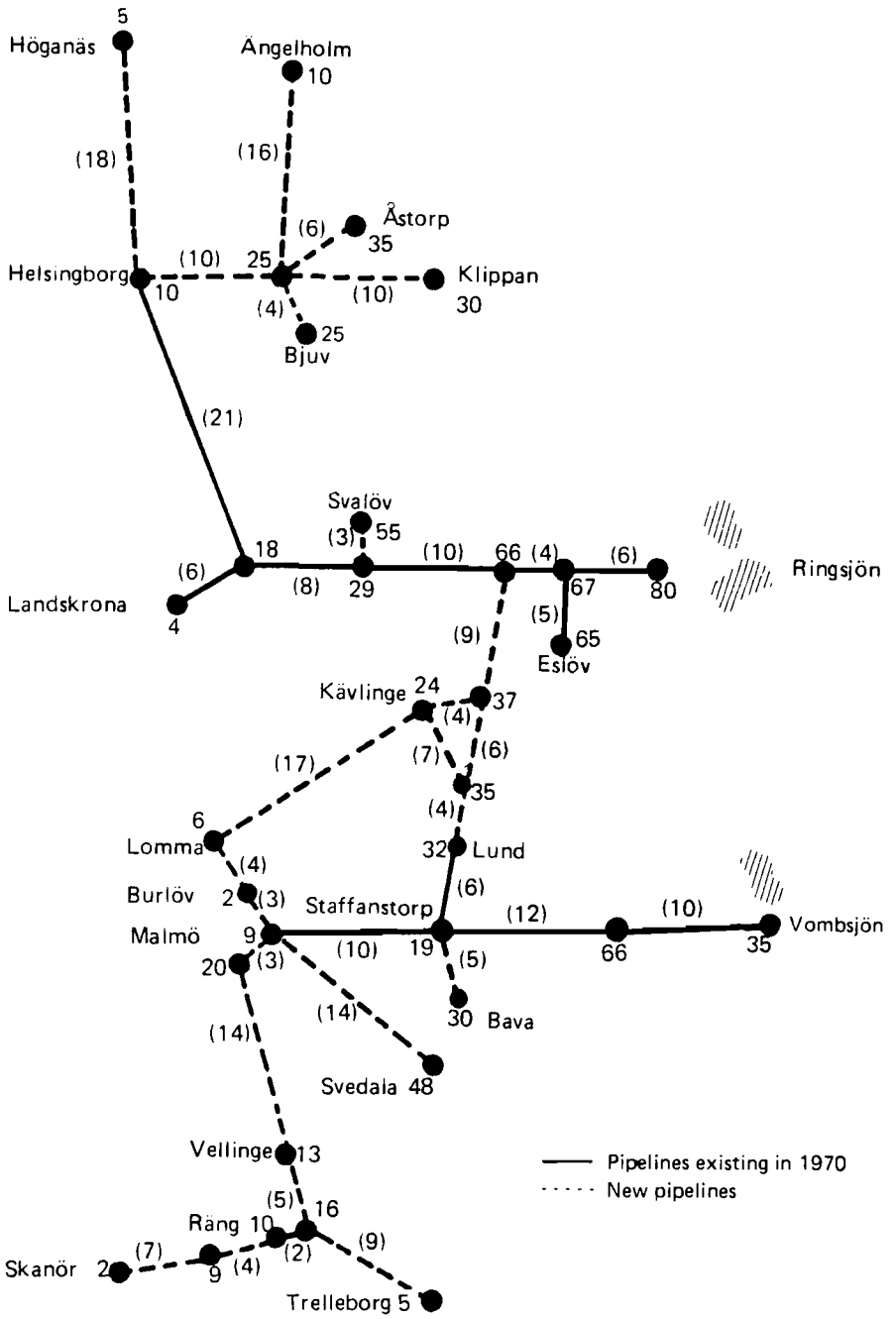

FIGURE A1 The water transmission network. The number at each node represents the elevation in m; the number in parentheses on each arc represents the distance in km.

supplied, as described in the text (p. 20), and this allows us to treat each arc of the transmission network independently. The cost analysis of the network is therefore carried out arc by arc.

The cost of water transmission includes the following components:

Cost of pipelines	$C_1 = c_1 L = (\gamma + \alpha D^{\beta})L$	(Skr)
Cost of pumps	$C_2 = c_2 fP$	(Skr)
Cost of electricity	$C_3 = c_3 P$	(Skr/yr)

where

c_1 = Unit cost of piping (Skr/m)
L = Length of pipe (m)
c_2 = Unit cost of pump (Skr/kW)
f = Safety factor
c_3 = Unit cost of electricity (Skr/kW-yr)
$P = (9.81/E)QH$ = Effective capacity of pump (kW)
Q = Flow of water in pipe (m^3/sec)
$H = H_0 + IL$ = Required pumping head (m)
H_0 = Difference in altitude between origin and destination of pipe (m)
I = Hydraulic gradient
E = Pumping efficiency
D = Pipe diameter (m)
α, β, γ = Coefficients

The total annual cost of transmission is given by

$$C = (C_1 + C_2)\mathrm{CRF} + C_3$$

where

$$\mathrm{CRF} = \frac{(1+i)^n\, i}{(1+i)^n - 1}$$ = Capital recovery factor
i = Interest rate
n = Amortization period (years)

The total cost C is a function of the pipe diameter D, the flow Q, the pumping head H, and the length of pipe L. These factors are related by the Hazen–Williams formula:

$$H = 10.7(\mathrm{Cw})^{-1.85}\, D^{-4.87}\, Q^{1.85}\, L$$

where Cw is the Hazen–Williams coefficient.

The economical pipe diameter D^* is obtained as a function of the flow Q by letting $\partial C/\partial D = 0$:

$$D^* = \left(\frac{4.87\,ab}{\alpha\beta\,\mathrm{CRF}}\right)^{1/(\beta+4.87)} Q^{2.85/(\beta+4.87)}$$

where

$$a = (c_2 f\,\mathrm{CRF} + c_3)(9.81/E)$$
$$b = 10.7(\mathrm{Cw})^{-1.85}$$

Similarly, the economical hydraulic gradient I^* is obtained as

$$I^* = \left(\frac{\alpha\beta\,\mathrm{CRF}}{4.87\,a}\right)^{\beta/4.87} Q^{(1.85\beta-4.87)/(\beta+4.87)}$$

The parameters are determined from Swedish data as follows: $\alpha = 477$ Skr; $\beta = 1.60$; $\gamma = 150$ Skr; $E = 0.63$; Cw = 100; $f = 1.33$; CRF = 0.0871 based on $i = 0.06$, $n = 20$ years; $c_2 = 1893$ Skr/kW; $c_3 = 613$ Skr/kW-yr.

The results are:

$$D^* = 0.928\,Q^{0.43} \qquad \text{(m)}$$

$$I^* = 2.99\,Q^{-0.28} \times 10^3$$

$$C_1 = (150 + 477\,D^{1.60})L \qquad \text{(Skr)}$$

$$C_2 = 39.2\,QH \times 10^3 \qquad \text{(Skr)}$$

$$C_3 = 9.54\,QH \times 10^3 \qquad \text{(Skr/yr)}$$

The cost of treating water at Vombsjön includes the costs of filtration, pumping, and chlorination. The treatment at Ringsjön consists of screening, sedimentation, coagulation, and filtration. Unfortunately the particular cost data on these unit processes were not available, so capital costs and the costs of operation and maintenance (O/M) were estimated using available data. The cost of treating on-site groundwater includes the costs of pumping, filtration, and chlorination, and these were also estimated. The results of the cost analysis are given in Table A2, where $\tilde{Q}$ is the flow of water through the treatment plant in $\mathrm{Mm}^3/\mathrm{yr}$.

TABLE A2 The cost of providing water from the three sources.

Water source	Cost	Value	Unit ($\times 10^6$)
Vombsjön	Capital	$C_K^V = 2.31\,\tilde{Q}^{0.74}$	Skr
	O/M	$C_M^V = 0.162\,\tilde{Q}^{0.91}$	Skr/yr
Ringsjön	Capital	$C_K^R = 3.68\,\tilde{Q}^{0.64}$	Skr
	O/M	$C_M^R = 0.410\,\tilde{Q}^{0.64}$	Skr/yr
Groundwater	Capital	$C_K^G = 2.38\,\tilde{Q}^{0.58}$	Skr
	O/M	$C_M^G = 0.263\,\tilde{Q}^{0.82}$	Skr/yr

APPENDIX B: MONOTONICITY

The weak least core is the set of optimal solutions to the linear program

$$\min \epsilon$$

subject to

$$\sum_N x_i = v(N)$$

$$\sum_S x_i \geqslant v(S) - \epsilon|S| \qquad \text{for all } S \subset N$$

which is equivalent to

$$\min \sum_N (x_i + \epsilon)$$

subject to

$$\sum_N x_i = v(N)$$

$$\sum_S (x_i + \epsilon) \geqslant v(S) \qquad \text{for all } S \subset N$$

This is equivalent to solving

$$\min \Sigma\, x_i' \tag{B1}$$

subject to

$$\sum_S x_i' \geqslant v(S) \qquad \text{for all } S \subset N$$

and letting $x_i = x_i' - \epsilon$, where $\epsilon = [\Sigma_N\ x_i' - v(N)]/n$. Since the x' program is independent of $v(N)$, an increase in $v(N)$ simply has the effect of increasing ϵ – and hence every component x_i – by the same amount. The same holds for the weak nucleolus, hence the weak nucleolus is monotonic. The proof of monotonicity of the Shapley value is left to the reader.

The proportional least core is the set of optimal solutions to the linear program

$$\min t$$

subject to

$$\sum_N x_i = v(N)$$

$$\sum_S x_i \geqslant (1 - t)v(S) \qquad \text{for all } S \subset N$$

where we assume that $v(S) > 0$ for some $S \neq N$ to ensure existence.

This is equivalent to solving (B1) and letting $x_i = x_i' v(N)/\Sigma_N\ x_i'$. An increase in $v(N)$ by a common proportion simply has the effect of increasing every component of x_i by the same proportion. The same holds for the proportional nucleolus, hence it is monotonic.

ACKNOWLEDGMENTS

We wish to thank Lennart de Maré, on leave at IIASA from the University of Lund, who provided us with much useful data and background information on the situation in Sweden, and commented extensively on the manuscript. We are also grateful to O. Menshikova and I. Menshikov, of the Computing Center of the Academy of Sciences of the USSR, who pointed out several errors in an earlier version of the manuscript. Finally, we wish to express our special thanks to Janusz Kindler, who, as leader of the Regional Water Management Task at IIASA, provided the inspiration for undertaking this study, and contributed many helpful comments on the organization and presentation of the results.

REFERENCES

Balinski, M.L., and H.P. Young (1974) A new method for Congressional apportionment. Proceedings of the National Academy of Sciences of the USA 71:4602–4606.

Balinski, M.L., and H.P. Young (1975) The quota method of apportionment. American Mathematical Monthly 82:701–730.

Balinski, M.L., and H.P. Young (1977) On Huntington methods of apportionment. SIAM Journal of Applied Mathematics C 33:607–618.

Balinski, M.L., and H.P. Young (1979a) Quotatone apportionment methods. Mathematics of Operations Research 4:31–38.

Balinski, M.L., and H.P. Young (1979b) The Webster method of apportionment. Proceedings of the National Academy of Sciences of the USA 77:1–4.

Baumol, W., and D. Bradford (1970) Optimal departures from marginal cost pricing. American Economic Review 60:265–283.

Bogardi, I., and F. Szidarovsky (1976) Application of game theory in water management. Applied Mathematical Modelling 1:16–20.

Charnes, A., J. Rousseau, and L. Seiford (1978) Complements, mollifiers, and the propensity to disrupt. International Journal of Game Theory 7:37–50.

Eckstein, O. (1958) Water Resource Development. Cambridge, Mass.: Harvard University Press.

Faulhaber, G. (1975) Cross-subsidization: pricing in public enterprises. American Economic Review 65:966–977.

Federal Inter-Agency River Basin Committee (1950) Proposed Practices for Economic Analysis of River Basin Projects. Washington, D.C.: U.S. Government Printing Office.

Grotte, J.H. (1970) Computation of and Observations on the Nucleolus, and the Central Games. M.Sc. Thesis, Cornell University.

Grotte, J.H. (1976) Dynamics of cooperative games. International Journal of Game Theory 5:27–64.

Heaney, J.P. (1979) Efficiency/equity analysis of environmental problems – a game theoretic perspective. In S.J. Brams, A. Schotter, and G. Schwödiauer (Eds.), Applied Game Theory, pp. 352–369. Vienna: Physica-Verlag.

Huntington, E.V. (1928) The apportionment of representatives in Congress. American Mathematical Society Transactions 30:85–110.

Inter-Agency Committee on Water Resources (1958) Proposed Practices for Economic Analysis of River Basin Projects. Washington, D.C.: U.S. Government Printing Office.

James, L.D., and R.R. Lee (1971) Economics of Water Resources Planning. New York: McGraw-Hill.

Loehman, E., and A. Whinston (1974) An axiomatic approach to cost allocation for public investment. Public Finance Quarterly 1:236–251.

Loehman, E., J. Orlando, J. Tschirhart, and A. Whinston (1979). Cost allocation for a regional coastwater treatment system. Water Resources Research 15:193–202.

Loughlin, J.C. (1977) The efficiency and equity of cost allocation methods for multipurpose water projects. Water Resources Research 13:8–14.

Maschler, M., B. Peleg, and L.S. Shapley (1979). Geometric properties of the kernel, nucleolus, and related solution concepts. Mathematics of Operations Research 4:303–338.

Megiddo, N. (1974) On the nonmonotonicity of the bargaining set, the kernel, and the nucleolus of a game. SIAM Journal of Applied Mathematics 27:355–358.

Neumann, J. von, and O. Morgenstern (1944) Theory of Games and Economic Behavior. Princeton, N.J.: Princeton University Press.

Okada, N. (1977) A Game-Theoretic Approach to the Analysis of Area-Wide, Multi-Modal Water Utilization System. Report of the Faculty of Engineering, Tottori University 8, September 1977.

Ramsey, F. (1927) A contribution to the theory of taxation. Economic Journal 37:47–61.

Ransmeier, J.S. (1942) The Tennessee Valley Authority. A Case Study in the Economics of Multiple Purpose Stream Planning. Nashville, Tenn.: Vanderbilt University Press.

Schmeidler, D. (1969) The nucleolus of a characteristic function game. SIAM Journal of Applied Mathematics 17:1163–1170.

Shapley, L.S. (1953) A value for *n*-person games. In H.W. Kuhn and A.W. Tucker (Eds.), Contributions to the Theory of Games, II (Annals of Mathematics Studies 28), pp. 303–306. Princeton, N.J.: Princeton University Press.

Shapley, L.S., and M. Shubik (1973) Game Theory in Economics – Characteristic Function, Core and Stable Set, Chapter 6, RAND Report R-904-NSF/6, Santa Monica.

Straffin, P., and J.P. Heaney (1980) Game Theory and the Tennessee Valley Authority. International Journal of Game Theory (in press).

Suzuki, M., and M. Nakayama (1976) The cost assignment of the cooperative water resource development: a game theoretical approach. Management Science 22:1081–1086.

Thomas, A.L. (1974) The allocation problem: Part two. In Studies in Accounting Research, No. 9. Sarasota, Fl.: American Accounting Association.

Water Resources Council (1962) Policies, Standards, and Procedures in the Formulation, Evaluation, and Review of Plans for Use and Development of Water and Related Land Resources. 87th Congress, 2nd Session, Senate Doc. 97.

Young, H.P. (1980) Cost Allocation and Demand Revelation in Public Enterprises. WP-80-130. Laxenburg, Austria: International Institute for Applied Systems Analysis.

Zajac, E. (1978) Fairness of Efficiency: An Introduction to Public Utility Pricing. Cambridge, Mass.: Ballinger.

AGRICULTURAL WATER DEMANDS IN THE SILISTRA REGION

Ilya V. Gouevsky, David R. Maidment, and Witold Sikorski

PREFACE

Interest in water resource systems has been a critical part of research at IIASA related to resources and the environment since the Institute's inception. As demands for water increase relative to supply, the intensity and efficiency of water resource management must be developed further. This in turn requires an increase in the degree of detail and sophistication of the analysis, including economic, social, and environmental evaluation of water resource development alternatives aided by application of mathematical modeling techniques, to generate inputs for planning, design, and operational decisions.

In 1977 IIASA initiated a concentrated research effort focusing on modeling and forecasting of water demands. Our interest in water demands derived from the generally accepted realization that these fundamental aspects of water resource management have not been given due consideration in the past.

This paper, the ninth in the IIASA water demand series, reports on the analysis of water demands of a large agroindustrial complex in the northeastern part of Bulgaria, covering a territory of about 2,700 km^2, with a population of some 175,000. With the aid of SWIM (*S*ilistra *W*ater for *I*rrigation *M*odel), which was developed at IIASA, several factors that influence both agricultural production and associated water demands have been analyzed. The major goal of the Silistra complex, i.e., to maximize the total crop and livestock production within the limited regional resources, has been taken into account in the analysis. (The user's guide to SWIM is available from IIASA on request.) The model allows analyses to be made of substitution possibilities in agricultural production (water for fertilizers, irrigated for nonirrigated crops, one subregion for another, and so on). The study, leading ultimately to the determination of an economically efficient level of irrigation development, may serve as an example for similar studies initiated elsewhere.

1 INTRODUCTION

In most countries agriculture consumes more water than all other sectors of the economy combined. The US National Water Commission (1973) reported that globally 77 percent of all water withdrawals and 87 percent of all consumptive use occur in agriculture. The demand for water in agriculture can be expected to rise in the future as more irrigation is developed. The UN Food and Agriculture Organization (1977b) has estimated that a \$100 billion (US) ($\$10 \times 10^9$) investment program in irrigation and drainage will be required to provide adequate food supplies to the world's population by 1990. In view of the very large investments required for developing water supplies to meet agricultural water demands, detailed studies of the nature of these demands are needed to ensure that the water is used productively and efficiently.

Research carried out at IIASA from 1976 to 1977 was aimed at improving the systems analysis methodology for studying water demands in a broad context of socioeconomic, engineering, and environmental issues. The application of this methodology at IIASA to a real-world agricultural problem was greatly facilitated by an agreement signed on 18 March 1977 between IIASA and the Bulgarian State Committee for Science and Technological Progress to promote technical cooperation in the development of the Silistra region of Bulgaria. Following the signing of this agreement, a case study of agricultural water demands in the Silistra region was begun at IIASA in collaboration with the Bulgarian Ministry of Agriculture and Food Industry. The goals of the case study were

- To provide the planners and decision makers of the Silistra region with detailed information about water demands and their impact on agricultural production in the region.
- To improve the systems analysis methodology for deriving and forecasting agricultural water demands by studying a real-world problem.

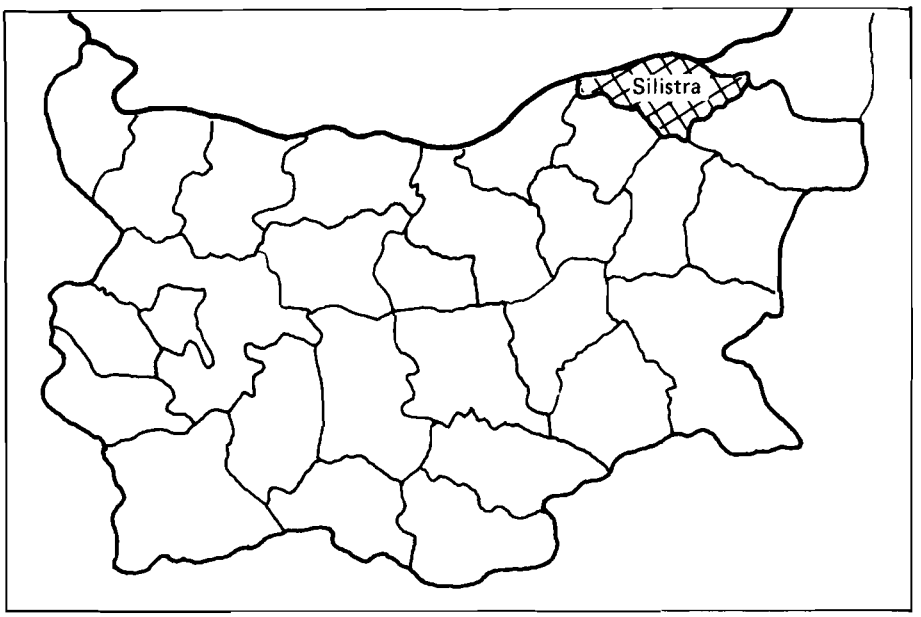

FIGURE 1a Location of the Silistra region in Bulgaria.

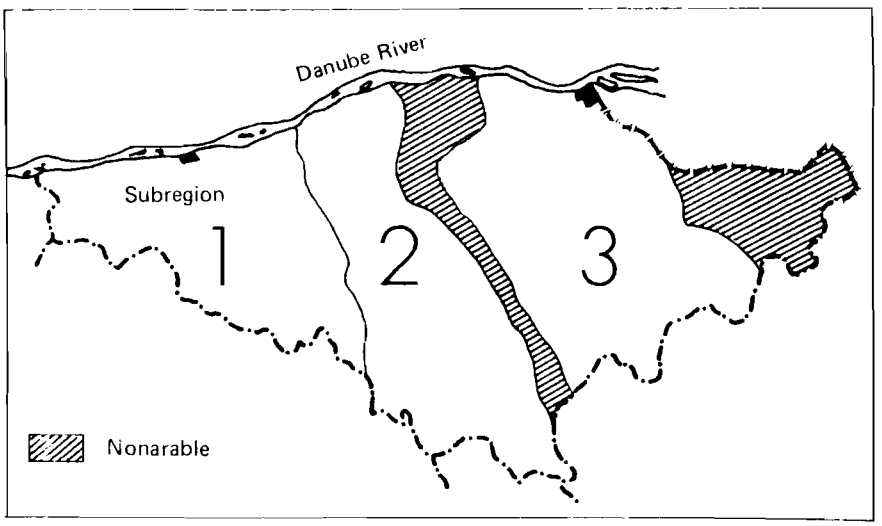

FIGURE 1b The Silistra region. There are 1,500 km^2 of arable land, which is 4.2 percent of the arable land in Bulgaria. The mean annual flow rate of the Danube River is 5,000 m^3/sec, and it is the only river in the region. Groundwater in the region is at a depth of 400 m.

The Silistra region has a population of 175,000, covers a territory of about 2,700 km^2, and is situated in the northeastern part of Bulgaria (Figure 1a). All agricultural activities in the region are organized into a large agroindustrial complex called Drustar. In the terminology that has been adopted in Bulgaria, an agroindustrial complex is an example of an aggregated agricultural system that consists of the following basic systems: crop production and processing, livestock production and processing, marketing, and environment. One administrative body is responsible for overall planning, development, and management of the complex.

The agroindustrial complex is a further development of the process of refining the management structure of agriculture in Bulgaria. There have been two turning points in this process. Until the early 1940s the agricultural activities in Bulgaria were spread over hundreds of thousands of small farms of a few hectares or less which had almost no mechanization. Following the socialist revolution in 1944, more cooperative farms were organized to better utilize the scarce resources available at that time. In the Silistra region cooperative farms were also organized which greatly improved the quantity and quality of the production as well as the living standards of the population. By the early 1970s it was recognized that further improvement of the existing 30 cooperative farms in the region required a new organization and management structure that could integrate all phases of the agricultural process, from the input resources to the final products. Thus all cooperative farms in the Silistra region were united in the present Drustar complex* which contains about 150,000 hectares (ha) of arable land.

Within the complex, crops are grown and harvested, stored, and fed to livestock, which are housed in concentrated feedlot areas. The Silistra region's planners consider self-sufficiency an important goal. As much as possible, they wish to supply all the region's needs from its own resources and export the surpluses. Because the management is integrated, it is reasonable to model the agricultural production system of the Silistra region as one unit. This is in contrast to modeling it as an assembly of separate units, as would be appropriate for regions with a different management structure and different goals.

Since rapid development is occurring, it is essential to choose the best way of directing future agricultural activities and investments. In the list of problems to be investigated in this respect, water resources appear to have a key role. There are two important reasons:

- Water resources within the region are limited to the bordering Danube River. No other rivers exist in the region. Groundwater is available only in small quantities or at depths exceeding 400 m, which makes it an unimportant resource as far as crop irrigation is concerned.

*The Drustar agricultural–industrial complex and the Silistra region are referred to interchangeably in the text.

- Vast irrigation development is to take place in the coming years to meet the feed requirements of meat- and milk-producing livestock – hence, to ensure stable agricultural production, a large reliable water supply has to be made available within the region.

The meteorological conditions in the region are favorable for crop and livestock production supported by irrigation. The average monthly rainfall in the irrigation season is 46 mm but extremes ranging from 0 mm to 137 mm have been recorded. The average monthly evapotranspiration for the same period is 171 mm, hence irrigation is necessary to ensure positive soil moisture balance over the vegetation season. The average water balance in the region under normal weather conditions is shown in Figure 2.

To overcome the difficulties associated with scarce water resources within the region and negative soil moisture balance, intensive investigations have been carried out over the past few years. As a result, a number of alternatives for

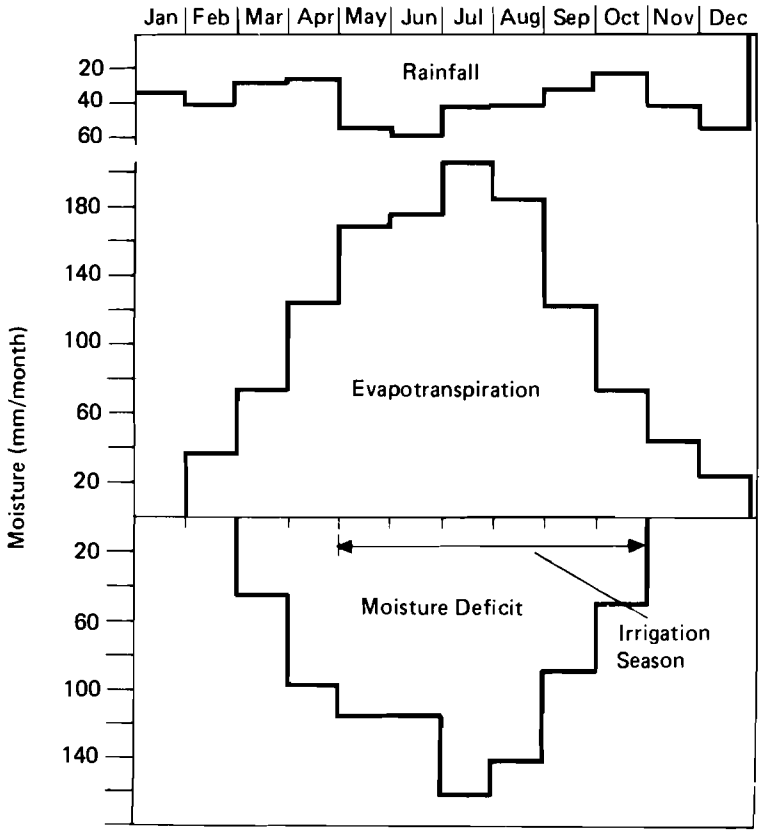

FIGURE 2 Average monthly water balance in the Silistra region.

augmenting the available water supply have been proposed. Some of them include the construction of reservoirs in various parts of the region; others combine the use of pumping stations and reservoirs, the construction of long-distance canals, and so on. The common characteristic of all alternatives is that, first, they rely on Danube River water and, secondly, all of the alternatives are rather costly. Obviously, one way of decreasing the supply cost would be to reduce agricultural water demands for irrigation, which constitute the major demand of the region, while keeping the production targets at the desired level. It is clear that keeping production at a certain level involves additional costs because other inputs must be substituted for water. The question is: Are these costs greater than the supply cost, and at what point is the water resource system in equilibrium, i.e., at what point is the incremental cost of additional supply equal to the incremental benefit that it produces?

Over the past 20 years there has been considerable interest in developing models that are able to answer one or both of these questions. Because of their great complexity and the planner's need to find "the best" solution in a set of feasible solutions, linear programming models have been employed from the very beginning. The models can be grouped into three categories: national, regional, and farm-level models. One of the first families of national models was developed at the Center for Agricultural and Rural Development (CARD) at Iowa State University in the United States beginning in 1954 (Heady and Agrawal 1972, Heady and Srivastava 1975, Nicol and Heady 1975). These models simultaneously consider (a) exogenous variables affecting food requirements, (b) government programs that control supply and increase food exports, (c) technological advances, and (d) the pricing of water through public investment in irrigation development. The models minimize total costs of crop and livestock production over a 25-yr time horizon. Duloy and Norton (1973) employed a similar concept for developing a model for the agriculture sector in Mexico. This model maximizes the sum of the producer and consumer surplus in national crop production. A similar model was developed by the UN Food and Agriculture Organization (1977a) in order to identify policy options for an optimal crop-mix pattern in long-term planning in Iraq.

Regional models receive the greatest attention in the literature. For example, Gisser (1970), Soltani-Mohammadi (1972), Voropaev (1973), and Dean *et al.* (1973) have developed regional agricultural models with heavy emphasis on crop production. Livestock production is considered as an exogenous variable. All of these models maximize net benefit difference between gross and production costs in the respective regions. The IIASA Food and Agriculture Program has also made a considerable effort to develop regional agricultural models (Carter *et al.* 1977).

Linear programming is a tool that can integrate the various production processes in agriculture, including water use, and hence can examine the major interrelationships between them. This is an attractive feature as far as the Drustar agroindustrial complex is concerned since this complex is a unified crop–

livestock agricultural system. Hence, linear programming was selected as the basic methodology for the study.

During the course of the study two versions of the *S*ilistra *W*ater for *I*rrigation *M*odel (SWIM) were developed, SWIM1 and SWIM2. SWIM1 derives agricultural water demands in the Silistra region taking into account only crop production, processing, and marketing (Gouevsky and Maidment 1977). It is a moderately sized linear program comprising 56 constraints and 68 decision variables. During July 1977, SWIM1 was developed and its results were reported in English and Bulgarian (see Figure 3).

After the results of SWIM1 were reviewed in Bulgaria, SWIM2 was developed. It takes into account three subregions within the Silistra region, livestock production and processing, and some environmental issues including different fertilizer application rates and manure disposal on the land. Some of the data were again revised in October 1977, and the model was run on the EC 1020 computer of the Central Computer and Management Center at the Ministry of Agriculture and Food Industry in Sofia.

The model and its results were presented during the second IIASA workshop on water demands, held in Laxenburg, Austria, from December 5 to 9, 1977. Following this workshop the final model was implemented on the ES1020 computer in Bulgaria where it is being further developed and refined.

This report is intended for the reader who wishes to familiarize himself with the modeling methodology and the type of results that can be produced. For the reader who also wishes to implement the SWIM2 model on his own computer, a users' guide has been prepared (Gouevsky *et al.* 1978). The users' guide illustrates all steps needed in computer implementation by means of a small linear programming model and then shows how to set up the input data

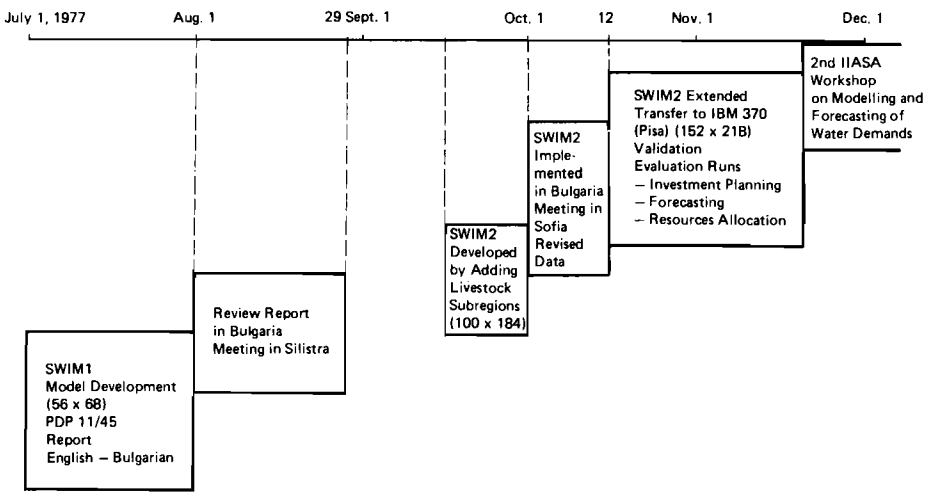

FIGURE 3 Progress of the Silistra case study.

to SWIM2 using a matrix generator. The full set of input data are given and also an example solution of SWIM2. These data are available on magnetic tape from the Resources and Environment Area of IIASA.

2 DESCRIPTION OF THE MODEL

2.1 The Agricultural Production System

There are about 1,500 km^2 (150,000 ha) of arable land in the Silistra region on which crops are grown to feed the livestock in the region and to meet the needs of the local population; 11,400 ha are irrigated, all with sprinklers. In the model, the region is divided into three main irrigation areas, all of which use Danube water.

The main objective of the model is to make a thorough analysis of factors that influence agricultural water demands and associated agricultural production in the three subregions, taking into account the major goal of the complex, which is to maximize the total net benefit from crop and livestock production with the limited regional resources. The model is intended to provide information for

- Estimating irrigation and livestock water demands and their distribution in space and time within a given year
- Forecasting the growth in these demands in response to different scenarios of growth in the numbers of livestock in the region
- Determining what proportion of the arable land within the complex should be developed for irrigation
- Evaluating the impact on water demands of various factors, including weather variability and the availability of other input resources (e.g., fertilizers)
- Estimating the demand function for water

For modeling purposes, agricultural production systems may be broken down into a number of subsystems as shown in Figure 4. Input resources such as land, water, and fertilizers go into producing crops whose output is processed for marketing or feeding to livestock. Crop production, supplemented by purchases from the market, is fed to livestock whose products are processed and sold. Livestock production may have substantial environmental impacts, such as those due to feedlot effluents, and these impacts may, in turn, affect crop production.

Those production processes modeled in detail for the Silistra region by SWIM2 are shown in Figure 5. The diagram indicates all processes that are involved in crop production and the uses of the crops. The input resources are land, water, seeds, fertilizers and chemicals, labor, machinery, fuel, and capital investments. Decision makers for the Silistra region consider that land is the only fixed input resource. All others are variable.

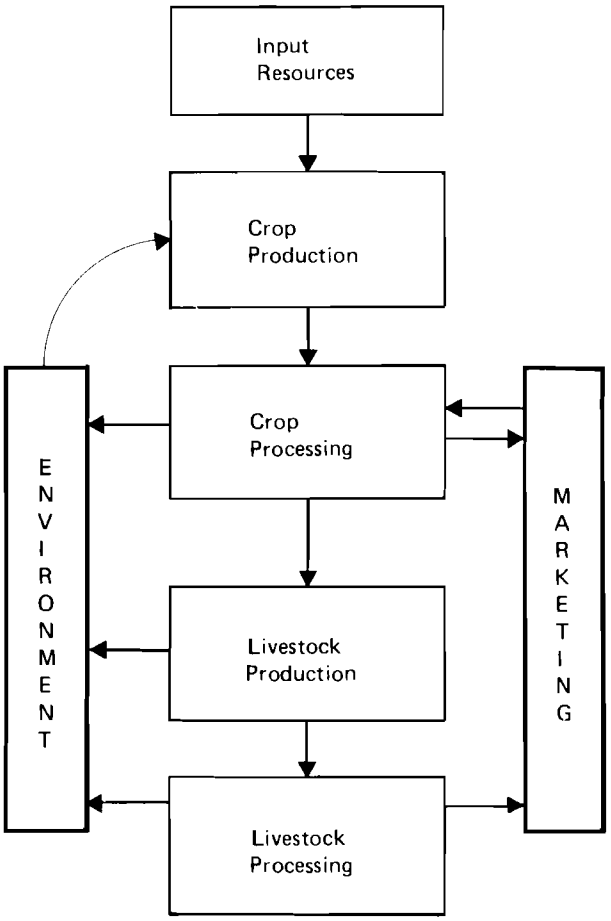

FIGURE 4 The agricultural production system.

Let us use wheat as an example. The input resources enter the crop production subsystem, which has various alternatives for producing wheat. It may be grown in any of the three subregions; it may or may not be irrigated; if it is irrigated, the usual amount of fertilizers may be supplied or these fertilizers may be reduced to 80 percent of their usual amounts. Thus, there are nine alternatives; no irrigation, irrigation with 80 percent fertilizers, and irrigation with 100 percent fertilizers, each of which can take place in any of the three subregions. In the next subsystem wheat undergoes processing to obtain grain, straw, flour, and bran.

The products are then distributed among different subsystems; grain goes to reserves and to livestock production, straw and bran go directly to livestock production, flour is sent to the market to meet the demands of the population.

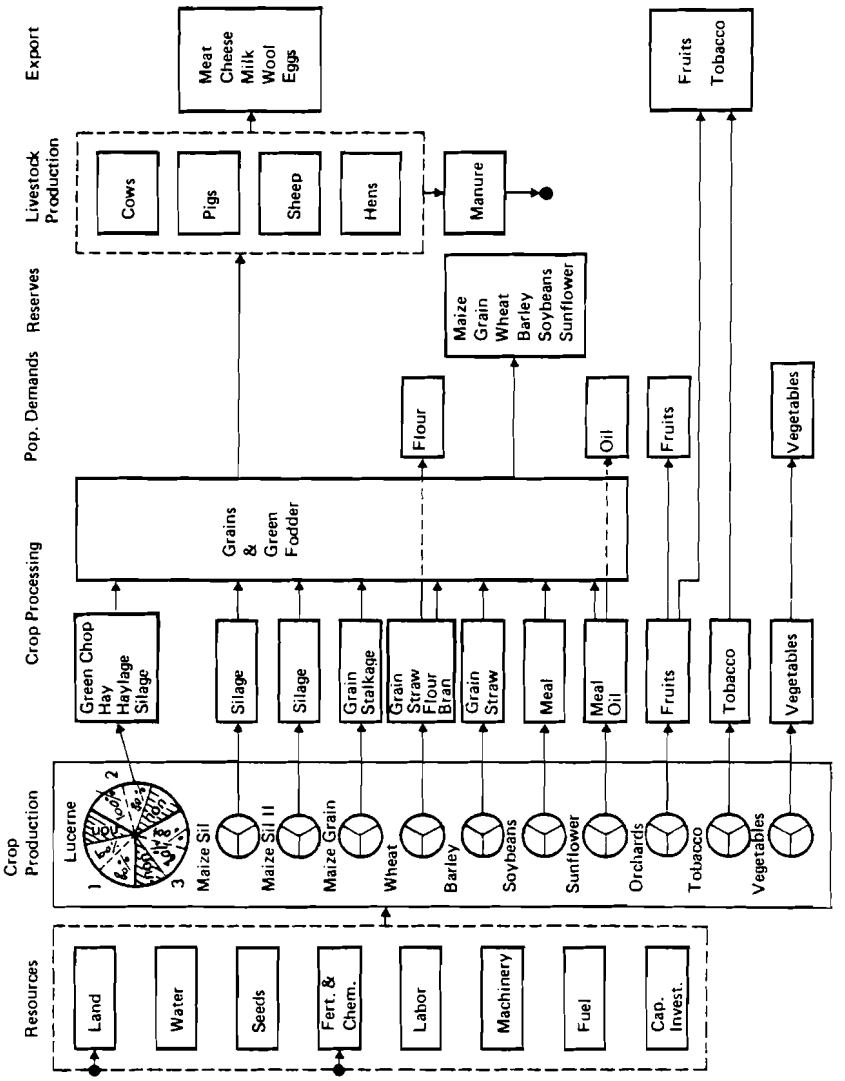

FIGURE 5 Agricultural production in the Silistra region.

Crop products feed four types of livestock – cows, pigs, sheep, and hens – all of which are housed in feedlots. Livestock products are exported from the Silistra region. The by-products of the livestock production subsystem, animal wastes from feedlots, are spread onto some of the land and partially substitute for fertilizers. These wastes may also have undesirable environmental impacts.

Water is one of the key parameters to be modeled in the system because it directly influences crop production, which in turn controls livestock production. The reverse also applies. If livestock numbers change, this will change the demands for crop production, and for irrigation and drinking water. These interrelationships are shown in Figure 6.

2.2 Modeling Assumptions

The decision makers for the Silistra region are considered to have a number of objectives in mind in planning the agroindustrial complex:

- *Maximum production*, so as to generate a high level of exports from the region and to meet the needs of the Silistra population for food and other agricultural products.
- *Efficient production*, i.e., minimum cost per unit of output. This implies that the flows of materials between the various processes in Figure 5 are in harmony with one another and that the least-cost combinations of inputs are used. It also involves an emphasis on using the most advanced technology (e.g., sprinkler rather than flooding systems are adopted for irrigation development).
- *Sustainable production*. Over the short term this involves minimizing the impact of weather variations by providing irrigation and production reserves. Over the long term, soil fertility must be maintained through

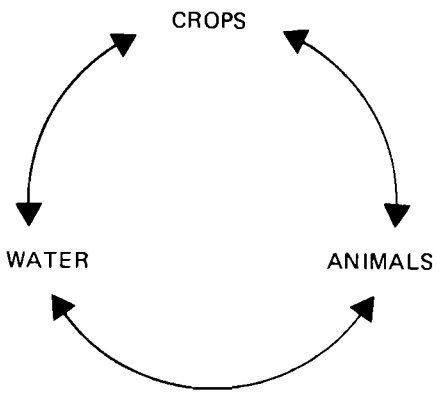

FIGURE 6 Relationship between water, crops, and livestock.

proper cultivation and crop rotation. A balance should also be maintained in the numbers of the different animals since if one animal becomes predominant the system is neither resilient to variations in market prices nor resistant to the spread of an animal disease.

These objectives have been substantially incorporated into SWIM2 either in its objective function or in its constraints. It may be noted that there could be other important objectives in the region that are not explicitly included in the model, such as increasing the efficiency of agricultural labor.

In the process of modeling agricultural production and deriving water demands, four basic assumptions have been made. (a) The agricultural system is modeled for 1 year. Depending on the coefficients included in SWIM2, this 1 year can represent the conditions of any specified year. SWIM2 does not contain year-to-year variations in its model structure, however. (b) The inputs and outputs of each of the seven subsystems shown in Figure 5 represent the decision variables in the model. It is further assumed that there are three types of relationships between decision variables:

- A linear-by-nature relationship; for example, the amount of seeds for planting a given crop is a linear function of the area to be planted. (See Figure 7(a)).
- A nonlinear relationship; for example, crop yield vs. fertilizer application. In this case the nonlinear function is linearized and the linear segments obtained are introduced as separate decision variables in the model (Figure 7(b)).
- A relationship where the decision maker is indifferent over a certain interval of variation of the dependent variable, or where the dependent variable is constant over a specified range of the independent variable (Figure 7(c)).

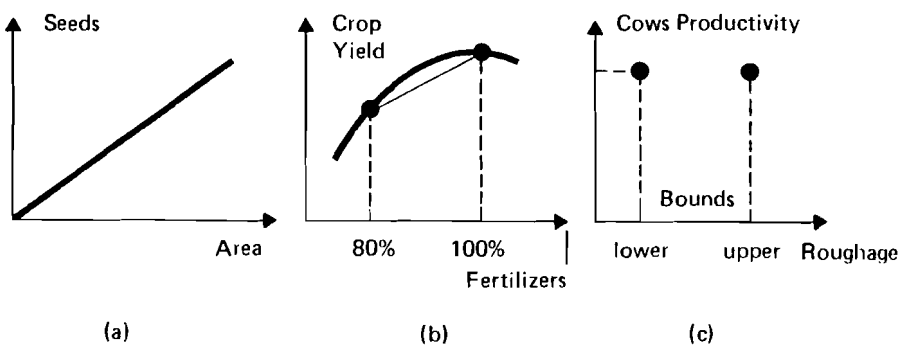

FIGURE 7 Relationships between decision variables.

(c) All costs, prices, and technological coefficients are known; economies of scale are not explicitly included. For example, in a given subregion the cost per hectare of bringing irrigation water to the field does not depend on the number of hectares irrigated. (d) No interest rate or investment is included in SWIM2 because, at present, interest rates are not considered to be the only and most important indicator of the socioeconomic value of investment in Bulgaria. For each piece of equipment purchased or facility developed by means of investment, the fixed cost is included in SWIM2 as an annual cost found from straightline depreciation of the investment over the useful working life of the facility. There are also other assumptions that relate to each of the subsystems described below.

2.3 Description of the Subsystems

2.3.1 INPUT RESOURCES

All input resources are introduced into SWIM2 as rates of use of resources per hectare of land or per animal. These rates may be taken directly from crop and livestock production manuals (e.g., Lidgi *et al.* 1976) and adapted to the region's conditions, or they may involve more sophisticated computations like those for irrigation water in this study.

Land. The main soil type of the region is chernozem (black earth). It is assumed that soil structure and productivity are uniform over the region. SWIM2 allows for different soil types in the three subregions shown in Figure 1b but there were no relevant data available concerning different soil types at the time of modeling. Out of 150,000 ha of arable land about 4,500 ha are reserved for seed production. The seed area is determined internally in the model solution. To allow for better land utilization SWIM2 takes into account the possibility of having maize silage as a second crop (maize silage II) after the midsummer harvest of wheat and barley. The model also computes the amount of irrigated or nonirrigated land planted with orchards and tobacco, as well as the irrigated area of vegetables. The areas of land planted in these three crops are fixed exogenous variables.

SWIM2 computes the cost of developing land for irrigation in two parts, the cost of bringing water to the fields and the cost of the sprinkler application equipment. The cost of all structures and equipment needed to bring water to the fields is expressed as a lumped cost in Lv/ha (1 leva (Lv) ≐ $1 (US)). This cost is 2,850 Lv/ha, 3,170 Lv/ha, and 2,750 Lv/ha in subregions 1, 2, and 3, respectively. These lumped costs are based on detailed engineering designs, using 1-in-4 dry year conditions, for developing more irrigation in these subregions that were already carried out. (A 1-in-4 dry year is one whose rainfall is exceeded on average in 3 years out of 4.) SWIM2 depreciates these costs over 25 years. Although SWIM2 computes the peak water demand rates in the irrigation season needed for engineering design and costing, there is no feedback in the model that changes the development cost per hectare as the peak demand rate changes. The costs of the sprinkler application equipment are described below.

SWIM2 assumes that the natural drainage of the soil in the Silistra region is sufficiently good that problems of waterlogging and soil salinization will not occur as irrigation is developed. In discussions with local officials it was confirmed that such problems have not been observed in irrigation areas.

Water. It was assumed that the Danube River is the only source of irrigation water and because of the rolling hills and potential for erosion, sprinkler irrigation is the only application method considered. The model computes the total amount of irrigation water as well as its distribution among subregions and various crops using 10-day intervals during the irrigation season from May to September. Unit crop demands are calculated by means of a soil moisture balance model.

This model uses the rainfall and evapotranspiration in each 10-day period from March to September as input data. Calculating forward in time, 60-mm irrigation is applied when soil moisture falls more than 60 mm below its capacity. Drainage occurs if excess rainfall fills soil moisture beyond its capacity.

Both normal weather conditions and 1-in-4 dry year conditions are analyzed. Using mean monthly data recorded at Silistra for each of the years 1961–70, normal weather conditions are defined for each month by averaging the 10 years of data. The conditions of 1961 are adopted as representing the 1-in-4 dry year by means of the probability analysis shown in Figure 8. Evapotranspiration

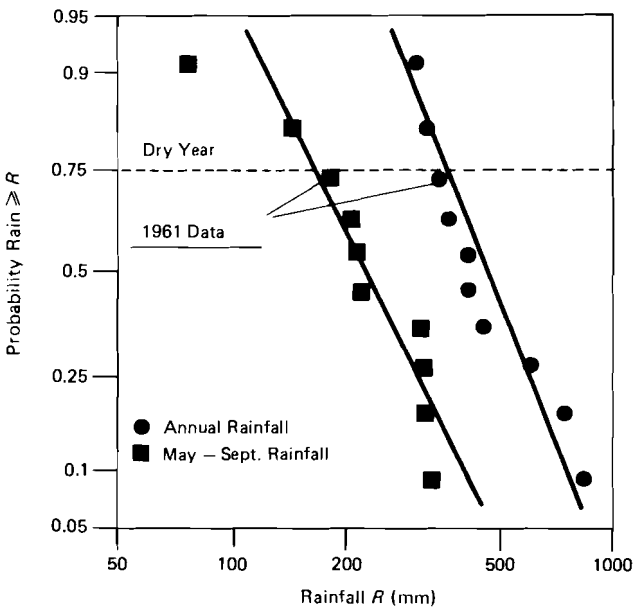

FIGURE 8 Probability analysis of rainfall. Source: Agrocomplect Silistra.

is computed from data on mean monthly temperature, humidity, windspeed, and cloudiness by the Penman method (Doorenbos and Pruitt 1977). An example of the soil moisture balance calculations for maize grain is shown in Figure 9. The procedure is described in detail in Appendix D.

A total water use efficiency of 50 percent is estimated on the basis of conveyance losses (5 percent), application losses (30 percent), and leaching requirements (15 percent). SWIM2 calculates the water use of each crop as the product of its unit crop water demand and the crop area. Then, to get the volume of water withdrawn from the Danube River, SWIM2 sums all crop water uses and divides the total by the efficiency. As in most irrigation systems, the price of irrigation water is subsidized and does not reflect the actual unit cost of supplying water. For this reason, a sensitivity analysis of water price, which is described in the analysis of the results (Section 3), has been performed. SWIM2 also computes livestock drinking water demands as the product of the unit water demand (liters/animal) for each type of animal, and the number of animals. This water is supplied from wells located near the Danube and subsequently transferred to the animal farms. The model does not consider treatment of wastewaters from the livestock feedlots.

Seeds. All seeds required for lucerne, maize, wheat, barley, soybeans, and sunflowers are assumed to be grown within the complex on nonirrigated land. SWIM2 computes the area of land needed for seed growing per hectare of field crop production by dividing the seed-planting rate for each crop by its seed crop yield rate and summing the resulting seed crop areas. The data used for seed-planting rates, seed crop yields, and the cost of seeds are given in Table A.1 in Appendix A.

Fertilizers and chemicals. Three nutrients must be supplied by artificial fertilizers: nitrogen, phosphorus, and potassium. The corresponding fertilizers are ammonium sulfate (34 percent active nitrogen), superphosphate (20 percent active phosphorus), and potassium sulfate (44.5 percent active potassium). The amount of each fertilizer needed per hectare is calculated so as to replace the nutrients removed by crop production with allowance for the natural ability of the soil to absorb or release nutrients. To estimate the effect on crop production of shortages in the supply of fertilizers, SWIM2 has an alternative for each crop that allows an application rate of only 80 percent of the fertilizer needed per hectare, with an associated loss in crop yield. The data on fertilizer application rates for all crops are given in Table A.2 in Appendix A. Their costs are given in Appendix C.

SWIM2 also allows for partial substitution of fertilizers by the nutrients in animal wastes from feedlots. The amount of nutrients in the animal wastes is given in Table A.3 in Appendix A. Although manure is generated throughout the year, the spreading of manure is limited by weather and transportation costs, so SWIM2 assumes that only 50 percent of the nutrients in the manure coming from the feedlots can substitute for the nutrients supplied by artificial fertilizers. As far as pesticides are concerned, there are too many individual chemicals involved to account for each one separately, as is done for fertilizers. Instead, a

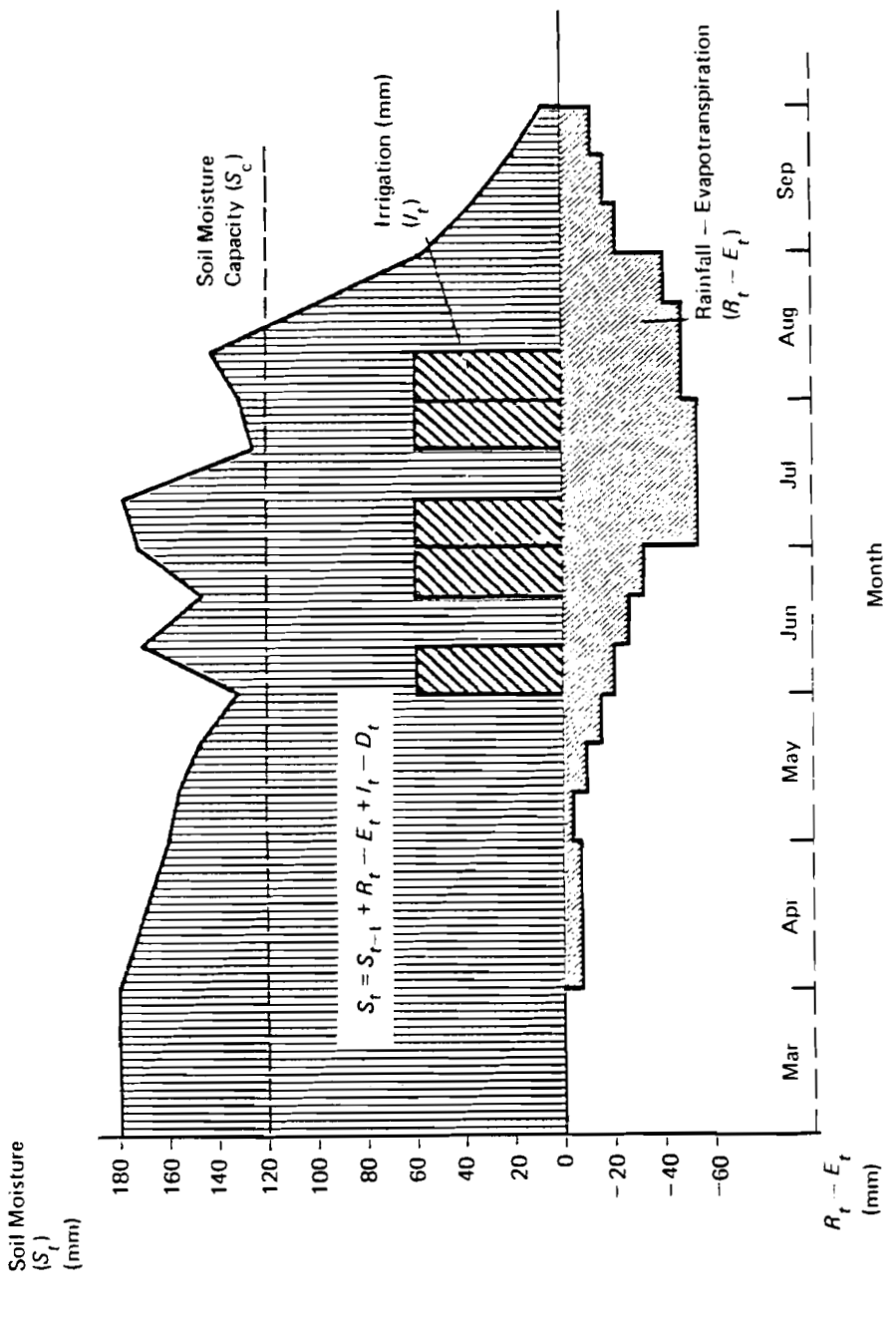

FIGURE 9 Soil moisture balance with irrigation.

lumped cost per hectare is specified for each crop and included as a cost per hectare in the production cost tables in Appendix C.

Labor, machinery, and fuel. These three inputs are interrelated in the sense that labor and fuel depend on the number of machines (the complex is considered to be fully mechanized).

Only one type of sprinkler irrigation system, called "Blue Arrow," is considered by SWIM2. "Blue Arrow" has fixed pipes that are towed from place to place by tractor. Other sprinkler systems, including side-roll and center-pivot systems, were considered when SWIM2 was being formulated, but data on their labor requirements, capital costs, and watering capacities were insufficient at that time to include them in the model as alternatives.

One "Blue Arrow" system consisting of eight lines of pipes can irrigate 10 ha/day. The purchase cost of 48,000 Lv is depreciated over a useful working life of 15 years. The number of "Blue Arrow" systems that are needed is computed by taking into account the area irrigated and the complementary relationships owing to the fact that not all crops are irrigated at the same time. As can be seen in Table A.6 in Appendix A, wheat and barley are irrigated only at the beginning of May when no other crops are irrigated. Hence, they can be irrigated by the equipment used for the other crops, provided that enough equipment is available. The same also applies to sunflowers and maize silage II, because the irrigation schedules of these two crops never coincide.

To determine the number of the other machines, such as tractors, that will be needed in the complex, the critical period in the schedule of field operations must be known when all of the available machines are being used. This schedule is shown in Table A.7 in Appendix A. SWIM2 finds the number of tractors, combine harvesters, and silage choppers in the following way. Assuming that there is some time lost due to bad weather during the critical period and that the working day has 10 hours, we calculated the number of working hours in the critical period. The area per hour that a machine can cover is known; hence, the area that can be covered by one machine during the critical period can be computed, and once the crop areas are fixed as a result of the model, the number of machines may be calculated.

For tractors the critical period is during spring cultivation from 20 March to 20 April; for combine harvesters it is during the wheat/barley harvest from 20 June to 20 July; and for silage choppers it is during the maize silage harvest in July.

The fuel needed by the field machinery is computed on the basis of the fuel used for individual field operations: plowing, cultivation, planting, and harvesting. The data on fuel use rates are presented in Table A.5 in Appendix A. For irrigated crops, the fuel use for harvesting is higher than for nonirrigated crops because of the higher yield.

For all machines and equipment two kinds of annual costs are considered: the fixed costs of depreciated capital investment over the machine life, and the variable costs of operation and maintenance.

The labor needed for field operations is calculated on the basis of the number of hours each machine is in the field with one operator per machine (Table A.4 in Appendix A). The additional labor required for administration and support services is not directly computed but is assigned a cost per hectare of land. Labor costs for irrigation are included in the total cost of irrigation.

Capital investments. SWIM2 accounts explicitly for the capital investments required for development of the complex. There are two types of capital investments distinguished in the model: irrigation capital investments and investments for machinery, feedlots, and perennial crops (orchards). The only cost of capital investments included in SWIM2 is their depreciation over the lifetime of the equipment. The lifetime is taken from the existing standards for Bulgarian conditions. For example, if a piece of equipment costs 10,000 Lv and its lifetime is 10 years, then the depreciated cost of capital is 10,000/10 = 1,000 Lv/yr. This coefficient is assigned as an annual cost in the objective function coefficient of the decision variable for this kind of equipment.

It should be noted that since SWIM2 is a static model of one year's conditions, the model shows the results of investments as if they were instantly in effect. It does not show the economic effect of staged investments over time.

In economic analysis involving the discounting of time streams of benefits and costs, the discount or interest rate employed plays a central role. This interest rate reflects the value of capital investment in alternative uses. Since SWIM2 does not contain discounting over time internally, it is not necessary to include an interest rate in the model. As is demonstrated in the analysis of the results, SWIM2 can be optimized for specified conditions in a sequence of future years linked by forecast growth in the numbers of livestock. In this case discounted time streams of benefits and costs could be obtained from the model's results.

2.3.2 CROP PRODUCTION AND PROCESSING

The key problems in modeling crop production are determining the crop production alternatives and the crop yields. There are nine alternatives introduced in SWIM2 for each crop. The crop may be grown in any of the three subregions using any of the three technologies (no irrigation, irrigation with 80-percent fertilizers, and irrigation with 100-percent fertilizers). The crop production costs for each crop, both irrigated and nonirrigated, are tabulated in Appendix C. The fertilizer use rates shown in these tables are for 100 percent of the requirements. In the model, lucerne is replanted every 3 and orchards every 15 years. Accordingly, the costs associated with their planting have been depreciated in a straight-line fashion over this period.

The crop yields are one of the most sensitive parameters of SWIM2. The relationships between crop yield, weather, fertilizer application, and irrigation are central to any analysis of irrigation. The yields used in SWIM2 under normal

TABLE 1 Crop yields (tons/ha).

	Irrigated		Nonirrigated	
CROP	100% fertilizer	80% fertilizer	Normal weather	Dry weather
Lucerne	11.0	9.5	5.5	5.1
Maize silage	48.0	42.0	28.0	14.0
Maize silage II	22.0	17.0		
Maize grain	9.0	7.5	4.3	2.4
Wheat	4.1	4.0	3.8	2.7
Barley	3.9	3.8	3.5	2.8
Soybeans	2.7	2.4	1.5	1.2
Sunflowers	2.2	2.15	2.0	1.5
Orchards	24.0	22.0	21.0	17.0
Tobacco	2.2	2.1	1.8	1.4
Vegetables	41.3			

NOTE: Maize silage II and vegetables are grown only with irrigation. Vegetables are grown only with 100-percent fertilizers.

weather conditions are based on average yields obtained in the Silistra region (Table 1). Because of lack of data, the yields are assumed to be the same regardless of the subregion in which the crops have been planted. However, the structure of SWIM2 permits the introduction of different yields in the subregions if this is justified.

At present, some crops are not grown with irrigation in the region. For these crops the increase in yield due to irrigation can only be based on experience gained in other regions with similar conditions. The decrease in yield in response to drought as well as the yield change in response to fertilizer application must be similarly estimated. In general, wheat, barley, and lucerne are more drought-resistant than the other crops because they are in the ground over the winter and the moisture absorbed by the soil during that time is not lost through cultivation in the spring. Maize is much affected by drought because it has a large amount of vegetative growth and small roots. The yield of irrigated crops during drought is assumed not to change because the loss in rainfall is made up by irrigation water.

Crop rotation to keep the natural productivity of the soil is explicitly introduced in SWIM2. Since SWIM2 is a static (1-year) model, the crop rotation is taken into account by constraining the ratio between the areas of field crops (lucerne, wheat, and barley) and interrow-cultivated crops (maize, soybeans, and sunflowers). This ratio can vary between 0.95 and 1.3.

The crops harvested from the field can be processed into a number of outputs (see Figure 5). Since the requirements for feeding livestock are expressed in terms of processed outputs, SWIM2 has some processing activities included in it.

Lucerne is grown for fodder, which can be green forage, hay, haylage, or silage. Silage can also be produced from maize. If maize is grown for grain, it is assumed that the stalks are harvested to be used as roughage. The processing of wheat includes milling for flour, in which case 78 percent of the grain becomes flour and 14 percent becomes wheat bran, which is fed to livestock. Maize and barley must be milled before being fed to animals but there are no significant weight losses in this process. Both wheat and barley straw are also harvested and processed for roughage. Soybeans and sunflowers are crushed and the oil is extracted, leaving a residual meal for livestock which amounts to 75 percent by weight of the soybean grain and 71 percent of the sunflower seeds. All the grain crops are assumed to undergo drying before being further processed or used. No cannery processing is assumed for fruits and vegetables. Drying is the only processing activity for tobacco considered in SWIM2.

2.3.3 USE OF CROP PRODUCTS

Crop products can be exported, set aside as reserves for the region, fed to livestock in the region, or used by the Silistra population. All estimates of product benefits used in SWIM2 are based on internal Bulgarian prices taken from Lidgi *et al.* (1976).

In the model, the requirements of the population for cooking oil and fruits are fixed. Vegetables are grown only for internal consumption in the region and their total production is constrained by the area planted.

The simplest way to account for the impact of dry weather on crop production is to build up reserves that can partially make up for crops lost because of bad weather. Reserves of grain crops only are considered. SWIM2 is based on normal weather conditions, but it also accounts for the additional amount of grain needed for feeding livestock if the year turns out to be a dry one. If a certain crop is grown without irrigation, the difference between the yield obtained in a normal year and that obtained in a dry year (shown in Table 1) is multiplied by the crop area to give the potential amount of the crop that goes to reserves. This potential amount is further multiplied by a coefficient, which takes into account that not every year in a given sequence is dry, to give the actual amount of reserves set aside. The reserves are assigned a benefit equivalent to the cost of purchasing an equivalent amount of grain from outside the region.

Since the agroindustrial complex is supposed to be a self-contained crop–livestock enterprise, the export of crops is limited only to fruits and tobacco. All excess feedstuff production is assumed to support the increase in the number of animals that provide the main export goods. The market for livestock production is assumed to be perfectly elastic. Imports of crop production are not allowed in SWIM2 (they were allowed in SWIM1).

The ultimate goal of the complex is to export livestock products from the region. Four types of animals are assumed to be raised in the complex: cows

with associated calves and heifers, sheep, pigs (breeding sows and pigs raised for slaughter), and hens. For ease in the subsequent analysis of diets, "structural" animals have been defined on the basis of the population structure of each type of animal.

1 structural cow	=	1 cow + 0.41 calves + 0.23 heifers
1 structural pig	=	1 fattening pig + 0.06 sow + 0.02 boar
1 structural sheep	=	0.5 milk ewe + 0.5 meat and wool ewe
1 structural hen	=	1 hen

The animals are in feedlots so their diets are controlled. These diets are made up of five feedstuffs: concentrated forage from grains, green forage freshly cut from the fields, silage, hay, and roughage from the harvest residuals of grain crops. Each animal must receive certain minimum amounts of energy and protein in a balanced diet of the five feedstuffs. To do this the weights of feedstuffs are converted into their energy equivalent in feed units, where one feed unit is the energy contained in 1 kg of oats. SWIM2 ensures that each animal receives a certain number of feed units and also keeps the number of feed units supplied by each of the feedstuffs within a specified range to maintain a balanced diet. Tables B.1 to B.3 in Appendix B contain the details. To maintain adequate levels of protein in the diets, SWIM2 does not permit the weight of high-protein feeds (soybeans and sunflowers) to be less than one-fourth of the weight of low-protein feeds (maize grain, wheat, and barley).

Animal products are calculated on an annual basis taking into account the population structure of each animal. In certain cases where improvements in productivity beyond 1975 levels can be expected as the complex develops, perspective productivities achievable by 1985 are used. One structural cow is assumed to produce annually 0.6 calves for slaughter at 6 months and 4,000 liters of milk and to have a milking life of 5 years. Pigs are raised to 120 kg live weight yielding a 75-kg slaughtered carcass. Sheep are milked for 180 days to produce 135 liters of milk, from which 13.5 kg of cheese are made. Hens lay 200 eggs over a 10-month laying season. The market prices for these products are taken from Lidgi *et al.* (1976).

2.4 General Mathematical Representation

The description that follows formalizes the relationships among the various subsystems in the complex into an aggregated linear programming format. Appendix E contains a complete mathematical description of the model and should be referred to if details are desired.

For ease in the explanation, all decision variables and constraints in the model are aggregated into 15 decision vectors and 18 sets of constraints, as shown in Table 2. The objective function *OB*, which has been adopted for the agricultural production in the region, maximizes the annual net benefits, i.e., the

TABLE 2 General structure of SWIM2, including decision vectors y, w^i, v^i, q^i, *and* x^i.

CONSTRAINTS	Crop production alternatives (y)	Fodder products (w^1)	Grain products (w^2)	Population crop products: Grain (v^1)	Population crop products: Other (v^2)	Grain reserves (v^3)	Export of other crop products (v^4)	Grain products for livestock (v^5)	Livestock: Numbers (q^1)	Livestock: Products (q^2)	Irrigation & drinking water demands (x^1)	Irrigation equipment (x^2)	Fertilizers (x^3)	Machinery (x^4)	Capital investments (x^5)	Right-hand side
Objective function	c^1	c^2	c^3	b^1	b^2	b^3	b^4		c^4	b^5	p^1	p^2	p^3	p^4	p^5	
Land balance	$A_{1,1}$															$\leqslant$ l
Irrigation & livestock drinking water	$A_{1,2}$								$A_{9,2}$		$-I$					$= 0$
Irrigation equipment	$A_{1,3}$											$-I$				$= 0$
Fodder production	$A_{1,4}$	$-I$														$= 0$
Grain production	$A_{1,5}$		$-I$													$= 0$
Grain production balance			$A_{3,6}$	$-A_{4,6}$		$-A_{6,6}$		$-A_{8,6}$								$= 0$
Other crop production balance	$A_{1,7}$				$-A_{5,7}$		$-A_{7,7}$									$= 0$
Livestock feedstuff requirements		$A_{2,8}$						$A_{8,8}$	$-A_{9,8}$							$\geqslant 0$
Livestock products									$A_{9,9}$	$-I$						$= 0$
Fertilizers	$A_{1,10}$								$-A_{9,10}$				$-I$			$= 0$
Machinery	$A_{1,11}$													$-I$		$= 0$
Capital investments	$A_{1,12}$								$A_{9,12}$			$A_{12,14}$		$A_{14,12}$	$-I$	$= 0$
Constrained irrigation water											I					$\leqslant$ w
Constrained fertilizers													I			$\leqslant$ f
Constrained capital investments															I	$\leqslant$ k
Grain products for population				I												$\geqslant$ g
Other products for population					I											$\geqslant$ r
Livestock numbers									I							$\geqslant$ n

difference between the value of marketed livestock and crop products, and their production cost. Vectors are in boldface.

$$OB = \max\Big[\mathbf{b}^1\mathbf{v}^1 + \mathbf{b}^2\mathbf{v}^2 + \mathbf{b}^3\mathbf{v}^3 + \mathbf{b}^4\mathbf{v}^4 + \mathbf{b}^5\mathbf{q}^2$$

crop and livestock production benefits

$$-\mathbf{c}^1\mathbf{y} \quad - \quad \mathbf{c}^2\mathbf{w}^1 - \mathbf{c}^3\mathbf{w}^2 \quad - \quad \mathbf{c}^4\mathbf{q}^1$$

crop production cost | crop processing cost | livestock production cost

$$-\mathbf{p}^1\mathbf{x}^1 - \mathbf{p}^2\mathbf{x}^2 - \mathbf{p}^3\mathbf{x}^3 - \mathbf{p}^4\mathbf{x}^4 - \mathbf{p}^5\mathbf{x}^5\Big]$$

input resources cost

where

$\mathbf{b}^1$ and $\mathbf{b}^2$ are the benefits form crop products sold to meet the requirements of the population in Silistra

$\mathbf{v}^1$ and $\mathbf{v}^2$ are the amounts of these crop products

$\mathbf{b}^3$ and $\mathbf{v}^3$ are the benefits per unit of grain reserves and the quantities of grain reserves, respectively

$\mathbf{b}^4$ and $\mathbf{v}^4$ are the benefits per unit of crop products exported and the quantities of crop products exported, respectively

$\mathbf{b}^5$ and $\mathbf{q}^2$ are the benefits per unit of livestock products and the quantities of livestock products, respectively

$\mathbf{c}^1$ and $\mathbf{y}$ are the crop production costs per hectare and the areas of crop alternatives, respectively

$\mathbf{c}^2$ and $\mathbf{w}^1$ are the unit costs of processing fodder products and the amounts of these products, respectively

$\mathbf{c}^3$ and $\mathbf{w}^2$ are the unit costs of processing grain products and the amounts of these products, respectively

$\mathbf{c}^4$ and $\mathbf{q}^1$ are the production costs per animal and the number of animals, respectively

$\mathbf{p}^1, \mathbf{p}^2, \ldots, \mathbf{p}^5$ are the prices of input resources

$\mathbf{x}^1, \mathbf{x}^2, \ldots, \mathbf{x}^5$ are the quantities of input resources

It may be noted that grain products for livestock $\mathbf{v}^5$ do not have a coefficient in the objective function because they are an intermediate product transferred straight into feeding livestock.

The objective function is maximized subject to the following set of constraints. Matrices denoted by $A_{i,j}$ are located in column i and row j of the linear programming tableau, Table 2.

2.4.1 LAND BALANCE

The area planted cannot exceed the available land area, both irrigated and non-irrigated:

$$A_{1,1}\mathbf{y} \leqslant \mathbf{l}$$

where

$A_{1,1}$ is a matrix that sums up the land used in each subregion
$\mathbf{l}$ comprises the areas of available land in the three subregions and the available irrigated land

2.4.2 DEMANDS FOR IRRIGATION WATER AND LIVESTOCK DRINKING WATER

$$A_{1,2}\mathbf{y} + A_{9,2}\mathbf{q}^1 - I\mathbf{x}^1 = 0$$

where

$A_{1,2}$ are the coefficients for irrigation crop water use per hectare
$A_{9,2}$ are the coefficients for livestock drinking water use per animal
I is the identity matrix that is introduced because the linear programming format does not allow variables on the right side of the constraint equations
$\mathbf{x}^1$ are the volumes of irrigation and livestock water demands

2.4.3 IRRIGATION EQUIPMENT

$$A_{1,3}\mathbf{y} - I\mathbf{x}^2 = 0$$

where

$A_{1,3}$ are the irrigation equipment requirements per hectare
$\mathbf{x}^2$ is the number of sets of irrigation equipment required

2.4.4 FODDER AND GRAIN PRODUCTION

$$A_{1,4}\mathbf{y} - I\mathbf{w}^1 = 0$$

$$A_{1,5}\mathbf{y} - I\mathbf{w}^2 = 0$$

where

$A_{1,4}$ and $A_{1,5}$ are the yields of fodder and grain crops, respectively
$\mathbf{w}^1$ and $\mathbf{w}^2$ are the quantities of fodder and grain products, respectively

2.4.5 GRAIN PRODUCTION BALANCE

The grain produced must equal the grain used.

$$A_{3,6}\mathbf{w}^2 - A_{4,6}\mathbf{v}^1 - A_{6,6}\mathbf{v}^3 - A_{8,6}\mathbf{v}^5 = 0$$

where

$A_{3,6}$, $A_{4,6}$, $A_{6,6}$, and $A_{8,6}$ are matrices that sum up, respectively, total grain production, population requirements of grains, reserves, and grain products for livestock

$\mathbf{v}^1$ are the quantities of population crop products

$\mathbf{v}^3$ are the amounts of grain reserves

$\mathbf{v}^5$ are the amounts of grain products for livestock

2.4.6 PRODUCTION BALANCE OF OTHER CROPS

$$A_{1,7}\mathbf{y} - A_{5,7}\mathbf{v}^2 - A_{7,7}\mathbf{v}^4 = 0$$

where

$A_{1,7}$, $A_{5,7}$, and $A_{7,7}$ are matrices that sum up the production of other crop (vegetables, tobacco, and orchards), their population requirements, and their exports, respectively

$\mathbf{v}^2$ are the amounts of other crops that go to the Silistra population

$\mathbf{v}^4$ are the amounts of exports of these other crops

2.4.7 LIVESTOCK FEEDSTUFF REQUIREMENTS

Livestock feed must at least meet minimum requirements.

$$A_{2,8}\mathbf{w}^1 + A_{8,8}\mathbf{v}^5 - A_{9,8}\mathbf{q}^1 \geqslant 0$$

where

$A_{2,8}$, $A_{8,8}$, and $A_{9,8}$ are matrices that sum up fodder products, grain livestock products, and animal diet requirements for these products, respectively

2.4.8 LIVESTOCK PRODUCTS

$$A_{9,9}\mathbf{q}^1 - I\mathbf{q}^2 = 0$$

where

$A_{9,9}$ are the amounts of livestock products generated per animal

2.4.9 FERTILIZERS, MACHINERY, AND CAPITAL INVESTMENTS

The nutrients that are needed must be supplied by fertilizer or manure.

$$A_{1,10}\mathbf{y} - A_{9,10}\mathbf{q}^1 - I\mathbf{x}^3 = 0$$

where

$A_{1,10}$ and $A_{9,10}$ are matrices of crop fertilizer requirements and manure generation, respectively

$\mathbf{x}^3$ are total requirements for each fertilizer

The machines that are needed must be available.

$$A_{1,11}\mathbf{y} - I\mathbf{x}^4 = 0$$

where

$A_{1,11}$ are the numbers of each type of machine needed per hectare of crop production

$\mathbf{x}^4$ are the total numbers of each type of machine needed in the complex

The capital investment used is summed up.

$$A_{1,12}\mathbf{y} + A_{9,12}\mathbf{q}^1 + A_{12,12}\mathbf{x}^2 + A_{14,12}\mathbf{x}^4 - I\mathbf{x}^5 = 0$$

where

$A_{1,12}$, $A_{9,12}$, $A_{12,12}$, and $A_{14,12}$ are matrices of capital investments for developing irrigated land, livestock farming houses, irrigation equipment, and machinery, respectively

$\mathbf{x}^5$ are amounts of capital investments for different purposes

It should be noted that the cost of capital $\mathbf{p}^5$ is actually zero in SWIM2 because no interest rate is used. The depreciated cost of capital is contained in the costs of the decision vectors requiring capital investment.

The last six constraints reflect direct limits on decision vectors and have been isolated to facilitate variations in these limits.

2.4.10 CONSTRAINED INPUT RESOURCES

The input resources used cannot exceed those available.

$$\mathbf{x}^1 \leqslant \mathbf{w} \qquad \mathbf{x}^3 \leqslant \mathbf{f} \qquad \mathbf{x}^5 \leqslant \mathbf{k}$$

where

w, **f**, and **k** are the amounts of available water, fertilizers, and capital investments, respectively

2.4.11 CONSTRAINED OUTPUTS

Some production outputs must meet target levels.

$$\mathbf{v}^1 \geqslant \mathbf{g} \qquad \mathbf{v}^2 \geqslant \mathbf{r} \qquad \mathbf{q}^1 \geqslant \mathbf{n}$$

where

g, **r**, and **n** are target levels of grain products for the Silistra population (flour and cooking oil), other products for the Silistra population (vegetables, peaches and tobacco), and numbers of livestock (cows, sheep, pigs, and hens).

The total dimension of the decision vectors $\mathbf{y}$, $\mathbf{w}^i$, $\mathbf{v}^i$, $\mathbf{q}^i$, and $\mathbf{x}^i$ is 218 decision variables interrelated by 152 constraints. The linear program for SWIM2 contains 2,050 data, which is about 6 percent data density in the tableau.

3 ANALYSIS OF THE RESULTS

To obtain the results of SWIM2, the IBM 370/168 computer at the CNUCE Institute of the National Research Council in Pisa, Italy, was used through the IIASA computer network. The linear programming package there is contained in the SESAME mathematical programming system (National Bureau of Economic Research 1972). An optimal solution is obtained in about 280 iterations.

About 70 solutions of SWIM2 were obtained. Each of the questions addressed has associated with it a few key variables in the model. To formulate a set of computer runs these variables are assumed to take a number of values within a certain range and the model is optimized for each of these values to obtain the required results.

First, the validity of the model's representation of the conditions in the Silistra region is examined by comparing its outputs with production statistics recorded in the region in 1975. Next, the consequences of investing capital in irrigation development are analyzed and the impact of restricting the input resources is investigated. Finally, various scenarios of future growth in water demands are determined on the basis of forecasts of the numbers of livestock in the region.

3.1 Validation of the Model

In general, validation is the process of ascertaining the agreement between the model's behavior and points of interest in a real situation (Thesen 1974). The goal of validation in the case of SWIM2 is to ensure that the model adequately reflects the overall realities of the Silistra agricultural production system. This would mean, for example, that its crop yields and animal diets are reasonably correct. The model can then be used with confidence to suggest policies for situations different from those currently practiced.

It should be noted that SWIM2 is an optimization and not a simulation model. As such, SWIM2 possesses internal decision-making capability to maximize net benefits subject to the set of constraints. A simulation model, by contrast, usually possesses no internal decision-making capability; it is intended only to mirror the actual conditions so that the effects of externally specified decisions can be evaluated.

Data on actual production outputs (e.g., tons of wheat and numbers of animals) from the Silistra region in 1975 are available in the *Bulgarian Statistical Yearbook* (Ministry of Information and Communications 1976). Unfortunately, these data do not include water withdrawals from the Danube River so it was not possible to check the model's computation of water withdrawals. For the validation, SWIM2 was run with an irrigated area of 11,400 ha, the amount of irrigated land in the region in 1975.

Aggregated production outputs recorded in the region are compared with the model's results in Figure 10. The model result shown is the sum of the optimized values of all relevant decision variables; for example, each crop has nine decision variables so the total grain production shown for five crops is the sum of 45 values. In order to avoid drawing a pair of bars for each of the animals, they have all been lumped together by defining a composite livestock unit based on the ratios of the numbers of pigs, sheep, and hens, to the number of cows in the region in 1975. These ratios are for pigs 8.4:1; for sheep 9.7:1; and for hens 27.8:1. One livestock unit = 1 cow + 8.4 pigs + 9.7 sheep + 27.8 hens. The ratios are preserved in this solution of SWIM2.

Compared with the 1975 data, SWIM2 gives 0.6 percent less grain, 24 percent less green fodder, and 20 percent more livestock. This is a fairly good agreement, because some of the 1975 production may have been exported from the region and not fed to animals, as SWIM2 assumes. It may be concluded that the model is reasonably valid at this level of aggregated production quantities.

The comparison begins to diverge, however, when details are considered. For example, Figure 11 compares the proportion of total grain production contributed by each crop. The model-optimal solution indicates that 13.1 percent of the grains should be soybeans, but soybeans were only 0.9 percent of production in 1975. Decision makers for Silistra have recognized the value of soybeans and progressively larger areas of it are being grown; however, no production of soybeans was recorded for 1974 (Ministry of Information and Communications

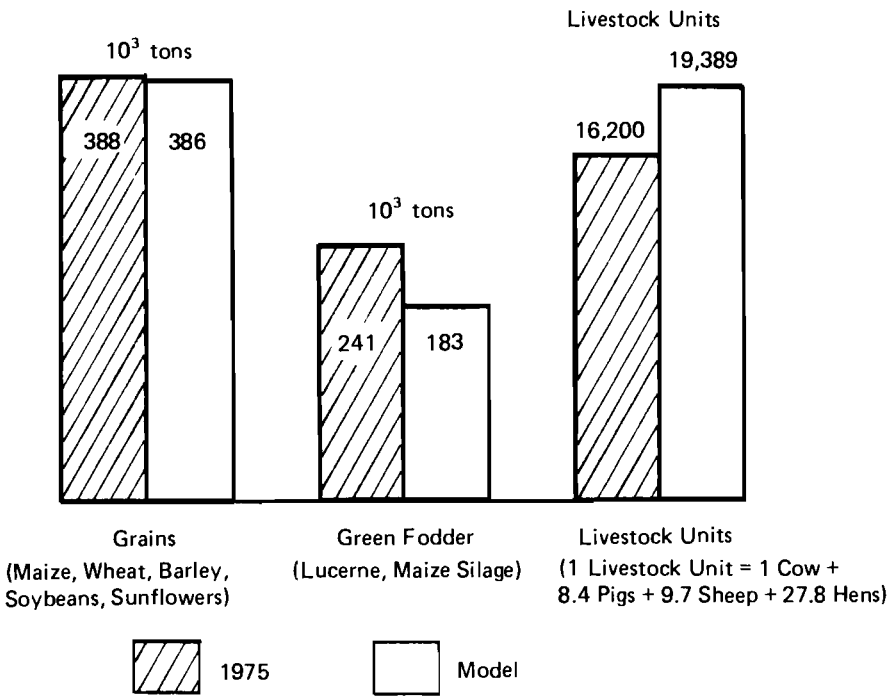

FIGURE 10 Comparison of aggregated production quantities.

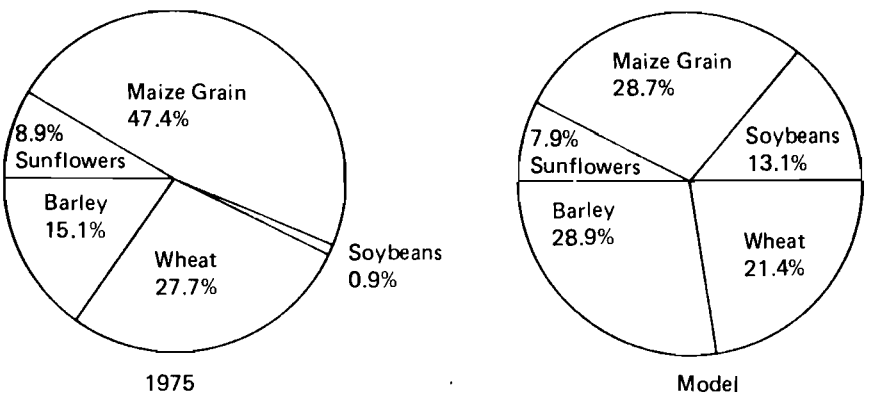

FIGURE 11 Distribution of grain production. SOURCE for 1975 statistics: Ministry of Information and Communications 1976.

1975). Therefore, this discrepancy between the model and the actual conditions may be attributed to the time required to introduce a new crop on a wide scale.

The model calls for more barley and less wheat than were grown in 1975. This may be due to the similar production technologies and costs of these two crops, which make it difficult for the model to choose between them. Small changes in the data can produce dramatic shifts in the balance between SWIM2's optimal areas of wheat and barley.

The results obtained from the validation run showed that the model is relatively realistic at an aggregated level. Individual crop areas, however, should not be taken too literally – other considerations, such as habit and methods of crop rotation, probably affect production in ways not included in the model.

3.2 Development of Irrigated Land

The most important factor in determining agricultural water demands is the area of land that is developed for irrigation. This development requires extensive capital investment to provide supply facilities at the water source, canals or pipes to bring the water to the field, and equipment to apply the water to the crops. Economic evaluation of this investment plays a central role in determining the area that will be developed.

3.2.1 INVESTMENT PLANNING

Developing irrigation increases both the benefits and the costs of an agricultural enterprise because production is intensified. The net benefits (benefits minus costs) of irrigation development are usually positive, but normally, as additional increments of land in a region are converted from dry land to irrigation, each additional increment in the irrigated area generates a smaller increase in the net benefits over the whole region, i.e., there are diminishing marginal returns on the investment. Before all the arable land is irrigated, a point can be reached at which the marginal cost of additional irrigation equals its marginal benefit. This point can be considered as the ultimate economical level of irrigation development.

In SWIM2, net benefits are found by subtracting from the benefits obtained by selling crop and livestock products the annual costs of production and depreciated capital investments. In the investment analyses the ratios between the numbers of animals were kept fixed at their 1975 values (1 cow: 8.4 pigs: 9.7 sheep: 27.8 hens) so that one type of livestock does not dominate the others in the complex.

In 1975, 11,400 ha of land were developed for irrigation in the Silistra region. Of the 150,000 ha of arable land included in SWIM2, only 139,700 ha are considered to be potentially irrigable for physical reasons, i.e., limitations of topography, slope, and soil type. With 11,400 ha irrigated, SWIM2 estimates the average annual net benefits as 105.6 million Lv/yr. The additional net benefits generated by investment to develop more irrigated area are shown in Figure 12.

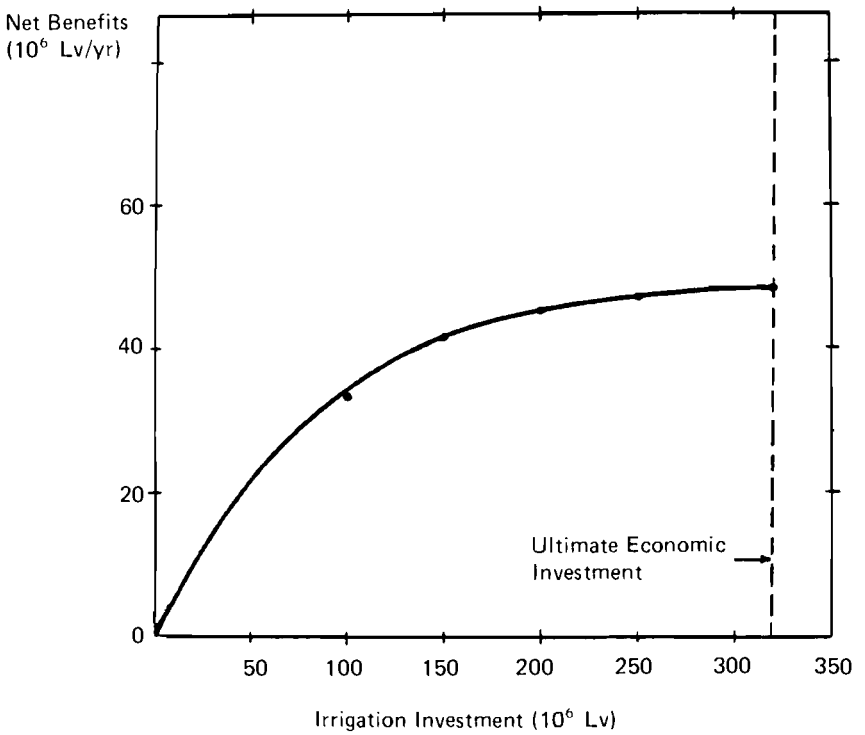

FIGURE 12 Net benefits of irrigation investment in the Silistra region.

This figure illustrates the principle of diminishing marginal returns on investment and identifies the ultimate economical investment as approximately 320 million Lv. This is the point of maximum additional net benefits and SWIM2 does not utilize any further investment funds made available. It should be noted that the investment shown in Figure 12 is just a total; it has no time dimension and could actually be provided in increments over many years. The additional net benefits shown in the figure are those that would occur on average each year after such an investment program had been completed.

The spatial distribution of future water demands depends on which subregion is chosen first for the development in irrigation. The investment to bring water to the field, expressed in Lv per hectare irrigated, is different for each of the three subregions. It is to be expected that as more investment funds are provided the subregions in which irrigation is relatively cheap will be developed first. This is demonstrated in Figure 13. Subregion 3 (2,750 Lv/ha) is developed first to the limit of its potentially irrigable area, followed by subregions 1 (2,850 Lv/ha) and 2 (3,170 Lv/ha). The ultimate economical investment is reached before subregion 2 is developed to its limit. The corresponding ultimate economical irrigation area is 105,500 ha, which is 70 percent of the arable land or 75 percent of the land considered to be potentially irrigable.

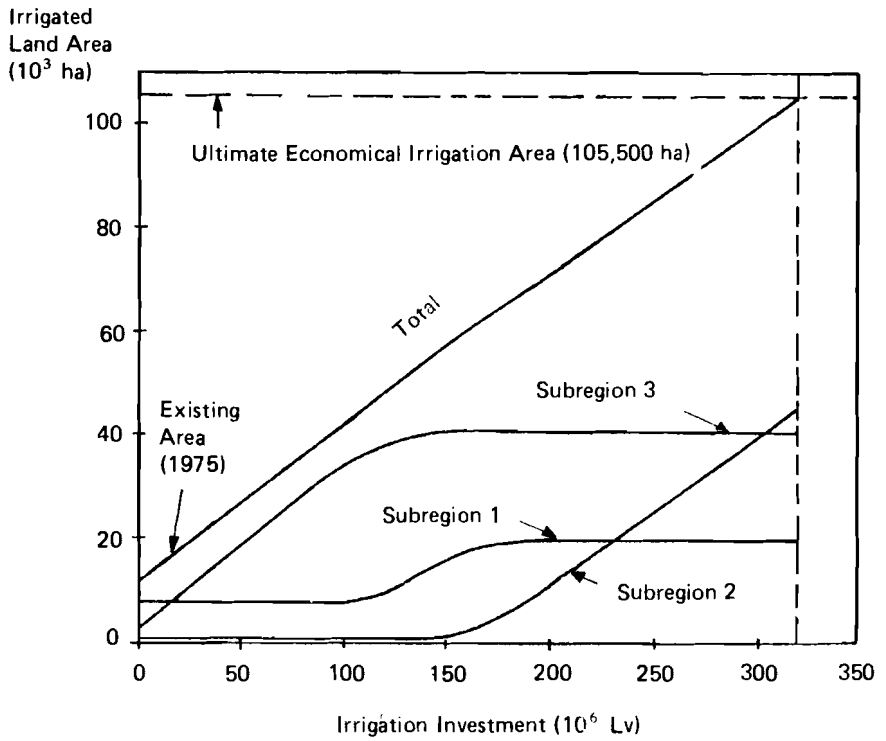

FIGURE 13 Irrigated area and investment.

The demands for Danube River water that result from developing the irrigated area are shown in Figure 14 for average weather and dry weather. (The dry weather condition is representative of a 1-in-4 year, as explained previously.) The extra water demanded during dry weather is that needed for a fixed irrigation area, i.e., SWIM2 assumes that in dry weather extra water is applied by longer sprinkling times to the area that would normally be irrigated under average weather conditions.

Under these assumptions, water demands for the 11,400-ha irrigated area are 78 X 10^6 m^3/yr and 103 X 10^6 m^3/yr for normal weather and dry weather. These demands increase approximately linearly with increasing irrigated area to ultimate economical levels of 585 X 10^6 m^3/yr (normal) and 820 X 10^6 m^3/yr (dry). The corresponding water withdrawal coefficients are 5,500 m^3/ha (550 mm) for normal weather and 7,750 m^3/ha (775 mm) for dry weather. Since an irrigation efficiency of 50 percent is assumed, these coefficients correspond respectively to 275 mm and 387 mm of consumptive use of irrigation water by the crops over the irrigation season.

If the results obtained from SWIM2 are extrapolated linearly to estimate water demands for the potentially irrigable area (139,700 ha), total withdrawals of 770 X 10^6 m^3/yr and 1,080 m^3/yr are found. These demands are 32 percent higher than those for the ultimate economical area. From this it may be con-

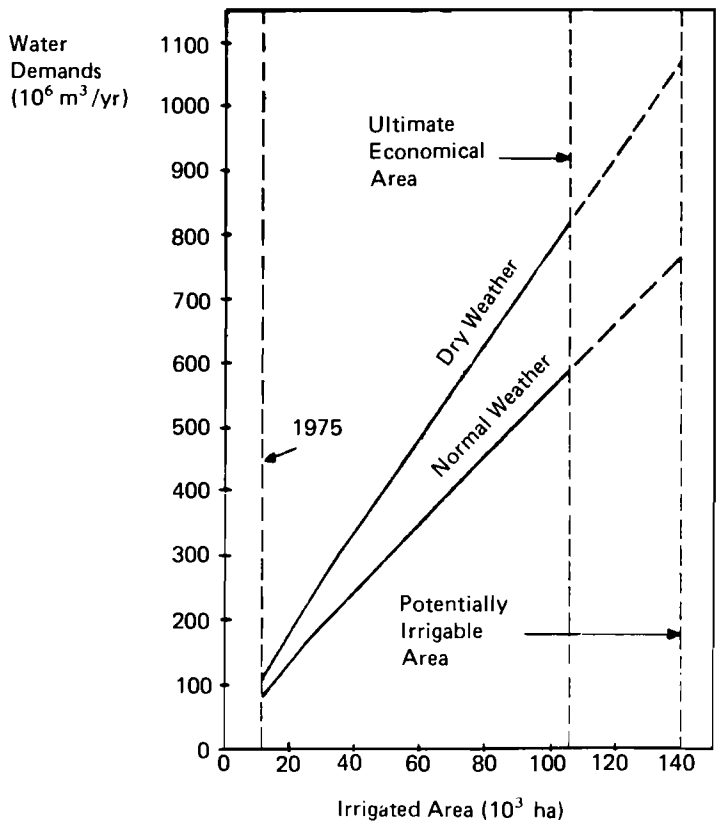

FIGURE 14 Water demands and irrigated area.

cluded that irrigation water demands in the Silistra region could be significantly overestimated if they are calculated from the potentially irrigable area.

3.2.2 DEMAND FUNCTION

The ultimate economical level of irrigation development identified previously is actually the point where the unit cost, or price, of water is equal to its marginal benefit. This is the point where the water resource system is in equilibrium. The sensitivity of this equilibrium point is an important criterion in determining how much investment should be made in irrigation. The variation in the amount of water demanded with its unit cost is expressed in the demand function shown in Figure 15.

The demand function for water in Figure 15 can be derived by differentiating net benefits from Figure 12 with respect to water demands, Figure 14. Using SWIM2, the demand function is obtained as the dual value (or shadow price) of the constraint on water when all other input resources, except land, are

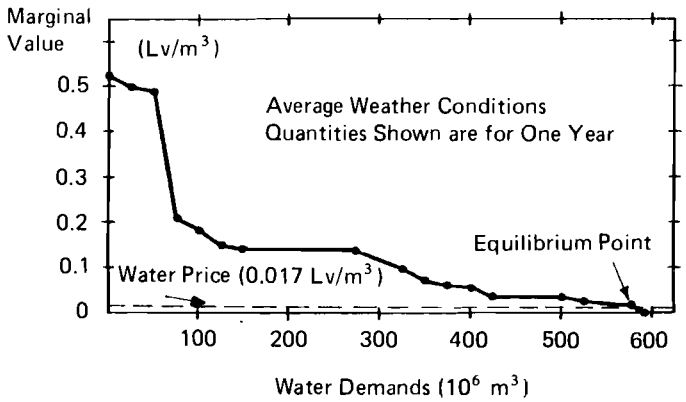

FIGURE 15 Demand function for irrigation water in Silistra region.

unconstrained. For a given level of demand the marginal value shown in this figure is the increase in average annual net benefits in the complex if one more cubic meter of water is supplied. This value is what the complex could afford to pay for that one extra cubic meter; hence, conceptually, the demand function is the locus of the points of equilibrium of the water system as the unit cost of water is raised.

As the limit on available water in SWIM2 is progressively decreased, a chain of impacts passes through the crop and livestock production systems. Reducing available water means that less area can be irrigated. Although the desirability of having production alternatives for reducing the amount of water per hectare was recognized, data on the consequent losses in crop yields were not available; hence SWIM2 does not allow for reducing the number of times a crop is irrigated or the amount of water applied in an irrigation. Reducing irrigated areas means that crop production falls; less crop products are then available for feeding livestock so the number of livestock that the complex can support is reduced. However, this does not mean that livestock will be slaughtered since the model is being used to look to the future to try to determine what the proper level of development of the complex should be.

The water price charged in the Silistra region (0.017 Lv/m^3) is small compared with its marginal value. The actual unit cost of water, based on the costs of the supply facilities, is estimated to be approximately 0.13 Lv/m^3 in the Silistra region. If this were charged as the water price, the demands at SWIM2's equilibrium point would fall to 275×10^6 m^3, which corresponds to 51,000 ha of irrigated land. The water demands of the 11,400 ha irrigated in 1975 lie in the range of very high marginal values, however, and would be unaffected even if such a price were charged.

There are 17 data points shown on the demand function. At each point something changes in the SWIM2 solution; for example, a different crop is irrigated or the livestock diets are changed. The relatively smooth nature of the demand function and the large number of solution changes on it reflect the

considerable ability of SWIM2 to substitute one input for another or one production process for another as external circumstances change.

The demand function shown in Figure 15 is for normal weather conditions. It could be expected that in dry weather conditions the demand for water would be larger and the price would be higher. Thus, the derived demand function for water in agriculture must be associated with a specific set of weather conditions. This is demonstrated for the Silistra region by Gouevsky and Maidment (1977).

It may be noted that most of the results presented from SWIM2 are based on maximizing net benefits from a fixed area of land, i.e., land is considered as the constraining resource rather than water. This is realistic since the Danube provides an abundant water supply. However, the demand function provides a mechanism by which the effect of water as the constraining resource can be explored, and this could be very useful in regions where the available water resources are limits to development.

3.2.3 RISK ANALYSIS

The risks in an agricultural enterprise are associated with fluctuating market prices, animal or crop diseases, and adverse weather conditions. A number of features of SWIM2 are designed to minimize those risks.

For products sold within Bulgaria there are few difficulties with fluctuating markets since internal prices and product flows are centrally planned. However, for products sold on international markets, less control is possible. Future international prices are uncertain. This is one of the reasons why the proportions of animals in the livestock population are kept fixed in the economic analyses made using SWIM2. With set international prices it would be possible to compute proportions that would maximize foreign exchange earnings; these new proportions could then be substituted for the old ones for the purpose of economic analysis. There was insufficient time during the study to pursue this point further.

Another reason for maintaining fixed proportions of the different types of livestock is to minimize the risk of animal disease. If one animal is allowed to dominate all others in the complex, the spread of a contagious disease could cripple livestock production. Likewise for crop production; SWIM2 follows certain crop rotations that prevent solutions in which one crop, such as maize, is grown everywhere in the region.

To allow for adverse weather conditions, SWIM2 sets aside reserves of each grain crop in proportion to the crop area and yield loss expected in dry weather. Developing irrigation also insures against production losses due to dry weather. Intuitively it seems clear that as a greater proportion of grain crops are irrigated there is less need to store reserves of them. This is demonstrated in Figure 16, which shows that about 12 percent of grain production is stored as reserves when a tenth of the grain crop area is irrigated, but only 5 percent goes to reserves when half the grain crop area is irrigated.

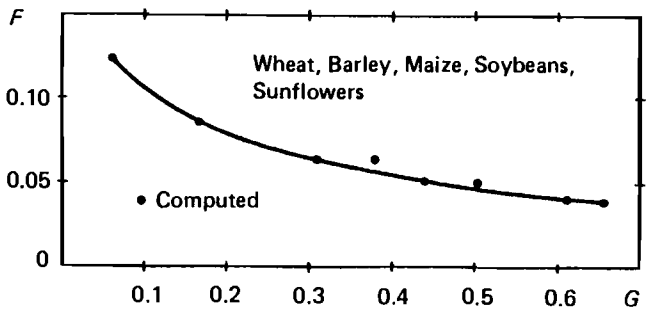

F = Proportion of Total Grain Products Going to Reserves
G = Irrigated Fraction of Total Grain Crop Area

FIGURE 16 Grain reserves and irrigation.

3.2.4 FERTILIZER RESTRICTIONS

As can be seen from the cost tables in Appendix C, fertilizers are one of the most expensive inputs in crop production. In addition, fertilizers contained in agricultural drainage can promote eutrophication in the receiving waters, although this is unlikely in the Silistra region since the Danube has such a large flow rate. Fertilizer applications may be restricted for either of these reasons. Highly productive crops usually require large amounts of fertilizers; SWIM2 has alternatives where crops can be grown with only 80 percent of their optimal requirements for fertilizers, with a consequential drop in crop yields.

Other methods that the complex can employ in adjusting to fertilizer restrictions are to switch to less productive crops, which will mean that crop and livestock production are reduced, or to attempt to maintain crop production by developing more irrigation, i.e., by substituting water for fertilizers.

The amount of irrigation water used, as ammonium sulfate fertilizer is restricted, is shown in Figure 17. From the model results it can be seen that less productive crops are used on the right portion of the figure until the number of livestock supported is reduced to 1975 levels. At this minimum point on the curve SWIM2 substitutes water for fertilizers. The substitution possibilities are limited, however, and the solution rapidly becomes infeasible.

3.3 Forecasting Water Demands

Forecasts of water demands are the basis for the design of supply facilities. Two types of information are needed: the *volume* that will be demanded in future years, and the distribution of the volume within a given year to produce *flow rates*. In the Silistra region the growth in water demands over time is linked to the overall agricultural development of the region; the numbers of livestock are the primary decision variables. The path of agricultural development of the

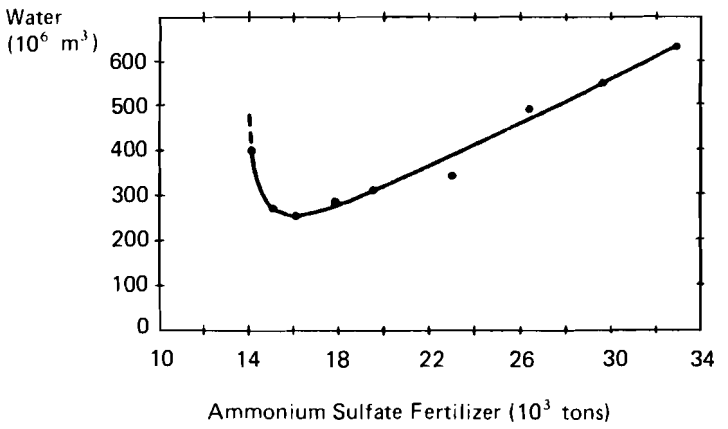

FIGURE 17 Water and fertilizers in the Silistra region.

Silistra region will be different depending on which of the animals (cows, pigs, sheep, or hens) predominates in the future. Cows and pigs may be more productive than milking sheep but Bulgarian sheep's cheese has an established image in international markets. The issue of which animals to concentrate on in the development of agricultural production is clearly a very complex one, involving many factors outside the scope of this study.

In order to illustrate the effect on water demands of various assumptions about the future growth in livestock, a set of scenarios has been developed. Each scenario corresponds to specified growth rates in the numbers of each type of livestock in the complex. These growth rates are all assumed to be linear from the base year 1975, i.e., a 2-percent growth rate means that in each subsequent year 2 percent of the number of livestock in 1975 are added to the total.

Four scenarios have been formulated with equal annual growth rates for each animal of 2, 4, 5, and 10 percent. Two additional scenarios favoring cows have also been formulated, one in which cows grow at 5 percent/yr and the other animals at 2 percent/yr, and another in which cows grow at 10 percent/yr and the others at 5 percent/yr.

For all the scenarios the numbers of livestock in the complex in 1980, 1985, 1990, 1995, and 2000 are computed and fed into SWIM2 as fixed variables. SWIM2 computes the most efficient production system needed to support these numbers of livestock.

The results for normal weather conditions are shown in Figure 18. For the faster-growth scenarios the ultimate economical level of development is reached before the year 2000 so the forecast was terminated at that level. It is striking that water demands grow about four to five times faster than the number of livestock. For example, in the scenario with a 5-percent livestock growth rate, water demands increase from 78.1 X 10^6 m^3/yr in 1975 to 340 X 10^6 m^3/yr in 1990, an increase of 335 percent or 22 percent/yr.

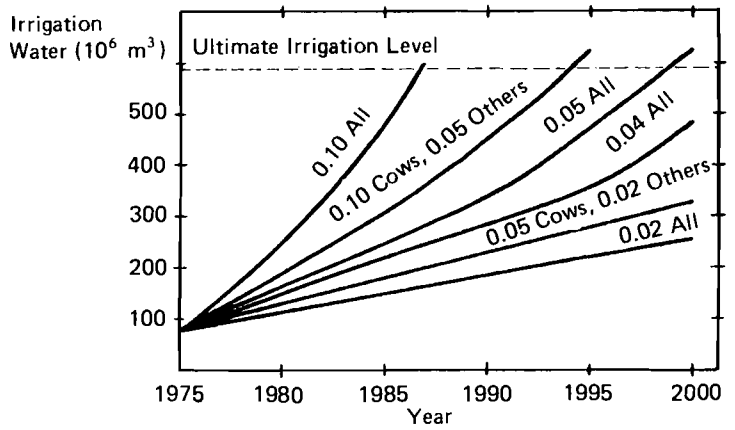

FIGURE 18 Comparison of water demand forecasts.

There is such a difference in the growth rates of water demands and livestock because the 1975 livestock numbers are almost entirely supported by nonirrigated crop production. To increase the livestock numbers, some of this land must be irrigated. It turns out that over a considerable range of livestock development, increases in irrigated area and water demands are linearly related to the number of livestock units (1 livestock unit = 1 cow + 8.4 pigs + 9.7 sheep + 27.8 hens), as shown in Figure 19. In this range each additional livestock unit requires the conversion of about 4 ha of nonirrigated land into irrigated land, 22,000 m^3/yr more irrigation water, and 175 m^3/yr more livestock drinking water, i.e., a 1-percent increase in the numbers of livestock in 1975 would require increases of 650 ha in irrigated land, 3.5 X 10^6 m^3/yr in irrigation water, and 2.8 X 10^6 m^3/yr more livestock drinking water. Future increases of livestock drinking water demands would, therefore, be less than 1 percent of the increases in irrigation water demands but livestock drinking water demands may still cause difficulties since these must be met by pumping groundwater.

As livestock development approaches twice the 1975 levels, more irrigation is needed per additional livestock unit because less productive crops begin to be irrigated. At this level of water demand, approximately 350 X 10^6 m^3/yr, the demand function for water (Figure 19) falls rapidly, also reflecting the decreasing productivity of irrigation.

Consider the "5 percent all" scenario in more detail. Irrigated land must be developed at the rate of about 3,000 ha/yr until 1995; this requires an investment of 10 million Lv/yr in irrigation. SWIM2 also computes the distribution of water demands over the irrigation season to enable the identification of the peak demand rate. For this scenario the growth in the peak demand rate can be seen in Figure 20. The peak demand rate rises from 19.7 X 10^6 m^3/10 days in 1975 to 79.2 X 10^6 m^3/10 days in 1995.

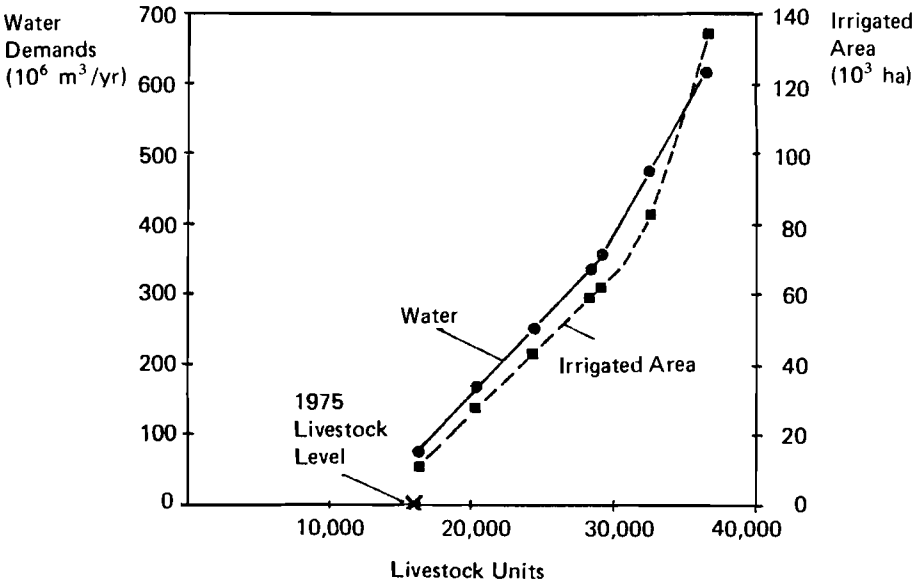

FIGURE 19 Livestock and irrigation.

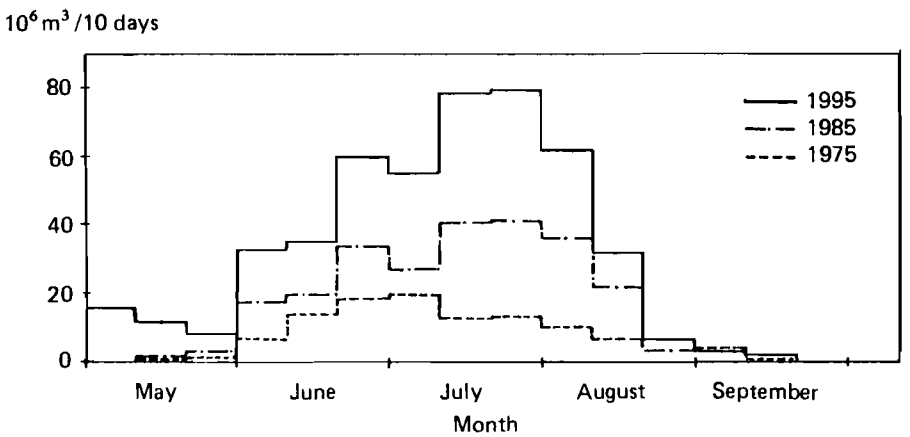

FIGURE 20 Water demands over the irrigation season.

It may be noted that the solutions of SWIM2 contain other data that may be of interest to regional planners, including the numbers of tractors and combine harvesters needed in the complex, annual requirements for fertilizers and fuel, and total quantities of the various types of crop production.

3.4 Sensitivity of the Results

In formulating a model, the relative importance of the parameters in the real system must be assessed. The more important parameters require detailed treatment in the model structure and more accurate input data. An assessment of the sensitivity of the model's output to changes in the parameters can show where improvements in the model structure or input data are needed and can give some indication as to how reliable the results are.

The experience accumulated during the study while performing more than 70 runs of SWIM2 demonstrates that there are five parameters that have a substantial influence on the results: animal benefits (value of animal products), crop production costs, crop yields, animal diets, and coefficients of irrigation water use. The main results described previously are sensitive to some parameters more than others (Table 3).

As far as the economic results from the model are concerned, the least reliable input data are those for animal benefits since these data involve assumptions about future market prices. In order to evalutate the effect of variations in the animal benefits on the net benefits of the system, SWIM2 was run for several values of animal benefits around the value adopted in the results previously described. From these runs it was found that a 1-percent change in the animal benefits produces a 0.9-percent change in the net benefits of the system. This indicates that there is little damping effect of the model itself on variations in these input data.

Since SWIM2 is available at IIASA and on the computer of the Ministry of Agriculture and Food Industry in Sofia, its input data and model structure can be improved where necessary and further results can be produced.

TABLE 3 Sensitivity of the model.

	Parameters				
Result	Animal benefits	Crop costs	Crop yields	Animal diets	Water coefficients
Validation		*	*	+	
Ultimate economic investment	*	*	+	+	
Demand function	*	+	*	+	*
Forecasting		+	*	*	*

NOTE: The symbols show how the main results from the model are sensitive to its input parameters: Blank – not sensitive, + – moderately sensitive, * – very sensitive.

4 CONCLUSIONS

A number of conclusions may be drawn from the results of the SWIM2 model. At the level of aggregated production quantities the model compares reasonably well with data recorded in the region in 1975. When more detailed comparisons are made there are some discrepancies between the model's results and the regional data, which is to be expected since the model optimizes rather than simulates the actual system.

An ultimate economical level of irrigation development, the level of maximum net benefit, is identified as the point where 70 percent of the arable land is irrigated. This area of irrigation corresponds to complete development of the potentially irrigable land in two of the three subregions within the Silistra region, and to partial development of the third subregion.

Water demands increase approximately linearly with increasing irrigated area to ultimate economical levels of 585×10^6 m^3/yr (under normal weather conditions) and 820×10^6 m^3/yr (under dry weather conditions). The corresponding water withdrawal coefficients are 5,500 m^3/ha (550 mm) under normal weather conditions and 7,750 m^3/ha (775 mm) under dry weather conditions. Since an irrigation efficiency of 50 percent is assumed, these coefficients correspond respectively to 275 mm and 387 mm of consumptive use of irrigation water by the crops. At these levels of development, water demands are quite sensitive to the price of water. Removing the existing price subsidy on water would reduce the ultimate economical irrigation area to about 35 percent of the arable land.

Further development of livestock production in the region beyond 1975 levels would require substantial investments in irrigation because the existing livestock are almost entirely supported by nonirrigated crop production. Over a substantial range of livestock development the associated demand for water and irrigated area varies linearly with the number of livestock. Each 1-percent increase in livestock from the 1975 levels requires about 650 ha of new irrigated land, or an increase of 4.5 percent in irrigated area. The corresponding increase in water demands amounts to 3.5×10^6 m^3/yr.

What are the advantages of using SWIM2 rather than the conventional methods of estimating agricultural water demands? The major advantage of SWIM2 is that it integrates the regional water demands with the crop and livestock production processes that determine these demands. This allows for various substitutions to be made among the inputs to these production processes (e.g., changing the composition of animals' diets) and among the production processes themselves (e.g., exchanging crops, converting land to irrigation). The integrated nature of the model is particularly important in the Silistra region because it corresponds to the centralized management structure controlling all aspects of agricultural production.

Although SWIM2 covers only a 1-year time period in each solution, it can be used to look at longer time horizons by forecasting various scenarios of the

growth in livestock numbers and by running SWIM2 for several future years to derive the corresponding forecasts of water demands. Since the numbers of livestock are the primary variables of interest to Silistra decision makers, SWIM2 provides a means for evaluating the impact of various livestock development strategies. However, these results should be interpreted carefully because SWIM2 does not discount benefits or costs over time, only one set of production coefficients has been used, and no economies of scale are included.

A number of limitations of SWIM2 may also be noted. The model is not truly dynamic since it does not contain internally the linkages of year-to-year evolution. Another limitation is that livestock processing is treated only in a very aggregated way. As with most models, improvement of the data on the more sensitive variables would improve the accuracy of the results. Better data on crop yields, crop production costs, prices for outputs, and water use coefficients would be especially useful.

Appendix A

TABLES OF INPUT RESOURCES

The following tables show the rates of application of various resources (seeds, fertilizers, machinery, and fuel) for each of the crops considered in the model. Also shown are time schedules for crop production activities and irrigation. The data given in this appendix are used to calculate tables of production costs in Appendix C.

TABLE A.1 Seed requirements.

Crop	Seeding rate (ton/ha)	Seed crop yield (ton/ha)	Cost of seeds (Lv/ton)	a_i
Lucerne				
irr[a]	0.020	0.3	5,504	0.0667
non[b]	0.020	0.3	5,504	0.0667
Maize silage				
irr	0.040	4.3	660	0.0093
non	0.030	4.3	660	0.0093
Maize silage II				
irr	0.019	4.3	660	0.0044
Maize grain				
irr	0.020	4.3	660	0.0046
non	0.015	4.3	660	0.0035
Wheat				
irr	0.308	3.8	130	0.0810
non	0.280	3.8	130	0.0740
Barley				
irr	0.209	3.5	120	0.0597
non	0.190	3.5	120	0.0543
Soybeans				
irr	0.100	1.5	700	0.0667
non	0.100	1.5	700	0.0667
Sunflowers				
irr	0.066	2.0	307	0.0330
non	0.060	2.0	307	0.0300

NOTE: a_i = Seeding rate ÷ seed crop yield.
[a]Irrigated.
[b]Nonirrigated.

TABLE A.2 Fertilizer requirements (ton/ha).

Crop	Ammonium sulfate	Superphosphate	Potassium sulfate
Lucerne			
irr, 80[a]	0.152	0.36	0.10
irr, 100[b]	0.190	0.44	0.13
non[c]	0.100	0.30	0.09
Maize silage			
irr, 80	0.640	0.72	0.22
irr,100	0.800	0.90	0.27
non	0.360	0.55	
Maize silage II			
irr, 80	0.640	0.42	0.22
irr, 100	0.800	0.53	0.27
Maize grain			
irr, 80	0.420	0.48	0.16
irr, 100	0.530	0.60	0.20
non	0.240	0.30	
Wheat			
irr, 80	0.260	0.29	0.18
irr, 100	0.325	0.36	0.22
non	0.250	0.28	
Barley			
irr, 80	0.168	0.19	0.10
irr, 100	0.210	0.24	0.14
non	0.167	0.15	0.07
Soybeans			
irr, 80	0.130	0.25	0.09
irr, 100	0.170	0.32	0.11
non	0.120	0.23	0.07
Sunflowers			
irr, 80	0.416	0.33	0.02
irr, 100	0.520	0.42	0.03
non	0.400	0.32	0.02
Orchards			
irr, 80	0.480	0.38	0.28
irr, 100	0.600	0.40	0.30
non	0.400	0.35	0.25
Tobacco			
irr, 80		0.40	0.25
irr, 100		0.50	0.32
non		0.60	0.40
Vegetables			
irr, 100	0.75	0.60	0.27

[a]Irrigated, 80-percent fertilizer.
[b]Irrigated, 100-percent fertilizer.
[c]Nonirrigated.

TABLE A.3 Amount of nitrogen, phosphorus, and potassium in animal wastes (ton/animal/yr).

Animal	Nitrogen	Phosphorus	Potassium
Cows	0.1042	0.0444	0.0743
Pigs	0.0364	0.026	0.0156
Sheep	0.0098	0.007	0.0042
Hens	0.00077	0.00055	0.00033

TABLE A.4 Labor requirements (man-h/ha).

	Tractor h					Combine h	
Crop	Plowing	Cultivation	Planting	Harvest	Total	June–July	Aug–Oct
Lucerne							
irr[a]	0.31	0.10	0.20	2.48	3.09		
non[b]	0.31	0.10	0.20	2.00	2.61		
Maize silage							
irr	0.94	0.48	0.33	2.50	4.25		
non	0.94	0.48	0.33	2.30	4.05		
Maize silage II							
irr	0.94	0.48	0.33	2.50	4.25		
Maize grain							
irr	0.94	0.48	0.35		1.77		0.80
non	0.94	0.48	0.35		1.77		0.80
Wheat							
irr	0.53	0.21	0.35		1.09	0.54	
non	0.53	0.21	0.35		1.09	0.54	
Barley							
irr	0.52	0.16	0.25		0.93	0.48	
non	0.52	0.16	0.25		0.93	0.48	
Soybeans							
irr	2.50	0.10	0.60		3.20		2.72
non	2.50	0.10	0.60		3.20		1.80
Sunflowers							
irr	0.80	0.32	0.44		1.56		0.56
non	0.80	0.32	0.44		1.56		0.56

[a] Irrigated.
[b] Nonirrigated.

TABLE A.5 Fuel requirements (l/ha).

Crop	Plowing	Cultivation	Planting	Harvesting (incl. straw)	Total fuel
Lucerne					
irr[a]	17	4	6	50	77
non[b]	17	4	6	42	69
Maize silage					
irr	21	20	5	126	172
non	20	19	5	68	112
Maize silage II					
irr	21	20	5	126	172
Maize grain					
irr	21	20	6	53	100
non	21	20	6	38	85
Wheat					
irr	8	4	7	41	60
non	8	4	7	34	53
Barley					
irr	9	4	7	37	57
non	9	4	7	30	50
Soybeans					
irr	19	3	9	34	65
non	19	3	9	34	65
Sunflowers					
irr	15	7	7	26	55
non	15	7	7	23	52

[a] Irrigated.
[b] Nonirrigated.

TABLE A.6 Irrigation schedule of crops.

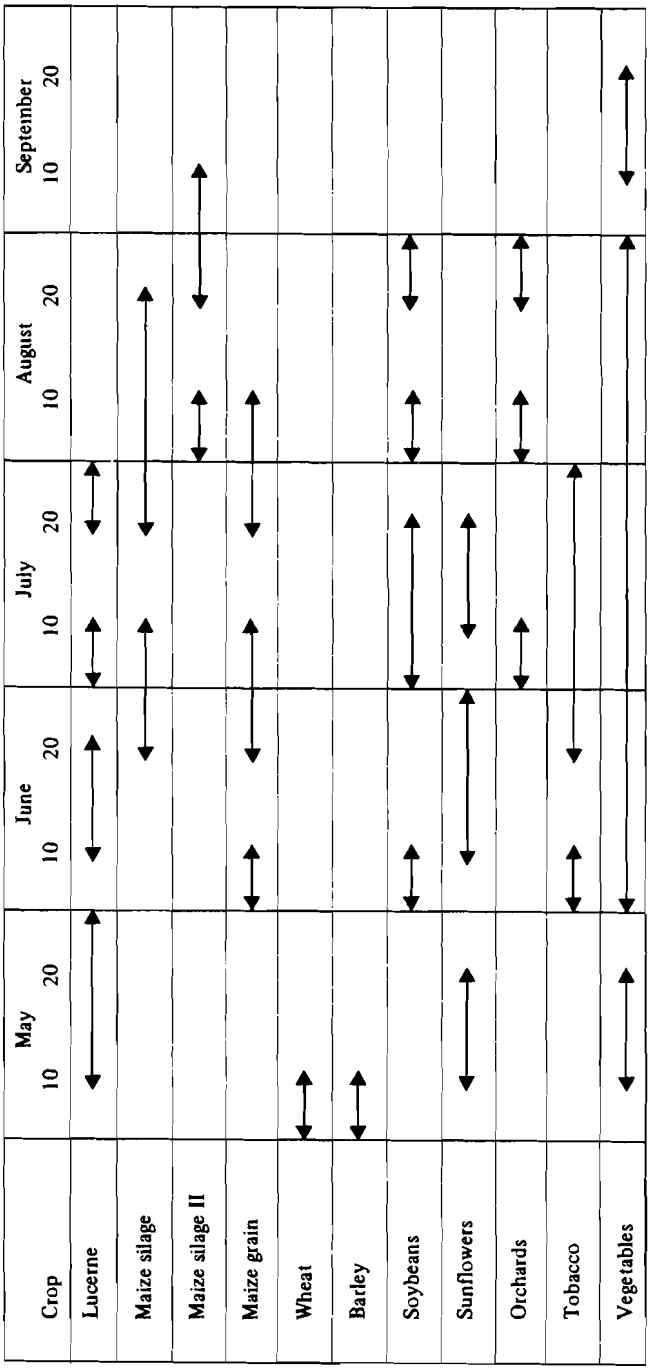

TABLE A.7 Schedule of field operations.

Appendix B

TABLES OF ANIMAL DIETS

This appendix contains the minimum and maximum amounts of energy content in the various feedstuffs forming the diet of each animal. The numbers of feed units (energy content) of each crop product are also given.

TABLE B.1 Animal diets (feed units/structural animal).

	Concentrated forage		Green forage		Silage		Hay		Roughage		Minimum amount of total feed units
Animal	min	max	min	max	min	max	min	max	min	max	required
Cows	4,284	5,881	404	901	549	929	437	1,029	0	354	6,415
Pigs	1,037										1,037
Sheep	118	158			51	94	49	90	0	54	370
Hens	57										57

TABLE B.2 Energy content of various forages.

Forage	feed units/ton
Concentrated	
maize grain	1,300
barley	1,200
wheat	1,200
wheat bran	370
soybean meal	1,150
sunflower meal	950
Green	
lucerne	200
Silage	
lucerne	340
maize silage	300
maize silage II	300
lucerne haylage	340
Hay	
lucerne	340

TABLE B.3 Energy content of roughages.

Roughage	feed units/ha
Maize grain stalks	
irrigated	
100% fertilizer	158
80% fertilizer	145
nonirrigated	72
Wheat straw	45
Barley straw	44
Sunflower residuals	830

Appendix C

TABLES OF PRODUCTION COSTS

For each crop, the following tables show all production costs associated with field cultivation activities. The costs are either attached to the land area (cost/ha) or to the input resources (cost/unit amount). The fixed costs attached to land are depreciated capital investments (machinery purchase). The variable costs include costs of application of the input resources (fertilizers and chemicals), labor other than that for operation of machines, and maintenance of the equipment. The total cost attached to land (e.g., 74.80 Lv/ha in Table C.1) is the unit cost used in the objective function of the linear programming for the crop area decision variable. The total land and resource cost (e.g., 163.71 in Table C.1) is the total production cost per hectare.

TABLE C.1 Nonirrigated lucerne production costs.

Cost	Seeds	Fertil-izer	Chem-icals	Machin-ery	Labor	Irrigation	Total costs
Attached to land (Lv/ha)							
fixed				11.00			
variable		3.20	46.00	8.70	5.90		
Total		3.20	46.00	19.70	5.90		74.80
Attached to resources							
seeds							
ton/ha	0.0066						
Lv/ton	5,504.00						
ammonium sulfate							
ton/ha		0.10					
Lv/ton		93.72					
superphosphate							
ton/ha		0.30					
Lv/ton		61.77					
potassium sulfate							
ton/ha		0.09					
Lv/ton		85.20					
fuel							
l/ha				69.00			
Lv/l				0.19			
operator-hour							
h/ha					2.61		
Lv/h					1.50		
water							
m^3/ha							
Lv/m^3							
Total (Lv/ha)	36.32	35.57		13.11	3.91		88.91
TOTAL land & resources (Lv/ha)	36.32	38.77	46.00	32.81	9.81		163.71

TABLE C.2 Irrigated lucerne production costs.

Cost	Seeds	Fertil-izer	Chem-icals	Machin-ery	Labor	Irrigation	Total costs
Attached to land (Lv/ha)							
fixed				27.00			
variable		3.20	46.00	23.00	15.40	29.45	
Total		3.20	46.00	50.00	15.40	29.45	144.05
Attached to resources							
seeds							
ton/ha	0.0066						
Lv/ton	5,504.00						
ammonium sulfate							
ton/ha		0.19					
Lv/ton		93.72					
superphosphate							
ton/ha		0.44					
Lv/ton		61.77					
potassium sulfate							
ton/ha		0.13					
Lv/ton		85.20					
fuel							
l/ha				77.00			
Lv/l				0.19			
operator-hour							
h/ha					3.09		
Lv/h					1.50		
water							
m^3/ha						3,000.00	
Lv/m^3						0.017	
Total (Lv/ha)	36.32	56.06		14.63	4.63	51.00	162.64
TOTAL land & resources (Lv/ha)	36.32	59.26	46.00	64.63	20.03	80.45	306.69

TABLE C.3 Nonirrigated maize silage production costs.

Cost	Seeds	Fertil-izer	Chem-icals	Machin-ery	Labor	Irrigation	Total costs
Attached to land (Lv/ha)							
fixed				40.00			
variable		8.00	7.68	34.47	12.88		
Total		8.00	7.68	74.47	12.88		103.03
Attached to resources							
seeds							
ton/ha	0.03						
Lv/ton	660.00						
ammonium sulfate							
ton/ha		0.36					
Lv/ton		93.72					
superphosphate							
ton/ha		0.55					
Lv/ton		61.77					
potassium sulfate							
ton/ha							
Lv/ton							
fuel							
l/ha				112.00			
Lv/l				0.19			
operator-hour							
h/ha					4.05		
Lv/h					1.50		
water							
m^3/ha							
Lv/m^3							
Total (Lv/ha)	19.80	67.71		21.28	6.07		144.86
TOTAL land & resources (Lv/ha)	19.80	75.71	7.68	95.75	18.95		217.89

TABLE C.4 Irrigated maize silage production costs.

Cost	Seeds	Fertil-izer	Chem-icals	Machin-ery	Labor	Irrigation	Total costs
Attached to land (Lv/ha)							
fixed				25.00			
variable		8.00	8.60	20.00	20.60	29.45	
Total		8.00	8.60	45.00	20.60	29.45	111.65
Attached to resources							
seeds							
ton/ha	0.04						
Lv/ton	660.00						
ammonium sulfate							
ton/ha		0.80					
Lv/ton		93.72					
superphosphate							
ton/ha		0.90					
Lv/ton		61.77					
potassium sulfate							
ton/ha		0.27					
Lv/ton		85.20					
fuel							
l/ha				172.00			
Lv/l				0.19			
operator-hour							
h/ha					4.25		
Lv/h					1.50		
water							
m^3/ha						3,000.00	
Lv/m^3						0.017	
Total (Lv/ha)	26.40	153.57		32.68	6.37	51.00	270.02
TOTAL land & resources (Lv/ha)	26.40	161.57	8.60	77.68	26.97	80.45	381.67

TABLE C.5 Irrigated maize silage II production costs.

Cost	Seeds	Fertil-izer	Chem-icals	Machin-ery	Labor	Irrigation	Total costs
Attached to land (Lv/ha)							
fixed				25.00			
variable		8.00	8.60	20.00	20.60	29.45	
Total		8.00	8.60	45.00	20.60	29.45	111.65
Attached to resources							
seeds							
ton/ha	0.019						
Lv/ton	660.00						
ammonium sulfate							
ton/ha		0.80					
Lv/ton		93.72					
superphosphate							
ton/ha		0.525					
Lv/ton		61.77					
potassium sulfate							
ton/ha		0.27					
Lv/ton		85.20					
fuel							
l/ha				172.00			
Lv/l				0.19			
operator-hour							
h/ha					4.25		
Lv/h					1.50		
water							
m^3/ha						1,800.00	
Lv/m^3						0.017	
Total (Lv/ha)	12.54	130.41		32.68	6.37	30.60	212.60
TOTAL land & resources (Lv/ha)	12.54	138.41	8.60	77.68	26.97	60.05	324.25

TABLE C.6 Nonirrigated maize grain production costs.

Cost	Seeds	Fertil-izer	Chem-icals	Machin-ery	Labor	Irrigation	Total costs
Attached to land (Lv/ha)							
fixed				32.00			
variable		8.00	26.00	24.45	7.15		
Total		8.00	26.00	56.45	7.15		97.60
Attached to resources							
seeds							
ton/ha	0.015						
Lv/ton	660.00						
ammonium sulfate							
ton/ha		0.24					
Lv/ton		93.72					
superphosphate							
ton/ha		0.30					
Lv/ton		61.77					
potassium sulfate							
ton/ha							
Lv/ton							
fuel							
l/ha				85.00			
Lv/l				0.19			
operator-hour							
h/ha					2.57		
Lv/h					1.50		
water							
m^3/ha							
Lv/m^3							
Total (Lv/ha)	9.90	41.02		16.15	3.85		70.92
TOTAL land & resources (Lv/ha)	9.90	49.02	26.00	72.60	11.00		168.52

TABLE C.7 Irrigated maize grain production costs.

Cost	Seeds	Fertil-izer	Chem-icals	Machin-ery	Labor	Irrigation	Total costs
Attached to land (Lv/ha)							
fixed				23.00			
variable		8.00	24.90	21.00	11.12	29.45	
Total		8.00	24.90	44.00	11.12	29.45	117.47
Attached to resources							
seeds							
ton/ha	0.02						
Lv/ton	660.00						
ammonium sulfate							
ton/ha		0.53					
Lv/ton		93.72					
superphosphate							
ton/ha		0.60					
Lv/ton		61.77					
potassium sulfate							
ton/ha		0.20					
Lv/ton		85.20					
fuel							
l/ha				100.00			
Lv/l				0.19			
operator-hour							
h/ha					2.57		
Lv/h					1.50		
water							
m^3/ha						3,000.00	
Lv/m^3						0.017	
Total (Lv/ha)	13.20	103.77		19.00	3.85	51.00	190.82
TOTAL land & resources (Lv/ha)	13.20	111.77	24.90	63.00	14.97	80.45	308.29

TABLE C.8 Nonirrigated wheat production costs.

Cost	Seeds	Fertil-izer	Chem-icals	Machin-ery	Labor	Irrigation	Total costs
Attached to land (Lv/ha)							
fixed				25.00			
variable		9.00	9.90	20.00	4.00		
Total		9.00	9.90	45.00	4.00		67.90
Attached to resources							
seeds							
ton/ha	0.28						
Lv/ton	130.00						
ammonium sulfate							
ton/ha		0.25					
Lv/ton		93.72					
superphosphate							
ton/ha		0.28					
Lv/ton		61.77					
potassium sulfate							
ton/ha							
Lv/ton							
fuel							
l/ha				53.00			
Lv/l				0.19			
operator-hour							
h/ha					1.63		
Lv/h					1.50		
water							
m^3/ha							
Lv/m^3							
Total (Lv/ha)	36.40	40.72		10.07	2.44		89.63
TOTAL land & resources (Lv/ha)	36.40	49.72	9.90	55.07	6.44		157.53

TABLE C.9 Irrigated wheat production costs.

Cost	Seeds	Fertil-izer	Chem-icals	Machin-ery	Labor	Irrigation	Total costs
Attached to land (Lv/ha)							
fixed				25.00			
variable		9.00	9.90	20.00	4.00	29.45	
Total		9.00	9.90	45.00	4.00	29.45	97.35
Attached to resources							
seeds							
ton/ha	0.28						
Lv/ton	130.00						
ammonium sulfate							
ton/ha		0.325					
Lv/ton		93.72					
superphosphate							
ton/ha		0.364					
Lv/ton		61.77					
potassium sulfate							
ton/ha		0.22					
Lv/ton		85.20					
fuel							
l/ha				60.00			
Lv/l				0.19			
operator-hour							
h/ha					1.63		
Lv/h					1.50		
water							
m^3/ha						600.00	
Lv/m^3						0.017	
Total (Lv/ha)	36.40	71.68		11.40	2.44	10.20	132.12
TOTAL land & resources (Lv/ha)	36.40	80.68	9.90	56.40	6.44	39.65	229.47

TABLE C.10 Nonirrigated barley production costs.

Cost	Seeds	Fertil-izer	Chem-icals	Machin-ery	Labor	Irrigation	Total costs
Attached to land (Lv/ha)							
fixed				20.00			
variable		3.00	9.60	15.80	1.80		
Total		3.00	9.60	35.80	1.80		50.20
Attached to resources							
seeds							
ton/ha	0.19						
Lv/ton	120.00						
ammonium sulfate							
ton/ha		0.167					
Lv/ton		93.72					
superphosphate							
ton/ha		0.15					
Lv/ton		61.77					
potassium sulfate							
ton/ha		0.07					
Lv/ton		85.20					
fuel							
l/ha				50.00			
Lv/l				0.19			
operator-hour							
h/ha					1.41		
Lv/h					1.50		
water							
m^3/ha							
Lv/m^3							
Total (Lv/ha)	22.80	30.87		9.50	2.11		65.28
TOTAL land & resources (Lv/ha)	22.80	33.87	9.60	45.30	3.91		115.48

TABLE C.11 Irrigated barley production costs.

Cost	Seeds	Fertil-izer	Chem-icals	Machin-ery	Labor	Irrigation	Total costs
Attached to land (Lv/ha)							
fixed				20.00			
variable		3.00	9.60	15.80	1.80	29.45	
Total		3.00	9.60	35.80	1.80	29.45	79.65
Attached to resources							
seeds							
ton/ha	0.209						
Lv/ton	120.00						
ammonium sulfate							
ton/ha		0.21					
Lv/ton		93.72					
superphosphate							
ton/ha		0.24					
Lv/ton		61.77					
potassium sulfate							
ton/ha		0.135					
Lv/ton		85.20					
fuel							
l/ha				57.00			
Lv/l				0.19			
operator-hour							
h/ha					1.41		
Lv/h					1.50		
water							
m^3/ha						600.00	
Lv/m^3						0.017	
Total (Lv/ha)	25.08	46.00		10.83	2.11	10.20	94.22
TOTAL land & resources (Lv/ha)	25.08	49.00	9.60	46.63	3.91	39.65	173.87

TABLE C.12 Nonirrigated soybean production costs.

Cost	Seeds	Fertil-izer	Chem-icals	Machin-ery	Labor	Irrigation	Total costs
Attached to land (Lv/ha)							
fixed				32.00			
variable		10.75	73.00	18.00	9.36		
Total		10.75	73.00	50.00	9.36		143.11
Attached to resources							
seeds							
ton/ha	0.10						
Lv/ton	700.00						
ammonium sulfate							
ton/ha		0.12					
Lv/ton		93.72					
superphosphate							
ton/ha		0.225					
Lv/ton		61.77					
potassium sulfate							
ton/ha		0.07					
Lv/ton		85.20					
fuel							
l/ha				65.00			
Lv/l				0.19			
operator-hour							
h/ha					5.00		
Lv/h					1.50		
water							
m^3/ha							
Lv/m^3							
Total (Lv/ha)	70.00	31.11		12.35	7.50		120.96
TOTAL land & resources (Lv/ha)	70.00	41.86	73.00	62.35	16.86		264.07

TABLE C.13 Irrigated soybean production costs.

Cost	Seeds	Fertil-izer	Chem-icals	Machin-ery	Labor	Irrigation	Total costs
Attached to land (Lv/ha)							
fixed				32.00			
variable		10.75	73.00	18.00	9.36	29.45	
Total		10.75	73.00	50.00	9.36	29.45	172.56
Attached to resources							
seeds							
ton/ha	0.10						
Lv/ton	700.00						
ammonium sulfate							
ton/ha		0.17					
Lv/ton		93.72					
superphosphate							
ton/ha		0.32					
Lv/ton		61.77					
potassium sulfate							
ton/ha		0.11					
Lv/ton		85.20					
fuel							
l/ha				65.00			
Lv/l				0.19			
operator-hour							
h/ha					5.92		
Lv/h					1.50		
water							
m^3/ha						3,000.00	
Lv/m^3						0.017	
Total (Lv/ha)	70.00	45.07		12.35	8.88	51.00	187.30
TOTAL land & resources (Lv/ha)	70.00	55.82	73.00	62.35	18.24	80.45	359.86

TABLE C.14 Nonirrigated sunflower production costs.

Cost	Seeds	Fertil-izer	Chem-icals	Machin-ery	Labor	Irrigation	Total costs
Attached to land (Lv/ha)							
fixed				20.57			
variable		9.00	26.00	16.80	5.00		
Total		9.00	26.00	37.37	5.00		77.37
Attached to resources							
seeds							
ton/ha	0.06						
Lv/ton	307.00						
ammonium sulfate							
ton/ha		0.40					
Lv/ton		93.72					
superphosphate							
ton/ha		0.32					
Lv/ton		61.77					
potassium sulfate							
ton/ha		0.02					
Lv/ton		85.20					
fuel							
l/ha				52.00			
Lv/l				0.19			
operator-hour							
h/ha					2.12		
Lv/h					1.50		
water							
m^3/ha							
Lv/m^3							
Total (Lv/ha)	18.42	58.96		9.88	3.18		90.44
TOTAL land & resources (Lv/ha)	18.42	67.96	26.00	47.25	8.18		167.81

TABLE C.15 Irrigated sunflower production costs.

Cost	Seeds	Fertil-izer	Chem-icals	Machin-ery	Labor	Irrigation	Total costs
Attached to land (Lv/ha)							
fixed				20.50			
variable		9.00	26.00	16.80	5.00	29.45	
Total		9.00	26.00	37.30	5.00	29.45	106.75
Attached to resources							
seeds							
ton/ha	0.066						
Lv/ton	307.00						
ammonium sulfate							
ton/ha		0.52					
Lv/ton		93.72					
superphosphate							
ton/ha		0.416					
Lv/ton		61.77					
potassium sulfate							
ton/ha		0.026					
Lv/ton		85.20					
fuel							
l/ha				55.00			
Lv/l				0.19			
operator-hour							
h/ha					2.12		
Lv/h					1.50		
water							
m^3/ha						2,400.00	
Lv/m^3						0.017	
Total (Lv/ha)	20.26	76.64		10.45	3.18	40.8	151.33
TOTAL land & resources (Lv/ha)	20.26	85.64	26.00	47.75	8.18	70.25	258.08

TABLE C.16 Nonirrigated orchards production costs.

Cost	Seeds	Fertil-izer	Chem-icals	Machin-ery	Labor	Irrigation	Total costs
Attached to land (Lv/ha)							
fixed				100.00			
variable		3.00	230.00	33.00	18.00		
Total		3.00	230.00	133.00	18.00		384.00
Attached to resources							
seeds							
ton/ha							
Lv/ton							
ammonium sulfate							
ton/ha		0.40					
Lv/ton		93.72					
superphosphate							
ton/ha		0.35					
Lv/ton		61.77					
potassium sulfate							
ton/ha		0.25					
Lv/ton		85.20					
fuel							
l/ha				70.00			
Lv/l				0.19			
operator-hour							
h/ha					56.00		
Lv/h					1.50		
water							
m^3/ha							
Lv/m^3							
Total (Lv/ha)		80.41		13.30	84.00		177.71
TOTAL land & resources (Lv/ha)		83.41	230.00	146.30	102.00		561.71

TABLE C.17 Irrigated orchards production costs.

Cost	Seeds	Fertil-izer	Chem-icals	Machin-ery	Labor	Irrigation	Total costs
Attached to land (Lv/ha)							
fixed				100.00			
variable		3.00	230.00	33.0	20.00	29.45	
Total		3.00	230.00	133.00	20.00	29.45	415.45
Attached to resources							
seeds							
ton/ha							
Lv/ton							
ammonium sulfate							
ton/ha		0.60					
Lv/ton		93.72					
superphosphate							
ton/ha		0.40					
Lv/ton		61.77					
potassium sulfate							
ton/ha		0.30					
Lv/ton		85.20					
fuel							
l/ha				87.00			
Lv/l				0.19			
operator-hour							
h/ha					69.00		
Lv/h					1.50		
water							
m^3/ha						2,500.00	
Lv/m^3						0.017	
Total (Lv/ha)		106.50		16.53	103.50	42.50	269.03
TOTAL land & resources (Lv/ha)		109.50	230.00	149.53	123.50	71.95	684.48

TABLE C.18 Nonirrigated tobacco production costs.

Cost	Seeds	Fertil-izer	Chem-icals	Machin-ery	Labor	Irrigation	Total costs
Attached to land (Lv/ha)							
fixed				25.00			
variable		5.00	240.00	5.00	8.00		
Total		5.00	240.00	30.00	8.00		283.00
Attached to resources							
seeds							
ton/ha							
Lv/ton							
ammonium sulfate							
ton/ha							
Lv/ton							
superphosphate							
ton/ha		0.60					
Lv/ton		61.77					
potassium sulfate							
ton/ha		0.40					
Lv/ton		85.20					
fuel							
l/ha				150.00			
Lv/l				0.19			
operator-hour							
h/ha					25.00		
Lv/h					1.50		
water							
m^3/ha							
Lv/m^3							
Total (Lv/ha)		71.14		28.50	37.50		137.14
TOTAL land & resources (Lv/ha)		76.14	240.00	58.50	45.50		420.14

TABLE C.19 Irrigated tobacco production costs.

Cost	Seeds	Fertil-izer	Chem-icals	Machin-ery	Labor	Irrigation	Total costs
Attached to land (Lv/ha)							
fixed				20.00			
variable		3.00	240.00	5.00	8.00	29.45	
Total		3.00	240.00	25.00	8.00	29.45	305.45
Attached to resources							
seeds							
ton/ha							
Lv/ton							
ammonium sulfate							
ton/ha							
Lv/ton							
superphosphate							
ton/ha		0.50					
Lv/ton		61.77					
potassium sulfate							
ton/ha		0.40					
Lv/ton		85.20					
fuel							
l/ha				100.00			
Lv/l				0.19			
operator-hour							
h/ha					25.00		
Lv/h					1.50		
water							
m^3/ha						2,500.00	
Lv/m^3						0.017	
Total (Lv/ha)		64.96		19.00	37.50	42.50	163.96
TOTAL land & resources (Lv/ha)		67.96	240.00	44.00	45.50	71.95	469.41

TABLE C.20 Irrigated vegetables production costs.

Cost	Seeds	Fertil-izer	Chem-icals	Machin-ery	Labor	Irrigation	Total costs
Attached to land (Lv/ha)							
fixed				38.00			
variable		10.00	184.00	12.00	40.00	29.45	
Total		10.00	184.00	50.00	40.00	29.45	313.45
Attached to resources							
seeds							
ton/ha	0.35						
Lv/ton	240.00						
ammonium sulfate							
ton/ha		0.75					
Lv/ton		93.72					
superphosphate							
ton/ha		0.60					
Lv/ton		61.77					
potassium sulfate							
ton/ha		0.27					
Lv/ton		85.20					
fuel							
l/ha				270.00			
Lv/l				0.19			
operator-hour							
h/ha					180.00		
Lv/h					1.50		
water							
m^3/ha						4,300.00	
Lv/m^3						0.017	
Total (Lv/ha)	84.00	130.35		51.30	270.00	73.10	608.75
TOTAL land & resources (Lv/ha)	84.00	140.35	184.00	101.30	310.00	102.55	922.20

Appendix D

COEFFICIENTS FOR IRRIGATION WATER USE

This appendix describes how the coefficients for irrigation water use in SWIM2 are derived. The general method is described first, followed by the details of rainfall, evapotranspiration, soil moisture capacity, the computation of the coefficients, and irrigation efficiency.

The aim of the computation is to find irrigation water use coefficients and an irrigation efficiency to use in the SWIM2 model to calculate the total volume of irrigation water over time, $W(t)$, that must be withdrawn from the Danube River.

$$W(t) = \frac{1}{e} \sum_{s=1}^{3} \sum_{i=1}^{11} \sum_{q=1}^{2} I_{si}^{q}(t)\, Y_{si}^{q} \qquad \text{(D.1)}$$

where

$W(t)$ is irrigation water demanded (m^3/10 days) in the complex

e is the irrigation efficiency

Y_{si}^{q} is amount of land (ha) in subregion s needed for production of crop i on an irrigated area using technology q

$I_{si}^{q}(t)$ is the irrigation water use coefficient in normal weather (m^3/ha/10 days) of crop i in subregion s using technology q at time t, $t = 1, \ldots, T$

There are 21 ($T = 21$) periods over the 7-month time horizon from 1 March to 31 September. Each month comprises three periods: days 1–9, 10–19, and 20–end. Although irrigation is not necessary before 1 May, the calculations of irrigation water use coefficients begin on 1 March to allow for soil moisture depletion during March and April. Hence, in the SWIM2 model, irrigation water use is accounted for in 15 periods, 3 per month from 1 May to 30 September.

The total water used in the irrigation season, X_{20}(m^3/yr), is computed as

$$X_{20} = \sum_{t=1}^{15} W(t) \qquad t = 1,2, \ldots, 15 \qquad \text{(D.2)}$$

The input data needed for SWIM2 to determine $W(t)$ and X_{20} are the irrigation water use coefficients $I_{si}^{q}(t)$ and the irrigation efficiency e, which is assumed to be constant for all crops and time periods. It is furthermore assumed that $I_{si}^{q}(t)$ do not vary with subregions s and with the technology of producing crops q. Since all calculations that follow exemplify the way that these coefficients are obtained for any of the 11 crops, the index i is omitted. In the text that follows, the irrigation water use coefficient in period t will be denoted by I_t.

D.1 METHOD

The analysis is carried out for 10 crops: lucerne, maize silage, maize silage II (sown after the barley and wheat harvests), maize grain, wheat, barley, soybeans, sunflowers, tobacco, and vegtables, under two weather conditions: average weather and a 1-in-4 dry year. The 1-in-4 dry year is chosen because this is the weather condition assumed by the Bulgarian Research Institute Vodproject in its design of pumps and pipelines for a new irrigation area in the Drustar complex. The calculations are not done for orchards although they are included in SWIM2 as a crop activity. The root depths appropriate for orchards in Silistra were not known precisely at the time and it was thought better to use directly the coefficients proposed by Vodproject, Sofia, than to assume a root depth arbitrarily.

Data on monthly mean rainfall, temperature, humidity, and wind speed, measured in Silistra in each year from 1961 to 1970, are used in deriving the SWIM2 coefficients. Average weather conditions for each month are estimated by averaging the 10 yr of data. The weather conditions for 1961 are chosen as the 1-in-4 dry year from a probability analysis of the rainfall that is described in Section D.2.

For each crop, the general soil moisture balance model shown in Figure D.1 is used:

$$\begin{gathered} S_t = S_{t-1} + R_t - E_t + I_t - D_t \qquad t = 1,2,\ldots,T \\ S_t, S_{t-1}, R_t, E_t, I_t, D_t \geqslant 0 \end{gathered} \tag{D.3}$$

where

S_t, S_{t-1} is available soil moisture at the end of periods t and $t-1$, respectively (mm)

R_t is rainfall in period t (mm/10 days)

E_t is evapotranspiration in period t (mm/10 days)

I_t is irrigation water use in period t (mm/10 days)

D_t is drainage in period t (mm/10 days)

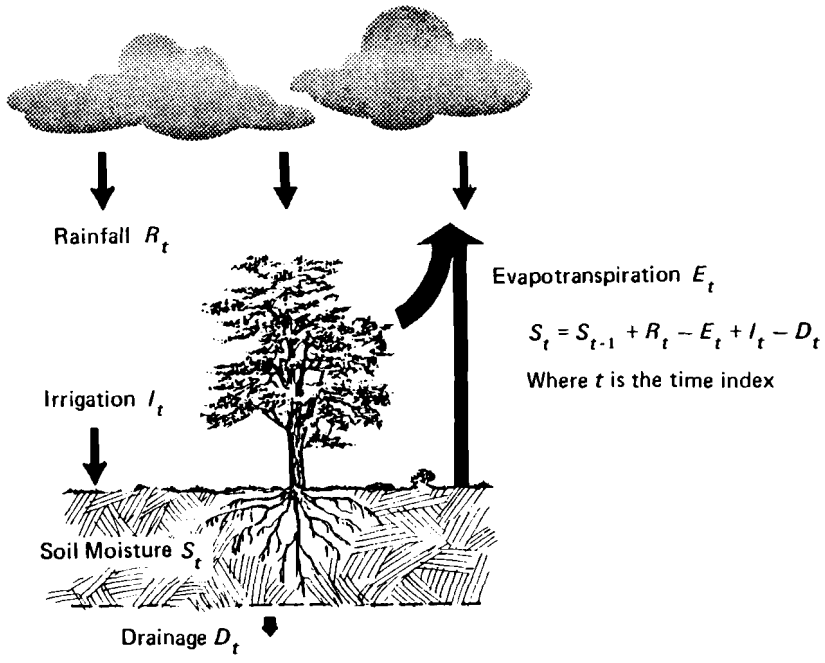

FIGURE D.1 Soil moisture balance model. Two analyses were done for each crop for average weather conditions (1961–1970) and for the 1-in-4 dry year (1961).

In the application of this model, a number of rules are specified to determine when irrigation and drainage occur. These are detailed in Section D.5. The calculations were done using a FORTRAN computer program that was run on the PDP 11/45 at IIASA; (a listing of the program is attached to the computational results in Gouevsky *et al.* (1978)).

The various components of the soil moisture balance model are described below in more detail.

D.2 RAINFALL

The mean monthly rainfall data recorded in Silistra from 1961 to 1970 are shown in Table D.1. To determine which year could be adopted as representing the 1-in-4 dry year, a probability analysis of both annual and irrigation season (May–September) rainfall is carried out (Chow 1964, Section 8).

In each case, the data are ranked according to depth of rainfall and assigned a rank number m ($m = 1$ for the greatest depth). The probability P that the actual rain fall R_a will equal or exceed each data value R is then estimated as:

$$P(R_a \geq R) = m/(n + 1) \qquad \text{(D.4)}$$

TABLE D.1 Monthly mean rainfall recorded at Silistra (mm).

Month	Year 1961	1962	1963	1964	1965	1966	1967	1968	1969	1970	Average 1961–70
Jan	27	20	35	6	0	161	26	56	15	8	35.4
Feb	28	38	45	21	36	8	18	14	130	82	42.0
Mar	24	40	18	8	25	43	27	14	18	58	27.5
Apr	27	71	21	11	34	23	12	1	48	26	27.4
May	58	38	34	39	137	50	16	8	53	104	53.7
Jun	38	12	31	67	31	116	80	36	136	54	60.1
Jul	54	21	21	30	33	20	31	66	99	55	43.0
Aug	29	2	26	68	6	37	52	58	36	104	41.8
Sep	0	3	31	107	0	92	36	49	10	2	33.0
Oct	17	20	11	33	6	31	22	32	0	56	22.8
Nov	9	41	7	37	54	151	4	65	4	36	40.8
Dec	41	23	40	24	60	96	53	21	186	16	56.0
Annual total	352	329	320	451	422	828	377	420	735	601	483.5

where n is the number of data (n = 10). The resulting probabilities are shown in Table D.2 and plotted in Figure 8. As an example of the exceedance probability calculations, consider the annual rainfall for 1961 (352 mm). This rainfall has rank 8 out of 10, so the probability that the observed rainfall in any given year will exceed 354 mm is estimated as 8/11 or 0.7273.

The rainfall in the 1-in-4 dry year will be exceeded in 3 years out of 4, or 75 percent of the time. The nearest exceedance probability to 0.75 is 0.7273 for rank m = 8. Since this probability happens to correspond to the year 1961 for both the annual and irrigation season rainfalls, the data for 1961 are adopted as representing the 1-in-4 dry year. It may be noted in passing that a similar attempt was made to locate an average year in Table D.2 (exceedance probability = 0.5), but no year was so clearly an average year as 1961 was a dry year. The nearest year to the average was 1968, for which a complete analysis of irrigation water use coefficients was carried out. It turned out, however, that the rainfall in March and April was abnormally low in 1968 so that the resulting irrigation water use coefficients were distorted by these unusual weather conditions. For this reason, the 1968 results were discarded and an average year was defined from the mean monthly data averaged over the 1961–70 period.

It would have been desirable to have a longer data series for rainfall to evaluate the design conditions more properly but, unfortunately, these data were not available. It would also have been desirable to use effective rather than total rainfall. The irrigation water use coefficients found from our analysis turn out to be a little higher, in most cases, than those computed by Vodproject, Sofia. If effective rainfall had been used, this difference would have been accentuated so this point was not pursued further.

TABLE D.2 Probability analysis of rainfall.

Rank (m)	Exceedance probability	May–September		Annual	
		Year	Rainfall (mm)	Year	Rainfall (mm)
1	0.0909	1969	334	1966	828
2	0.1818	1970	319	1969	735
3	0.2727	1966	315	1970	601
4	0.3636	1964	311	1964	451
5	0.4545	1968	217	1965	422
6	0.5454	1967	215	1968	420
7	0.6363	1965	207	1967	377
8[a]	0.7273	1961	179	1961	352
9	0.8182	1963	143	1962	329
10	0.9091	1962	76	1963	320

[a] 1-in-4 dry year.

D.3 EVAPOTRANSPIRATION

Evapotranspiration includes both evaporation of water from the soil surface and transpiration through the plant leaves. Since the contribution of these two components varies according to the stage of plant growth, the actual evapotranspiration E_t is found as:

$$E_t = k_c P_t \tag{D.5}$$

in which k_c is a coefficient depending on the crop and its stage of growth and P_t is the potential evapotranspiration (mm/10 days) for a reference crop (grass) grown over a wide area with unlimited soil moisture.

Potential evapotranspiration was computed using the Penman method as described by Doorenbos and Pruitt (1977). Of all the methods of measuring potential evapotranspiration without an evaporation pan, the Penman method has been found in many parts of the world to be one of the best. Potential evapotranspiration is found as the sum of an energy component (from solar radiation) and an aerodynamic component (from transport of the moisture away from the plant and soil surface).

This requires concurrent measured data on temperature, humidity, wind speed, and cloudiness. Monthly mean data for 1961–70 were obtained for the first three of these factors (Tables D.3 to D.5). Cloudiness was estimated by relating it to temperature using 1974 data. Temperature and cloudiness have a hysteresis-type relationship owing to the heating and cooling of the earth (Figure D.2). Given the monthly mean temperature the cloudiness can then be found. For radiation calculations Silistra is located at latitude 44° N.

TABLE D.3 Monthly mean temperature recorded at Silistra (°C).

Month	Year 1961	1962	1963	1964	1965	1966	1967	1968	1969	1970	Average 1961–70
Jan	−0.5	−1.5	−7.3	−4.7	1.3	−1.1	−2.3	−1.3	−5.5	0.5	−2.24
Feb	2.2	0.3	−0.2	0.3	−2.1	6.7	−0.3	3.9	−0.5	2.0	1.23
Mar	9.1	4.6	3.2	4.6	5.8	7.3	6.9	6.5	1.7	7.3	5.70
Apr	14.6	12.0	10.6	12.7	9.1	14.0	11.0	15.0	10.9	13.8	12.37
May	15.8	18.2	17.8	17.6	16.0	17.1	17.0	20.7	18.7	15.5	17.44
Jun	21.2	20.3	21.7	22.2	21.4	19.5	19.8	21.5	20.3	20.3	20.82
Jul	22.5	23.3	24.3	22.7	23.2	23.6	28.0	22.3	20.5	23.6	23.40
Aug	22.4	24.5	24.3	21.3	20.7	22.9	23.3	21.1	22.6	21.6	22.47
Sep	18.4	18.4	19.6	13.7	19.6	17.8	19.2	18.6	18.2	17.3	18.08
Oct	12.4	13.4	13.1	14.6	11.0	16.5	14.0	11.8	11.8	10.9	12.95
Nov	9.4	10.0	10.7	8.9	5.4	8.1	8.0	7.8	11.4	8.9	8.86
Dec	0.6	−1.5	−1.3	3.4	3.7	2.1	2.1	0.1	1.5	3.4	1.41

TABLE D.4 Monthly mean humidity recorded at Silistra (%).

Month	Year 1961	1962	1963	1964	1965	1966	1967	1968	1969	1970	Average 1961–70
Jan	83	89	82	83	83	88	81	82	84	86	84.1
Feb	80	81	83	83	77	80	83	82	87	82	81.8
Mar	65	77	75	80	77	74	75	67	86	73	74.9
Apr	66	70	73	65	74	74	67	56	70	68	68.3
May	77	66	72	72	72	68	67	62	62	74	69.2
Jun	72	65	60	71	67	70	70	66	73	71	68.5
Jul	65	65	67	65	63	66	62	66	76	68	66.3
Aug	64	59	62	67	65	70	80	73	68	72	68.0
Sep	62	67	66	74	69	74	74	73	74	69	70.2
Oct	79	75	73	76	70	78	80	75	71	76	75.3
Nov	79	86	70	84	83	89	80	89	66	76	80.2
Dec	81	85	85	87	89	85	81	85	89	86	85.3

TABLE D.5 Monthly mean wind speed recorded at Silistra (m/sec).

Month	Year 1961	1962	1963	1964	1965	1966	1967	1968	1969	1970	Average 1961–70
Jan	2.1	2.4	4.5	3.8	3.4	2.7	2.5	4.1	3.9	2.6	3.20
Feb	2.7	4.6	3.8	4.4	4.8	2.7	3.2	2.3	4.3	3.4	3.62
Mar	3.6	4.6	4.5	3.3	3.0	3.0	2.5	3.5	4.7	2.7	3.54
Apr	4.1	3.5	3.6	4.0	3.6	2.8	3.6	4.3	3.5	3.1	3.61
May	3.4	3.6	3.3	3.5	2.8	4.3	3.6	4.2	3.9	3.2	3.58
Jun	2.7	2.2	3.4	2.7	3.1	0.6	2.5	2.7	3.1	2.3	2.53
Jul	3.7	3.1	2.4	2.5	2.6	2.4	1.8	2.6	2.1	2.6	2.58
Aug	2.8	2.7	3.3	2.7	2.4	2.6	1.7	2.5	2.0	2.2	2.49
Sep	2.4	3.1	2.2	3.7	2.3	2.0	2.1	2.4	2.1	1.7	2.40
Oct	3.6	2.8	2.8	2.2	1.6	2.1	2.3	1.9	1.8	2.1	2.32
Nov	2.4	3.0	3.4	2.5	2.2	2.6	2.2	3.4	3.9	3.2	2.88
Dec	3.6	5.2	2.7	2.7	1.8	2.7	3.5	2.1	3.9	2.3	3.05

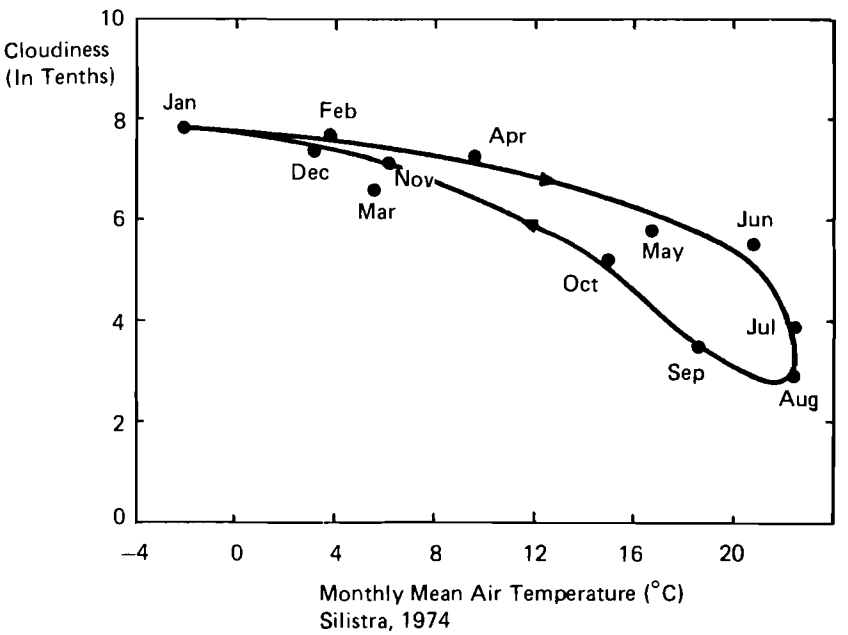

FIGURE D.2 Cloudiness and temperature.

All of these data are inputs to the calculation of potential evapotranspiration by the Penman method. The data obtained at each step in the calculations are shown in Table D.6, in which Doorenbos and Pruitt's notation is used. It may be noted that evapotranspiration is computed from March to October 1961, since the other months do not enter the soil moisture analysis. The average January temperature (– 2.24 °C) is too low to permit calculation of evapotranspiration.

The crop coefficients k_c are estimated for each plant and stage of growth also by reference to Doorenbos and Pruitt (1977). The scheduling of planting and harvesting in the Drustar complex was considered in defining the length and timing of the growing season for each crop. This growing season was further subdivided for definition of k_c according to the growth characteristics of each crop. Generally, actual evapotranspiration is around 0.4 of the potential when the crop has just been sown; the proportion rises as the crop grows to a maximum when full vegetative growth has been completed; as the grain is being formed evapotranspiration again falls below the potential. Values of k_c can therefore be defined for the various stages of crop growth, as shown in Figure D.3. The values adopted for each crop are shown in Table D.7.

D.4 SOIL MOISTURE CAPACITY

The soil moisture available to plants is contained in the depth d in meters of the soil penetrated by the roots. The amount of moisture contained in this zone varies with the characteristics of the soil. A water-holding capacity H (mm water/m soil) may be defined as the amount of water retained in the soil once it has been saturated and after all drainage has ceased. Soils with fine texture (silt-clay) have a high water-holding capacity (200 mm/m), while sandy soils have a lower value of H (60 mm/m).

Not all moisture contained in the soil is available to the plants because their roots do not penetrate everywhere and some water is bound very tightly to the soil particles. Some proportion p (usually 50 percent) of the total soil moisture is considered to be readily available to the plants. The plant can therefore be regarded conceptually as if it were sitting in a tank of water (see Figure D.4) whose capacity S_c is computed as:

$$S_c = pHd \tag{D.6}$$

For the Drustar complex, the fine chernozem soil is predominant, so a value of 200 mm/m (Doorenbos and Pruitt 1977: 86) is adopted for H. The values for p and d for each crop are given in Table D.8. The resulting values of S_c range from 24 mm (vegetables) to 220 mm (lucerne). As mentioned previously, it was not possible to estimate reliably the root depth d for orchards so the irrigation water use coefficients proposed for orchards by the Vodproject, Sofia, were adopted without further analysis.

TABLE D.6 Evapotranspiration data from Penman method.

	T_{av} (°C)	RH_{av} (%)	Wind (U) (m/sec)	Cloud (tenths)	e_a (mbar)	e_d (mbar)	$e_a - e_d$ (mbar)	$f(U)$	$1-W$	Aero. Term. $(1-W)f(U)$ (e_a-e_d)	R_a (mm/day)
Average 1961–70											
Feb	1.2	82	3.6	7.6	6.7	5.5	1.21	1.11	0.58	0.78	7.6
Mar	5.7	75	3.5	7.4	9.1	6.8	2.27	1.09	0.51	1.26	10.6
Apr	12.4	68	3.6	6.8	14.4	9.8	4.61	1.11	0.41	2.10	13.7
May	17.4	69	3.6	6.0	19.9	13.7	6.2	1.11	0.35	2.41	16.1
Jun	20.8	69	2.5	5.1	24.6	17.0	7.6	0.90	0.30	2.05	17.2
Jul	23.4	66	2.6	3.5	28.8	19.0	9.8	0.88	0.28	2.41	16.6
Aug	22.5	68	2.5	2.8	27.3	18.6	8.7	0.90	0.29	2.27	14.7
Sep	18.1	70	2.4	3.7	20.7	14.5	6.2	0.83	0.34	1.75	11.9
Oct	13.0	75	2.3	5.6	15.0	11.3	3.7	0.81	0.41	1.23	8.7
Nov	8.9	80	2.9	6.5	11.4	9.1	2.28	0.95	0.47	1.02	6.0
Dec	1.4	85	3.1	7.7	6.8	5.8	1.02	0.99	0.58	0.58	4.7
1961											
Mar	9.1	65	3.6	7.0	11.6	7.5	4.06	1.11	0.46	2.07	10.6
Apr	14.6	66	4.1	6.5	16.6	11.0	5.6	1.23	0.38	2.62	13.7
May	15.8	77	3.4	6.3	18.0	13.8	4.13	1.06	0.36	1.58	16.1
Jun	21.2	72	2.7	4.9	25.2	18.1	7.06	0.90	0.30	1.91	17.2
Jul	22.5	65	3.7	3.8	27.3	17.7	9.54	1.13	0.29	3.13	16.6
Aug	22.4	64	2.8	2.9	27.1	17.3	9.75	0.92	0.29	2.60	14.7
Sep	18.4	62	2.4	3.6	21.2	13.1	8.04	0.83	0.34	2.21	11.9
Oct	12.4	79	3.6	5.8	14.4	11.4	3.0	1.11	0.42	1.40	8.7

(TABLE D.6 *Continued.*)

	$^n/N$	R_a	R_{ns}	$f(T)$	$f(e_d)$	$f(^n/N)$	R_{nl}	R_n	W	Rad. Term. WR_n (mm/day)	P (mm/day)	P (mm/mo.)
Average 1961–70												
Feb	0.34	3.19	2.39	11.2	0.237	0.406	1.08	1.31	0.42	0.55	1.33	37
Mar	0.36	4.56	3.42	12.0	0.225	0.424	1.15	2.27	0.49	1.11	2.37	73
Apr	0.42	6.30	4.73	13.2	0.202	0.478	1.27	3.46	0.59	2.04	4.14	124
May	0.50	8.05	6.04	14.0	0.177	0.55	1.36	4.68	0.65	3.04	5.45	169
Jun	0.55	9.03	6.77	14.8	0.158	0.595	1.39	5.38	0.70	3.77	5.82	175
Jul	0.70	9.96	7.47	15.3	0.148	0.73	1.65	5.82	0.72	4.19	6.60	205
Aug	0.76	9.26	6.95	15.1	0.150	0.784	1.78	5.17	0.71	3.67	5.94	184
Sep	0.66	6.90	5.18	14.2	0.172	0.694	1.70	3.48	0.66	2.30	4.05	122
Oct	0.52	4.44	3.33	13.3	0.192	0.568	1.45	1.88	0.59	1.11	2.34	73
Nov	0.45	2.85	2.14	12.5	0.207	0.505	1.31	0.83	0.53	0.44	1.46	44
Dec	0.33	1.95	1.43	11.2	0.234	0.397	1.04	0.42	0.42	0.18	0.77	24
1961												
Mar	0.40	4.77	3.56	12.6	0.219	0.46	1.27	2.26	0.54	1.24	3.31	103
Apr	0.45	6.50	4.88	13.6	0.194	0.505	1.33	3.65	0.62	2.20	4.82	145
May	0.47	7.81	5.86	13.8	0.176	0.523	1.27	4.59	0.64	2.94	4.52	140
Jun	0.56	9.11	6.84	14.8	0.153	0.604	1.37	5.47	0.70	3.83	5.74	172
Jul	0.67	9.71	7.28	15.1	0.155	0.703	1.65	5.63	0.71	4.00	7.13	221
Aug	0.75	9.19	6.89	15.1	0.157	0.775	1.84	5.05	0.71	3.59	6.19	192
Sep	0.69	7.08	5.31	14.3	0.181	0.721	1.87	3.44	0.68	2.34	4.61	138
Oct	0.15	4.39	3.30	13.2	0.191	0.559	1.48	1.82	0.58	1.06	2.46	76

AFTER: Calculated using methodology from Doorenbos and Pruitt 1977.

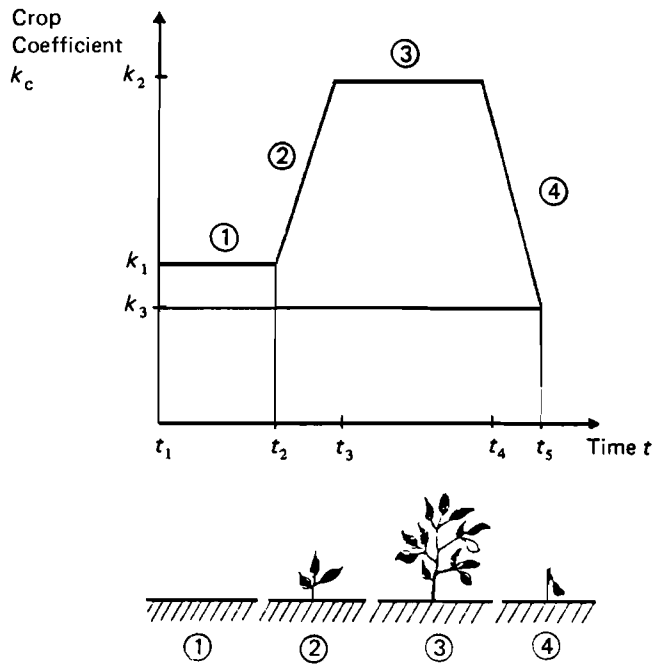

FIGURE D.3 Parameters of the crop coefficients.

TABLE D.7 Crop coefficients.

Crop	t_1	t_2	t_3	t_4	t_5	k_1	k_2	k_3
Lucerne[a,b]		3	7	19		0.38	0.80	
Maize silage[b]	7	10	14	19		0.38	1.00	
Maize silage II[b]	13	15	18	22		0.28	1.00	
Maize grain	5	8	12	18	22	0.38	1.00	0.55
Wheat[a]		3	6	10	13	0.38	1.00	0.25
Barley[a]		3	6	10	12	0.38	1.00	0.25
Soybeans	6	8	12	18	21	0.38	0.80	0.45
Sunflowers	3	6	10	15	18	0.38	0.90	0.4
Tobacco	5	8	12	15	18	0.38	0.90	0.4
Vegetables	6	9	12	18	21	0.38	1.00	0.4

MAR APR MAY JUN
NOTE: The time index t refers to 10-day periods as follows: 1 2 3 4 5 6 7 8 9 10 11 12
JUL AUG SEP OCT
13 14 15 16 17 18 19 20 21 22. Times given in the table refer to the beginning of the period. The stages of crop growth are shown in Figure D.3.

[a]No stage 1.

[b]No stage 4.

d = Depth
p = Proportion of Soil Water Available to Plant
H = Water-holding Capacity of the Soil

FIGURE D.4 Soil moisture capacity.

TABLE D.8 Values of d and p and resulting soil moisture capacity for each crop.

Crop	Root depth d (m)	Proportion p	Soil moisture capacity S_c (mm)[a]
Lucerne	2.0	0.55	220
Maize silage	1.5	0.50	150
Maize silage II	1.0	0.50	100
Maize grain	1.5	0.60	180
Wheat	1.2	0.55	132
Barley	1.2	0.55	132
Soybeans	1.0	0.50	100
Sunflowers	1.2	0.45	108
Tobacco	1.0	0.35	70
Vegetables	0.6	0.20	24

[a] $S_c = 200\,pd$.

It should be noted that the soil moisture capacities so computed refer to the water available to the plants, not to the total water in the soil. The soil moisture analysis described in Section D.5 also refers to this available water.

D.5 COMPUTATION OF CROP WATER USE COEFFICIENT

All of the input data needed to compute the crop water use coefficients I_t by means of Eq. (D.3) have now been developed. Rainfall and potential evapotranspiration may be compared in Table D.9. In an average year potential evapotranspiration exceeds rainfall from March through October or November, which creates a potential moisture deficit throughout the growing seasons. The accumulated precipitation over the winter months (November to February) exceeds potential evapotranspiration so the soil moisture reservoir can be assumed full on 1 March, the date on which the earliest field cultivation operations begin.

To facilitate the computation it is assumed that a standard depth of irrigation water of 60 mm could be applied in one irrigation during a 10-day period. This standard depth is also used by the Vodproject in their analysis for the Silistra

TABLE D.9 Rainfall and potential evapotranspiration for Silistra (mm/month).

	Potential Evapotranspiration		Rainfall	
Month	1961–70	1961	1961–70	1961
Jan			35	27
Feb	37		42	28
Mar	73	103	28	24
Apr	124	145	27	27
May	169	140	54	58
Jun	175	172	60	38
Jul	205	221	43	54
Aug	184	192	42	29
Sept	122	138	33	0
Oct	73	76	23	17
Nov	44		41	9
Dec	24		56	41

region. The choice of the 60-mm irrigation depth is made because most of the crops have more than 150 mm of available moisture; to refill this amount in one irrigation would require continuous sprinkling for about 1 day, which would probably be an excessive irrigation time because the land is sloping and the soil is susceptible to erosion.

The irrigation equipment is assumed to be of the "Blue Arrow" type which consists of stationary pipes and sprinklers that are towed by tractor from one position in the field to the next. Under standard conditions, "Blue Arrow" applies 6.9 mm/h so the 60-mm depth adopted corresponds to an irrigation time of 8.7 h in each position. This is consistent with the usual practice, enabling the sprinklers to be moved twice a day, once in the morning and once in the evening.

The computations are begun on 1 March when it is assumed that the soil moisture reservoir is full ($S_0 = S_c$). Rainfall and potential evapotranspiration are considered to be constant over the month and the values of R_t and P_t for each 10-day period are found as one-third of the monthly values given in Table D.9. To get E_t, Eq. (D.5) is used. Since the value of k_c in this equation can change within the month, E_t is not constant over the month. Computations proceed forward in time. Typically, in each 10-day period, a trial value S'_t of soil moisture at the end of the period is computed as:

$$S'_t = S_{t-1} + R_t - E_t \tag{D.7}$$

Various possibilities exist depending on the value of S'_t.

- If $S'_t > S_c$, then drainage D_t

$$D_t = S'_t - S_c \tag{D.8}$$

  occurs and the final soil moisture $S_t = S_c$
- If $S_c - 60 < S'_t \leqslant S_c$, then no irrigation or drainage occurs and $S_t = S'_t$
- If $S'_t \leqslant S_c - 60$, then irrigation I_t of 60 mm occurs and $S_t = S'_t + 60$

A slightly different procedure is adopted for vegetables since their S_c of 24 mm is so small. I_t is computed so as to meet the deficit of rainfall and no drainage is assumed to occur.

The calculations are terminated on 30 September since only harvesting remains to be done after this date. Near the end of the growing season it is not appropriate to continue irrigating grain crops because dryer soils encourage the formation of grain and make it easier for the harvesting machines to function. To account for this, the accumulated deficit S''_t until the end of the growing season is computed:

$$S''_t = \sum_{\tau=t+1}^{T} (E_\tau - R_\tau) \tag{D.9}$$

When the available soil moisture S_t is sufficient to meet this expected deficit, i.e., $S_t \geqslant S''_t$, then irrigation calculations are terminated. It should be noted that this soil moisture refers to available rather than total moisture in the soil. Allowing S_t to fall near zero at the end of the growing season means that the crop is at no time under moisture stress. Considerable moisture may still remain in the soil – see Eq. (D.6).

An example of this calculation for maize grain under average weather conditions is shown in Table D.10. Irrigation occurs when S'_t falls to 120 mm or below. The calculations are determined after period 16 because available soil moisture (S_t = 145 mm) is enough to meet the expected future deficit (S''_t = 136 mm).

In all, 20 analyses of this type are carried out (10 crops, 2 weather conditions). The values of I_t so derived for each irrigated crop in each 10-day period are then substituted into SWIM2's tableau in the column of that irrigated crop activity, and the row of that 10-day period and weather condition. SWIM2 computes $W(t)$ and X_{20} – see Eqs. (D.1) and (D.2) as part of its solution procedure, given also the estimate of irrigation efficiency detailed in section D.6. The sum over all periods of the I_t values for each crop is shown in Table D.11. The details of the distribution of I_t over time are contained in the computational results in Gouevsky *et al.* (1978).

D.6 IRRIGATION EFFICIENCY

The crop water use coefficients determined by the analysis described in the preceding sections represent the amount of water actually needed in the root

TABLE 10 Soil moisture balance for maize grain (Silistra region, average weather conditions, soil moisture capacity – 180 mm).

	March			April			May			June			July			August			September		
Period	1	2	3	4	5	6	7	8	9	10	11	12	13	14	15	16	17	18	19	20	21
P_t	24	24	24	41	41	41	56	56	56	58	58	58	68	68	68	61	61	61	41	41	41
k_c	0.38	0.38	0.38	0.38	0.38	0.38	0.38	0.48	0.59	0.69	0.79	0.90	1.00	1.00	1.00	1.00	1.00	0.89	0.78	0.66	0.55
E_t	9	9	9	16	16	16	21	27	33	40	46	52	68	68	68	61	61	54	32	27	23
R_t	9	9	9	9	9	9	18	18	18	20	20	20	14	14	14	14	14	14	11	11	11
S_{t-1}	180	180	180	180	173	166	159	156	147	132	172	146	174	180	126	132					
S'_t	180	180	180	173	166	159	156	147	132	112	146	114	120	126	72	85					
S_t	180	180	180	173	166	159	156	147	132	172	146	174	180	126	132	145					
S''_t																136	89	49	28	12	0
D_t	0	0	0	0	0	0	0	0	0	0	0	0	0	0	0	0					
I_t	0	0	0	0	0	0	0	0	0	60	0	60	60	0	60	60					

TABLE D.11 Crop water use coefficients (mm).

Crop	Average year	1-in-4 dry year
Lucerne	300	420
Maize silage	300	360
Maize silage II	180	300
Maize grain	300	420
Wheat	60	120
Barley	60	120
Soybeans	300	360
Sunflowers	240	300
Tobacco	250	300
Vegetables	450	530
Orchards	180	240

zone of the plants. To find the corresponding amount of water needed to be withdrawn from the Danube River, estimates of leaching requirements and irrigation efficiency must be made.

The quality of the irrigation water withdrawn from the Danube River is not high. Drinking water for livestock must be pumped from groundwater. Although no data on water quality were obtained during the course of the project, it may be presumed that the Danube River contains some salts and other wastes from the six countries upstream of Silistra. To ensure that these salts do not remain in the root zone following irrigation and cause soil salinization and crop damage, enough extra water must be irrigated onto the land to wash, or leach, the salts down through the root zone of the plants. This leaching requirement is estimated to be 15 percent of the intake water using the procedure of Ayers and Westcot (1976). Local experts in Silistra say that problems of soil salinization or drainage associated with irrigation in the Drustar complex have not yet occurred on the 11,400 ha under irrigation, but such problems may occur in the future.

Irrigation efficiency estimates must account for the losses in bringing water to the field and in applying it to the soil. Using the procedure of Bos and Nugteren (1974), application losses are estimated at 30 percent of intake water. These losses are due to the evaporation of water between the time it leaves the sprinkler and the time it hits the ground, and to the nonuniform areal distribution of sprinkling.

Losses of 5 percent have been allowed in the conveyance system. These are rather low but may be attainable in the Drustar complex because the water is pumped in a closed system diirectly up from the Danube River to the fields. These data for losses assume very efficient management of irrigation.

The total of the losses and leaching requirements is 50 percent of the intake water from the Danube (Figure D.5). While this percentage may seem rather low,

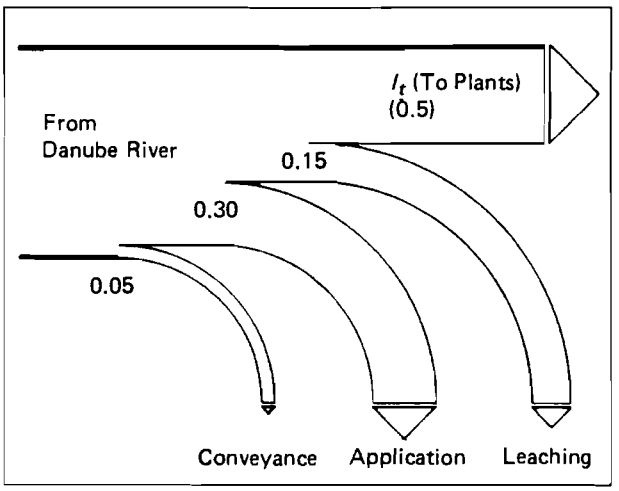

FIGURE D.5 Components of water use.

the international survey carried out by Bos and Nugteren (1974) demonstrates that only a very few irrigation projects have a project efficiency (water used by crop/intake water from source) as high as 50 percent. Most often the efficiency is around 30 percent. Thus the estimate of 50 percent made here could be assumed as being near the maximum attainable and is consistent with the goals of advanced technology and efficient management adopted by the planners of the Drustar complex.

Appendix E

MATHEMATICAL DESCRIPTION OF SWIM2

This appendix formalizes the description of the model in Section 2. Following Figure 5, all input resources, crop production alternatives, crop products, and livestock variables have been designated by X, Y, V, and Q, respectively. The further subdivision of these variables is explained below.

E.1 OBJECTIVE FUNCTION

The objective function OB adopted for the Drustar agricultural–industrial complex maximizes the annual net benefit, i.e., the difference between the benefit from the marketed products and the total production cost in the complex:

$$OB = \max\Bigg[\underbrace{\sum_{j=1}^{4} b_j Q_j}_{\substack{\text{livestock}\\ \text{production}\\ \text{benefits}}} + \underbrace{\sum_{g=14}^{24} b_g V_g}_{\substack{\text{crop pro-}\\ \text{duction}\\ \text{benefits}}} - \underbrace{\sum_{r=1}^{24} P_r X_r}_{\substack{\text{input re-}\\ \text{sources}\\ \text{cost}}}$$

$$- \underbrace{\sum_{s=1}^{3}\sum_{i=1}^{11}\sum_{k=1}^{2}\sum_{q=1}^{2} C_{si}^{kq}\, Y_{si}^{kq}}_{\substack{\text{crop}\\ \text{production}\\ \text{cost}}} - \underbrace{\sum_{i=1}^{11} C_i W_i}_{\substack{\text{crop pro-}\\ \text{cessing}\\ \text{cost}}} - \underbrace{\sum_{j=1}^{4} C_j Q_j}_{\substack{\text{live-}\\ \text{stock pro-}\\ \text{duction}\\ \text{cost}}}\Bigg] \qquad \text{(E.1)}$$

where

Q_j is the number of animals j; $j = 1$ (cows), $j = 2$ (sheep), $j = 3$ (pigs), $j = 4$ (hens)

b_j is the export benefit from animal j (Lv/animal)

V_g is the amount of crop product g for export, for meeting population demands, or for reserves; $g = 14$ (cooking oil), $g = 15$ (flour), $g = 16$ (domestic fruits), $g = 17$ (export fruits), $g = 18$ (tobacco), $g = 19$ (vegetables), $g = 20$ (reserves of maize grain), $g = 21$ (reserves of wheat), $g = 22$ (reserves of barley), $g = 23$ (reserves of soybeans), and $g = 24$ (reserves of sunflowers)

b_g is the benefit from commodity g (Lv/ton)

X_r is the amount of input r required for the crop and livestock production in the complex, $r = 1, \ldots, 24$

P_r is the price (Lv/unit of resource) of input r

Y_{si}^{kq} is amount of land (ha) in subregion s, $s = 1, 2, 3$, needed for production of crop i on irrigated ($k = 1$) or nonirrigated ($k = 2$) land with 80-percent fertilizer application ($q = 1$) or 100-percent fertilizer application ($q = 2$). The crops i are as follows: $i = 1$ (lucerne), $i = 2$ (maize silage), $i = 3$ (maize silage II), $i = 4$ (maize grain), $i = 5$ (wheat), $i = 6$ (barley), $i = 7$ (soybeans), $i = 8$ (sunflowers), $i = 9$ (orchards), $i = 10$ (tobacco), and $i = 11$ (vegtables)

C_{si}^{kq} is the cost (Lv/ha) for producing crop i on land located in subregion s with technologies k and q

W_i is the amount (tons) of total crop product i subject to processing, $i = 1, \ldots, 11$

C_i is the cost (Lv/ton) of processing (grain drying, transportation to storage) of crop product i

C_j is the cost (Lv/animal) of providing farm houses for animal j

E.2 CONSTRAINTS

There are three general types of constraints in the model: physical constraints (irrigated and nonirrigated land, water and fertilizer availability), demand constraints, and material balance constraints (equations). For ease in comparing the mathematical description and the linear programming format, the constraints are expressed in detail.

E.2.1 Physical Constraints

E.2.1.1 IRRIGATED LAND

The amount of land already developed and the amount to be developed are constrained in the three subregions by the following inequalities:

$$\sum_{\substack{i=1 \\ i \neq 3}}^{11} \sum_{q=1}^{2} Y_{si}^{1q} - I_s \leqslant EI_s \qquad s = 1,2,3 \tag{E.2}$$

where

Y_{si}^{1q} is the area (ha) of crop i planted in subregion s on irrigated land ($k = 1$) at rate of fertilizer application q

I_s is the amount of irrigated land (ha) to be developed in subregion s

EI_s is the amount (ha) of irrigated land already developed in subregion s; EI_s is a given constant for all s

E.2.1.2 IRRIGATED AND NONIRRIGATED LAND IN EACH SUBREGION

SWIM2 accounts explicitly for crops planted on irrigated and nonirrigated land in the following way:

$$\sum_{\substack{i=1 \\ i\neq 3}}^{11} \sum_{q=1}^{2} Y_{si}^{2q} + I_s + AS \leqslant AL_s \qquad s = 1,2,3 \tag{E.3}$$

where

Y_{si}^{2q} is the area (ha) of crop i in subregion s fertilized at rate q on nonirrigated land ($k = 2$)

AL_s is the total arable land (ha) in subregion s

AS is the area (ha) of crops for seeds (crops for seeds are planted on nonirrigated area only in region 2, i.e., $AS = 0$ for $s = 1,3$)

E.2.1.3 TOTAL IRRIGATED LAND TO BE DEVELOPED

$$IL = \sum_{s=1}^{3} I_s \tag{E.4}$$

where IL is the total irrigated land (ha) to be developed in the region

E.2.1.4 AREAS OF TOBACCO, ORCHARDS AND MAIZE SILAGE II

Although tobacco and orchards may be grown on irrigated or nonirrigated areas, the total amount of land occupied by the crops is restricted.

$$\sum_{k=1}^{2} \sum_{q=1}^{2} Y_{si}^{1q} \leqslant A_{is} \qquad s = 1,2,3 \qquad i = 9,10 \tag{E.5}$$

where

A_{is} is the area (ha) allowed for growing orchards ($i = 9$) and tobacco ($i = 10$) on subregion s

$$\sum_{q=1}^{2} Y_{s3}^{1q} - 0.5 \sum_{q=1}^{2} Y_{s5}^{1q} - \sum_{q=1}^{2} Y_{s6}^{1q} \leqslant 0 \qquad s = 1,2,3 \tag{E.6}$$

where

Y_{s3}^{1q} is the area (ha) of maize silage II planted on half of the area Y_{s5}^{1q} of wheat, and all the area Y_{s6}^{1q} of barley in subregion s using technology q; $k = 1$ because maize silage II is grown only on irrigated area

E.2.1.5 CROP ROTATION

Crop rotation is taken into account in SWIM2 by constraining the ratio of field crops (lucerne, wheat, and barley; $i = 1, 5, 6$) to interrow-cultivated crops (maize silage, maize grain, soybeans, and sunflowers ($i = 2, 4, 7, 8$)).

$$\sum_{i=1,5,6} \sum_{s=1}^{3} \sum_{k=1}^{2} \sum_{q=1}^{2} Y_{si}^{kq} - 0.95 \sum_{i=2,4,7,8} \sum_{s=1}^{3} \sum_{k=1}^{2} \sum_{q=1}^{2} Y_{si}^{kq} \geqslant 0 \quad \text{(E.7)}$$

$$\sum_{i=1,5,6} \sum_{s=1}^{3} \sum_{k=1}^{2} \sum_{q=1}^{2} Y_{si}^{kq} - 1.3 \sum_{i=2,4,7,8} \sum_{s=1}^{3} \sum_{k=1}^{2} \sum_{q=1}^{2} Y_{si}^{kq} \leqslant 0 \quad \text{(E.8)}$$

E.2.2 Demand Constraints

This set of constraints spells out all crop and livestock production requirements for population, export, and reserves.

E.2.2.1 CROP CONSTRAINTS

The amount of crop products generated from each crop is as follows (all amounts are in tons unless otherwise indicated):

$$W_i = \sum_{s=1}^{3} \sum_{k=1}^{2} \sum_{q=1}^{2} d_{si}^{kq} Y_{si}^{kq} \qquad i = 1, \ldots, 11 \quad \text{(E.9)}$$

where

d_{si}^{kq} is crop yield (ton/ha)
W_i is total crop production of crop i

Some of the crop products W_i are processed further to obtain subproducts V_g in the following way:

E.2.2.1.1 Lucerne Subproducts.

$$W_1 = \sum_{g=1}^{4} a_{1g} V_g \quad \text{(E.10)}$$

where

W_1 is lucerne production
V_g, $g = 1, 2, 3, 4$, are the amounts of lucerne green chop, hay, haylage, and silage, respectively

a_{1g} is a rate of conversion of lucerne production into green chop, hay, haylage, and silage

E.2.2.1.2 Maize Silage Balance

$$V_5 = W_2 + W_3 \tag{E.11}$$

where

V_5 is the total amount of maize silage
W_2 is the amount of maize silage
W_3 is the amount of maize silage II

E.2.2.1.3 Wheat Subproducts

$$W_5 = M_w + V_8 + V_{21} \tag{E.12}$$

$$V_{15} = a_F M_w \tag{E.13}$$

$$V_{15} \geqslant PF \tag{E.14}$$

$$V_{13} = a_B M_w \tag{E.15}$$

where

W_5 is wheat grain production
M_w is wheat milled for flour and bran
V_8 is the amount of wheat feedstuff
V_{21} is the amount of wheat reserves
V_{15} is flour production
a_F is the amount of flour produced from one ton of wheat
PF is the amount of flour for meeting population requirements
V_{13} is bran production
a_B is the amount of bran produced from one ton of wheat; note that $a_F + a_B < 1$ because of losses associated with flour and bran production

E.2.2.1.4 Sunflower Subproducts

$$W_8 = V_9 + V_{24} \tag{E.16}$$

$$V_{14} = a_L V_9 \tag{E.17}$$

$$v_{14} = \geqslant \text{Oil} \tag{E.18}$$

$$V_{12} = a_M V_9 \tag{E.19}$$

where

W_8 is sunflower grain production
V_9 is sunflower for oil and meal production
V_{24} is the amount of sunflower reserves
V_{14} is sunflower oil production
V_{12} is sunflower meal production
a_L and a_M are the amount of oil and meal in one ton of sunflower production; $a_L + a_M < 1$ since amounts of oil and sunflower meal cannot exceed the total sunflower production

Oil is the specified amount of cooking oil for meeting population requirements

E.2.2.1.5 Other Grain Products Balance

$$W_4 = V_6 + V_{20} \tag{E.20}$$

$$W_6 = V_7 + V_{22} \tag{E.21}$$

$$W_7 = V_{10} + V_{23} \tag{E.22}$$

where

W_4, W_6, and W_7 are the amounts of maize grain, barley, and soybeans
V_6, V_7, and V_{10} are the amounts of maize grain feedstuff, barley feedstuff, and soybeans feedstuff
V_{20}, V_{22}, and V_{23} are amounts of reserves of maize grain, barley, and soybeans

E.2.2.1.6 Roughage Production. Various roughages (stalks, straw) can be processed further to obtain forage for some of the animals (cows, sheep). In the model only the nutrient content of stalks and straw is taken into account in the following way:

$$V_{11} = \sum_{s=1}^{3} \sum_{\substack{i=4 \\ i \neq 7}}^{8} \sum_{k=1}^{2} \sum_{q=1}^{2} f_{si}^{kq} Y_{si}^{kq} \tag{E.23}$$

where

f_{si}^{kq} is the feed unit content per hectare of crop i planted in subregion s using technologies k and q
V_{11} is the total amount of feed units of the roughage forage

E.2.2.1.7 Fruit Production

$$W_9 = V_{16} + V_{17} \tag{E.24}$$

$$V_{16} \geqslant PR \tag{E.25}$$

where

W_9 is total fruit production
V_{16} is fruit production for domestic consumption PR
V_{17} is fruit production for export

E.2.2.1.8 Tobacco and Vegetable Production. Tobacco and vegetables are not subject to any constraints except for the constrained area already explained in Section E.2.1.4. Tobacco and vegetable products are denoted by V_{18} and V_{19}

E.2.2.1.9 Crop Production Reserves. To meet crop production requirements in case of drought, reserves are built up in the following way:

$$V_g = h \sum_{s=1}^{3} \sum_{k=1}^{2} \sum_{q=1}^{2} Y_{sg}^{kq} (d_{sg}^{kq} - d^{-kq}_{sg}), \qquad g = 20,21,22,23,24 \tag{E.26}$$

where

V_g is the amount of reserves of crop product g
$g = 20$ (maize grain), $g = 21$ (wheat), $g = 22$ (barley)
$g = 23$ (soybeans), $g = 24$ (sunflowers)
h is a coefficient taking into account how many successive years in a given sequence are dry
Y_{sg}^{kq} is the area of crop i producing crop product g, $i = 4, 5, 6, 7, 8$ for $g = 20, 21, 22, 23, 24$, respectively
d_{sg}^{kq} is the crop yield of crop i producing crop product g in normal weather
d^{-kq}_{sg} is the crop yield of crop i producing crop product g in dry weather

E.2.2.2 LIVESTOCK PRODUCTION CONSTRAINTS

E.2.2.2.1 Livestock Feedstuff. There are five types of feedstuff required by the animals in the complex: green forage, hay, silage, concentrated forage, and roughage. To account for them the following equations are introduced:

$$F_g = V_1 f_{1g} \tag{E.27}$$

$$F_h = V_2 f_{2h} \tag{E.28}$$

$$F_s = (V_3 f_{3s} + V_4 f_{4s} + V_5 f_{5s}) \tag{E.29}$$

$$F_r = V_{11} \tag{E.30}$$

$$F_c = (V_6 f_{6c} + V_7 f_{7c} + V_8 f_{8c} + V_{10} f_{10c} + V_{13} f_{13c} + V_{15} f_{15c}) \tag{E.31}$$

where

F_g, F_h, F_s, F_r, and F_c are total amounts of feed units (f.u.) of green forage, hay, silage, roughage, and concentrated forage available to animals

V_1 is the amount of green forage (tons)

V_2 is the amount of hay (tons)

V_3, V_4, and V_5 are the amounts (tons) of lucerne haylage, silage, and maize silage (including maize silage II)

V_{11} is the amount of roughage feed units

V_6, V_7, V_8, V_{10}, V_{13}, and V_{15} are the amounts (tons) of maize grain, barley, wheat, soybean, bran, and sunflower meal allocated to livestock production

$f_{1g}, \ldots, f_{15c}$ is the feed unit content in 1 ton of each product

E.2.2.2.2 Livestock Diets. To ensure certain productivity of animals, they have to be fed by some or by all of the products specified in Eqs. (E.27)–(E.31). Furthermore, each animal diet is specified within the following upper and lower limits:

$$Q_j D_{\alpha j}^{\min} \leqslant F_\alpha j \leqslant Q_j D_{\alpha j}^{\max} \qquad \alpha = \text{g,h,s,r,c} \qquad j = 1,2,3,4 \tag{E.32}$$

$$\sum_{\text{all } \alpha} F_{\alpha j} \geqslant A_j \qquad j = 1,2,3,4 \tag{E.33}$$

$$\sum_{j=1}^{4} F_{\alpha j} = F_\alpha \qquad \alpha = \text{g,h,s,r,c} \tag{E.34}$$

where

Q_j is the number of animals j, $j = 1$ (cows), $j = 2$ (sheep), $j = 3$ (pigs), $j = 4$ (hens)

$D_{\alpha j}^{\min}$ and $D_{\alpha j}^{\max}$ are the minimum and maximum amount of feed units of feedstuff α required by animal j

$F_{\alpha j}$ is the total amount of feed units fed to animal j

A_j is the total amount of feed units required by animal j

F_α is the total amount of feed units of feedstuff α required in the complex

E.2.2.2.3 Protein Content of Livestock Feedstuff. Feed units are the energetic component of animal diets. The other component to be supplied to livestock is protein. There are several ways to account for protein content in the

livestock diets; the simplest one has been chosen, i.e., to specify the ratio B of high-protein feeds to low-protein ones:

$$V_{10} + V_{12} \geqslant B(V_6 + V_7 + V_8 + V_{13}) \qquad \text{(E.35)}$$

where

V_{10} and V_{12} are the tons of soybeans and sunflower meal in livestock diets
V_6, V_7, V_8, and V_{13} are the tons of maize grain, barley, wheat, and wheat bran in livestock diets

E.2.2.2.4 Livestock Balance. To account for the existing livestock and that which is to be developed in the future, the following equations are introduced in SWIM2:

$$(Q_j - Q_j^E) + I_j - Q_j^D = 0 \qquad j = 1,2,3,4 \qquad \text{(E.36)}$$

where

Q_j is the total number of animals j grown in the complex
Q_j^D is the number of animals j to be developed in the complex
Q_j^E is the number of existing animals j
$I_j \geqslant 0$ is a dummy variable, i.e., the number of animals to be developed Q_j^D is equal to 0 if $Q_j < Q_j^E$, and $Q_j^D = Q_j - Q_j^E$ if $Q_j - Q_j^E$; in other words, either I_j or Q_j^D is equal to 0.

In addition to Eq. (E.36) there are three more equations that keep the ratio between animals in a certain proportion corresponding to their present numbers.

$$Q_j = R_j Q_1 \qquad j = 2,3,4 \qquad \text{(E.37)}$$

where

R_j is the ratio of the number of animals of type j to the present number of the first animal (cows)

Constraint (E.37) is relaxed when SWIM2 is used as a forecasting tool.

E.2.3 Material Balance of Input Resources

The material balance equations, while not actual constraints, take into account various inputs to crop and livestock production, like seeds, fertilizers, water, machinery, labor, fuel, and capital investments. The structure of SWIM2 allows these inputs to be constrained when necessary, as was done with water, capital investments, and fertilizers.

E.2.3.1 SEED REQUIREMENTS

SWIM2 computes the amount of all seeds and the respective seed areas required for growing crops.

$$X_r = \sum_{s=1}^{3} \sum_{k=1}^{2} \sum_{q=1}^{2} S_{sr}^{kq} Y_{sr}^{kq} \qquad r = 1,5,6,7,8 \tag{E.38}$$

$$X_2 = \sum_{s=1}^{3} \sum_{k=1}^{2} \sum_{g=1}^{2} \sum_{r=1}^{4} S_{sr}^{kq} Y_{sr}^{kq} \tag{E.39}$$

where

X_r is the number of tons of seeds required to produce crop r; $r = 1$ (lucerne), $r = 2$ (maize silage), $r = 3$ (maize silage II), $r = 4$ (maize grain), $r = 5$ (wheat), $r = 6$ (barley), $r = 7$ (soybeans), $r = 8$ (sunflowers)

Y_{sr}^{kq} is the amount of land (ha) occupied by crop r in subregion s with irrigation ($k = 1$) or without ($k = 2$) using fertilizer application rate q

S_{sr}^{kq} is the seeding rate (ton/ha) required to produce crop r on irrigated ($k = 2$) land using fertilizer application rate q

Equation (E.39) takes care of different crops using the same kind of seeds; in our case these crops are maize silage, maize silage II, and maize grain.

To determine the total seed area the following equation has been introduced in SWIM2:

$$AS = \sum_{s=1}^{3} \sum_{r=1}^{8} \sum_{k=1}^{2} \sum_{q=1}^{2} \frac{S_{sr}^{kq}}{d_{sr}^{kq}} Y_{sr}^{kq} \tag{E.40}$$

where

AS is the area (ha) occupied by all seeds

d_{sr}^{kq} is the crop yield (tons/ha); in SWIM2 $k = 2$ because seeds are grown on nonirrigated land

E.2.3.2 FERTILIZER REQUIREMENTS

There are three essential types of fertilizers used in the Drustar complex: ammonium sulfate, superphosphate, and potassium sulfate. The first set of constraints describes the required amount of each fertilizer:

$$x_r = \sum_{s=1}^{3} \sum_{i=1}^{11} \sum_{k=1}^{2} \sum_{q=1}^{2} f_{sir}^{kq} Y_{si}^{kq} - AP \sum_{j=1}^{4} m_{jr} Q_j \qquad r = 9,10,11 \tag{E.41}$$

where

x_r is the amount of fertilizer r required in the complex (tons); $r = 9$ (ammonium sulfate), $r = 10$ (superphosphate), $r = 11$ (potassium sulfate)

f_{sir}^{kq} is the fertilizer rate of fertilizer r for crop i planted in subregion s using technologies k and q (tons/ha)

Q_j is the number of animals of type j

m_{jr} is the amount of animal waste (manure) generated by animal j that can substitute for one ton of fertilizer r (tons/animal)

AP is the amount of manure that can be utilized: $0 \leqslant AP < 1$; this coefficient takes care of the fact that (a) manure is generated all year but it is used only during a few months, and (b) farm houses are concentrated on a restricted number of places and the use of the whole amount of manure involves substantial transportation costs

E.2.3.3 FUEL REQUIREMENTS

Fuel is required for operating tractors, various combines, and grain processing equipment. The total amount of fuel required, X_{12}, is determined by the following equation:

$$x_{12} = \sum_{i=1}^{11} \sum_{s=1}^{3} \sum_{k=1}^{2} \sum_{q=1}^{2} L_{si}^{kq} Y_{si}^{kq} \tag{E.42}$$

where

L_{si}^{kq} is the fuel rate for production of crop i in subregion s using technologies k and q (liters/ha)

E.2.3.4 LABOR REQUIREMENTS

The labor is actually the machine-hours of field work needed (assuming 1 operator/machine). SWIM2 does not account for labor required in the processing industry because these activities are not considered in detail in the model.

In principle, all machine-hours could be lumped together to obtain the total number of hours required. In this study, however, we separate machine-hours required for tractors, combines (June and July), and combines (August and October). The latter two can be operated by people coming from outside the region.

$$X_{13} = \sum_{i=1}^{11} \sum_{s=1}^{3} \sum_{k=1}^{2} \sum_{q=1}^{2} t_{si}^{kq} Y_{si}^{kq} \tag{E.43}$$

where

t_{si}^{kq} is the number of tractor-hours per hectare required for field activities on crop area Y_{si}^{kq}

X_{13} is the total number of tractor-hours for the whole corp area

$$X_{14} = \sum_{i=5}^{6} \sum_{s=1}^{3} \sum_{k=1}^{2} \sum_{q=1}^{2} CJ_{si}^{kq} Y_{si}^{kq} \tag{E.44}$$

where

CJ_{si}^{kq} is the number of combine-hours per hectare in June and July required for the harvesting of crop area Y_{si}^{kq}; $i = 5$ (wheat), $i = 6$ (barley)

$$X_{15} = \sum_{i=4,7,8} \sum_{s=1}^{3} \sum_{k=1}^{2} \sum_{q=1}^{2} CA_{si}^{kq} Y_{si}^{kq} \tag{E.45}$$

where

CA_{si}^{kq} is the number of combine-hours per hectare in August and September required for the harvesting of crop area Y_{si}^{kq}; $i = 4$ (maize grain), $i = 7$ (soybeans), $i = 8$ (sunflowers)

E.2.3.5 MACHINERY REQUIREMENTS

To convert the machine-hours already specified in the last section into a more meaningful number, which is the number of machines needed, an estimate has to be made about the critical time in the combination of activities on all crops when all tractors or combines are put into use.

E.2.3.5.1 Tractor Requirements

$$X_{16} = \frac{1}{T_t} \sum_{\substack{i=1 \\ i \neq 5,6}}^{11} \sum_{s=1}^{3} \sum_{k=1}^{2} \sum_{q=1}^{2} m_{si}^{kq} Y_{si}^{kq} \tag{E.46}$$

where

X_{16} is the total number of tractors needed for crop production

m_{si}^{kq} is the number of machine hours per hectare for crop i planted in subregion s using technologies k and q over the critical period. In our case, this period is from 20 March to 20 April (see Table A.7)

T_t is the total number of hours available over the critical period; $T_t = (D - Dw)W_t$, where D is the number of calendar days in the critical period; D_w is the number of days taken off because of holidays or bad weather conditions in this period; W_t is working hours per day

E.2.3.5.2 Combine Requirements

$$X_{17} = \frac{1}{T_c} \sum_{i=4,7,8} \sum_{s=1}^{3} \sum_{k=1}^{2} \sum_{q=1}^{2} mc_{si}^{kq} Y_{si}^{kq} \tag{E.47}$$

where

X_{17} is the total number of combines needed for crop harvesting

mc_{si}^{kq} is the number of machine hours per hectare for harvesting of crop i planted in subregion s using technologies k and q

T_c is the total number of hours available over the critical period; T_c is determined in the same way as T_t in (E.46).

E.2.3.5.3 Silage Chopper Requirements.

$$X_{18} - \frac{1}{T_{sc}} \sum_{i=2}^{3} \sum_{s=1}^{3} \sum_{k=1}^{2} \sum_{q=1}^{2} ms_{si}^{kq} Y_{si}^{kq} \qquad \text{(E.48)}$$

where

X_{18} is the number of silage choppers required

ms_{si}^{kq} is the number of machine hours per hectare for harvesting of maize silage and maize silage II over the critical period

T_{sc} is the total number of hours available over the critical period

E.2.3.5.4 Irrigation Equipment Requirements. To evaluate the amount of irrigation equipment, the productivity of this equipment (hectares per sprinkler) has to be found as well as the schedule of crop irrigation. The latter is needed to avoid excessive investment in a piece of equipment, i.e., to account for the fact that this equipment can be moved from one place to another over the irrigation season to irrigate different crops.

The information given in Table A.6 can serve as a guideline to determine the amount of irrigation equipment. It is obvious from this table that irrigation equipment for maize silage II is complementary to that for sunflowers. On the other hand, the equipment for wheat and barley can be combined and made complementary to that for all other crops. All these relationships can be formalized as follows:

$$X_{19} = \frac{1}{S_p} \left[\sum_{\substack{i=1 \\ i \neq 3,5,6}}^{11} \sum_{s=1}^{3} \sum_{q=1}^{2} Y_{si}^{1q} \right] + E^3 + E^{5,6} + D - EI \qquad \text{(E.49)}$$

where

S_p is the productivity of the irrigation equipment (ha/sprinkler)

Y_{si}^{1q} are irrigated areas of crop i planted in subregion s using technology q

E^3 is the extra irrigation equipment needed for maize silage II

$E^{5,6}$ is the extra irrigation equipment needed for wheat and barley

X_{19} is the total amount of new irrigation equipment needed

EI is the amount of existing irrigation equipment

D is a dummy variable: the amount of new irrigation equipment X_{19} is equal to zero if

$$\frac{1}{S_p}[\cdot] + E^3 + E^{5,6} < EI$$

and

$$X_{19} = \frac{1}{S_p}[\cdot] + E^3 + E^{5,6} - EI$$

if

$$\frac{1}{S_p}[\cdot] + E^3 + E^{5,6} \geqslant EI$$

In other words, either X_{19} or D is equal to zero.

The variables E^3 and $E^{5,6}$ are determined by Eqs. (E.50) and (E.51). Equation (E.50) takes into account that maize silage II is complementary to sunflowers, and Eq. (E.51) that wheat and barley are complementary to all other crops (except vegetables).

$$\frac{1}{S_p}\left[\sum_{s=1}^{3}\sum_{q=1}^{2} Y_{s8}^{1q} - \sum_{s=1}^{3}\sum_{q=1}^{2} Y_{s3}^{1q}\right] + E^3 - D^3 = 0 \qquad \text{(E.50)}$$

$$\frac{1}{S_p}\left[\sum_{i\neq 5,6,8}^{10}\sum_{s=1}^{3}\sum_{q=1}^{2} Y_{si}^{1q} - \sum_{i=5}^{6}\sum_{s=1}^{3}\sum_{q=1}^{2} Y_{si}^{1q}\right] + E^3 + E^{5,6} - D^{5,6} = 0 \qquad \text{(E.51)}$$

where

$E^{5,6}$ is the amount of extra irrigation equipment needed for wheat and barley; D^3 and $D^{5,6}$ are dummy variables with the same properties as D in (E.49).

E.2.3.5.5 Water Availability. SWIM2 accounts for both the total amount of irrigation water over time in normal weather and dry weather, and for the livestock drinking water.

The total amount of water for irrigation is determined by the following equation:

$$W(t) = \frac{1}{e}\sum_{i=1}^{11}\sum_{s=1}^{3}\sum_{q=1}^{2} I_{si}^{q}(t) Y_{si}^{q} \qquad t = 1, \ldots, T \qquad \text{(E.52)}$$

where

$I_{si}^{q}(t)$ is the irrigation water use coefficient in normal weather (m^3/ha) of crop i planted in subregion s using technology q at time t; t is a time index in 10-day periods over the irrigation season

$W(t)$ is the amount of water required for all crops at time t
e is irrigation efficiency

The irrigation water demanded by each of the three regions is:

$$W_s = \frac{1}{e} \sum_{i=1}^{11} \sum_{q=1}^{2} \sum_{t=1}^{15} I_{si}^{q}(t) Y_{si}^{q} \qquad s = 1,2,3 \tag{E.53}$$

The total irrigation water demanded, X_{20}, in the complex is $\Sigma_{s=1}^{3} W_s$.

SWIM2 also computes irrigation water demands in case of a dry year, X_{21}, in the following way:

$$X_{21} = \sum_{i=1}^{11} \sum_{s=1}^{3} \sum_{q=1}^{2} \sum_{t=1}^{15} \tilde{I}_{si}^{q}(t) Y_{si}^{q} \tag{E.54}$$

where

$\tilde{I}_{si}^{q}(t)$ is the irrigation water use coefficient in dry weather (m^3/ha) of crop i planted in subregion s using technology q at time t

To determine the livestock demands for drinking water, X_{22}, the following constraint is introduced in SWIM2:

$$X_{22} = \sum_{j=1}^{4} L_j Q_j \tag{E.55}$$

where

L_j is the livestock water use coefficient (m^3/animal)
Q_j is the number of animals j

E.2.3.5.6 Capital Investments. The capital investments are split into two parts: (a) irrigation capital investments and (b) investments for machinery and livestock farm houses.

$$X_{23} = \sum_{s=1}^{3} i_s I_s + c_c X_{19} \tag{E.56}$$

where

X_{23} is the capital investment in irrigation (Lv)
i_s is the capital investment to bring water to the field (Lv/ha)
I_s is the amount of irrigated land (ha) to be developed in subregion s
c_c is the capital cost of irrigation equipment (Lv/equipment)
X_{19} is the total amount of irrigation equipment required

$$X_{24} = i_t X_{16} + i_c X_{17} + i_p X_{18} + \sum_{j=1}^{4} h_j Q_j \tag{E.57}$$

where

X_{24} is the capital investment for machinery and livestock farm houses

i_t, i_c, i_p are the capital investments (Lv/machine) for tractors, combines, and choppers

h_j is the capital investment for livestock farmhouses (Lv/animal)

Q_j is the number of animals j

ACKNOWLEDGMENTS

The authors wish to express their appreciation to Dr. J. Kindler, the task leader of the Regional Water Demand and Management Task of IIASA's Resources and Environment Area, for his continual guidance and encouragement during the course of the study. Other IIASA scientists who provided valuable assistance include Dr. H. Carter, Dr. J. Guise, and Dr. W. Orchard-Hays. The authors are also grateful for the help of many IIASA support staff.

Special thanks are due to Professor E. Hristov of the State Council of Bulgaria, and Mr. V. Manahilov, Dr. V. Genkov, and Dr. S. Stoykov of the Ministry of Agriculture and Food Industry, Sofia, for their help in carrying out the case study and implementing the model in Bulgaria.

The research was partially supported with funds provided by the Volkswagenwerk Foundation and by the Rockefeller Foundation.

REFERENCES

Ayers, R.S., and D.W. Westcot. 1976. Water Quality for Agriculture. Irrigation and Drainage, Paper 29, Rome: UN Food and Agriculture Organization.

Bos, M.G., and J. Nugteren. 1974. On Irrigation Efficiencies. Publication 19. Wageningen, the Netherlands: International Institute for Land Reclamation and Improvement.

Carter, H., C. Csaki, and A.I. Propoi. 1977. Planning Long Range Agricultural Investment Projects: A Dynamic Linear Programming Approach. RM-77-38. Laxenburg, Austria: International Institute for Applied Systems Analysis.

Chow, V.T. 1964. Handbook of Applied Hydrology. New York: McGraw-Hill.

Dean, G.W., H.O. Carter, Y. Isyar, and C.V. Moore. 1973. Programming model for evaluating economic and financial feasibility of irrigation projects with extended development periods. Water Resources Research 9(3):546–555.

Doorenbos, J., and W.O. Pruitt. 1977. Crop Water Requirements. Irrigation and Drainage, Paper 24, Rome: UN Food and Agriculture Organization.

Duloy, J.H., and R.D. Norton. 1973. CHAC, A programming model of Mexican agriculture. In Multi-Level Planning: Case Study in Mexico, edited by L.M. Goreux and A.S. Manne. Amsterdam: North-Holland/American Elsevier.

Gisser, M. 1970. Linear programming models for estimating the agricultural demand function for imported water in the Pecos River basin. Water Resources Research 6(4):1025–1032.

Gouevsky, I.V., D.R. Maidment, and W. Sikorski. 1978. User's Guide for Silistra Water for Irri- of Silistra Case Study. RM-77-44. Laxenburg, Austria: International Institute for Applied Systems Analysis.

Gouevsky, I.V., D. Maidment, and W. Sikorski. 1978. User's Guide for Silistra Water for Irrigation Model. Available from the Resources and Environment Area of the International Institute for Applied Systems Analysis, Laxenburg, Austria.

Heady, E.O., and R.C. Agrawal. 1972. Operations Research Methods for Agricultural Decisions. Ames: Iowa State University Press.

Heady, E.O., and U.K. Srivastava, eds. 1975. Spatial Sector Programming Models in Agriculture. Ames: Iowa State University Press.

Lidgi, M., ed. 1976. Handbook for Agricultural Economists (Spravochni na Agrarikonomista). Sofia: Zemizdat.

Ministry of Information and Communications. 1975. Statistical Yearbook 1974 (Statisticheski Godishnik 1974). Sofia (in Bulgarian).

Ministry of Information and Communications. 1976. Statistical Yearbook 1975 (Statisticheski Godishnik 1975). Sofia (in Bulgarian).

National Bureau of Economic Research. 1972. Sesame Reference Manual. Cambridge, Massachusetts.

Nicol, K.J., and E.O. Heady. 1975. A Model of Regional Agricultural Analysis of Land and Water Use, Agricultural Structure, and the Environment: A Documentation. Ames: Iowa State University Press.

Soltani-Mohammadi, G.R. 1972. Problems of choosing irrigation techniques in a developing country. Water Resources Research 8(1):1–6.

Thesen, A. 1974. Some notes on systems models and modelling. International Journal of Systems Science 5(2):145–152.

UN Food and Agriculture Organization. 1977a. Perspective Study of Agricultural Development for the Republic of Iraq: Allocation of Seasonal Water Resources for an Optimal Pattern of Crop Production (A Linear Programming Approach). ESP/PS/IRQ/77/Rev/3. Rome.

UN Food and Agriculture Organization. 1977b. Water for Agriculture. UN Water Conference, Mar del Plata, Argentina. Conference Document E/Conf. 70/11. Rome.

US National Water Commission. 1973. Water Policies for the Future. Washington, DC Water Information Center.

Voropaev, G.V. 1973. Irrigation reserves associated with optimization of water resources utilization. Problems of Water Resource Management and Use (Problemi Reguliro-vaniya i Ispolzovaniya Vodnih Resursov). Moscow: Nauka (in Russian).

POSSIBLE CLIMATIC CONSEQUENCES OF A MAN-MADE GLOBAL WARMING

H. Flohn

PREFACE

There is increasing concern about man's impact on climate. While studying this problem, one comes to realize that this influence is not so much felt as a variation of the average values of global climate, such as temperature and pressure. Of concern is instead a change in the climatological patterns, with the average values changing very little. This could be a change in rainfall patterns, for example. Among other effects, increasing levels of carbon dioxide could cause a man-made global warming.

While it is impossible to determine such changes in climate patterns given the present state of the art, we consider it perhaps useful to study the changes that occurred in the climate patterns of the past. Today's highly sophisticated knowledge in paleometeorology allows us to undertake such a venture – a research activity that may also be crucial for our understanding of the forthcoming CO_2 problem.

This study follows along these lines, and makes use of information available as of March 1980. This report was written for the study on "Energy Systems and Climate" [Project Number FP/0700-75-02(717)], sponsored jointly by the United Nations Environment Programme (UNEP) and IIASA.

SUMMARY

Although climatic changes and modifications are mainly observed in the atmosphere, they in fact occur within the climatic system – the atmosphere, oceans, soil and vegetation, snow and ice – and can affect the multiple interactions between these subsystems. As Figure S1 shows, the time scales relevant to the subsystems can vary between a few days, in the case of the atmosphere, for instance, and up to 10^6 years, in the case of the Antarctic ice dome.

This paper examines both natural processes and man-made effects that may play a role in climate change, to provide the background for the development of a scenario of future climate change. The sensitive internal interactions between the atmosphere and thin drifting sea ice that lead to ice formation and melting are discussed, as well as the interaction between the atmosphere and the oceans in the regions of frequent upwelling along the equator and some coasts. The role of the heavily glaciated Antarctic continent in causing a marked hemispheric asymmetry of both the atmospheric–oceanic circulation and the positions of the large climatic belts is then examined. A possible partial instability of the West Antarctic ice sheet and its role in sea-level changes is also discussed.

The paper turns next to man-made impacts on the climate. Some, such as direct heat output, atmospheric pollution, changes in surface albedo (reflectivity), heat storage, and water budget, are obvious on a local scale. More important, however, are the implications of the increase in carbon dioxide and some atmospheric trace gases. Their long residence time, between 5 and about 50 years, their large-scale turbulent mixing caused by the atmospheric circulation, and, above all, their absorption in the infrared portion of the spectrum produce a combined greenhouse effect, which tends to warm the troposphere and cool the stratosphere.

Attempts to model the relationship between CO_2 concentrations and temperature changes are then reviewed, in order to quantify the greenhouse effect that may be associated with given levels of CO_2. It is found that the

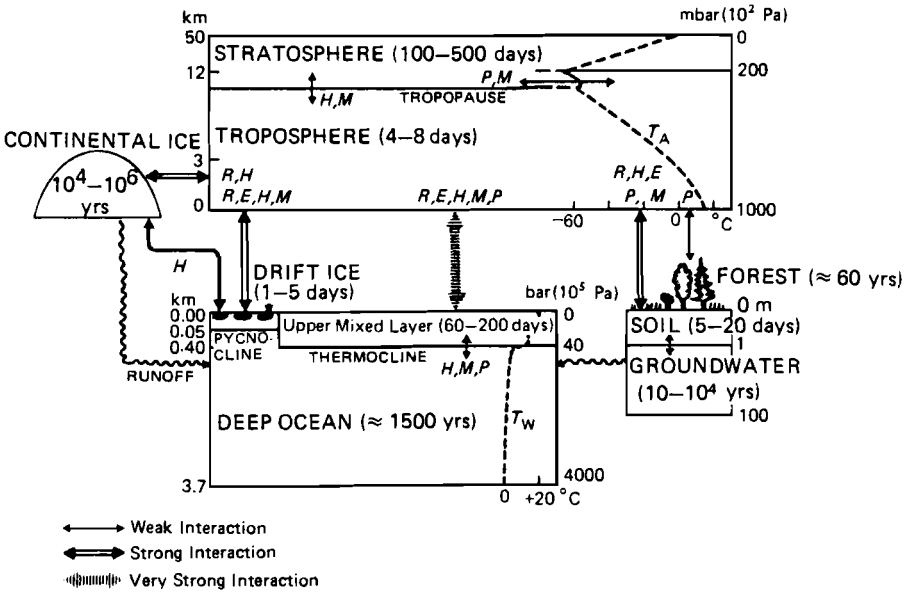

FIGURE S1 The climatic system, showing the time scales characteristic of its subsystems and the interactions between the subsystems. R is radiation; H is heat; E is evaporation; M is momentum; P is particles or gases; T_W is water temperature; and T_A is atmospheric temperature.

best models available indicate an average 3 °C warming of the surface layers in low and middle latitudes, with a doubling of the CO_2 concentration. This warming increases to 5–10 °C in polar latitudes, due to the feedback between snow or ice, surface albedo, and temperature. The effect of other trace gases, especially of nitrous oxide, one of the final products of nitrogen fertilizers, adds some 50% or more to the CO_2 effect – accelerating the expected global warming. An estimate of future temperature evolution, dependent on the initial growth rate of CO_2 concentrations, is made, using one of the most reliable radiation models for the relation between CO_2 content and typical temperature change (together with a selection of logistic CO_2 growth functions).

Evidence of temperature fluctuations in recent years is examined next. It is found that a man-made global warming of 0.2 °C, assumed to have occurred over the past 80 years, can be accounted for by natural fluctuations. Evidence shows that an increase of 0.4–0.5 °C is likely to occur between 1990 and 2000.

Paleoclimatic phases characterized by warm temperatures are then identified, to see if current man-made warming and expected future warming has been paralleled by past warm phases during the long historical evolution of the earth's climate, and to study the nature of the climate during the warm phases. Table S1 provides information on selected paleoclimatic warm phases, including estimates of the middle-latitude temperature differences that characterized the phases, and CO_2 levels equivalent to the increased temperatures. The CO_2 levels associated with the estimated temperature differences are based on two extreme versions of the Augustsson–Ramanathan model (1977). "Virtual" CO_2 content refers to a CO_2 level that has been adjusted to reflect the additional greenhouse effect of other trace gases. It is assumed that the increase in other trace gases adds 50% to the greenhouse effect of CO_2 alone (the "real" CO_2 content).

Since really comprehensive models of the climatic system as a whole and its interactions are not yet available and cannot be expected to be forthcoming soon, a scenario based on these warm paleoclimatic phases is discussed in this paper. Such a scenario can be used as a conditional forecast only if the following natural factors remain constant: no change in the solar constant, no major cluster of volcanic eruptions, no disintegration of the West Antarctic ice sheet, and no changes in cloudiness. Furthermore, the changes in the boundary conditions since the occurrence of past warm phases, i.e., changes in vegetation, sea level, and mountain formation, must also be taken into account.

Examination of past climates as a basis for a global warming scenario. Evidence is brought together showing that during the Medieval warm phase (~ 1,000 AD), the sea ice around Greenland retreated, causing more northerly cyclone tracks and frequent dry anticyclonic conditions for Europe. Evidence for the Holocene warm period (~ 6,000 years ago) indicates that it was nearly everywhere more humid than today, especially in the arid belt of the Old World. There the desert was replaced by semiarid grassland densely populated by cattle-raising nomads. The role of natural and man-triggered processes, such as the retreat of the North American ice sheet and the beginning of desertification, during this epoch is also discussed. It is concluded that under present boundary conditions a return to a similar regional climate is unlikely.

During the warmest interglacial period 120,000 years ago, more warming, i.e., +2.0–2.5 °C, occurred, accompanied by marked shifts of vegetation belts and coastal lines due to a sea-level rise of 5–7 m. A partial disintegration of the West Antarctic ice sheet probably played an important role in climatic change during this period. As in the Holocene warm period, the climate was somewhat more moist than today in many areas for which data are available. (Immediately after the Eem sensu stricto phase of this warm interglacial period, an abrupt cooling occurred; such abrupt occurrences of cooling, sometimes of a nearly glacial intensity, have also been observed for other interglacials, lasting for several centuries.)

The real CO_2 level equivalent to a 2.5 °C warming, as occurred during the last interglacial period, can be estimated to be 550 ppm ± 10%, if one assumes

TABLE S1 Atmospheric CO_2 content equivalent to estimated temperature differences (ΔT) during selected paleoclimatic phases.

Paleoclimatic warm phases	ΔT(°C)[a]	Virtual CO_2 content[b,d](ppm)	Real CO_2 content[c,d](ppm)
Medieval warm phase (1,000 yrs ago)	+1.0	420–490	385–430
Holocene warm phase (6,000 yrs ago)	+1.5	475–580	420–490
Eem Interglacial (120,000 yrs ago)	+2.0	530–670	460–555
	+2.5	590–760	500–610
Ice-free Arctic ocean (12–2.5 X 10^6 yrs ago)	+4.0	780–1150	630–880

[a]Estimated temperature increase over the current temperature in low and temperate latitudes.
[b]Unit expressing the combined greenhouse effect stemming from real CO_2 and atmospheric trace gases.
[c]Assuming a 50% contribution of trace gases to the expected increase in virtual CO_2.
[d]The ranges in virtual and real CO_2 content are based on two extreme versions of the Augustsson–Ramanathan model (1977); the most likely value lies between the extremes.
SOURCE: The data presented in this table are based on results from the Augustsson–Ramanathan model (Augustsson and Ramanathan, 1977).

the contribution of trace gases to the CO_2 greenhouse effect to be 50%. The warming in the Arctic would reach about 6–8 °C, probably reducing the Arctic sea ice to its central core between Siberia and Canada, and causing at the same time a poleward displacement of climatic belts by several hundred kilometers.

If CO_2 concentrations reached 750 ppm ± 16%, an average global warming of 4 °C would occur. *Model studies and paleoclimatic investigations indicate that this value is close to the critical threshold of a complete disappearance of the drifting Arctic sea ice.* The sensitivity of this sea ice (whose average thickness is only 2–3 m) to changes in such climatic factors as length of melting period, heat flow from the ocean, and salinity (due to a possible reduction of freshwater inflow), indicates that such a disappearance would probably take no more than a few decades, or even less. Due to the delay caused by the heat storage capacity of the ocean, the above-mentioned temperature increase of 4 °C may be considered a minimum value.

Paleoclimatic evidence collected by the Deep Sea Drilling Program has revealed that a permanently open Arctic sea existed until 2.5 or 3.0 X 10^6 years ago. In contrast, the East Antarctic continent has been glaciated for the past 12–14 X 10^6 years. The evidence shows that for about the last 10 X 10^6 years before the beginning of the present glacial–interglacial cycle, an Antarctic ice dome of today's height (or higher) coexisted with an open Arctic ocean,

with temperate or boreal forests extending to lat 81–83 °N, interspersed only with some local mountain glaciers; no evidence of tundra or permafrost in the soil has been found.

The implications of a possible coexistence of an ice-free Arctic and a glaciated Antarctic. The evidence from the Deep Sea Drilling Program is quite surprising since such a contrast between a heavily glaciated pole and an ice-free pole must have created a hemispheric asymmetry of the atmospheric–oceanic circulation that was much stronger than the asymmetry existing today. Such an asymmetry of the climate would cause the southern arid areas to expand to the vicinity of the equator, displace the meteorological (and thermal) equator to near lat 10 °N or even more (leaving the equatorial rain belt only in the northern hemisphere), and shift the northern arid belt to lat 35–45 °N, extending it even to the southern part of central Europe. This shift of climatic belts must be seen as a consequence of fundamental circulation theories. With the temperature difference between the equator and the North Pole decreasing, the area of the tropical–subtropical circulation belt increases, while the temperate and subpolar belt of westerlies contracts toward the North Pole. Since no comprehensive climate model of this unexpected pattern has been designed so far, detailed forecasts of regional climates after such an event are not possible. Simple extrapolation of the climate of the late Tertiary ($12–2.5 \times 10^6$ years ago) is not admissible because of the displacement of continental coasts and the formation and lifting of most of today's mountains at and since that time. Still, the stability of this pattern over a period of as long as ten million years must now be considered a fact. A return to this pattern would most probably lead, after a series of catastrophic weather extremes, to a displacement of the earth's climatic zones by 400–800 km. This would necessarily affect mankind as a whole, beneficially in some areas, but destructively in many others, drastically changing freshwater supply and agricultural productivity.

1 INTRODUCTION

The recent discussion on the physical background of climatic fluctuations aims at one of the basic problems of meteorology and the geophysical sciences as a whole (see GARP 1975). Climatogenesis occurs not only within the atmosphere but within the overall climatic system. As Figure 1 shows, this system consists of several interacting subsystems with quite different time scales (or "memories" in the usual scientific jargon). The climatic history of the past 5,000 years indicates that this system is fairly well balanced, for only secondary climatic fluctuations occurred during this period. But even these seriously disturbed man's economy and challenged his bare existence in marginal areas of the polar or arid zones.

1.1 NATURAL CLIMATOGENIC PROCESSES

Many climatic changes are caused by natural feedback processes within the climatic system; for example, an expansion of the Arctic sea ice is at the same time both a cause and an effect of climatic fluctuations. Such internal climatogenic processes are discussed in Chapter 2 of this report.

Other natural causes of climatic fluctuations are external and operate with little or no feedback. The examples given most frequently include heavy volcanic eruptions of the explosive (Plinian) type; such eruptions produce large numbers of small particles in the submicron range, which float in the stratosphere (in the Junge layer at about 20–22 km), concentrate in polar regions, and absorb and scatter some components of solar radiation. This leads to worldwide cooling that increases with high-latitude feedback between snow, albedo (reflectivity), and temperature (Mass and Schneider 1977, Oliver 1976, Pollack *et al.* 1976). The frequency with which these eruptions occur varies greatly (Lamb 1970, Kennett 1977a, Kennett and Thunell 1975, 1977b); as in the case of earthquakes, they are apparently triggered by the slow, but discontinuous, motion of the tectonic plates of the earth's crust.

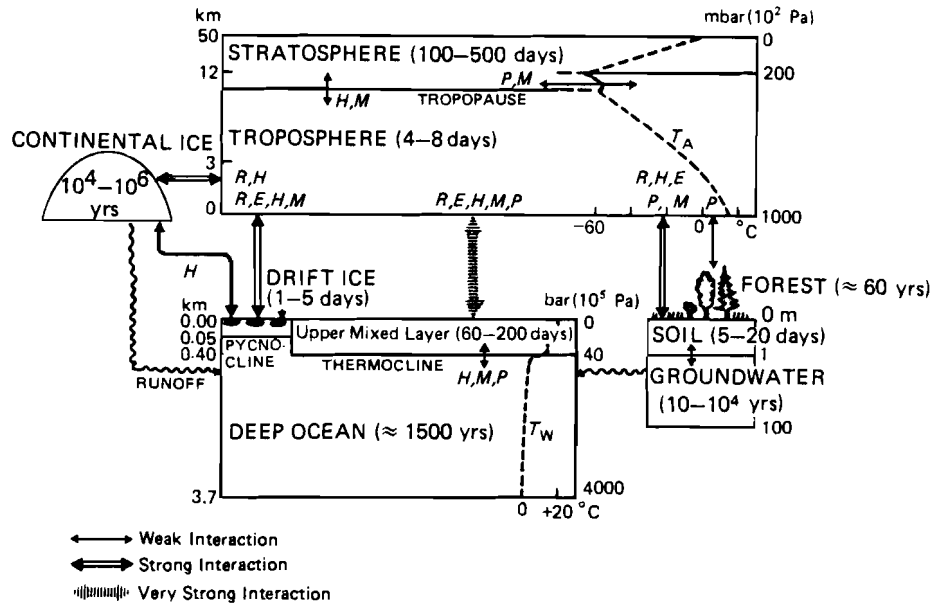

FIGURE 1 The climatic system, showing the time scales characteristic of its subsystems and the interactions between the subsystems. R is radiation; H is heat; E is evaporation; M is momentum; P is particles or gases; T_W is water temperature; and T_A is atmospheric temperature.

The possibility that short-lived fluctuations of solar radiation in the visible and near-infrared part of the spectrum induce climatic change is still controversial among specialists; continuous high-precision measurement above the level of pollutants in the denser layers of the atmosphere is needed, preferably by means of a satellite. There are also strong variations in the particle emission of the sun (protons) and in solar radiation in the far-ultraviolet or roentgen range. The possible role of such variations in the climate- and weather-producing troposphere [below 200 millibars (mbar) or approximately 12 km] is also still controversial and will not be discussed here. Other extraterrestrial factors affecting the climate are negligible.

1.2 MAN-MADE CLIMATOGENIC EFFECTS

It is generally agreed that man-made effects have been perceptible until now only locally or on a microscale, e.g., in cities or industrial centers (see Bach 1976a, 1976b). The role of atmospheric dust (in the 1–10 μm range) has sometimes been overrated, though it may be important in some deserts or semi-

deserts (notably in Central Asia and the Middle East), or in large metropolitan areas. The effect of atmospheric dust depends not only on the size and quality of the particles, but also on the surface albedo; it seems to have a warming effect, at least in continental areas. Waste heat affects the climate only on a local scale; even if it were to increase substantially, the short residence time of enthalpy in the atmosphere – on the order of hours and days – would probably inhibit its impact. In contrast to the rather short residence time of tropospheric particles, which is on the order of days or weeks, the residence time of infrared-absorbing gases, such as CO_2, is on the order of years and decades. Because of their importance in climatogenic processes, i.e., in creating a "combined greenhouse effect," a detailed treatment of the role of these pollutants is provided in Chapter 3.

Omitted from this discussion are some slow, but certainly important, man-made changes which affect the climate via the biosphere and the soil. These include destruction of natural vegetation in order to create arable land or pastures (causing soil erosion and desiccation of swamps, lakes, and marshes); large-scale irrigation (now affecting about 2.3×10^6 km^2); building of reservoirs (now covering about 0.5×10^6 km^2, not including the multitude of small tanks and ponds); and sealing of the earth's surface with concrete and other building materials. The climatic effect of these activities occurs through changes in several physical parameters: surface albedo and roughness, soil moisture and evapotranspiration, terrestrial (infrared) radiation, and absorption of radiation by water vapor. All of these processes are first relevant on a local scale; on a global scale they operate quite slowly. Still, continental surfaces have been subject to exponentially increasing changes at least since the Neolithic revolution about 8,000 years ago. Such man-made effects are probably even much older; Paleolithic man already knew how to use fire for hunting (e.g., in Australia).

At least 30% of the continents, some 45×10^6 km^2, are now affected by such activities. According to statistics from the Food and Agriculture Organization (FAO), destruction of natural vegetation has reached an alarming rate (see Polunin 1980). These statistics indicate that the annual rate of destruction of tropical forests (which play a big part in the CO_2 cycle) is 110,000 km^2. These surface changes tend to increase the surface albedo everywhere and are one of the few man-made processes that lead to cooling, at least in cases where the decrease in evapotranspiration does not cause an increase in sensible heating. Recent estimates (i.e., by Sagan *et al.* 1979) indicate that this effect is quite small in the context of the "human time scale" of 50–100 years; however, destruction of vegetation may have contributed to the global cooling since the Neolithic revolution.

1.3 METHODS FOR PREDICTING CLIMATIC CHANGE

Due to the complexity of the climatic system (see Figure 1) and the lack of models suitable for simulating the important interactions between its subsystems,

any attempt to predict climatic changes *in toto* is useless at the present time, at least if the forecast is to cover a period longer than one year. Most sobering in this respect is the fact that external effects on the climatic system are as yet unpredictable and will remain so for some time. Still, there is some hope that *conditional* predictions (also defined rather approximately as "predictions of the second kind") may be feasible. Such predictions may start with the assumption that external climatogenic effects, and perhaps also some of the internal interactions, do not change. One may then ask the question, What are the climatic consequences of a given man-made process, for instance, an increase in CO_2? If all other factors are held constant, it should be possible, with the help of simplified or more sophisticated models, to outline the possible individual or combined effects of processes produced or triggered off by man. In this way our understanding of climatogenic processes can be systematically improved.

In spite of the remarkable progress we have made in designing physical–mathematical models of atmospheric circulation, no model can yet adequately describe the climatic system as a whole, including the highly effective positive or negative feedback mechanisms within and between its subsystems. Manabe and Holloway (1975) provide a careful and critical evaluation of the existing limitations of surface climate modeling, using Köppen's classification for comparing model results and reality. No model has yet demonstrated, with sufficient accuracy and horizontal resolution, an ability to simulate the present surface climate with its seasonal variation – one of the most demanding and convincing tests of model capability. A major drawback is the lack of effective parameterization of subgrid-scale processes; another is the limited capability of even the most powerful computers available. Still, these sober statements should not underrate the achievement of enthusiastic model designers. There is little doubt that in the foreseeable future more advanced climate models, probably combining deterministic and stochastic approaches, will be able to present satisfactory solutions, at least for conditional predictions.

In recognition of the present state of modeling, a scenario based on past climate behavior is discussed in this report, and no attempt is made to use comprehensive physical–mathematical models. This scenario is a scientific tool based on historical and geological information. It may be considered essentially (but not exclusively) an empirical approach with specific limitations. Since it is necessary to study climate behavior over many epochs (the Medieval warm period 1,000 years ago, the Holocene warm period 6,000 years ago, the last Interglacial 10^5 years ago, and earlier epochs reaching back 10^6-10^7 years), the boundary conditions of the climatic system vary to such a degree that past experience can only be used as a first guide to what may happen in the foreseeable future – like sensitivity tests for a fairly sophisticated model. Also, in spite of the nearly unimaginable time scale on which the scenario is based, our interest in future climate change has to be restricted to what could be considered man's time scale, the next 50–100 years.

Because of the unpredictability of and uncertainty about many natural climatogenic processes, a scenario describing the possible future evolution of the climate must assume no major change in solar radiation, no unusual clustering of major volcanic eruptions, and no unusually large advance ("surge") of the Antarctic ice shelves. Because of our present lack of knowledge, it is also necessary to assume no significant variation in average cloudiness, for the interaction between radiation (dependent on wavelength) and clouds (dependent on size distribution of droplets and crystals, on cloud type and altitude, and on pollution particle content) is not well understood. However, many scientists feel that this concern should not be overemphasized (Cess 1976, 1977). One reason is that most clouds are formed or dissolved in ascending or subsiding motion of different scales; due to the law of conservation of mass all vertical motions are well balanced. Only a few percent of low-level stratus and thin cirrus trails can now be manipulated by man. A second reason is that global warming due to infrared absorption (the "greenhouse effect") decreases with height and reverses its sign in the stratosphere. In this case the overall thermal stability of the troposphere will decrease; consequently, the frequency of stratus clouds will also decrease, while vertical mixing will increase. Roads (1978) demonstrated that fractional cloudiness and relative humidity may even decrease with increasing temperature.

Compared with a model, the scenario discussed in this report has one advantage: it describes a situation that has in fact occurred and that may therefore arise again. Learning from history means checking how nature has solved the complete set of equations simultaneously and on-line, in all subsystems and at all scales, with a fully four-dimensional, i.e., time-dependent, approach. Since the boundary conditions are varying slowly, but permanently, climatic history can never repeat itself in all details, but rather only in substance. In this analysis, the main objective of scenarios is to serve as a preliminary guide for impact studies. Since the time scale of the phases of geophysical evolution described in our scenario can vary greatly, the scenario should not be conceived as a necessary sequence or as a substitute for climate prediction.

1.4 ORGANIZATION OF THE REPORT

Natural processes which can play an important role in climate change are presented in Chapter 2 of this report. In section 2.1 the formation and melting of polar sea ice is discussed, with emphasis on factors which may produce changes in the area and thickness of drift ice. Evidence of the recession or advancement of Arctic sea ice in the historical past is also reviewed. Section 2.2 addresses the role of the Antarctic continental ice sheet, focusing on the partial latent instability of the ice, which could possibly lead to catastrophic ice surges or deglaciation of western Antarctica. In section 2.3 the discussion turns to the asymmetry of the global atmospheric circulation at the current time, due to the contrast between the heavily glaciated Antarctic continent and the Arctic,

with its thin cover of drift ice. Finally, in section 2.4 the phenomena of equatorial upwelling of the ocean, El Niño, and the hydrologic balance are discussed, with attention to their significance for ocean water temperatures and evaporation. Changes in the parameters describing these phenomena during selected paleoclimatic phases are reviewed. As a whole Chapter 2 provides the background for the later discussion of a possibly ice-free Arctic and the implications of such a situation for the climate.

Chapter 3 focuses on climatic changes produced or triggered off by man, specifically the "greenhouse effect," or global warming, caused to a great extent by the release of CO_2 and trace gases into the atmosphere, but also by increases in such factors as the water vapor content of the atmosphere due to human activities, or to equatorial downwelling of the ocean. Attempts to model the relationship between atmospheric concentrations of CO_2 and trace gases, and the magnitude of global warming are then reviewed. Finally, paleoclimatic phases characterized by warm temperatures are identified and associated with levels of CO_2 that could be expected to produce such warming in the future.

In Chapter 4 existing evidence of the most recent temperature fluctuations is examined, taking into account the difficulty of distinguishing natural fluctuations from a real warming trend. The lack of representative data on such parameters as air temperatures, rainfall, and the extension of sea ice at the end of the melting season is discussed.

Chapter 5 focuses on the characteristics of selected warm paleoclimatic phases, i.e., the Medieval warm period, the Holocene warm period, and the last Interglacial period. Underlying this description of climatic history is the question, To what extent could history repeat itself, under varying boundary conditions, if global warming equal to that which obtained in earlier eras is reached in the future? Evidence regarding such factors as the extension of Arctic sea ice, cultivated land areas, tree lines, sea level, air and water temperatures, and rainfall during these eras is presented.

Chapter 6 takes a serious look at one scenario of climate change in the future: the possibility for the coexistence of an ice-free Arctic and a glaciated Antarctic. The discussion begins with a review of factors which could lead to global temperature increases large enough to cause the complete disappearance of Arctic sea ice – temperatures higher than those which obtained during all the warm climatic phases of the past two million years. Particular attention is then paid to the plausibility of the ice-free Arctic–glaciated Antarctic scenario, and to the great hemispheric asymmetry of atmospheric and ocean circulation that this situation would imply. Evidence of the existence of just such a situation during the late Tertiary period is introduced, lending weight to the argument that the scenario merits sober consideration. Finally, climatic implications of such a unipolar climatic asymmetry are examined, for instance, changes in the global water budget, a world-wide rise in the sea level, and melting of the continental ice caps.

2 NATURAL INTERNAL CLIMATOGENIC PROCESSES

2.1 THE ROLE OF POLAR SEA ICE

2.1.1 The General Process of Ice Formation and Melting

Large areas in both polar regions are permanently or seasonally covered by a thin blanket of ice floes separated by narrow strips of open water (polynyas or leads). The ice floes are covered by snow for most of the year and have an albedo of almost 80%. This is in contrast to the albedo of open water, which is only 8–12% in polar regions when the sun is low in the sky. During the melting season (which in the central Arctic is restricted to about ten weeks between mid-June and the end of August), the albedo of the ice floes decreases to about 60%; superficial ponds of meltwater occur, which appear light blue when seen from an airplane.

The area of polynyas relative to ice floes varies between 2 and 3% in winter and up to 12–20% in the melting season (Vowinckel and Orvig 1970, Untersteiner 1975). The thickness of the Arctic drift ice is often quoted to be 2–3 m on the average. However, the thickness of individual floes actually varies with age and ranges between 0.5 m and more than 6 m (Thorndike 1975). This has been verified by submarine expeditions and satellite microwave measurements of surface emissivity.

Typical values for the heat and radiation budget of the polar ice are very difficult to determine under such conditions. In winter the turbulent fluxes of sensible and latent heat from the polynyas – where the open ocean water (water temperature $T_W \approx -2$ °C) is in direct contact with the cold air below the polar inversion (air temperature $T_A \approx -30$ °C) – are more than 100 times as large as those at the surface of the ice floes, and sometimes have an opposite sign (Vowinckel and Orvig 1973). Recent measurements of the sensible heat flux at natural leads (with the fetch varying between 7 and 80 m) north of Barrow, Alaska yielded values of 250–450 W/m^2; this exceeds the solar radiation in the Sahara (Andreas *et al.* 1979). Even during polar summer with

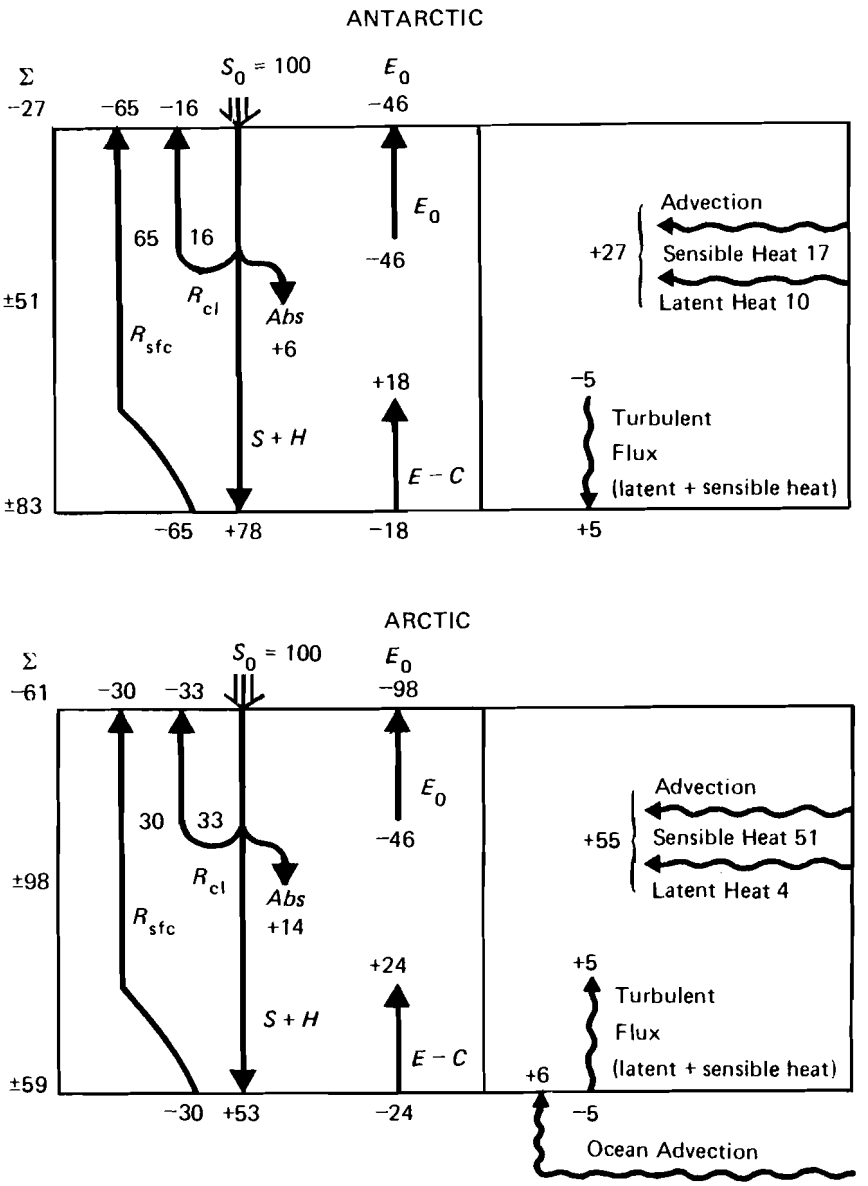

FIGURE 2 Estimated heat budgets of the atmosphere above the Antarctic and the Arctic, in 100 units of solar radiation at the top of the atmosphere (S_0). E_0 is outgoing terrestrial (infrared) radiation; *Abs* is solar radiation absorbed by the atmosphere; R_{cl} (R_{sfc}) is radiation reflected by clouds and the earth's surface; $S + H$ is global (sun and sky) radiation at the earth's surface; $E - C$ is effective infrared surface radiation. The data, with some modifications, are taken from Schwerdtfeger (1970) and Vowinckel and Orvig (1970). Source: Flohn (1978a).

permanent daylight, polynyas with a diameter of several kilometers can suddenly freeze over because of cold air advection. Thus, the heat budget values given in Figure 2 can only be rough estimates.

In a very careful study, Maykut and Untersteiner (1971) simulated the physical processes of ice formation and melting, on the basis of observations made in 1957–1958 and assuming a horizontally homogenous ice cover. In this one-dimensional model of the ocean–ice–snow–air multiphase system, two processes are particularly effective in reducing ice thickness: lowered surface albedo (e.g., related to the duration of the melting season and to pollution by dust or oil wastes) and increased ocean water temperature. Model runs showed that during the melting season about 50 cm of ice melts from above, while during the rest of the year a similar amount freezes from below. A possible increase in salinity (and thus density) of the ocean water is not considered in the model. This could occur, for instance, after an artificial deviation of part of the freshwater flow from big rivers in Siberia and Canada for irrigation purposes (Aagard and Coachman 1975; for new data on future plans for Siberia and Central Asia see Hollis 1978). More sophisticated three-dimensional time-dependent models of the multiphase system are now under development in large international research programs, and more complete solutions, including all feedback mechanisms, may be expected (Washington *et al.* 1977, Hibler 1979).

2.1.2 Arctic Drift Ice

At present the ice-forming processes occur in a shallow ($\approx$ 50 m), but very stable, surface layer of the Arctic ocean (Figure 3). Excess low-saline water and ice leave the Arctic basin with the strong and narrow East Greenland Current. If the freshwater inflow is significantly reduced, the salinity and density of the surface layer of the ocean must increase, reducing its stability. In a non-stratified ocean with turbulent vertical exchange, no permanent ice cover would be possible.

Arctic drift ice is driven by winds and ocean currents. A large anticyclonic gyre circles clockwise around the central core of the Arctic ice between Greenland, Alaska, and Siberia (Rothrock 1975). The total area of the Arctic drift ice varies between 7×10^6 km^2 in late summer and 14×10^6 km^2 in spring (Walsh and Johnson 1979). Thus only one-half of the maximum ice cover is seasonal, with a thickness of 50–100 cm. The average residence time of an ice crystal in a floe between freezing and melting is on the order of 5–10 years.

2.1.3 Recession and Advancement of Arctic Drift Ice in the Past

In contrast to the high stability of the central core of Arctic ice, which has existed for at least 7×10^5 years and probably for more than 2×10^6 years,

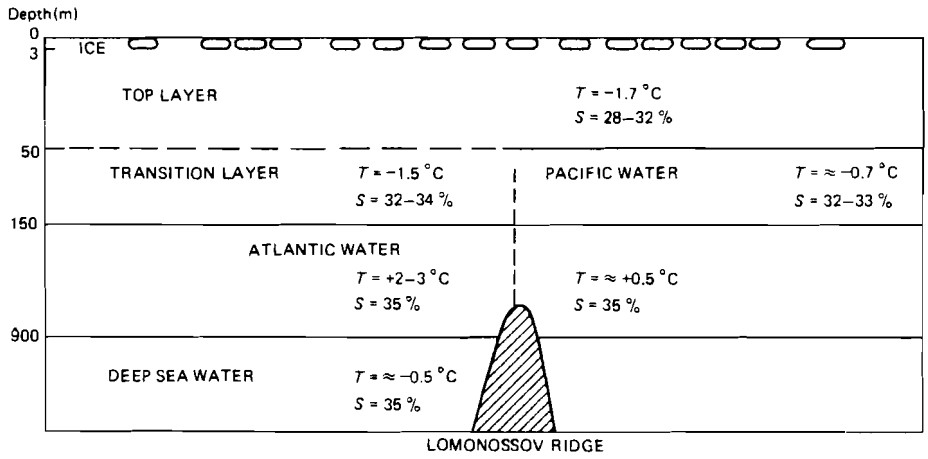

FIGURE 3 A schematic diagram of the stratification of the Arctic Ocean. T is temperature (°C); and S is salinity (%).

the marginal parts of the ice in the Atlantic sector between Greenland, Svalbard, and Novaya Zemlya underwent large fluctuations within historical times. After gradually receding to Greenland's northern coast (≈ 81 °N), the ice began to advance along the eastern coast about the year 1320, sometimes blocking Iceland and the Denmark Strait until late summer. During the late seventeenth and early eighteenth centuries, the ice advanced several times towards the Faroes and even Norway (Lamb 1979). Occasionally Eskimos and polar bears stranded on a floe were carried as far as the coast of Scotland. The total area of Arctic ice may have varied by more than 20% during the last millenium, while the southern edge of the ice shifted by more than 2,000 km.

The large-scale advance of the ice during the Little Ice Age (1550–1850, with severe precursors around 1320 and 1430) seems to be correlated with several phenomena: a rearrangement of cyclone tracks in the far south, a much more frequent occurrence of blocking anticyclones above the then cold surface waters north and west of the British Isles, frequent outbreaks of polar air across the Alps in western and central Europe, and an increase in cyclonic activity and rainfall in the Mediterranean. "Low index" circulation patterns prevailed over most parts of the mid-latitude belt of westerlies in the northern hemisphere, and – as happens occasionally today – cold high-tropospheric troughs frequently penetrated into the interior tropics, causing anomalous rainfall. The contrasts between albedo and heat budget along the edges of the ice are of paramount importance for the formation of cold air above the ice and thus for the position of tropospheric frontal zones.

Polar ice shifts were rare during the warm period of 1931–1960. Since then, however, there has been some modest readvancement of the ice (shown in Figure 4 for Iceland), coinciding with some of the most unexpected climatic

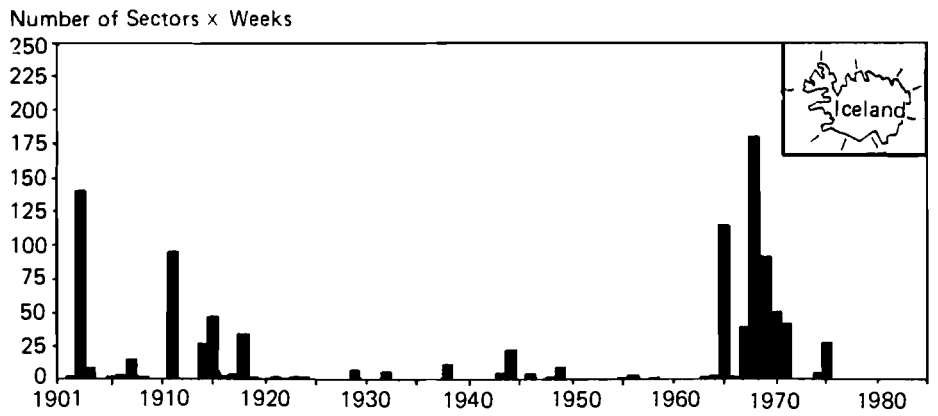

FIGURE 4 Sea ice fluctuations on the coasts of Iceland (measured in terms of the number of coastal sectors affected times duration of the ice in weeks), 1901 to the present. Source: Meteorological Service of Iceland (G. Sigtryggson).

anomalies of recent years. Among them were the severe winters of 1968/69 in the USSR and 1976/77, 1977/78, and 1978/79 in parts of North America, an unbroken series of six or seven unusually mild winters in western and northern Europe, and the coincidence of a serious western European drought with abundant rainfall in the central part of the USSR during the summer of 1976. Other anomalies were the three most severe seasons in this century of Greenland icebergs in the Newfoundland area (1971–1973) and frequent heavy gales in the North Sea area between 1972 and 1976.

Such quasi-stationary, atypical weather patterns demonstrate the simultaneous occurrence of large positive and negative anomalies of temperature and rainfall, known as the "North Atlantic seesaw" (van Loon and Rogers 1978). This phenomenon is correlated with a general cooling of the interior Arctic (see Figure 9), but masks the small temperature variations averaged along the parallels of latitude.

The physical reasons for such cooling (or warming) in the polar zone are not well understood. Flohn (1974a) hypothesizes the occurrence of one or more volcanic explosions which produce great masses of stratospheric particles; due to the stratospheric circulation system, these particles converge and subside above the interior Arctic (north of $\approx 75\,^{\circ}$N) and Antarctic, forming a dust layer at an altitude of 10–15 km (easily visible from an airplane). At this altitude the dust layer lasts longer than in mid-latitudes because of the relative absence of exchange processes between the troposphere and the stratosphere. By back-scattering and absorption, the dust layer may reduce solar radiation, surface temperature, and the duration of the melting season. Consequently, the average thickness of the ice may increase, reducing the heat flow between ocean and atmosphere. This in turn may lead to cooling and to an extension of the ice, for thin seasonal ice grows faster than thick perennial floes.

2.1.4 *Antarctic Drift Ice*

In contrast to the Arctic ice, the Subantarctic drift ice is largely seasonal (≈ 85%). In winter an extremely cold, thin surface layer develops above the Antarctic ice dome, with average minimum temperatures below −70 °C, repeatedly reaching −88 °C. This cold layer spreads outward, cools the sea surface, and produces an extended seasonal cover of drift ice about 100–150 cm thick. (Unlike the situation in the Arctic, a low-salinity surface layer of the ocean does not develop). This drift ice is thus mainly produced by the extremely cold winds descending and blowing out of the Antarctic continent during the cold season, which is characterized by a strongly negative radiation balance. Its area increases from 3.5×10^6 km² in late summer to about 22×10^6 km² in spring. The most productive region is the Weddell Sea in the Atlantic sector; a large tongue of drift ice frequently extends from this sea towards ENE. At the end of the season, the total area of Antarctic ice is no less than $36–38 \times 10^6$ km². Since both the areal extension of the coldest air and the position of the tropospheric baroclinic zone depend on the extension of drift ice, the southern hemispheric circulation is characterized by a time lag of 2–3 months with respect to the sun's radiation.

Two sharp extensions of the Subantarctic drift ice and the cold Antarctic surface water come in contact with the warmer water of the middle latitudes. In the Atlantic sector the drift ice and cold surface water reach lat 48–50 °S, while in the vast South Pacific they extend approximately to lat 60 °S. Thus, in contrast with the Arctic, the climatic influence of the Antarctic is strongest in the Atlantic sector; Bouvet Island (54 °S) is almost completely glaciated, whereas Helgoland (54 °N) is a summer bathing resort.

In addition to the enormous area of sea ice, the large-scale tabular icebergs of the Antarctic should be mentioned. These have an average depth of 200–400 m and extend for many square kilometers. In extreme cases they are as big as the Netherlands (≈ 30,000 km²). They break off from the large Antarctic ice shelves, their last debris reaching sometimes as far as lat 35 °S in the Atlantic. From the point of view of climate, they are mainly important because of the large amount of heat they need for the melting process.

2.2 THE ROLE OF THE ANTARCTIC CONTINENTAL ICE SHEET

About 15 years ago a new, unorthodox ice age hypothesis was proposed by the New Zealand geochemist A.T. Wilson (1964). His basic assumption was that the combined action of pressure from above and geothermal heat flow from below must necessarily lead to melting at the bottom of a sufficiently thick body of ice. In this case the quite stable "cold" ice could become mobilized with the help of regelation processes, which are well known from "temperate" or "warm" glaciers in mid-latitude mountains. He assumed that a latent instability of the Antarctic ice parallels the rare surges of some Arctic or mountain

glaciers. Thus the Antarctic ice could possibly move forward catastrophically on all sides, forming a quasi-permanent ice shelf of 20–30 × 10^6 km^2; the consequence would be a general cooling of the earth and the sudden initiation of a glaciation of the continents in the northern hemisphere. One of the most exciting discoveries that confirmed one of Wilson's basic assumptions was made by Gow *et al.* (1968) at Byrd station (80 °S, 120 °W). They observed how the bottom of an ice core (2,163 m) met with meltwater under high pressure.

Discussion of this hypothesis has led to some important modifications (e.g., Hughes 1973, Flohn 1974b), but has left the fascinating basic idea untouched. Model computations by Budd (1975a, 1975b) have demonstrated the interaction of the physical processes involved. Hughes (1975, 1977) has outlined the current form of Wilson's hypothesis in the following terms. While the bulk of the eastern Antarctic ice is stable and rests at a level well *above* sea level (except for a few small, widely dispersed meltwater lakes), the smaller ice dome of western Antarctica (between South America and long 140 °W) rests on bedrock largely *below* sea level. In western Antarctica the ice may not be stable; the boundary between the floating shelf ice and the slowly moving parts of the continental ice is not fixed, and it has been suggested (see Hughes 1975, Mercer 1978) that the western Antarctic ice sheet once disappeared in the geological past. The present situation has apparently not yet reached an equilibrium stage (Hughes 1975); thus there is some risk of a catastrophic deglaciation of parts of western Antarctica in the foreseeable future (Mercer 1978). An event of this kind could create a worldwide rise in the sea level of 4–6 m (Mercer 1978). Its possible mechanism and time scale are unknown (see p. 68 for further discussion).

The Antarctic ice sheet, with a volume of about 26 × 10^6 km^3, contains by far the largest freshwater reserve of the globe, at an average temperature below −30 °C. Its mass balance is probably positive (Schwerdtfeger 1970), on the order of 3 cm water-equivalent per year. This figure is somewhat uncertain since some of the outflow components of this vast continent, such as snowdrift, are not yet well known. It should be mentioned that the possible positive mass balance of the Antarctic ice sheet is inconsistent with the very slow worldwide rise in the sea level of about 1.1 mm/yr. Geophysically, however, sea level fluctuations are extremely complex and far from being understood.

2.3 THE ASYMMETRY OF THE GLOBAL ATMOSPHERIC CIRCULATION

One of the basic features of global atmospheric circulation, and consequently of the wind-driven mixed oceanic layer, is its asymmetry with respect to the equator – a fact not covered satisfactorily by most textbooks. The asymmetry is accounted for by one of the fundamental parameters of atmospheric circulation, the *thermal Rossby number* Ro_T:

$$Ro_T = U_T/r\Omega$$

where $U_T = \Delta z\, \partial u/\partial z \propto \Delta y\, \partial T/\partial y$ is the vertical shear of zonal wind u (or the "thermal wind" proportional to the meridional temperature gradient $\partial T/\partial y$) of a layer Δz, r is the earth's radius, $y(z)$ the meridional (vertical) coordinate, and Ω the angular speed of the earth's rotation. This dimensionless number describes the thermal zonal wind, depending on the temperature difference between equator and pole, in units of the rotational speed of a point on the earth's equator (464 m s^{-1}).

It is easy to determine the meridional equator–pole temperature difference in the troposphere, at least for the layers above the surface of the Antarctic ice dome. This is done at the Amundsen–Scott station at 90 °S, altitude 2,800 m. Table 1 gives the results of a survey based on data for an uninterrupted seven-year period. If the results of the South Pole station survey (in which the surface pressure averaged 681 mbar) are used to represent the 700 mbar level, the error introduced is only about 0.5 °C. Taking into account the systematic error, the data presented in Table 1 demonstrate that the Antarctic troposphere is actually about 11 °C colder than the Arctic troposphere in the equivalent seasons. This is true in spite of the fact that in summer the Antarctic ice dome has the highest solar radiation of the whole globe; its surface albedo of 84–89% is also the highest.

A meridional equator–pole temperature difference results that is almost symmetric during northern winter/southern summer, but greatly asymmetric (17 °C versus 44 °C) during northern summer/southern winter. This causes a much stronger atmospheric circulation in the southern hemisphere, which crosses the equator and displaces the intertropical convergence zone (ITCZ) towards the north. The zonally averaged position of the "meteorological equator" – defined as the latitude of lowest pressure in the tropics and of a change in sign of the average meridional wind component – varies seasonally between 0° and almost 15 °N, and reaches 6 °N on an annual average (Flohn 1967). In July the thermal Rossby number is more than 250% higher above the southern hemisphere than above the northern hemisphere.

The quite different heat and radiation budgets of the two polar regions explains this asymmetry. The nearly landlocked Arctic ocean (85%) with a thin and perforated cover of drift ice contrasts with the isolated Antarctic continent with an ice sheet more than 2 km thick. Figure 2 (from Flohn 1978a) compares the preliminary data that are available on the heat and radiation budgets of Antarctica (Schwerdtfeger 1970, partly revised) and the Arctic interior (Vowinckel and Orvig 1970). Among the most essential points of difference are the higher albedo (reflectivity R_{sfc}) of the Antarctic ice, the region's lower cloudiness and atmospheric water vapor content [that affect the reflection from clouds (R_{cl})], and the varying atmospheric infrared emission (E_0). Of minor importance are the turbulent fluxes of sensible and latent heat (evaporation) from the surface, which are directed upward above the Arctic Ocean and downward above Antarctica.

TABLE 1 Average temperatures (°C) in the 300/700 mbar layer.

	January	July	Annual average
Equator (E)	..[a]	..[a]	−8.6
North Pole (N)	−41.5	−25.9	−35.9
South Pole ((S)	−38.3	−52.7	−47.7
Difference E–N	32.9	17.3	27.3
Difference E–S	29.7	44.1	39.1

[a]The difference in the average temperature of the mid-troposphere in January and July is less than 0.4 °C.
SOURCE: Flohn (1967, 1978a).

In both regions the negative radiation budget at the top of the atmosphere must be maintained by quasi-horizontal advection from temperate latitudes; this advection is much higher in the Arctic, due to the variation of the land–sea distribution with longitude. Compared with atmospheric advection, the oceanic advection in the Arctic is rather small, since the warm Atlantic water submerges below cold, shallow surface waters.

The significance of the asymmetry of the global atmospheric circulation for climate change will be shown in Chapter 6, in which the possibility of an ice-free Arctic is discussed.

2.4 EQUATORIAL UPWELLING, EL NIÑO, AND THE HYDROLOGIC BALANCE

One of the most unusual cases of climatic variability is the irregular fluctuation of sea surface temperatures and of rainfall in a long, narrow belt along the equator across both the Pacific and the Atlantic (but not across the equatorial Indian Ocean). This belt coincides with the "equatorial dry belt" of classical climatology, for which a physical interpretation was first given by J. Bjerknes (1969).

In the Pacific and Atlantic Oceans the actual sea surface temperature drops, in a latitudinal belt between about 0° and 4 °S, from the average value of tropical oceans (26–27 °C) to 18–22 °C. In some cases, especially on the leeward side of islands, it drops to even less than 15 °C. The occurrence of penguins on the equatorial Galapagos Islands is a striking example of bio-climatic adaptation to the lower sea temperature. Bjerknes's explanation of this phenomenon starts with the wind-driven Ekman flow in the shallow upper mixed layer of an ocean, which extends down only 50–100 m to the top of the thermocline; it separates, with several strong discontinuities, the cold waters of the deep ocean from the warm mixed layer. By integrating the Ekman drift with increasing depth down to the level where the wind-driven component disappears, one obtains a direction perpendicular to the wind, with an anti-cyclonic deviation of the current to the right in the northern hemisphere, and

to the left in the southern hemisphere. Since zonal winds prevail in tropical latitudes, several phenomena (see Figure 5) can be interpreted by means of the meridional component of the Ekman drift (ED_y). This can be written as follows:

$$ED_y = -(\rho f)^{-1} \vec{\tau}_x$$

Here x and y denote the zonal and meridional components, $\vec{\tau}$ the surface stress vector of wind v (proportional to v^2), ρ the density, and f the Coriolis parameter ($f = 2\Omega \sin \phi$, with angular velocity Ω and latitude ϕ). Because of $\sin \phi$, the sign of f is reversed at the equator, and ED_y diverges on both sides of the equator in a generally easterly wind. In the Indian Ocean, where westerlies prevail throughout the year in a narrow band along the equator, the change in the sign of f leads to a convergence of the Ekman drift at $\phi = 0$, where $(\rho f)^{-1}$ becomes indefinite.

A more thorough elucidation should start from the rotation (vorticity) of the wind stress field. At the lower boundary of the ED layer, the vertical flow component w of the water can be expressed as:

$$w = (\rho f)^{-1} \operatorname{rot}_z \vec{\tau}$$

where the vorticity $\operatorname{rot}_z \vec{\tau} = \partial \vec{\tau}_y / \partial x - \partial \vec{\tau}_x / \partial y$, and x, y are the zonal and meridional coordinates, respectively.

Due to the asymmetry of the atmospheric (and oceanic) circulation, as discussed above, the southeast trade winds cross the equator and reach about lat 5–8 °N, with the streamlines usually turned clockwise. This clockwise turn is equivalent to a cyclonic curvature in the southern hemisphere (rot_z v negative); but with the crossing of the equator and the change in the sign of f, the curvature of the flow by definition becomes anticyclonic in the northern hemisphere (Figure 5). Since the sign of vorticity is the same on both sides of the equator (see Figures 2–6 in Hantel 1972), while f in the denominator disappears at the equator ($\phi = 0$) (and is quite small in its immediate vicinity), w must be highly positive just south of the equator, indefinite at $\phi = 0$, and highly negative just north of the equator. In this case one observes a more or less permanent trend of upwelling (or downwelling) just south (or north) of the equator, together with a marked increase in water temperature when the equator is crossed from south to north.

The asymmetry of the circulation peaks in northern summer/southern winter, with a lag of 1–3 months with respect to the sun's position. As a result, the seasonal maximum of upwelling in the belt 0–4 °S occurs from June to September, i.e., at the time when the symmetry of the wind field (in relation to the equator) reaches its minimum and southerly components of the trade winds predominate. The upwelling cool water (with an average w on the order of 0.5–1 m/d) stabilizes the atmosphere if the temperature of the sea surface T_W is less than that of the air T_A. In this case the flux of sensible heat proportional to the temperature difference $T_W - T_A$ is directed downward to the sea;

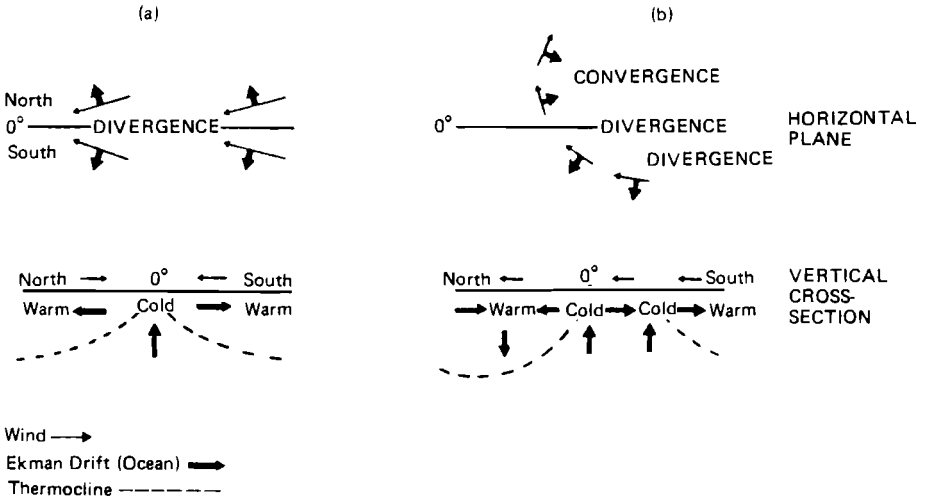

FIGURE 5 Equatorial flow patterns and upwelling for (a) the symmetric case and (b) the asymmetric case.

the relative humidity of the air increases, and evaporation (which is proportional to the vertical gradient of specific humidity at the surface of the water q_w minus the specific humidity of the air q_A) decreases sharply. Recent evaluations of maritime observations made on a meridional strip at the Galapagos (long 85–90 °W) have revealed that the average evaporation in the belt 0–3 °S decreases to 1.0 mm/d in winter (May–October) and to 0.8 mm/d in summer (November–April), compared with 2.8–3.5 mm/d in the adjacent latitudes on both sides (Trempel 1978); representative values for tropical oceans are somewhat higher (120–150 cm/yr). Similar values have been obtained from a larger data set (1953–1965) for the equatorial Atlantic (Henning and Flohn 1980).

Equatorial upwelling currently prevails in the air–sea system. However, marked changes and reversals do occur at irregular intervals, frequently during northern winter/southern summer, when the southern circulation nearly equals the intensity of the northern circulation. At such times the intertropical convergence zone (ITCZ), representing the boundary between both circulations (also called the meteorological equator), tends to be close to $\phi = 0°$. Along the coasts of Ecuador and Peru, these abnormal periods coincide with the replacement of upwelling cool and nutritious water by a sterile layer of warm water. The result is a drastic reduction in the fish catch for man and seabirds. At the equator, the sign of the vertical flow component w apparently reverses, producing a downwelling trend. This anomaly usually starts around Christmas and has therefore been called *El Niño* ("the little boy").

Recent investigations (Barnett 1977, Wyrtki 1977) have demonstrated the large variability of the winds and ocean currents, in addition to the variability

of sea surface temperature and rainfall. The average intensity of the large zonal ocean currents – which is nearly proportional to the small zonal slope of the sea level – varies by ±50% over the period of 12 consecutive months. Similarly, the wind stress varies on the average between +44% and −25% over similar periods and as much as +100% and −52% during particular months (Wyrtki 1977). Upwelling or downwelling is controlled by the divergence of the Ekman drift only in the central equatorial Pacific. In the Galapagos area and along the Peruvian coast, changes in the wind field over large distances (≈ 10,000 km) are much more effective than local variations (Barnett 1977). While upwelling coincides with high zonal winds (trade winds), downwelling occurs during periods of diminishing trade winds. An equatorial (Kelvin) wave reverses the vertical circulation in the ocean, causing the El Niño phenomenon to occur almost simultaneously between 80 °W and about 160 °E, i.e., over a distance of 120° longitude or approximately 13,000 km (Doberitz 1968). It is accompanied by torrential rainfall, by thermodynamic instability ($T_W > T_A$), and by lower relative humidity, which in turn causes increased evaporation. Since the correlation between sea surface temperature and rainfall is positive (and well above the 3σ level of significance; see Flohn 1972), rainfall variations are enormous and larger than anywhere else in the world. For instance, at Nauru (0.5 °S, long 169 °E), the rainfall during consecutive 12 month periods varies between 95 mm and over 5,000 mm (as was observed between 1916 and 1918). Irregular fluctuations suppress the usual seasonal variations.

Generally speaking, equatorial upwelling, with rainfall and evaporation at a minimum, occurs during periods of strong atmospheric circulation (today mainly controlled from the southern hemisphere); equatorial downwelling (El Niño), with high rainfall and evaporation, is coincident with periods of weak circulation. The fact that the Pacific and Atlantic are practically closed basins in equatorial latitudes leads to some complications. In past epochs with stronger or weaker zonal circulation – i.e., during some parts of the glacial (strong) and interglacial (weak) epochs – upwelling or downwelling may each have occurred more than 90% or even 100% of the time.

There is evidence that the fluctuations in water temperature T_W and thus also in evaporation were even stronger during the glacial and interglacial epochs. A permanent southerly flow like that which existed in glacial times increases upwelling, and continuously spreads cool water to both sides (Doberitz 1968 and 1969). While thermal stability ($T_W < T_A$) increases, evaporation decreases and may even be reversed to condensation ("dew") on the cool surface of the water (with $q_w < q_A$). Conversely, in interglacial periods with distinctly weaker circulation, the tropical warm water (with temperatures of 26–27 °C) may have affected the weather and climate more than 90% of the time, with high instability, evaporation, and rainfall. Since the change between upwelling and downwelling modes depends on $\vec{\tau}$, which is proportional to v^2, relatively weak variations in atmospheric circulation can lead to enormous variations in evaporation and rainfall.

The great importance of these processes for oceanic evaporation as well as for the global water balance will be illustrated by an analysis of conditions during the peak of the last glaciation (about 24,000 to 14,000 years ago) and of the last interglacial period (about 125,000 years ago). The climate during these two epochs was almost everywhere more arid or more humid than at present. This may be tentatively interpreted in the following way. The area involved in the temperature fluctuations may have been only an equatorial ocean belt in the Pacific and Atlantic between lat 10 °S and 10 °N, extending over 52×10^6 km^2. Little evidence is available for the Indian Ocean. Gardner and Hays (1976) and Prell *et al.* (1976) have evaluated T_W on the basis of a great number of ocean cores. Of particular interest is core A 180-73 located at lat 0°, long 23 °W. The investigators found that 18,000 years ago, at the peak of the last glaciation, T_W in August was approximately 16 °C, 7–8 °C colder than it is now at this location. During an earlier glacial peak 55,000 years ago, T_W dropped to about 14 °C. In contrast, at the peak of the last interglacial period 125,000 years ago, T_W was approximately 26 °C. (In subtropical latitudes, however, T_W has remained essentially unchanged.) February temperatures were only 1–3 °C cooler at the peak of the last glaciation 18,000 years ago than they are today; this indicates a strong upwelling during southern winter with an extension of the southerly circulation (due to an expansion of the Subantarctic seasonal ice).

These data, obtained for a sufficient number of ocean cores, using different biostatistical techniques, are accurate within ±1–2 °C. They indicate that the low value of evaporation E (obtained by Trempel at the Galapagos) of 0.8–1 mm/d or 30–36 cm/yr, with $T_W = 18–19$ °C, is not exceptional; when T_W drops to 14 °C, the value of E may reverse completely.

The present value of E for the area involved in temperature fluctuations, as discussed above, is about 132 cm/yr or 69×10^3 km^3/yr (Baumgartner and Reichel 1975). In a glacial phase, 36 cm/yr may be considered representative of this large area, yielding only 19×10^3 km^3/yr, i.e., a regional loss of 50×10^3 km^3, or 72%, occurs. For the global budget, one must take into account the decrease in E caused by the Arctic sea ice and extending to lat 45 °N (Atlantic only). For an area of 14×10^6 km^2, this yields a loss ranging from $E = 73$ cm/yr to $E = 15$ cm/yr, or 8×10^3 km^3. Furthermore, the drop in the global sea level by at least 100 m produces a loss in ocean area of 20×10^6 km^2 and of $E = 12 \times 10^3$ km^3. The expansion of the Subantarctic drift ice 600 km northward in summer and winter (Hays *et al.* 1976) and over an area of about 14×10^6 km^2 yields a further loss in evaporation of at least 5×10^3 km^3. One obtains altogether a loss of $50 + 12 + 8 + 5 = 75 \times 10^3$ km^3, which is 15% of the global annual budget (496×10^3 km^3), or 18% of total oceanic evaporation (425×10^3 km^3).

In a warm interglacial phase with permanent downwelling, E may have reached 155 cm/yr or 81×10^3 km^3/yr (for the Pacific and the Atlantic together). Here we may take into consideration the change in the area of the

Arctic drift ice from 10^7 km^2 to 7×10^6 km^2; this may further increase E by 2×10^3 km^3. The total increase in E is then $12 + 2 = 14 \times 10^3$ km^3/yr or 3% of the global evaporation. This figure may be too small, however, because continental changes have been neglected. Even more significant is the drastic change in the evaporation of equatorial oceans from about 80×10^3 km^2/yr during the interglacial period to 20×10^3 km^2/yr during the glacial period. This is the physical background for the nearly complete disappearance of equatorial rain forests during the glacial phases and their replacement by semihumid grasslands (see Shackleton 1977).

The equatorial ocean belt discussed above plays a key role in large-scale climatic change. J. Bjerknes (1969) has shown empirically the effects of changes in T_W in that area on worldwide atmospheric flow patterns. The circulation model developed by Rowntree (1972) also demonstrated these effects. The importance of the equatorial ocean belt has become even more evident since Bacastow (1976) and Newell (1978) showed, on the basis of records from Mauna Loa, Hawaii, and South Pole stations, that, after accounting for seasonal fluctuations, the time variations of the increase in atmospheric CO_2 are in line with the irregular change between upwelling and downwelling. Newell (1978) indicated that this correlation essentially depends on the nutrient content of the upwelling deep water; during a cool phase the photosynthesis rate in this water is high and much CO_2 is removed from the atmosphere, while during a warm phase the uptake of CO_2 by the ocean is weak. This leads to a marked positive correlation between the annual increase in atmospheric CO_2 and the sea surface temperature in the equatorial Pacific. During the 1958–1974 period, the average increase in CO_2 in the air during five downwelling years was 1.11 ppm/yr; in contrast, during five years with maximum upwelling, the average CO_2 increase was only 0.57 ppm/yr (Keeling and Bacastow 1977, data averaged from Mauna Loa and the South Pole). In the latter case, time variations in water vapor content and in the CO_2 increase rate are positively correlated. This contributes much to a better understanding of the internally coherent processes controlling the climatic variations on a 1,000-year scale during the peak of the last glacial period and the Holocene period. These variations included aridity and drastic reduction of tropical forests 18,000 years ago, together with strong cooling of equatorial (but not of subtropical) oceans; they included as well a peak in precipitation and expansion of tropical forests far into the arid zone 12,000–6,000 years ago, together with equatorial warming and weakening of the trade winds (see Shackleton 1977).

3 MAN-MADE CLIMATOGENIC PROCESSES: THE "COMBINED GREENHOUSE EFFECT" OF CARBON DIOXIDE AND ATMOSPHERIC TRACE GASES

3.1 FACTORS CONTRIBUTING TO THE GREENHOUSE EFFECT

Any analysis of the impact of an increasing "greenhouse effect" (warming of the earth's surface and the lower layers of the atmosphere) on future climate must take into account that, in addition to CO_2 (Schneider 1975), some other, at least partially man-made, gases play an important role in creating the effect. Like CO_2, these gases absorb terrestrial radiation, particularly in the window region between 7.5 and 12 μm, just below the region of strong CO_2 absorption (12–18 μm) (Ramanathan 1975, Wang *et al.* 1976). Also involved in the greenhouse effect is water vapor, the strongest absorber of infrared radiation. The global amount of evaporation (and precipitation) has recently been estimated to be 496×10^3 km^3/yr, equivalent to a water column of 973 mm/yr (Baumgartner and Reichel 1975). Man-made evaporation over land areas amounted to 1,800 km^3/yr in 1965 (Lvovich 1969), and may rise to about 2,500 km^3/yr by the beginning of the 1980s (Flohn 1977a). This amount is equivalent to only 0.5% of the global value, which is certainly within the limits of error. With a global warming of the atmosphere, the evaporation of the oceans will rise appreciably. This has been simulated by some of the most realistic models available (see Manabe and Wetherald 1975, Wetherald and Manabe 1975). Also, because of the importance of equatorial upwelling and downwelling for evaporation (see Chapter 2), other significant changes in the atmospheric water vapor content are to be expected. Even a slight increase in "precipitable water," which is at present equivalent to a water column of only 25 mm, will contribute to the greenhouse effect (Manabe and Wetherald 1980).

While future increases in CO_2 concentrations have been investigated by many authors, the role of trace gases has only recently been recognized. Wang *et al.* (1976) have used a one-dimensional radiative–convective model with fixed relative humidity to study the impact of these gases. In their model the role of clouds is accounted for in two ways, by assuming a fixed cloud-top altitude (CTA) and a fixed cloud-top temperature (CTT). According to their

investigations, the combined effect of man-made trace gases is on the same order of magnitude as the effect of CO_2. Thus any neglect of these processes would cause a serious underestimation of the total greenhouse effect. Table 2 presents data from Wang (1976) in condensed form.

As well, Table 2 contains results from a similar one-dimensional radiative–convective model describing the CO_2–temperature relationship (Augustsson and Ramanathan 1977; also see Figure 6). In contrast to the frequently cited Manabe–Wetherald model (Manabe and Wetherald 1975), these models are one-dimensional and neglect atmospheric dynamics and transports. The radiation–cloud interaction is not included, nor is feedback between temperature and snow–ice albedo. Thus their results are only representative of low and middle latitudes; in subpolar and polar latitudes, the effect of CO_2 on the temperature must be multiplied by a factor of about 3, as recent empirical data indicate (Borzenkova *et al.* 1976). Results from the Augustsson–Ramanathan model (Figure 6) do not differ greatly from the results obtained by Manabe and Wetherald (1975). With a doubling of CO_2, the former model yields a warming of 1.98 °C (CTA) and 3.2 °C (CTT), while the latter model yields a warming of 1.92 °C for lat 0–30° and of 2.20 °C for lat 0–50°. Figure 7 provides results from a more recent version of the Manabe–Wetherald model, showing the role of a quadrupling of the CO_2 content. The results of other recent radiation models of the CO_2–temperature relationship are scattered around the model results described above (Schneider 1975, Bach 1978, Rowntree and Walker 1978; for a review see Ramanathan and Coakley 1978). In a recent critical examination of all existing model results, an independent Ad Hoc Study Group of the US National Research Council estimated that the most probable global warming which would result from a doubling of CO_2 is near 3 °C, with an error possibly as great as ±1.5 °C (National Academy of Sciences 1979). Further discussion would go beyond the scope of this paper.

The first two rows in Table 2 show that both the Augustsson–Ramanathan and the Wang models agree quite highly in estimating the CO_2 greenhouse effect, assuming that temperature increases nearly linearly with CO_2 until the amount of CO_2 doubles for the first time (Figure 6). The future changes in the O_3 and H_2O content of the stratosphere, due to increasing supersonic traffic, are probably too high as calculated by the Wang model, since it is doubtful that this traffic will reach the levels assumed in the model. While infrared absorption, influenced by a decrease in O_3 and an increase in stratospheric H_2O, may produce additional warming, it is assumed here that the two effects tend to cancel out (third and fourth rows in Table 2).

One of the most important atmospheric trace gases is nitrous oxide (N_2O), produced by denitrification of fertilizers in the soil. A large increase in this gas seems unavoidable, if one considers all the complexities of the nitrogen cycle in the environment, including the atmospheric residence time of nearly 70 years (Söderlund and Svensson 1976, Hahn and Junge 1977). During the 1962–1974 period, the annual average increase in nitrogen fertilizers was as high as

TABLE 2 Infrared-absorbing trace gases and their greenhouse effect.

Constituents	Present concentration	Expected Increase in concentration(%)[a]	Greenhouse effect (° C)	
			CTA[b]	CTT[c]
CO_2	320 ppm[d]	+100%	1.98	3.2
CO_2	330 ppm[d]	+25%	0.53	0.79
O_3	0.34 cm	−25%	−0.34	−0.47
H_2O (Stratosphere)	3 μg/g	+100%	0.65	1.03
N_2O	0.28 ppm[d]	+100%	0.44	0.68
CH_4	1.6 ppm[d]	+100%	0.20	0.28
CCl_2F_2 + CCl_3F	0.2 ppb[e]	factor of 20	0.36	0.54
CCl_4 + CH_3Cl	0.6 ppb[e]	+100%	0.01	0.02
NH_3	6 ppb[e]	+100%	0.09	0.12
C_2H_4	0.2 ppb[e]	+100%	0.01	0.01
SO_2	2 ppb[e]	+100%	0.02	0.03

[a] All the growth rates assumed in the Wang model are estimated for 2020 AD; the Augustsson–Ramanathan model is independent of time.
[b] Model version in which the cloud-top altitude is held constant.
[c] Model version in which the cloud-top temperature is held constant.
[d] Parts per million.
[e] Parts per billion (10^9).
SOURCES: The CO_2 data in the first line are taken from the Augustsson–Ramanathan model (Augustsson and Ramanathan 1977); all others are taken from the Wang model (Wang *et al.* 1976).

10.7% (Pratt *et al.* 1977). Even with just a linear growth rate, one could expect an increase of 170% by the year 2000, rather than 100% as Wang assumed for 2020. Pratt estimates an increase of 200 to 450% between 1974 and 2000, while Hahn and Junge more cautiously estimate a rise of 100 to 160%. Using conservative assumptions, Hahn (1979) estimates the greenhouse effect of N_2O alone to be about 25% of that of CO_2; together with NH_3 and HNO_3, the effect of N_2O is estimated by Hahn to be about 37% of that of CO_2.

Another important atmospheric trace gas is CH_4, which is considered a conversion product of CO. Its presence is strongly correlated with the burning of fossil fuels. Finally, the contribution of chlorofluoromethanes (CFMs) to the greenhouse effect derives from their chemical inertness and thus from their long atmospheric residence time, estimated at 30–50 years. Since strong efforts are being made to prohibit the use of these substances in refrigerators, aerosol spray cans, and so on, we may expect a drastic reduction in their rate of increase in the atmosphere (from a factor of 20 to a factor of 3), and assume a linear reduction in the corresponding greenhouse effect. The greenhouse effect of all other gases is small compared to that of the gases discussed above.

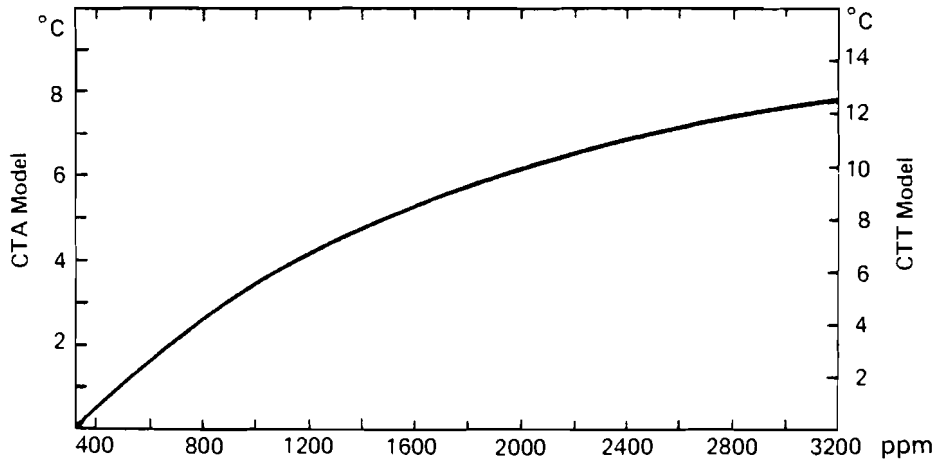

FIGURE 6 CO_2 concentrations (ppm) and increases in surface temperatures (°C) at representative middle latitudes. Results from both the CTA (fixed cloud-top altitude) and CTT (fixed cloud-top temperature) versions of the Augustsson–Ramanathan model (1977) are shown.

The selection of an appropriate model to account for the role of clouds deserves attention, since, due to our ignorance of some important parameters, we still cannot handle adequately the important cloud–radiation feedback. While Augustsson and Ramanathan prefer to hold the cloud-top altitude (CTA) constant, Wang *et al.* consider a constant cloud-top temperature (CCT) a more plausible assumption. The CTA model appears to be more consistent with the assumption of constant relative humidity. Table 2 shows that the CTA model is less sensitive to the presence of CO_2 and atmospheric trace gases than the CTT model. Though the results of the CTA model may seem somewhat more convincing at the present time, results from the CTT model should also be considered. In any case, the possible role of clouds should not be overestimated, as was argued in Chapter 1.

3.2 ESTIMATION OF THE FUTURE COMBINED GREENHOUSE EFFECT

Taking the results from Wang's model for CO_2 and using his estimated growth rates as a first order assumption, one may expect an increase in atmospheric CO_2 from 330 to 412 ppm, equivalent to a warming of 0.53 °C (CTA) or 0.79 °C (CTT). In addition, one may expect a warming of 0.81 °C (CTA) or 1.19 °C (CTT) associated with the presence of N_2O, CH_4, CFM, and other gases. This produces 150% more warming, with both the CTA and the CTT models, than would be caused by CO_2 alone. If one includes the full effects of supersonic transport (O_3 and H_2O) as calculated by Wang *et al.*, the atmosphere

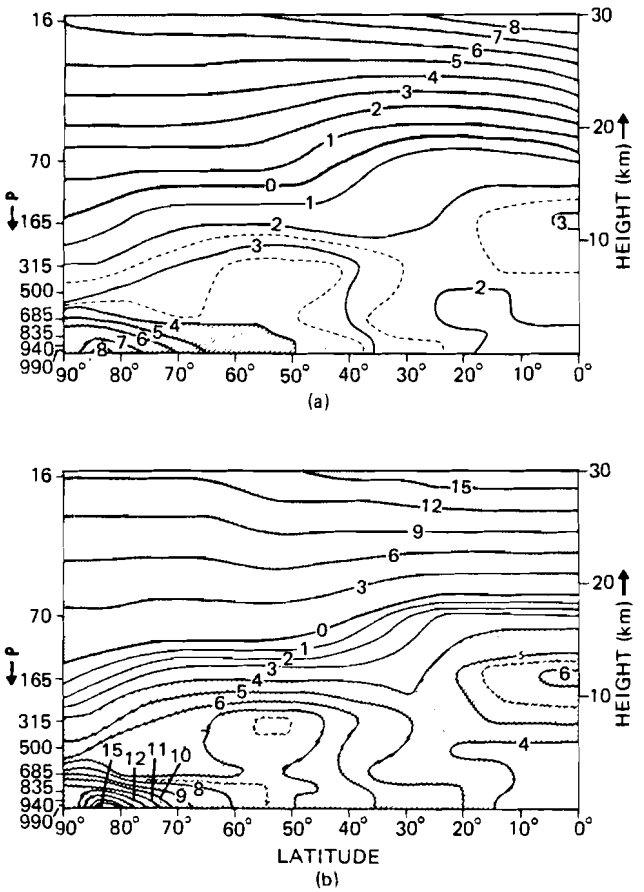

FIGURE 7 Temperature change (°C) in a vertical–meridional section of the atmosphere after (a) doubling and (b) quadrupling of the CO_2 content, including atmospheric dynamics. The ocean is treated as a swamp. Note the strong warming of the lower polar atmosphere due to the snow–albedo–temperature feedback. Source: Manabe and Wetherald (1980).

would be further warmed by 0.31 °C (CTA) or 0.56 °C (CTT). In other words, the greenhouse effect would be 212% or 288% larger than if CO_2 alone were considered. However, this possible additional effect is disregarded in this paper, and thus the estimates given here are more likely too low than too high (see Flohn 1978c). This is especially true in view of the possible increase in water vapor discussed in Chapter 5.

Like the well-known ozone band at 9.6 μm, the atmospheric trace gases dealt with above have narrow absorption bands in the infrared window between the strong absorption bands of H_2O and CO_2. It should be realized, however,

that two of the N_2O absorption bands are situated on the flanks of the much stronger bands of H_2O and CO_2 (at 7.78 μm and 17.0 μm respectively) (Wang *et al.* 1976, Figure 1). In view of the enormous differences in concentration among the atmospheric gases, it is necessary to further investigate the question of overlapping. According to Wang *et al.*, an additive effect can be safely assumed. The physical processes of trace gases in the window region (7.5–12 μm) are similar to those of H_2O and CO_2 on both flanks of the window; together these gases act as venetian blinds attached to the atmospheric window.

In an unpublished paper Ramanathan recently described a sophisticated radiative–convective model for estimating in detail the role of other infrared trace gases. Model results indicate that a possible increase in tropospheric O_3 may play a significant role, due to photochemical processes involving CO and CH_4. Preliminary results from Ramanathan's model do not differ greatly from the estimates used below.

To account for the effects of the atmospheric trace gases, 50% will be added to the expected future increase in CO_2 content (i.e., to the 320 ppm base used by Wang *et al.*), and this combined greenhouse effect (CGE) will be expressed in units of virtual CO_2 concentration given in ppm. This would be equivalent to a 67% contribution of real CO_2 to the virtual CO_2 level at any given time. A less conservative approach would be to add 100% to the expected increase in CO_2 content, equivalent to only a 50% contribution of real CO_2 to the virtual CO_2 level. The right-hand columns of Table 3 give the real CO_2 value for given levels of virtual CO_2, using the relation between the combined greenhouse effect and temperature shown above in Figure 6. Although the more conservative assumption of a 50% addition to the expected increase in CO_2 is preferred, results obtained using the assumption of a 100% addition are also presented in Table 3.*

The expected increase in atmospheric CO_2 strongly depends on the future evolution of the global CO_2 budget. A report of a working group of specialists at the Dahlem Conference (Stumm 1977) – based on various models with logistic growth curves – estimated maxima of atmospheric CO_2 concentrations at between 1,100 ppm and 1,600 ppm. At a more recent IIASA workshop (Williams 1978), participating specialists tentatively concluded that there would be a "manifold increase" in CO_2 if all economically exploitable fossil fuels were burned, and if the CO_2 growth rate could not be reduced to less than 3%. In a critical survey, Junge (1978) estimated an increase in atmospheric CO_2 by a factor of nearly 3 until the year 2050, with a further increase after this date. A rather realistic model of the global carbon cycle and the biosphere (Olson 1978) yielded a doubling of atmospheric CO_2 around 2040, and an increase by a factor of 4–6 (or even higher) by the twenty-second century. These model estimates of a possible manifold increase in atmospheric CO_2 due to fossil fuels

*In a recent lecture (Münster, March 1980), Ramanathan proposed the assumption of a 30% addition at the current time, increasing to 70% over the next 50 years.

TABLE 3 Atmospheric CO_2 content equivalent to estimated temperature differences (ΔT) during selected paleoclimatic phases.

Paleoclimatic phase	ΔT(°C)[a]	Virtual CO_2 content[b] (ppm)		Approximate real CO_2 content (ppm)			
				CTT[c]		CTA[d]	
		CTT[c]	CTA[d]	+100%[e]	+50%[f]	+100%[e]	+50%[f]
Current perception of warming	+0.5[g]	365	395	342	350	360	375
Medieval warm phase	+1.0	420	490	370	386	405	432
Holocene warm phase	+1.5	475	580	398	422	450	492
Eem Interglacial	+2.0	530	670	426	460	495	555
	+2.5	590	760	455	500	540	610
Ice-free Arctic ocean	+4.0	780	1150	555	630	740	880

[a]Estimated temperature increase over the current temperature.
[b]Unit expressing the combined greenhouse effect stemming from real CO_2 and atmospheric trace gases.
[c]Version of the Augustsson–Ramanathan model in which cloud-top temperature is held constant.
[d]Version of the Augustsson–Ramanathan model in which cloud-top altitude is held constant.
[e]Assuming a 100% contribution of trace gases to the expected increase in virtual CO_2.
[f]Assuming a 50% contribution of trace gases to the expected increase in virtual CO_2.
[g]Based on the current CO_2 concentration of 330 ppm.
SOURCE: The data presented in this table are based on results from the Augustsson–Ramanathan model (Augustsson and Ramanathan 1977).

would remain unchanged, if the net contribution of the biosphere to the CO_2 budget would indeed remain small. This important point has been made independently by many specialists at recent conferences (i.e., presentations made by B. Bolin, W.S. Broecker, C.D. Keeling, H. Oeschger, and others at the Conference on Energy and Climate, Münster/Westfallen, March 1980).

In respect to the future evolution of the global CO_2 budget, a very controversial question is the role of the widespread destruction of existing virgin forests – 110,000 km^2/yr according to FAO statistics (see Polunin 1980). This destruction is another source of increases in atmospheric CO_2.

In light of the findings discussed above, it is clear that a scenario of future climatic evolution for the case of man-made global warming should be based on the role of the combined greenhouse effect – described in terms of atmospheric CO_2 content – with respect to temperature. In Table 3, best estimates of temperature differences (ΔT) during selected paleoclimatic stages are given, based on all available data (without regard to unknown geophysical causes); these estimates are then converted into equivalent threshold values of CO_2 with the aid of the Augustsson–Ramanathan model (see Figure 6). In this way

past climatic stages can be used as scenarios for possible future climate modifications.

Results from the CTA version of the Augustsson–Ramanathan model, as well as from the more sensitive CTT version, are presented in Table 3. The first threshold that may be selected is the level of warming that can be unambiguously derived from current data sources. This "level of perception" of a quasi-global warming is estimated at 0.4–0.5 °C. Looking at results from the CTA version and the last two columns in Table 3, one finds a corresponding real CO_2 level of 360–375 ppm.

The other threshold values shown in Table 3 are estimates of representative temperature changes over land areas during some selected paleoclimatic stages, such as the early Middle Ages (about 900–1100 AD), the Postglacial (Holocene) Optimum (about 6,500–5,500 years ago), and the Eem stage of the last Interglacial.

Considering possible consequences, one of the most important questions is, When will these combined greenhouse effect thresholds occur? The answer depends heavily on developments and decisions in the fields of economics and politics in a pluralistic society – events far outside the author's field of expertise. Only a first-order estimate, based on a logistic growth rate model, can be tentatively given. Figure 8 gives a time scale for the expected temperature levels derived from the CTA version of the Augustsson–Ramanathan model, shown previously in Figure 6. (The curves labeled temperature in Figure 8 are in fact curves of virtual CO_2 content.) Figure 8 is also based on the combined greenhouse effect and the logistic CO_2 growth rate model developed by Zimen (1977a, 1977b). Zimen's model is based on the assumption that the biosphere does not act as a CO_2 source and that the airborne fraction of CO_2 (presently 53–56%) remains constant. Assuming that recent CO_2 growth rates of 3.5–4% per year continue, the 0.4–0.5 °C "level of perception" of a quasi-global warming will be reached between 1990 and 2000. Under the same assumption the CTT model would yield a date between 1985 and 1990.

Assuming a logistic growth rate between 3 and 4%, the 1.5 °C threshold (equivalent to the Holocene warm period) could be reached between 2005 and 2030, and the 2.5 °C threshold (equivalent to the Eem period) between 2020 and 2050. Figure 8 also contains estimates based on the apparently unrealistic growth rates of 1–2%; on the basis of these rates any immediate climatic risk appears to be avoidable. Several processes contribute to the uncertainty of the time scale: on one hand, the airborne fraction of CO_2 should increase with time, due to the increasing CO_2 content and acidification of the oceanic mixed layer; on the other hand, the thermal inertia caused by the storage capacity of the ocean may be responsible for a time-lag of an equilibrium temperature of several years or even decades. Thus for present purposes, it seems more appropriate to label the stages of the scenario using approximately equivalent levels of virtual CO_2 instead of fixed calendar years.

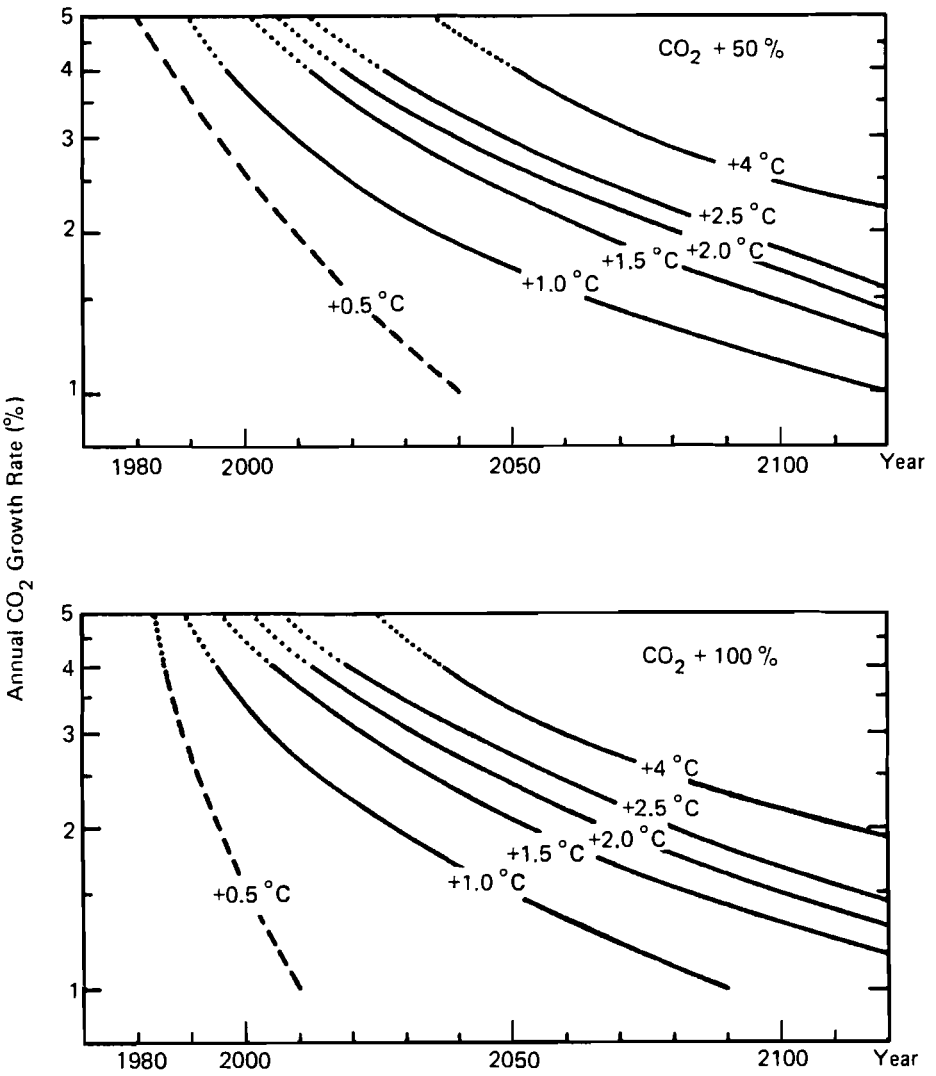

FIGURE 8 Extrapolation of the combined greenhouse effect to the year 2120 using logistic CO_2 growth rates. In the upper graph the contribution of trace gases to the combined greenhouse effect is taken into account by adding 50% to the estimated CO_2 level; in the lower graph the contribution of trace gases is taken into account by adding 100% to the estimated CO_2 level. The logistic CO_2 growth rates are taken from Zimen (1977a), and the temperature values are taken from Figure 7 of this paper.

4 RECENT CLIMATIC HISTORY AND THE PERCEPTION OF A GLOBAL WARMING

At the present time, global or hemispheric variations in surface temperature T_a can be detected only with the help of an existing network of climate stations situated almost exclusively on the continents and on a number of islands. This network has many gaps, especially in oceanic regions where the small number of stationary weather ships has been reduced drastically since 1973. The unevenly distributed stations are not sufficiently representative to account for the large irregular anomalies occurring over months, seasons, and years – a lot of noise is due only to the inadequacy of the station network. Thus interannual hemispheric temperature variations on the order of 0.2–0.3 °C can be hardly distinguished from noise.

Several papers provide an overview of the most recent temperature fluctuations. Yamamoto *et al.* (1975) have presented monthly data on T_a from 343 stations on the northern hemisphere for the period 1951–1973. They objectively analyzed the data with a cubic spline technique using moving three-month averages. Typically the most striking variations occurred in the latitude belt 60–85 °N; a significant reduction in temperature occurred after a volcanic eruption, with time delays on the order of 3 to 12 months. The effect of stratospheric dust of volcanic origin has also been analyzed with a much longer data series by Oliver (1976) and Mass and Schneider (1977). Yamamoto *et al.* (1977) have also extended their analysis to 431 stations, including some in the southern hemisphere, using time-series data for the 1957–1972 period. Still longer series of annual averages have been analyzed by Borzenkova *et al.* (1976) for several latitudinal bands between 82.5 °N and 17.5 °N, including the meridional gradient in the belt between 75 and 25 °N. The interannual fluctuations are large, especially in Subarctic and Arctic latitudes. For example, such fluctuations amounted to 0.5 °C in the belt between 57.5 and 72.5 °N, and to 0.63 °C in the polar belt between 72.5 and 87.5 °N, both in the 1940–1975 period. The hemispheric average reached a maximum around 1938, dropped approximately 0.5 °C by about 1963, and has been rising slightly since then, especially at the polar cap.

In high southern latitudes the period since 1943 has been characterized by a weak warming trend (Damon and Kunen 1976, Yamamoto *et al.* 1977). Records kept over long periods in the Subantarctic (Limbert 1974) and New Zealand (Salinger and Gunn 1975) indicate the same trend. The equatorial belt has undergone only short-lived fluctuations. According to a quite recent synthesis presented by nine investigators from the USA, Japan, and the FRG (Kukla *et al.* 1977b), interannual fluctuations explain most of the variance observed, and occur over most of the northern hemisphere and over parts of the southern hemisphere. The long-term trends are significantly weaker – i.e., on the order of 0.01–0.02 °C per year (also see Walsh 1977) – than the interannual fluctuations. This noise apparently demonstrates the role of internal feedback mechanisms within the climatic system and of short-lived external effects, such as volcanic events. These data do *not* show a reversal in the cooling trend of the last decades, especially not in the temperature of the upper air; only the surface temperature data from the Arctic and Subantarctic show an increase or remain more or less constant.

A comparison of these findings indicates the great difficulty in obtaining representative data on current temperature changes. This is especially true for the Arctic region, where the Asiatic and American sectors can have quite opposite trends (Walsh 1977); this indicates a longitudinal displacement of the center of the polar cold vortex, as is demonstrated by averages for the tropospheric layers (e.g., 500/1000 mbar).

Since all climatic variations are subject to large longitudinal changes which can frequently mask the latitudinal changes, it is preferable to use maps (van Loon and Williams 1976, 1977) and/or empirical orthogonal functions (Walsh 1977) for an adequate description of climatic change, at least for parameters such as pressure, geopotential, or temperature. A good example of climatic variability dependent on longitude is the Greenland/NW Europe seesaw (van Loon and Rogers 1978), which has been known for more than two centuries. Similar cases probably also occur in other areas because of the quasi-stationary behavior of the long waves of the atmospheric westerlies.

Unfortunately, most investigations have concentrated on temperature changes, and little is known about large-scale rainfall patterns, which have perhaps the greatest impact on economy and society. Here records from single stations often are unrepresentative and inhomogeneous. The use of areal averages is meaningful only if the available data are internally coherent. This is often not the case because of the rather rapidly diminishing spatial correlations, such as in the Mediterranean. Recent evaluations have demonstrated the role of the longitudinally-oriented Walker circulation in the tropics (Bjerknes 1969, Doberitz 1969, Flohn and Fleer 1975, Hastenrath 1976, 1977).* This circulation today is responsible for a seesaw correlation between equatorial

*The Walker circulation was so named by J. Bjerknes in 1969; it was originally called the Southern Oscillation by Sir Gilbert Walker in the 1920s. An index for the Walker circulation has been given by Wright (1975).

upwelling and downwelling in the Atlantic and in the Pacific (Doberitz 1969; see also Chapter 2 of this report). This is similar to the seesaw between the Pacific and Indonesia with the Indian Ocean, as was outlined by Walker and his successors (Berlage 1957, 1966). For a review of the numerous investigations in this context, see Wright (1977).

The recent *cooling* of the northern hemisphere, starting about 1940, has been on the order of −0.3 or −0.4 °C; this is apparently contradictory to the hypothesis of man-made *warming*. But note that the temperature trend in middle and high southern latitudes has at the same time reversed. One interpretation has been given by Damon and Kunen (1976), who consider the development in the southern hemisphere to represent the true CO_2 warming trend. This trend is masked in the northern hemisphere by cooling, due to man-made particles and volcanic eruptions. Both explanations are not very convincing; in particular the latter is brought into question by the recent occurrence of volcanic eruptions in the tropics south of the meteorological equator (Bali, 1963; Galapagos, 1968). Another possible interpretation is that the natural cooling of the northern hemisphere – probably partly due to volcanic activity, which was at a minimum between 1912 and 1948 – would have reached −0.6 °C, without the assumed warming due to CO_2 and equivalent to about +0.2 °C. Because of the high interannual variability, this argument cannot be verified. A look at past climatic data indicates a variation of ±0.5–0.6 °C around a moving 100-year average during the last centuries; this is a reasonable limit for natural fluctuations. In the northern hemisphere, such a warming can be observed on the basis of 5-year or 10-year averages; this is above the noise level produced by interannual variability.

There are some signs (see Kukla *et al.* 1977b) that the post-1945 cooling has already passed its climax. Since about 1974 the polar region has not been as extremely cold as it was between 1964 and 1972, when the Arctic ice was progressing toward Iceland and Newfoundland (see Figure 9). The years 1978 and 1979 still do not show an upward trend; indeed, for the polar cap (65–90 °N), 1979 is the coldest year. Other evidence can be found in the monthly surface temperature maps *Grosswetterlagen Europas* issued by the FRG Weather Service (also see Walsh 1977 and Walsh and Johnson 1979). The opposite trend in high latitudes of both hemispheres and the small changes observed in low latitudes indicate that the cooling of the Arctic between 1940 and 1970 was *not* a global phenomenon. If future man-made warming is superimposed on the natural fluctuations occurring at irregular intervals over several decades, it should intensify the natural warming episodes and weaken (or even reverse) the natural cooling episodes. A warming of about 0.5 °C above the noise level, maintained for a period of about ten years, would coincide with the expected tendency. Only this might be a sufficiently convincing argument to override scientific scepticism. Using an objective procedure (based on records from 12 stations along 60 °N), Madden and Ramanathan (1980) have shown that at present no convincing sign of a CO_2-induced warming can be detected. This may result from other

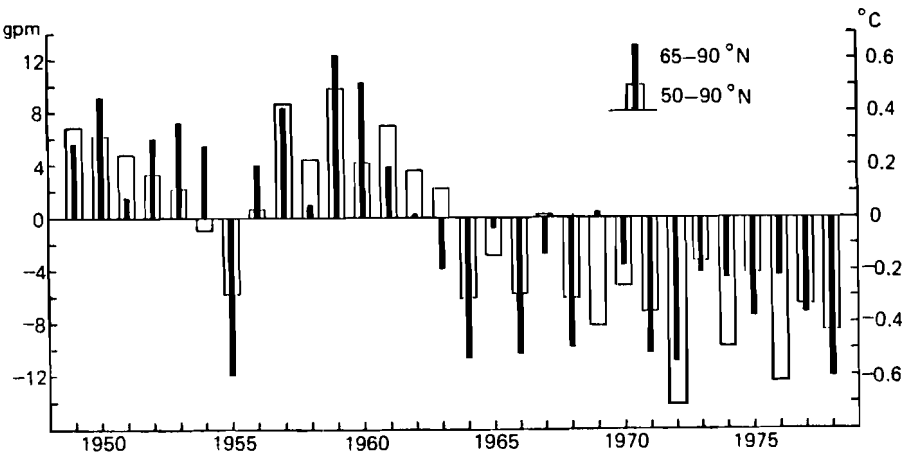

FIGURE 9 Deviations of the average annual temperature of the 500/1000 mbar layer above the polar caps from the 1949–1973 average, 65–90 °N and 50–90 °N. Gpm stands for geopotential meters. Source: Dronia (1974) with amendments provided by the author.

(natural or man-made) climatogenic effects and/or from failure to consider thermal ocean inertia. It is also not clear whether all short-lived fluctuations are of a deterministic or a stochastic nature. An interesting attempt to outline possible CO_2-induced climatic change until the year 2000 has been made by Wigley *et al.* (1980), comparing the 5 warmest and 5 coldest years during the last 50 years.

The evidence presented above thus suggests that a *global warming of 0.5 °C* can be assumed to be a reasonable threshold for a general perception of warming – even if it may still be impossible to distinguish quantitatively between the contributions of natural versus anthropogenic processes. Beginning about 1990, a repetition of some climatic patterns of the 1931–1960 reference period (to avoid the misleading term "normal") can be expected; this reference period was one of the warmest periods during the last 500 years, and was also characterized by a relatively low interannual variability in some regions (such as India), but not in western and central Europe, where severe winters and exceptional wet or dry summers were observed in the 1940s (see, for example, Ratcliffe *et al.* 1978).

A more general notion of recent short-lived climatic fluctuations can be obtained from the monthly maps of the 500/1000 mbar layer for large areas of the northern hemisphere, published in *Grosswetterlagen Europas* since 1949, as mentioned above; the thickness of this layer is proportional to the temperature, and represents the average temperature of the lower half of the atmospheric mass (≈ 0–5 km).

Figure 9 (updated after Dronia 1974) gives the deviation of area averages from a 25-year average (1949–1973) for the polar cap 65–90 °N and for lat 50–90 °N for each calendar year. This procedure suppresses all longitude-dependent variations. In the 500/1000 mbar layer, the systematic deviations of the individual radiosondes are generally below 0.5 °C and can be neglected, at least in the case of area averages. The year-to-year variations are still relatively large. A good example is the year 1955, when a great anomaly centered in the Pacific. The marked cooling during 1962–1964 cannot be interpreted as having been caused by the Agung eruption in Bali in early March 1963, although this event probably contributed to the cooling. Since 1963 the average temperature of the lower troposphere in polar latitudes has remained a few tenths of a degree cooler than it was before. A worldwide comparison for the years 1958–1976, based on 63 evenly spaced radiosonde stations (Angell and Korshover 1978), has verified a warming trend in high southern latitudes, indicating a cooling in northern and southern temperature latitudes, as well as increasing temporal variability in the tropics. In all latitude belts, 1976 was one of the coldest years on record.

In addition to such temperature data, it is necessary to obtain in the near future continuous records of some integrating parameters, such as the extension of sea ice at the end of the melting season in the northern and southern hemispheres (in August or late February, respectively). This is especially important for the North Atlantic sector where the greatest fluctuations are to be expected. The Commission on Snow and Ice of the International Union of Geophysics and Geodesy (IUGG) collects data for many mountains on glacier variations. For our purposes the extended permanent ice fields and snowbeds in high latitudes are of paramount interest, rather than valley glaciers in alpine mountains that, in quite a number of cases, only respond to local conditions. The variations in the size of glaciers at the end of the melting period should be monitored, including the relative area of snowbeds in the partly unglaciated Queen Elizabeth Islands (Canadian Archipelago) and in similar islands in the Siberian sector of the Arctic.

Special mention should be made of the following ice fields (Hattersley-Smith 1974): Iceland–Vatnajökull, Hofsjökull, Langjökull (partly controlled by volcanic and geothermal activity), Drangajökull (NW); Baffin Island–Penny Ice Cap (66–67 °N), Barnes Ice Cap (70 °N); Devon Island–field at 75 °N; Axel Heiberg Island–field at 79–81 °N, (studied since 1959); Norway–Folgefonn (60 °N), Hardangerjökull, Jostedals Breen, Svartisen (67 °N); Svalbard–Edge Island, Nordaustlandet; and Severnaja Zemlja–field at 78–81 °N. In the southern hemisphere, the large Patagonian ice field situated at lat 48–50 °S should also be mentioned (Schwerdtfeger 1956, 1958).

A continuous evaluation of the snow-covered land area based on satellite data (Kukla *et al.* 1977b) is also necessary. According to recent experience (1971–1972), the early appearance of a continuous snow cover in the autumn is of great importance for the evolution of cold-season surface temperatures on boreal continents.

5 EXAMINATION OF PAST CLIMATES AS A BASIS FOR A GLOBAL WARMING SCENARIO

5.1 MEDIEVAL WARMING

According to the wealth of evidence collected by Lamb [1977a (see especially Chapters 13 and 17), 1979] the early Middle Ages represent the warmest period of the last millennium. The temporal peak of this warm period differs slightly between areas (Dansgaard *et al.* 1975, Alexandre 1977, Wigley 1977). The most remarkable period was between about 900 and 1050. It was characterized by unusually warm and hospitable conditions in Arctic latitudes (Barry *et al.* 1977), with a disappearance of sea ice in the East Greenland Current, cereal cultivation in Iceland and Norway up to 65 °N (and even experimentally in Greenland), and Eskimo settlements as far north as Ellesmere Land and the New Siberian Islands.

During this period, forests in Canada advanced up to 100 km north of the present timberline, simultaneously with an upward shift of the tree line in many European mountains. This indicates a temperature increase of around +1 °C, compared with average temperatures between approximately 1916 and 1950 (Table 4). Frequent droughts occurred all over Europe south of 60 °N. The Caspian Sea stood at −32 m, i.e., lower than today's level, after losing much water for irrigation. (This sea subsequently rose 12 m by the 14th century.) In the Mediterranean region, the Dead Sea was nearly as low as it is now (Klein 1977), but the northern part of the Sahara was definitely wetter. Crossing the desert by horse caravan has been reported for that time (Nicholson 1980), and the end of earlier cattle rearing around the Kufra oasis (now near the center of aridity) has also been traced to this period. China and Japan had warm summers (Chu 1973, Yoshino 1978), but severe winters in China, with freezing of the lakes near the banks of the Yangtse Kiang River, have been reported.

In North America, there is evidence of large cultivated areas and a remarkable urban center in Illinois and Iowa (Bryson and Murray 1977). Tree ring data from California mountains also indicate higher temperatures but low

TABLE 4 Estimated climate parameters for Central England during selected periods.

Climatic Periods	Temperature (°C)			Rainfall			
	Annual average	July–Aug.	Dec.–Feb.	Annual	July–Aug.	Annual Evaporation[b]	Annual Runoff[b]
"Atlantic"[c] (6,000 yrs ago)	10.7	17.8	5.2	110–115[a]	–[e]	108–114[a]	112–116[a]
Little Optimum[d] (1150–1300 AD)	10.2	16.3	4.2	103[a]	85[a]	104[a]	102[a]
Little Ice Age (1550–1700 AD)	8.8	15.3	3.2	93[a]	103[a]	94[a]	92[a]
Recent warm period (1916–1950 AD)	9.4	15.8	4.2	932 mm		497 mm	435 mm

[a]Percent of 1916–1950 average.
[b]Calculated according to Turc's formula.
[c]Holocene warm period.
[d]Data probably also valid for 900–1050 AD.
[e]No evidence available.
SOURCE: Lamb (1977).

rainfall, similar to southwest Colorado. Evidence from the tropics is very scanty. Rains concentrated in the southern part of Ethiopia (Nicholson 1976), while Nile floods were low and Lake Turkana was high. No data are available for India. Long-lasting warming on the Antarctic coast, together with a period of marked drought and forest fires in New Zealand, has been reported.

One interpretation of these data (Lamb 1977a) suggests a northward shift of the cyclone track by 3–5° latitude to 60–65 °N and high pressure conditions over Europe, similar to the warmest and driest summers of the 1931–1960 period; in winter, a similar pattern occurred during this period in the north, which has frequently been related to a "blocking" pattern with severe winters and extended droughts, especially in eastern Europe. Such a pattern would be consistent with the marked retreat of ice from the Greenland seas during the early Middle Ages. Since the speed of the East Greenland Current is higher than the melting time of ice floes, a retreat of the Atlantic drift ice to latitudes north of 80 °N is indicated. Cooling in northern Greenland after 1160 (Dansgaard 1975) coincides with a marked advance of glaciers in the Alps and other mountain ranges, and with a reappearance of Arctic sea ice around 1320. Extreme climatic anomalies and severe famines also occurred throughout Europe and a long drought period (200 years) affected Iowa and Illinois, leading to mass emigration from these areas (Bryson and Murray 1977).

This wave of anomalies announced, after several interruptions, the transition towards the Little Ice Age (1550–1850).

5.2 THE HOLOCENE WARM PERIOD AND THE HUMID SAHARA

The history of the retreat of the melting ice domes of North America and northern Europe after the peak of the last ice age 18,000 years ago is fairly well known (see Lamb 1977a, Chapter 16). While the smaller Scandinavian ice sheet finally disappeared more than 8,000 years ago (Figure 10), the North American ice sheet still covered about 50% of its former area at that time (Figure 11), disintegrating after a catastrophic incursion of the sea into Hudson Bay, probably about 7,800–7,600 years ago (Hughes 1977). Separate ice sheets remained; the Labrador ice did not disappear until about 4,500 years ago, while some ice fields of about 35,000 km^2 in interior Baffin Island have apparently survived until today. This created a marked longitudinal asymmetry of the atmospheric circulation between 8,000 and 6,500 years ago (Lamb 1977a), which faded out 4,500 years ago. During this episode, Eurasia and Africa experienced the warmest epoch of the last 75,000 years, but eastern North America remained relatively cool, especially in summer, with frequent outbreaks of polar air. This caused a predominance of southwesterly winds over the Atlantic, probably producing an intensification of the Gulf Stream and its northward-flowing branches. In winter, the frequent occurrence of anticyclonic ridges at long 0–20 °W would be consistent with frequent outbreaks of polar air also over central and eastern Europe, extending with copious precipitation to the Mediterranean Sea and northern Africa.

The present description of the climate during the Holocene warm period refers mainly to the peak of the epoch, around 6,000 years ago. Data are given here in radiocarbon years; their conversion into calendar years, with a possible difference of up to 12%, appears to be a matter of controversy. Insufficient time resolution of the data available does not yet allow treatment of the existing fluctuations on a 100-year or even a 500-year scale.

During the peak of the Holocene period, forests in western Canada and in western Siberia extended 200–300 km farther north than they do today. The summer temperature has been estimated to have been 2–3 °C higher than at present. Subarctic forests also covered the northernmost islands of Norway and the whole of the Taimyr peninsula. This warm period, however, came to an end around 4,800 years ago, when, because of a polar outbreak lasting no longer than about 200 years, the Canadian timberline moved more than 300 km south (Nichols 1975). Almost simultaneously with this relatively brief event, important climatic shifts towards a "neoglacial" climate – similar to the Little Ice Age between 1550 and 1850 AD – occurred in many areas, together with a gradual desiccation of the present Arid Belt.

At the peak of the warm period the waters of the Kuroshio, between Taiwan and Japan, were up to 6 °C warmer than now (Taira 1975). With some

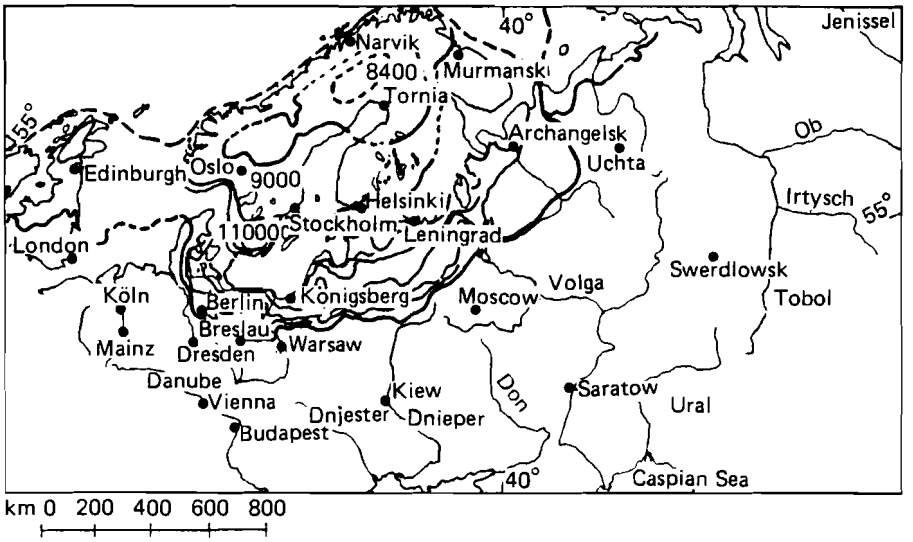

FIGURE 10 European ice margins during the last glaciation, 18,000–8,000 years ago. The map is based on Woldstedt (1969).

delay, the interior Arctic experienced its warmest level during the Holocene period about 4,500 years ago; open waters flowed in the fjords and along the northern coasts of Spitzbergen, Greenland, and Ellesmere Island, allowing Siberian driftwood to reach these coasts up to lat 83 °N (Vasari *et al.* 1972, Barry 1977). However, there is no indication that the core of the present Arctic drift ice between Greenland, Alaska, and eastern Siberia disappeared during the Holocene warm period. Regarding the sea level, only conflicting evidence is available for a worldwide rise of a few meters at the time; this question will be considered in the following chapter of this report.

In the Subantarctic ocean, the very rapid shrinking of the mainly seasonal Antarctic drift ice led to a warming peak as early as 9,000 years ago (Hays 1978). Similarly, the Holocene warm period had already started more than 7,000 years ago (Starkel 1977) in eastern Siberia, an area in which no major ice sheets had formed during the previous glaciation. At Lake Biwa in central Japan, the warm period was initiated over 8,000 years ago (Fuji 1976). The transition between the glacial and interglacial (Holocene) modes of the atmospheric–oceanic circulation was very complex, superimposed by a series of abrupt changes between cold and warm phases (i.e., Bölling, Alleröd phases: see Lamb 1977a) between about 13,500 and 10,800 years ago. At the end of this period, the tropical oceans became slightly warmer than they are now; this was probably accompanied by a substantial weakening of the tropical (Hadley) circulation. Increasing evaporation raised the water vapor content of the tropical air, leading to a rapid expansion of the tropical rainbelt and

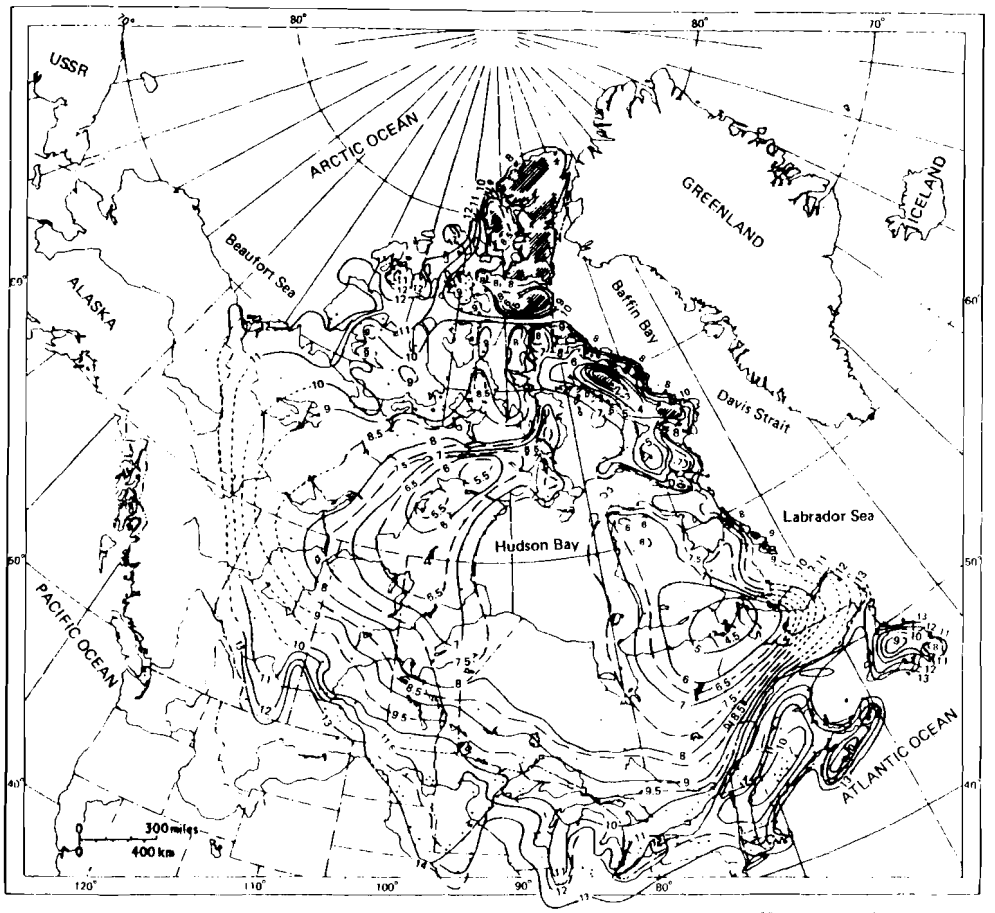

FIGURE 11 Isochrones of the withdrawal of the North American (Laurentide) ice sheet. The numbers in the body of the map are dates expressed in 10^3 years before the present time. Dots show where radiocarbon dates have been established. Moraines, coastlines, and all other available evidence have been used. Source: Bryson *et al.* (1969), reprinted in Lamb 1977a.

rain forests (which had been drastically reduced during the previous ice age) towards higher latitudes (Rognon and Williams 1977, Shackleton 1977).

For England and Wales, Lamb has given estimates of the basic climatic parameters, including those representing other climatic stages of interest (see Table 4). On the mid-latitude oceanic coasts the probable temperature increase was 1.5–2 °C.

In other continental areas the increase was lower, at least in northeastern North America. In the area between 85° and 95 °W, a triangle of prairie vegetation extended into Wisconsin and Illinois, reaching a maximum about 7,000 years ago (Bernabo and Webb 1977). Together with some areas in southwest Siberia

and in eastern Turkey, this is one of the few areas that was drier during the Holocene period than it is now. The occurrence of thermophilous species in European and Asiatic forests (Frenzel 1967, 1968a, 1968b) indicated somewhat higher temperatures and rainfall. Permafrost in eastern Siberia retreated several hundred kilometers north of its present position; a similar retreat in Canada and Alaska can be assumed because of the northward extension of the vegetation lines. In the mountains the upper tree line shifted upward by 100–150 m, which indicates a warming of nearly 1 °C compared to current temperatures.

In subtropical latitudes, the present arid areas enjoyed wetter conditions during the Holocene warm period. Since everywhere the temperature was higher or similar to today's temperature, this humid climatic phase (Sarnthein 1978) must have been related to higher precipitation and caused by higher evaporation of the tropical oceans (see the discussion in Chapter 2 of this report on equatorial upwelling, El Niño, and the hydrologic balance). This was probably correlated with a weakening of the subtropical anticyclones and the trade winds. In this connection, there is evidence of a correlation between a prolonged warm and humid period and a weakening of the coastal oceanic flow (with upwelling) in California earlier than 5,400 years ago (Pisias 1979).

Perhaps the most surprising feature of the Holocene warm period is the recently established occurrence of a marked humid period in the Sahara, as well as in the deserts of the Middle East (Nicholson 1976, Williams and Faure 1980). Since parts of this humid phase occurred simultaneously on both flanks of the desert, the model of a parallel shift of climatic zones towards north or south, as the seasonal variations suggest, cannot be considered applicable in all cases. Evidence based on current data supports the idea of a tendency towards synchronous shrinking or expansion of the Arid Belt on *both* flanks. (On a much shorter time scale, Nicholson (1980) found this tendency in the 16th and 19th centuries, together with a prolonged rainy summer season.) During the first phase of this moist period – between about 11,000 and 8,000 years ago (see Figure 12) – tropical rains expanded northward. Mediterranean rains, under the influence of the dwindling northern ice sheets, still dominated along the northern margins, with frequent outbreaks of cold air occurring even during summer (Flohn and Nicholson 1980). Marked troughs in the high tropospheric layer, extending diagonally across the Sahara, could have induced tropical disturbances; these in turn could have crossed the arid zone as "Sahara depressions," initiating more frequent rains even in the central belt between lat 21° and 26 °N, as shown in Figure 13 (Flohn 1971). Lake Mega-Chad stood about 40 m higher, with an area of nearly 320,000 km^2 (comparable to the present Caspian Sea). During the peaks of the Holocene period this lake had an outlet to the Benuë–Niger catchment. The onset of the Holocene rainfall caused the sedimentation rate in the sea off the Niger delta to increase by a factor of 20 (Pastouret *et al.* 1978). Similarly, Lake Turkana (formerly Lake Rudolf) emptied into the White Nile catchment (Butzer *et al.* 1972). Even in

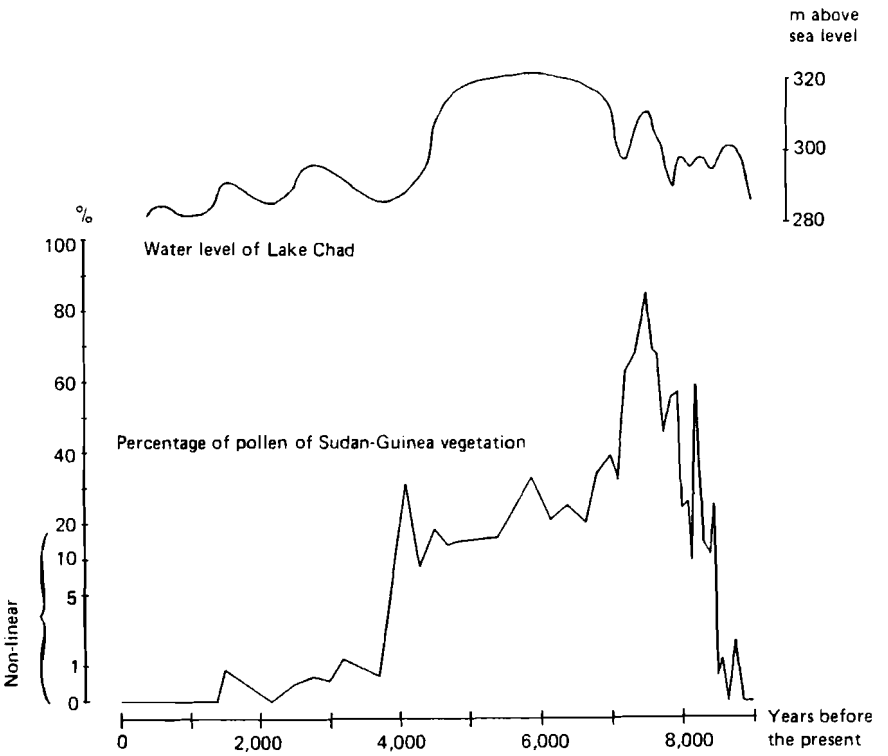

FIGURE 12 Upper curve: water level of Lake Chad (Mega-Chad) during the Holocene period. Lower curve: percentage of pollen in Sudan–Guinea vegetation over time during the Holocene period, representing the contribution of tropical rainfall to the total amount of rainfall. This vegetation may represent an area with an annual rainfall of 80–120 cm. The time scale 8,000 and more years before the present may be too compressed, possibly due to errors in C_{14}-dating. The upper curve is after Servant (1973) and the lower curve is based on Maley (1977a and 1977b).

the now hyperarid center of the Sahara between the Kufra Oasis and the Tibesti Mountains – which today has less than 5 mm of rain per year – permanent rivers were flowing (Pachur 1975), indicating at least 200 mm, and more probably 300–400 mm, of rainfall per year. The grasslands in this area were utilized by many groups of cattle-raising nomads (Gabriel 1977).

Similar evidence has been found throughout the Arid Belt of the Old World between Mauretania (long 17 °W) and Rajasthan (long 77 °E), including the Afar–Danakil depression and the Arabian interior. At the margin of the Tharr desert in India (which now has an average annual rainfall of about 250 mm) rainfall increased to values of 500–800 mm during a long moist period between about 10,500 and 3,600 years ago (Singh *et al.* 1974, Bryson and Murray

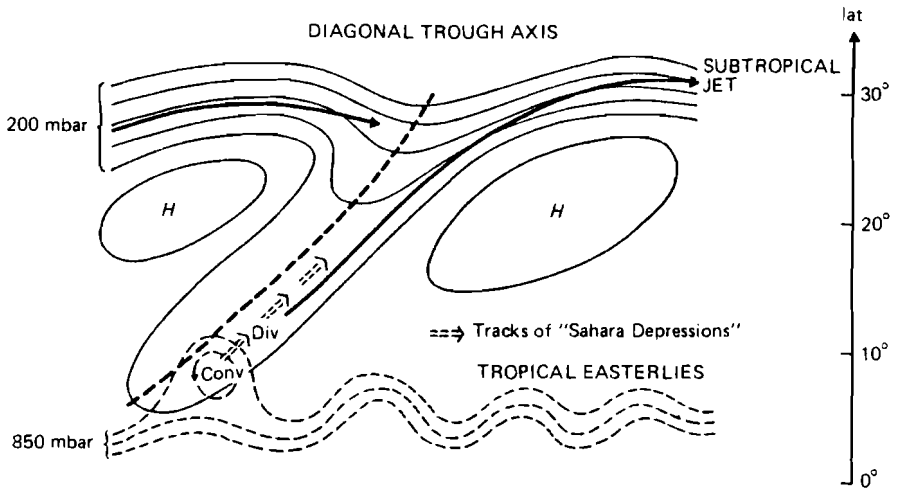

FIGURE 13 Interaction between "diagonal" upper troughs in the subtropical westerlies (200 mbar or ≈12 km) and tropical easterlies with traveling vortices (850 mbar or ≈1.5 km). Coincident low convergent (CONV) and upper divergent (DIV) motions produce "Sahara depressions"; these move in a northeast direction ahead of the upper trough, which is visible from satellites as an elongated cloud band. Source: Flohn 1971.

1977). This temporal variation in rainfall is shown in Figure 14. The individual fluctuations may be uncertain, as well as the dates for the beginning and the end of the moist period; still, the occurrence of a long moist period at this time agrees well with evidence from more than 30 other spots lying more than 8,000 km apart [*cf.* the summary review by Rognon and Williams (1977)]. Here again, both monsoonal summer rains and extratropical winter rains increased, overlapping in many parts of the Arid Belt.

Throughout the area of the present Arid Belt, gradual desiccation set in about 5,500 years ago, interrupted by relatively wetter periods. It seems noteworthy that according to most recent data, the early high civilizations (the Old Empire of Egypt from the first to the fourth dynasties, the Near East urban centers between Jericho and Ur, the Indus culture) started at the end of this relatively wet period, and had to fight increasing desiccation. North of about lat 35 °N the displacement of the winter rains towards the south lead to a dry period in Anatolia and Iran (Butzer 1975); good evidence has been found of a simultaneous lowering of Lake Van in eastern Anatolia by 300–400 m and salinization of its waters (Kempe 1977).

Evidence about the Holocene climatic history of the arid southwest of the USA is poor, except for the existence of a freshwater lake in central New Mexico in this moist period.

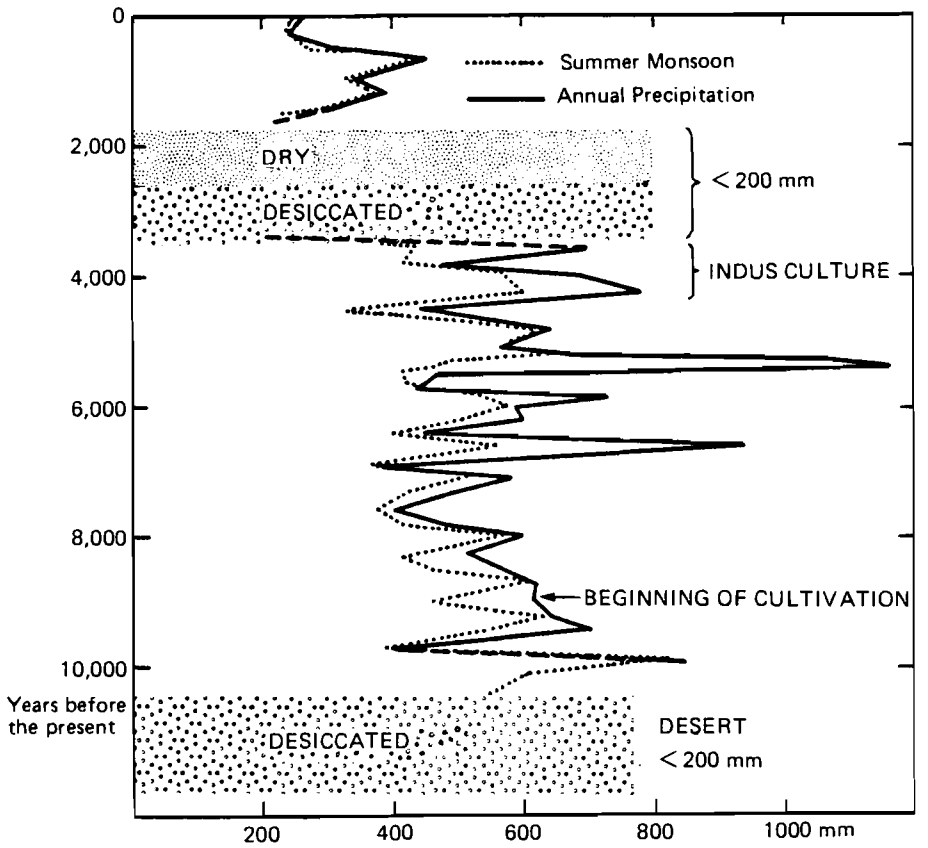

FIGURE 14 Rainfall estimates for Rajasthan, India, 10,000–2,000 years ago, based on evidence from pollen. (In the periods indicated by shaded areas, no pollen and thus no rainfall data are available.) The data are taken from Bryson and Murray (1977) and Singh *et al.* (1974).

Climatic conditions in Australia during the Holocene warm period were quite similar; increased precipitation occurred at the northern *and* southern margins of the desert together with a slight warming in the mountains of New Guinea, even at altitudes above 2,500 m (Bowler *et al.* 1976a). In contrast, the evidence available for southern Africa (van Zinderen Bakker 1976) indicates that the interior plateau had warmer, but drier, semidesert conditions.

At this point it is necessary to raise the question, To what extent can this climatic history repeat itself under varying boundary conditions? There were two such essential boundary conditions during the early Holocene period, i.e., until about 5,500 years ago: the presence of limited and shallow, but not

negligible, permanent ice sheets in eastern Canada, and the absence of desertification processes triggered by man.

These permanent ice sheets seem to have disappeared eventually, fairly parallel to the desiccation which started about 5,500 years ago. The importance of these ice sheets as a boundary condition can be understood if one takes into account the effect which a permanent cold source in eastern Canada could have had on the circulation pattern in the European section; similar to today's conditions in spring, the effect would have been frequent blocking anticyclones in the region of the British Isles and Scandinavia, with increasing cyclonic activity in the Mediterranean. This would have been effective especially in late spring, summer, and fall, and would have been accompanied by frequent deep troughs over eastern and central Europe, extending diagonally into northern Africa (see Figure 13). Similar conditions could only be expected in the near future if a permanent snow cover were to develop in the area of Baffin Island and Labrador; this is unlikely to occur in the next decades, but is not absolutely impossible, as will be discussed in the concluding chapter of this report.

Increasing desertification triggered by man (Hare 1977) has probably contributed to the slow and gradual desiccation process. Rainfall data collected in many arid regions since 1890 (Rajasthan) or 1904 (southern Tunesia) do *not* reveal a downward trend. Models designed by Charney (1975), Berkofsky (1976, 1977), Ellsaesser *et al.* (1976), and Joseph (1977) describe man-made destruction of vegetation as the cause of increasing surface albedo and intensification of the subsidence processes which should reduce effective rainfall. A reversal of such desertification processes (soil erosion, deflation, destruction of vegetation, groundwater depletion, and salinization) seems possible only if repeated large-scale rainfall triggers the growth of an adequate vegetation cover that can be protected against overgrazing and the ever-increasing strain caused by rapid population growth. Only then could the weak positive feedback effect, "desertification–increasing albedo–increasing subsidence–less rainfall–extended desertification," be interrupted and (possibly!) reversed. This would necessitate a major concerted effort on the part of many nations. From the discussion of the Holocene ice sheets in eastern Canada, one may conclude that no substantial change in rainfall along the northern margins of the Old World Arid Belt is to be expected. On the southern flank this might be possible if, as is expected, the subtropical anticyclones become slightly less intensive and are displaced towards higher latitudes. This would weaken the trade winds of the northern hemisphere and decrease coastal and equatorial upwelling, leading to increased evaporation and a higher water vapor content.

From the discussion of desertification triggered by man, it appears that, given our present population growth, reconstruction of the natural vegetation cover is a socioeconomic problem; several decades may pass before a reliable long-term increase in rainfall could be achieved through such reconstruction. Here much additional research of a truly interdisciplinary nature is certainly needed.

5.3 THE LAST INTERGLACIAL PERIOD (EEM SENSU STRICTO)

Recent investigations of ocean cores in low and middle latitudes, as well as of continental loess deposits in Austria and Czechoslovakia, have indicated that over the past 2–2.5 million years a sequence of at least 17 large-scale glaciations has occurred on northern continents. These were interrupted by an equal number of interglacial periods with a climate similar to the present one. Detailed data are available only for more recent events, especially for the last glaciation between about 73,000 and 14,000 years ago. This glaciation had two major glacial peaks at the beginning and end, and at least five shorter periods with a slightly warmer climate (interstadials). For the controversial subject of chronology, see, for example, Kukla (1977a).

The last interglacial period, defined here as stages 5a–5e after Emiliani and Shackleton (1974), lasted, with two important interruptions, from about 130,000 to 75,000 years ago. While the climate in Europe and Asia during this period has been carefully described by Frenzel (1968a), information on North America is hardly adequate for a regional description, and evidence for other continents is almost completely lacking. Detailed investigations of the climate at the earliest peak of the last interglacial (Eem sensu stricto, or stage 5e as defined above) around 125,000 years ago are being carried out by the CLIMAP group (Cline and Hays 1976). The group is evaluating the large number of accessible ocean cores to obtain a realistic estimate of sea surface temperatures and salinities. Since the Eem sensu stricto was apparently the warmest of all interglacial periods, a climatic interpretation of this subperiod is given below.

In northern and eastern Europe the climate during this subperiod was much more oceanic than it is at present. This was mainly due to the high sea level, about 5–7 m above today's level. Scandinavia was isolated from the continent by an oceanic channel between the Baltic and the White Sea. The sea also penetrated deeply into the continent in western Siberia, along the Ob and Yenisey flood plains up to lat 62 °N. Table 5 gives a selection of climatic data from polar and mid-latitudes in Eurasia and North America. Temperatures were generally 2–3 °C higher than today, (even higher in some areas) and slightly more humid (for details, see Frenzel 1967, 1968a, and 1968b). The forests in the current cool/temperate zone were then thermophilous; deciduous trees like oak, linden, elm, hazel, and hornbeam prevailed. The occurrence of hippopotamus, forest elephants, and lions in southern England is a remarkable feature of this warm climate (Lamb 1977a, p. 188). Thermophilous forests in eastern Siberia indicated a marked retreat of permafrost up to lat 57 °N (now around lat 50 °N); boreal forests extended up to the coastlines of the time. While the coasts were inundated by the high eustatic sea level, the high temperature estimates suggest a seasonal retreat of Arctic drift ice far away from the coasts. Marginal parts of the Arctic drift ice were probably displaced poleward, but the central core of the ice in the ocean between Greenland, Alaska, and eastern Siberia has remained unchanged, at least since the beginning of the

TABLE 5 Estimated climatic differences between the Eem period and the present.

Area	Temperature (°C)			Annual rainfall (mm)
	January	July	Annual average	
Denmark	+2	+1–2	+1.5	0
GDR and northern FRG	+1–2	+3	+2.5	0
Central Poland	+3–4	+3	+3	+50
Northeast Poland	+3–5	+3–5	+5	+50
Byelorussia	+5–6	+5	+6	0
Central Russia	+9–10	+2	+5	+100
Northwest Ukraine	+2–3	±0	+1	+50
Western Siberia	+4	+3	+3	+100[b]
Central Siberia	–[a]	–[a]	+6	–[a]
Toronto	+3–4	+2	+2–4	+250
Southeast Alaska	–[a]	+4–5	–[a]	–[a]
Banks Islands (72 °N)	–[a]	+4–5	–[a]	–[a]

[a]No evidence available.
[b]Rough estimate.
SOURCE: Frenzel (1967).

Brunhes paleomagnetic epoch 700,000 years ago (Herman 1977). Worldwide comparisons of ocean cores indicate that during this stage the sea level stood at least 6 m higher than at present, as evidenced at Barbados, Hawaii, New Guinea, Mallorca, and on the lower Thames.

The duration of the Eem (stage 5e) was only on the order of 10,000 years. It was terminated by a markedly abrupt and relatively short period of cooling, during which the global ice volume both increased and decreased, possibly causing a change of 60–70 m in the sea level (rather than 100 m or more as occurred during the last ice age). In the Eem period, Atlantic polar water with some seasonal ice retreated north of lat 76 °N for about 8,000 years, while subtropical waters, which apparently did not extend north of 44 °N in the Holocene period, reached 52 °N (Kellogg 1976).

Two other warm phases (5c and 5a) followed, but with fewer thermophilous forests and a lower sea level. Figure 15 gives a simplified diagram of the vegetation history of a peat bog core in northeast France (Woillard 1975, 1978), illustrating the apparent brevity of the two interrupting cold episodes on the continent. The second cooling (locally called Melisey II), which occurred during stage 5b (Emiliani and Shackleton 1974), apparently coincided with several marked events in northern Greenland at lat 76 °N (Dansgaard *et al.* 1972), in a deep cave in southern France (Duplessy *et al.* 1970), in peat bogs in California and northern Greece (Adam 1978, Wijmstra 1978), and in many ocean cores of the Caribbean (Kennett and Huddlestone 1972). The worldwide occurrence

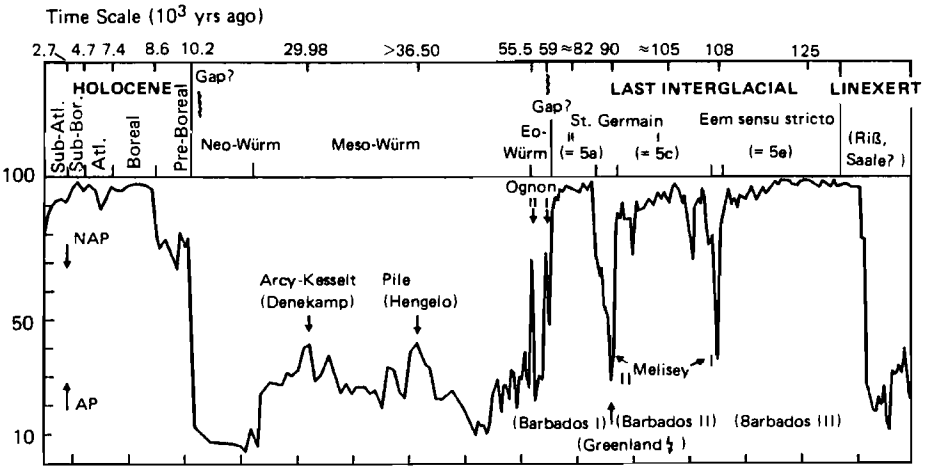

FIGURE 15 A simplified vegetation history from a fossil bog in southern Vosges (northeast France). The time scale in 10^3 years before the present is given on the x-axis, and the percentage of forest pollen (AP) vs. nonarboreal pollen (NAP) is given on the y-axis. Sub-Atl. is Sub-Atlanticum; Sub-Bor. is Sub-Boreal; Atl. is Atlanticum. Emiliani–Shackleton stages (5a, 5c, and 5e) are shown in the 'Last Interglacial' portion of the graph. The beginning of the Eem sensu stricto is misplaced slightly to the left; it should coincide with the sudden rise of AP. The figure is a simplified version of a figure appearing in Woillard (1975).

of stages 5a–5e (Emiliani–Shackleton) is verified by many complete oceanic and continental cores in all latitudes.

In all interglacial periods for which good evidence exists, except for the present one, such rather abrupt coolings with a Subarctic or Arctic climate have been observed to last only for several centuries or 1,000–2,000 years ("abortive glaciations") (see Woillard 1979). The physical mechanism of such abrupt, but certainly natural events, recurring approximately once every 10,000 years, is not yet known; the possible role of clustering of volcanic eruptions or of Antarctic surges is still an open question (see Chapter 2 of this report and Flohn 1979).

Little is known about low latitudes; the occurrence of a long humid phase, with a deep lake in the Afar Triangle west of Djibouti (see Gasse and Delibrias 1976), and also along the western African coast (Diester–Hass 1976), suggests conditions similar to those prevailing during the early Holocene period.

6 IS A COEXISTENCE OF AN ICE-FREE ARCTIC AND A GLACIATED ANTARCTIC POSSIBLE?

6.1 CAUSES AND TIME SCALE OF A POSSIBLE OPENING OF THE ARCTIC OCEAN

The most fascinating, and also most controversial, problem of the future evolution of man's climate is the possibility of a complete disappearance of the drift ice of the Arctic ocean (which was discussed in Chapter 2). The sensitivity of the multiphase air–snow–ice–ocean system (see Figure 1) is demonstrated by the relatively large amount of seasonal melting (from above) and freezing (from below), on the average about 50 cm/yr. Unfortunately, no figures are available for a sample of years; recent experience based on ice and weather ship data suggests high interannual variability. In particular, the system is highly sensitive to the heat flow of the ocean below, to the albedo of the ice–snow surface during the melting season, and certainly to the length of the melting season (which ends with the first snow cover). After demonstrating the sensitivity of the system, Budyko discussed the possibility of artificial removal of the Arctic sea ice, and then designed simple semiempirical models based on the heat balance of the earth–atmosphere system (Budyko 1962, 1969, 1972). He noted that small increases in the solar constant or an increase in the atmospheric CO_2 content might lead rather rapidly to an ice-free Arctic ocean, substantially increasing the surface temperature by about 6–8 °C in summer, but by more than 20 °C in winter.

Since Budyko's work, arguments for and against such a drastic evolution – which probably went beyond the imagination of many responsible scientists – have been discussed, in private circles much more than in publications. Since no sufficiently realistic model of the climatic system is available, including the physical and dynamical interaction and the feedback processes between atmosphere, drift ice, and ocean, this problem cannot be satisfactorily resolved at the present time. Fletcher *et al.* (1973) made one of the first attempts to simulate atmospheric circulation under the conditions of an ice-free Arctic ocean, on the basis of the Mintz–Arakawa model. As Figure 16 shows, the essential result of the

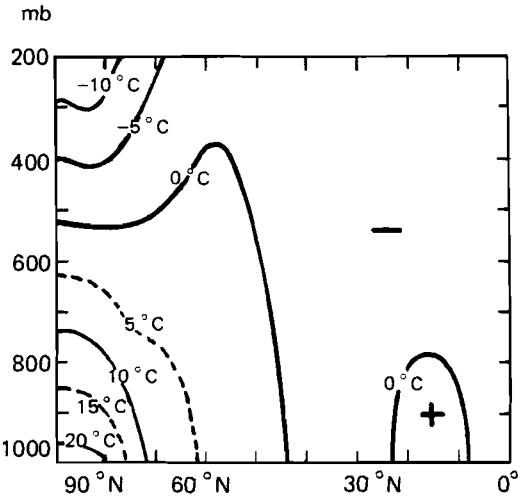

FIGURE 16 Temperature change obtained from the simulation of atmospheric circulation under conditions of an ice-free minus an ice-covered Arctic, using the Mintz–Arakawa model. The figure is based on Fletcher *et al.* (1973).

simulation is a warming of the lower troposphere north of about lat 45 °N, together with a cooling of the upper troposphere and a marked destabilization of the polar atmosphere. Changes in tropical latitudes are probably uncertain.

Simple one-dimensional models have also frequently been investigated since Budyko's initiative (e.g., Sellers 1969, 1973). One of the most important simplifications was to define the latitude of boundary ϕ_p of the polar zone as equivalent to an average latitudinal temperature of the warm half-year of −1 °C (Budyko 1974); then the planetary albedo, as seen from space, was taken to be 0.62 for the northern polar cap and 0.77 for the southern polar cap. This procedure introduces parameterization of the highly effective snow–albedo–temperature feedback. According to Budyko's 1974 monograph, the relationship between ϕ_p and solar radiation has the form of a hysteresis loop; ϕ_p is larger when the incoming radiation, as the determining parameter, increases from a value lower than the original value, and smaller when the incoming radiation decreases from a value higher than the original value. This is shown in Figure 17 (after Figure 8 in Budyko 1974). In another diagram (Budyko 1974, Figure 9) he demonstrates the relation between the average planetary air temperature and solar radiation; there the difference between points E (ice-free regime) and 3 (present situation) is equivalent to a change of about 4 °C from the current temperature. This is higher than the temperature increase in all warm phases (1–2.5 °C) during the last 2 × 10^6 years, but the difference is not very big. If one accepts Budyko's model as a reasonable first guess, the possibility of such an ice-free regime cannot be excluded. Furthermore, temperature

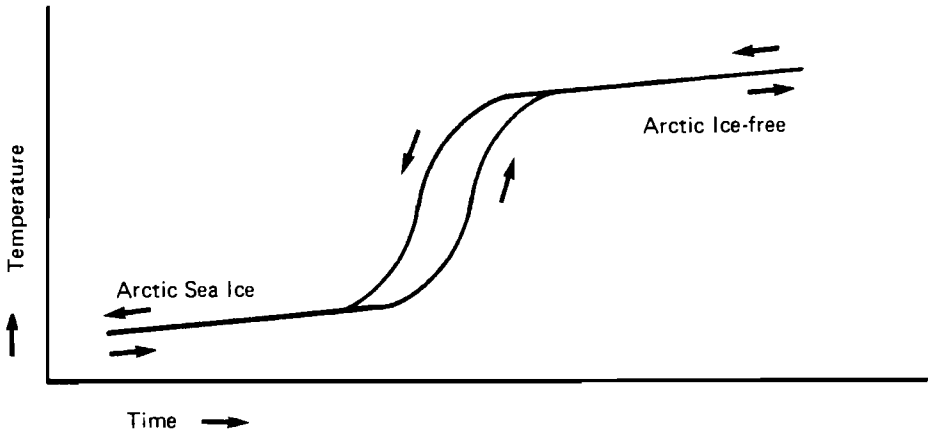

FIGURE 17 Expected temperature change due to hysteresis in the case of formation or disappearance of Arctic sea ice. The arrows pointing to the left indicate ice formation, while arrows pointing to the right indicate disappearance of the ice. The graph is a simplified version of a graph appearing in Budyko (1974).

estimates based on vegetation patterns during relevant past epochs, as the late Tertiary, also suggest a temperature about 4 °C higher than the present temperature in the northern hemisphere (see the next section of this chapter). In this case, however, the hysteresis loop is followed from above and not from below, as must be expected in a possible future evolution.

Looking at seasonal variations in the heat budget of the Arctic sea ice, Maykut and Untersteiner (1971) have stressed the roles of surface albedo and oceanic heat flow; their estimate of the oceanic heat flow (1.5 kcal/cm^2/yr $\approx$ 2 W/m^2) is much too small according to more recent data, and should be increased by a factor of 6 to 7 (Aagard and Greisman 1975). Surface albedo during the melting season plays an effective role only in the case of surface pollution through dust or oil wastes. As for the oceanic heat flow, the flux of sensible heat is, on an annual average, slightly less than 10% of net solar radiation as well as of the infrared terrestrial radiation (Figure 2; see also Vowinckel and Orvig 1970); this is also true for the flux of latent heat (evaporation) in the same upward direction. Since the annual net radiation at the surface is quite small at present, the heat flux from the ocean is approximately equal to the sum of the flux of sensible heat and the flux of latent heat into the atmosphere.

During the melting season the melting process of the sea ice takes only 50–60 days (plus an additional 20 days for snowmelt), leading to a phase transition of about 15–20% of the average mass of an ice floe. In the remaining months a similar amount freezes from below. It is obvious that interannual changes in the heat budget – which should be on the order of ±20% or even

higher – may significantly alter these estimates. They have been verified in substance by only a few 12-month surveys. If one assumes only a 10% increase in summer melting and a 10% decrease in cold season freezing, for a period of a few years, the destruction of a 2–3 m ice floe would take a short time. If the melting season started 1–2 weeks earlier, perhaps as a consequence of advective warming, this would most certainly lead to a substantial imbalance in the sensitive mass budget. However, there is also a negative feedback; in winter the accretion rate is negatively correlated with thickness, i.e., thin ice accretes much faster than thick ice, because of the higher value of the upward heat flux (Thorndike *et al.* 1975). In contrast, a positive correlation exists during melting.

Under given assumptions, a seasonal disappearance of the Arctic sea-ice cover has recently been found in two model computations. Manabe and Stouffer (1979) used a spectral atmospheric model coupled with a static mixed-layer ocean, which allows for seasonal heat storage, evaporation, and the formation and decay of sea ice. If the CO_2 content of the atmosphere is assumed to be 1,200 ppm, model results show a disappearance of sea ice during summer and fall after about 10 model-years, when fairly stable climatic conditions have been reached (see Figure 18). Parkinson and Kellogg (1979) arrived at a similar result with a newly developed sea-ice model, under the assumption of a general increase in the air temperature of 5 °C. None of these models has been run over a longer period, taking into consideration storage of radiational heat in the open sea with its low albedo during summer.

According to the large areal fluctuations of the ice over the last millenium (discussed in the section on Medieval warming in Chapter 5), there is little doubt that at least the marginal sections of the Arctic drift ice can disappear rather rapidly. This argument is not valid for the central core; its existence has been verified by several independent lines of evidence at least for the period since the Brunhes–Matuyama boundary 0.7 million years ago, and it has probably existed for the last 2.3 million years. However, if the global warming exceeds the range of temperature fluctuations (up to +2.5 °C) during the last 6–8 glacial–interglacial cycles, this argument is no longer true; with an average warming of 4 °C or more, as occurred in the late Tertiary, disappearance of the central core of the drift ice is almost certain. This would be equivalent to an increase in the virtual CO_2 level by a factor of almost 3. The equivalent increase in the real CO_2 level would be by a factor of about 2.5 (see Table 3).

The atmospheric heat budget above an ice-free Arctic ocean is completely different from that which presently exists. Disregarding earlier attempts to analyze this heat budget, some calculations by Vowinckel and Orvig (1970, p. 220) will be presented here as the most complete approach available. The heat budget equation for a column above the Arctic cap (75–90° lat) between the earth's surface (sfc) and the top of the atmosphere (TA) may be written as follows:

$$R_{\mathrm{sfc}}\downarrow - R_{\mathrm{TA}}\uparrow + F_{\mathrm{a}} + F_{\mathrm{s}} \triangleq 0$$

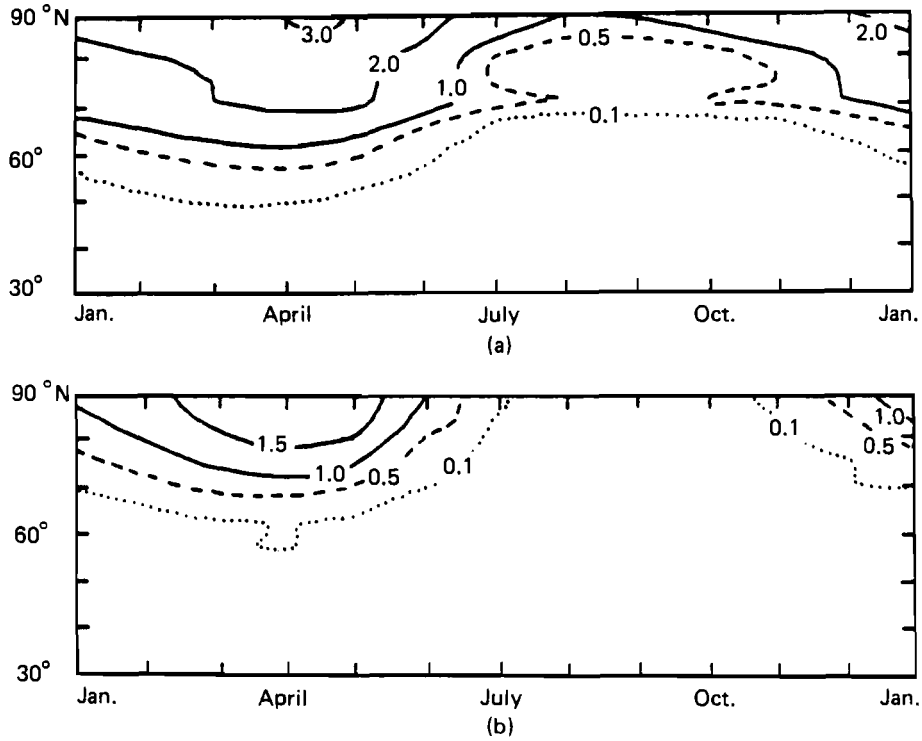

FIGURE 18 Seasonal variations in Arctic ice thickness (m) in (a) the standard case and (b) after quadrupling of the CO_2 content. A thickness of 10 cm may represent the southern boundary of sea ice. The figure is based on computations from Manabe–Stouffer's spectral atmosphere/mixed ocean model (1979).

where R = net radiation flux, F = northward heat transport across lat 75 °N by ocean (s) and atmosphere (a). In equilibrium, the divergence of the downward radiation flux, div $R = R_{sfc} - R_{TA}$, must equal the convergence of the horizontal flux of sensible and latent heat. Table 6 gives estimates for the individual terms, assuming, in the case of an ice-free Arctic ocean, either a cloudless atmosphere or a closed stratus cover. Both assumptions are unrealistic, but the role of clouds of different altitude, thickness, and extension for the radiation fluxes is not yet well understood. Somewhat more realistic is the assumption of a cloudless sky during summer (from May to August), when the continents favor a thermal circulation with subsidence over the sea; for the rest of the year a closed stratus should prevail (see the last line of Table 6). The data are given in watts/m^2 (1 kcal/cm^2/yr = 1 kilolangley/yr = 1.327 W/m^2).

The most interesting result is that of a positive annual net radiation budget, div R (Table 6, last line); in this case heat would be available for export from the Arctic. The advective oceanic heat flux F_s is, according to the most recent evaluation (Aagard and Greisman 1975), 10.6 W/m^2 – much larger than

TABLE 6 Energy budget estimates (W/m^2) for an ice-free Arctic ocean.

	R_{sfc}	R_{TA}	div R	$F_a + F_s$
Present conditions	+3.3	+100.8	−97.5	+97.5
Ice-free, no clouds	29.4	59.1	−29.7	+29.7
Ice-free, closed stratus	42.7	92.9	−50.2	+50.2
Ice-free, seasonally varying[a]	62.1	58.3	+3.8	−3.8

[a] Assuming a cloudless sky during summer, and a closed stratus cover during the rest of the year.
SOURCE: Vowinckel and Orvig (1970).

the value calculated in most earlier investigations. (For instance, Vowinckel and Orvig arrived at the value ≈ 7 W/m^2). One of the most important factors is the export of ice by the East Greenland Current; this contributes about 50% to the warming of the Arctic ocean, since the ice is melted externally. In an earlier analysis with much greater uncertainties, Donn and Shaw (1966) obtained an imbalance of +26.3 kilolangley/yr (≈ 35 W/m^2). The heat surplus is in line with the obvious consideration that, during the cold season, heat and water vapor should be exported from an ice-free ocean towards the continents; the continents certainly should be colder than an open ocean in subpolar latitudes. An open Arctic ocean should receive an annual net radiation of 30–60 W/m^2 at the surface (Table 6). If one assumes $R_{sfc} = 45$ W/m^2, allowing 40% for evaporation in summer (when the small flux of sensible heat is probably downward), then 27 W/m^2 or 20 $kcal/cm^2$ are available for heat storage in the sea. For a 50 m mixed surface layer, this yields an average heat storage of 4 cal/g, which is equivalent to a warming of 4 °C in one single summer. In winter, infrared emission increases with temperature; therefore if the surface temperature increases from −35 °C to 0 °C, the blackbody radiation increases by only about 60%. But due to the much higher water vapor content, atmospheric counter-radiation will also rise substantially, so that the net infrared radiation of the ocean surface may not change much. These estimates permit the conclusion that a new equilibrium water temperature will be reached after a few years, which should be indeed substantially higher than the melting temperature of saltwater; Budyko's estimate of +8 °C cannot be so far from reality. This would also be consistent with the air temperatures estimated for late Tertiary vegetation at the highest latitudes.

It should not be forgotten that the fate of the Arctic sea ice also depends on the low salinity of the shallow upper layer of the sea (see Figure 3). A balance exists between the outflow of the surface water via the East Greenland Current and the seasonal inflow of fresh water from the enormous Siberian and Canadian rivers. Due to the urgent need for increased irrigation in the central Asian part of the USSR, several large diversion schemes have been developed for western Siberia, including an advanced canal system (Hollis 1978). In this scheme, provision is made for a diversion of up to 300 km^3 freshwater per year, which is about 23% of the present runoff into the Kara Sea (1,283 km^3/yr).

It has been pointed out that any large-scale loss of freshwater inflow tends to raise the salinity of the Arctic Ocean, to decrease its stability, and to contribute eventually to a reduction in the present sea-ice balance; no quantitative investigation is available as yet.

6.2 COEXISTENCE OF AN OPEN ARCTIC OCEAN AND A GLACIATED ANTARCTIC CONTINENT DURING THE LATE TERTIARY

One of the main arguments against a possibly ice-free Arctic ocean in the foreseeable future has been the existence of the highly glaciated Antarctic continent. Indeed it is not easy to imagine a completely asymmetric planet with one pole ice-free, and the other one covered by an ice sheet more than 2 km thick. Still, a similar asymmetry probably existed for more than 20–30 million years during the Permo–Carboniferous glacial period about 250 million years ago. At that time, however, several of the earth's continents formed one giant supercontinent (Gondwana); it was situated at higher latitudes of the southern hemisphere and included the pole. In the northern hemisphere most of our present coal deposits were formed during this period in forest swamps similar to the Everglades in southern Florida. The boundary conditions on the earth's surface are different today, but not so much different: one pole is situated on a fairly large, completely isolated ice-covered continent, while the other pole is situated in a deep, almost landlocked ocean with a thin skin of floating ice. To some extent, this causes an asymmetric circulation of atmosphere and ocean, as was discussed in Chapter 2 (see also Flohn 1978a).

Regarding the background of a possible evolution of an ice-free Arctic ocean, it is of paramount interest that exactly the same situation did in fact exist immediately before the onset of the Pleistocene, with its sequence of glacial and interglacial periods in the northern hemisphere and a more or less constant glaciation of the Antarctic. As the results of the Deep Sea Drilling Program have shown, the Antarctic ice had developed to its present size about ten million years (i.e., a period five times the duration of the Pleistocene) before the formation of Arctic drift ice. In two recent reviews Kennett (1977a) and Frakes (1978) evaluated the available evidence, and arrived at only slightly different results. At the end of the period in which a glaciated Antarctic and ice-free Arctic coexisted, in the Pliocene (about 2–5 million years ago), the early hominids, our ancestors, lived in a savanna environment in equatorial East Africa learning how to use pebbles as weapons and as tools. (Unfortunately they did not yet know how to record climate.) To what extent climatic changes may have affected the ape–man transition is not yet known.

For the last 50–70 million years, Antarctica has been situated near the South Pole. It was once connected with Australia and other parts of the former Gondwana continent. Both poles were ice-free throughout the Mesozoic and the early Tertiary (about 200–50 million years ago) (Schwarzbach 1974). During these eras the atmospheric circulation was probably dominated by the

tropical Hadley cells reaching to lat 50–60°, with strong seasonal variations (Flohn 1964b). The meridional extension of Australia and Antarctica caused warm oceanic currents and prevented any glaciation until the beginning of the Eocene (55 million years ago). Soon thereafter, Australia separated from Antarctica and drifted northward at an average speed of 5 cm/yr, while Antarctica remained nearly fixed (Kennett *et al.* 1977c). After a long period of increasing winter snow, with possible local glaciations in West Antarctica and steadily decreasing water temperatures (small surface–bottom differences), the first significant drop in temperature occurred 38 million years ago, near the boundary between the Eocene and Oligocene eras. This drop especially affected the bottom layers (i.e., a 5 °C decrease within less than 10^5 years, which was remarkably abrupt for the time; see Figure 19).

At this time substantial Antarctic sea ice formed, coinciding with the development of widespread glaciation in parts of the Antarctic continent (Kennett 1977a). As under present conditions, the cold and dense bottom water spread outward into all oceans, causing a considerable worldwide crisis for deep-sea fauna. After further climatic fluctuations of more geological importance, including a significant global cooling during the Oligocene (38–22 million years ago), a notable Antarctic ice cap formed during the middle Miocene epoch (15–12 million years ago) and became a permanent feature; it probably was still "warm," i.e., with temperatures close to the melting point. This formation occurred roughly at the same time as volcanic activity sharply increased, as many ocean drillings have shown (see Figure 20; also Kennett *et al.* 1977c). After the formation of the ice cap, the first mountain glaciers in southern Alaska appeared, as well as the first cold-water fauna in northernmost Japan (Kanno and Masuda 1978); a marked drop in the surface temperature also occurred in the high latitudes of the Pacific (Savin *et al.* 1975).

The highest glacial maximum, characterized by a "cold" and slowly moving Antarctic ice dome, was reached at the end of the late Miocene or Messinian (6.5–5 million years ago), when the ice volume was larger than it is today. At this time the height of the ice dome must have been several hundred meters higher, and the Ross shelf ice extended several hundred km farther north. This glacial maximum was accompanied by a remarkable global cooling, by an extension of cold Antarctic surface waters 300 km northward, and by a high carbonate sedimentation rate at the equatorial Pacific, indicating strong upwelling of nutritious cool water (Saito *et al.* 1975). Seven to ten cyclic temperature changes were observed, with minima as cold as in the cold phase of the last glaciation. This is not necessarily indicative of a global cooling, but does show the intensity of the equatorial upwelling. One of the most important consequences was a "glacial-eustatic" drop in sea level 40–50 m below today's level, due to the storage of water in the Antarctic ice dome. During each drop the Gibraltar Strait, or its predecessor, became dry and isolated the Mediterranean; the latter completely evaporated 8–10 times to a depth of 3,700 m and filled

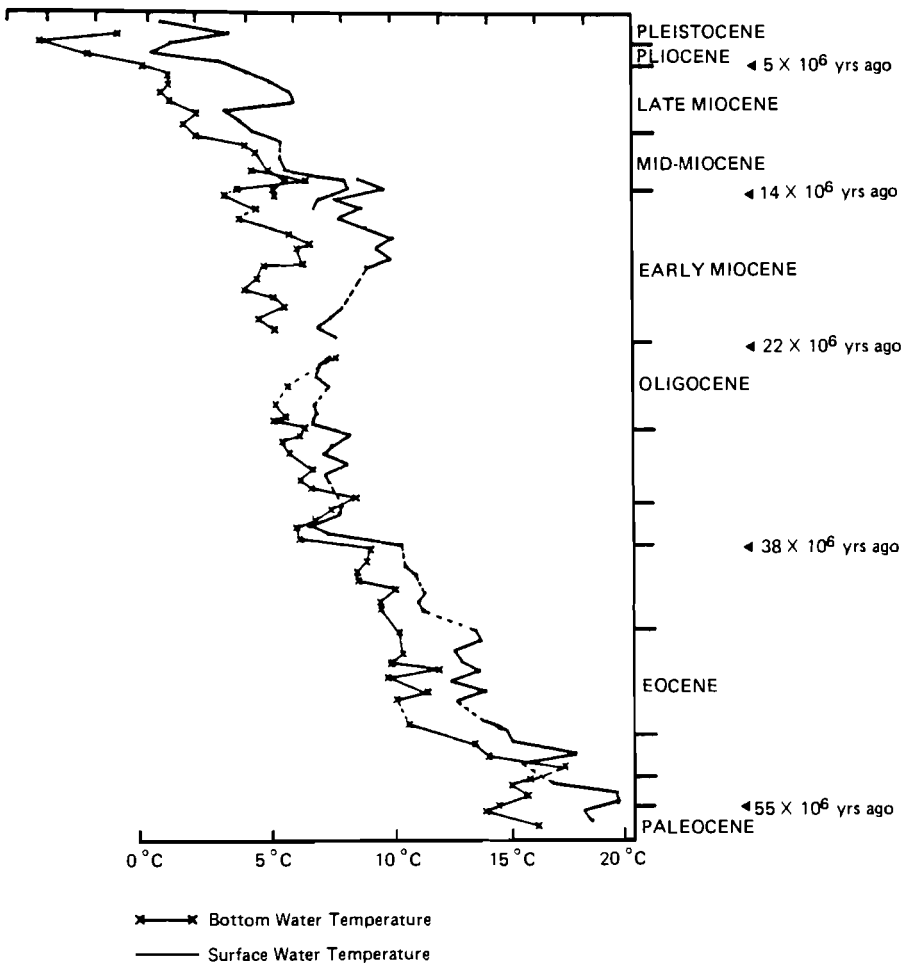

FIGURE 19 Evolution of surface and bottom (isotopic) temperatures in the Subantarctic (about 50 °S, 160 °E) since the late Paleocene about 58 X 10^6 years ago. The figure is based on two figures which appeared in Kennett (1977a).

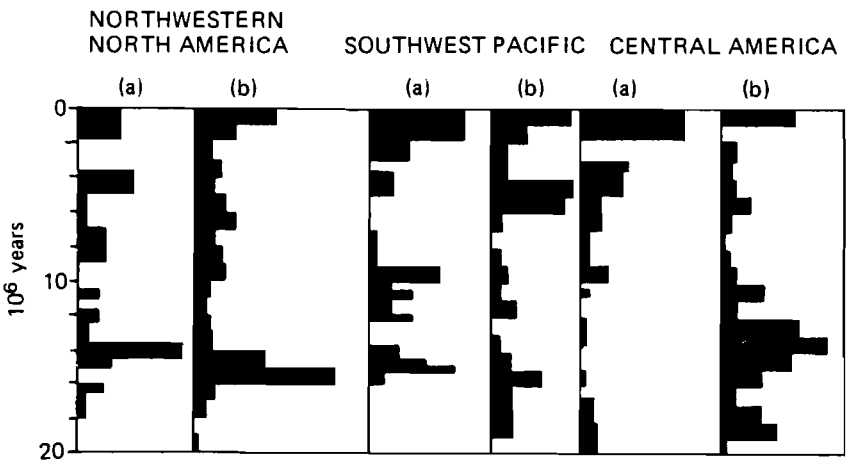

FIGURE 20 Volcanic activity in some circum-Pacific provinces during the late Tertiary and Quaternary, measured by volcanic ash from (a) deep sea sediments and (b) terrestrial volcanic sequences. Source: Kennett *et al.* (1977c).

again, leaving a laminated salt layer 300–500 m thick (Hsü *et al.* 1973, 1977). This lamination and the paleoclimatic history of equatorial Pacific sediments indicate a cyclic behavior on a time scale of about 10^5 years, lasting for about 0.5 million years; the cyclic behavior was probably caused by orbital elements similar to those in effect during the Pleistocene.

During and after that time, the Arctic enjoyed a cool to temperate climate with boreal forests extending up to the northernmost tip of land. In the late Miocene and Pliocene the entire shelf north of Asia and Alaska fell dry, and the continents extended 200–600 km farther north, e.g., in Siberia up to 81 °N, and in Canada up to 83 °N (Hopkins 1967). The distribution of vegetation in Siberia shortly before the first appearance of ice on the European continent (during the late Pliocene, about 2.5 million years ago) has been mapped with the aid of a rich data base, published mainly by Soviet authors (Frenzel 1968a, 1968b). No evidence of tundra or widespread permafrost could be found. Summer temperatures have been estimated to have been about 3 °C higher in western Europe, but 4–5 °C higher in eastern Europe. There and in Siberia annual and winter temperatures must have been 5–10 °C higher than at present (Frenzel 1968a, 1968b). Since the relative and absolute heights of many mountains were significantly lower than they are now (as is demonstrated by the flat or rolling topography now covering the highest levels of some mountains – the Rax "plateau" in Austria is a good example) oceanic rainfall could penetrate farther inland. Precipitation has been estimated to have been 300–400 mm higher (Frenzel 1968a, 1968b). In a few areas, such as in California and northwest Iceland, local glaciers were formed simultaneously with the boreal forests, but produced no significant large-scale climatic effect. Simultaneous glaciation of parts of Greenland can be assumed, but there is no

evidence for it, due to the strong, and probably permanent, glacial erosion since that time. Along the coasts of Alaska well-developed boreal mixed forests extended more than 800 km north of some of the present tree lines. The fossil insect fauna at lat 66 °N resembled the insect fauna now living in the Vancouver–Seattle area at lat 48–50 °N (Hopkins 1971).

During the Pliocene (5–2 million years ago) the Ross Ice Shelf in Antarctica extended beyond its present boundary, and glaciation started in southern South America [about 3.6 million years ago (Mercer 1976)]. From ice-rafted pebbles one may infer that, simultaneously with a northward shift of the boundary of the cold Antarctica surface water, Antarctic tabular icebergs occurred and also spread northward, reaching even farther north than during the Pleistocene glaciations.

Of special interest is the climate of the middle and lower latitudes. After many careful investigations, Lotze (1964) compiled maps of the position of the evaporite belt during past climatic periods, i.e., the position of the arid zone of playas and sebkhas, where soluble salts were sedimented in dry pans. The northern limits of the northern arid belt during the Quaternary, late Tertiary, and early Tertiary, taken from Lotze's maps, is presented in Figure 21; a southward shift from an average latitude of about 47 °N in the early and middle Tertiary to 42 °N in the late Tertiary, and to 38 °N in the Quaternary is indicated in the figure. In the context of this paper, only the displacements during the latter epochs are important. The multiple desiccation of the Mediterranean that occurred during the Messinian – a short portion of the Miocene/Pliocene epoch 6.5–5 million years ago – aggravated the arid conditions in southern Europe. Evidence of a similar southward shift of the vegetation belts of North America has been compiled by Dorf (1960) (Figure 22).

During the Messinian, even the southern part of central Europe was partly arid, with steppes or desert vegetation near Vienna (Schwarzbach 1974, Hsü 1974). Southwest Germany was also drier than it is now (Schwarzbach, in Nairn 1964). While tropical marine microfossils had occurred abundantly in the Atlantic up to lat 58 °N before these events, this boundary retreated during the desiccation of the Mediterranean on the eastern side of the Atlantic to about lat 33 °N. Tropical species could not enter the Mediterranean after its reopening during the early Pliocene (5 million years ago), though such species were able to reach farther than lat 50 °N in the Gulf Stream region. This indicates a great longitudinal contrast, probably caused by the wind-driven surface currents of the oceans.

Many regional temperature and precipitation estimates have been made (e.g., Mägdefrau 1968, Schwarzbach 1974). Since in the late Tertiary many of our present mountains existed only in rudimentary form, these numerical data cannot be considered representative of conditions in the near future. This is obvious, for example, in the case of the now arid continental basin of Nevada or the Mojave desert, which enjoyed a rather moist maritime climate near sea level during the late Miocene. Summer temperatures were then 4 °C lower, and winter temperatures were 8–10 °C higher than at present (Schwarzbach

FIGURE 21 Displacement of the northern boundary of the northern hemisphere arid zone during the early Tertiary (30–50 X 10^6 years ago), late Tertiary (5–15 X 10^6 years ago), and Quaternary (0–2 X 10^6 years ago) periods, measured by the position of the evaporite belt. The figure is based on several figures which appeared in Lotze (1964).

1974). During the same time periods, southwest Germany enjoyed a subtropical or, later, warm to temperate climate (Mägdefrau 1968). In the tropics, the extension of savanna climates with seasonal rains was much wider than it is today, but the equatorial rain forest with perennial rain was smaller. In the Oligocene and Miocene (Maley 1980), the vegetation patterns of the African continent revealed the same marked asymmetry as in the Miocene and Pliocene. While the southern Sahara was covered with a tropical humid or at least semihumid vegetation (which has persisted in southern Nigeria), southern Africa and the Zaire basin were dry and sometimes fully desertic. Evidence of the same aridity has also been observed in northern Australia, especially for the period after the Messinian peak of the Antarctic glaciation (Kemp 1978).

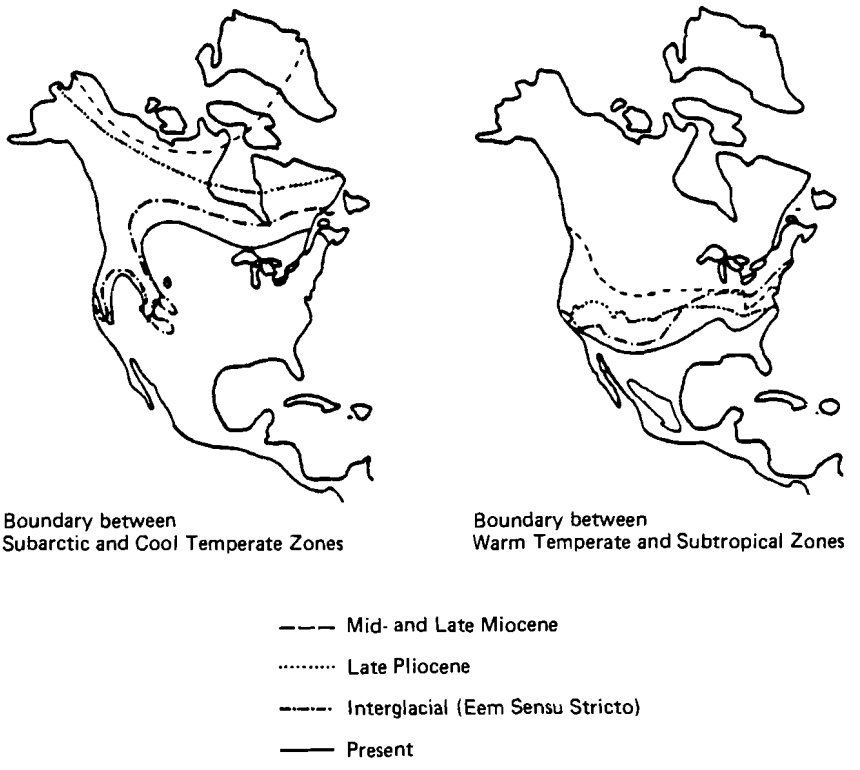

FIGURE 22 Displacement of vegetation boundaries in North America from the mid- and late Miocene periods to the present. The figure is based on Dorf (1960).

Although certainly still incomplete, this evidence indicates that the hemispheric asymmetry of the general atmospheric and oceanic circulation was substantially greater between the middle Miocene and the Pliocene than it is now (Flohn 1978a). The shape and position of the continents was then by and large similar to present conditions. Large-scale glaciation of the northern continents did not start until 2.5×10^6 years ago; the formation of Arctic drift ice began only after that date, about 2.3×10^6 years ago, when the meltwater produced a shallow, stable low-saline upper layer in the Arctic ocean (Herman 1977). Further evidence of an ice-free Arctic ocean earlier than 3×10^6 years ago is found in the vegetation boundaries described by Frenzel (1968) for Siberia and by Hopkins (1967, 1971) for Arctic North America and the Chukchi peninsula. Thus, the simultaneous existence of a continental ice dome in the Antarctic and a substantially ice-free Arctic ocean is well established for the period between, at least, about 12 and 2.5×10^6 years ago, a period characterized by a high degree of stability in spite of second-order climatic fluctuations. This strange situation must have caused marked hemispheric circulation asymmetries of both the atmosphere and the ocean.

6.3 SOME IMPLICATIONS OF A UNIPOLAR CLIMATIC ASYMMETRY

The discovery of the coexistence of a fully glaciated Antarctic continent and an open Arctic ocean, for no less than 10×10^6 years immediately before the Pleistocene, is indeed important. It could be made because of the evidence accumulated by the "Glomar Challenger" during the Deep Sea Drilling Project. The notion appears so contradictory to traditional climatological views that no more than reluctant adoption can be expected. One of the most urgent tasks to pursue next is a careful and critical survey of the vast geological literature on a global scale. This must be done, however, in cooperation between geologists and meteorologists, and with full knowledge of the basic laws of planetary circulation and their consequences.

Attention must be paid, first of all, to the fundamental circulation theorem set forth by V. Bjerknes in 1897 (see Palmén and Newton 1969); according to this theorem, temperature decreases with height and latitude in the three-dimensional baroclinic structure of the earth's atmosphere, while atmospheric density decreases with height but increases with latitude. Not being parallel, isothermal and isopycnic surfaces cut each other at small angles, forming flat tubes (solenoids). The circulation theorem states that in such a baroclinic field the intensity of a thermal circulation (which is driven by differences in heating according to latitude and height) depends only on the number of solenoids, i.e., on the temperature change (gradient) along an isopycnic surface. Since the slope of such a surface is only 1:300 to 1:2,000, the isopycnic temperature gradients nearly equal the horizontal gradients. On a rotating planet, this thermal circulation is distorted by the Coriolis force; in the earth's atmosphere, the zonal (E–W) components of motion, introduced by the earth's fast rotation, are much stronger than the meridional and vertical components.

It cannot be the task of this report to outline the physical concepts of atmospheric circulation (see, for example, Palmén and Newton 1969) or of oceanic circulation; the latter is driven mainly by the wind near the surface, and at greater depths by solenoids between surfaces of constant temperature and density (depending on salinity). Note, however, that the intensity of atmospheric circulation, given the earth's rotation and the composition (density) of the atmosphere, depends first of all on the meridional temperature difference between the equator and the poles. The data presented in Table 1 of this paper shows that, even today, the equator–pole temperature difference is about 40% higher in the southern than in the northern hemisphere.

For conservative extrapolation of the relation between temperature and height for the case of an ice-free Arctic in winter, one may assume (as in Figure 23) an average surface temperature of +4 °C (instead of the current −34 °C), and a moist adiabatic lapse rate from the cloud base at about 950 mbar up to at least 500 mbar. [This instability probably leads to a cooling of the upper troposphere, e.g., at 300 mbar (~ 9 km) from the current −58 °C to about −62 °C; see also Figure 16.] This means an average tropospheric warming of

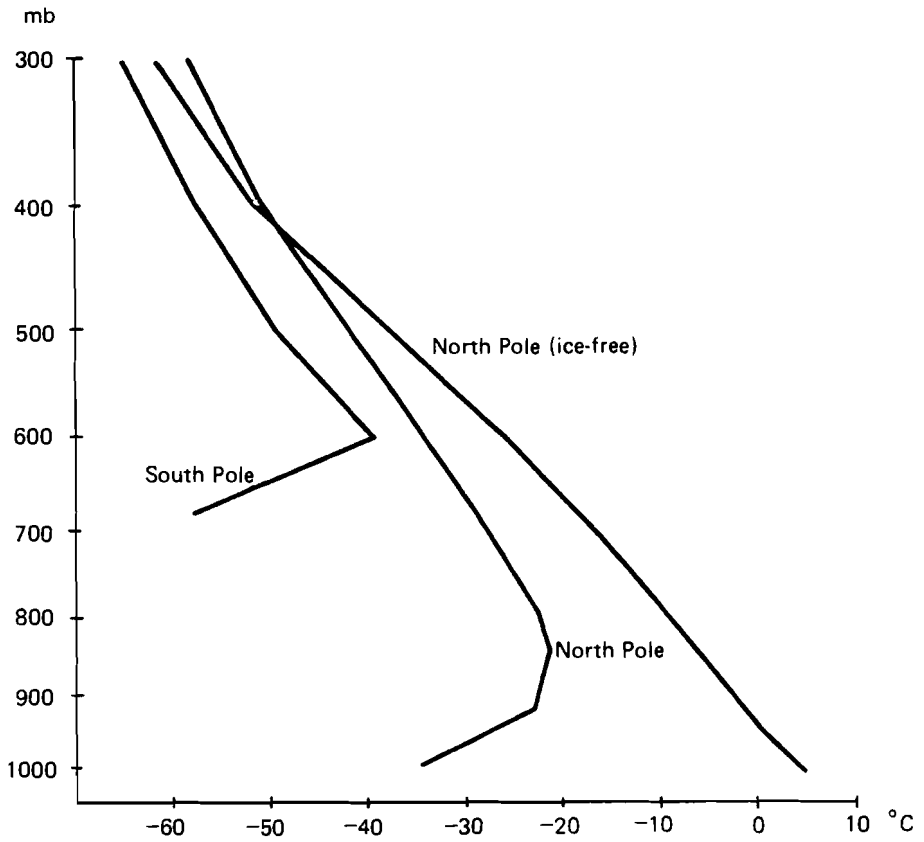

FIGURE 23 Current winter temperatures above the North Pole and South Pole, and estimated winter temperatures which might prevail above an ice-free North Pole.

11.5 °C. A corresponding tropospheric warming of only 2–3 °C can be expected for summer, when the surface inversion is shallow and unimportant. For the 300/700 mbar layer, assumed representative for the purposes of a hemispheric comparison (see Chapter 2, especially Table 1), the temperature increase in winter is only +4 °C, and the summer increase +2 °C. A conservative estimate of a +3 °C annual average increase results. In this case, the average temperature difference of this layer between the equator and the North Pole would decrease to 24 °C; still, the temperature difference would remain at 37 °C above the southern hemisphere, where it would be slightly more than 50% higher than in the northern hemisphere. Here the assumption is made that the greenhouse effect does not significantly alter the meridional temperature gradient; this is certainly not quite realistic and subject to further revision.

Under the conditions of such a unipolar temperature asymmetry, one fundamental quantity of the atmospheric circulation could be extrapolated. Remember that in a rotating atmosphere there are two fundamentally different modes of meridional exchange of conservative properties, such as angular momentum or enthalpy (Palmén and Newton 1969). The first mode can be conceptualized as a helical motion within a latitudinal band, symmetric about the rotational axis, and driven by a thermal circulation in a meridional/vertical plane between the equator and the subtropics; this is the tropical circulation or Hadley cell. The exchange processes of the second mode in higher latitudes are mainly due to traveling and quasi-stationary eddies, advecting warm or cold air poleward or equatorward on both sides of a vortex or long wave, within a belt of westerlies; this belt, identical with the meandering edge of a huge polar vortex, is part of the extratropical or Ferrel circulation. The average boundary between the two modes (which in reality permanently interact) is characterized by the belt of subtropical anticyclones near the surface and by the maximum of baroclinic westerly winds (i.e., the subtropical jet stream) in the upper troposphere, both in positions which nearly coincide.

It has been shown (Smagorinsky 1963) that the stability or instability of eddies in a baroclinic current depends on a simple criterion related to the circulation theorem, i.e., the ratio between the meridional temperature gradient and the vertical lapse rate. Since the latter depends mainly on the water vapor content of the atmosphere (as will be discussed below), the behavior of the eddies is by and large controlled by the meridional temperature gradient. The eddies tend to be unstable in the Ferrel circulation, but stable in the Hadley cell where the meridional temperature differences are weak. The latitude-dependent threshold of the so-called Z-criterion then indicates, at the same time, the seasonally varying position ϕ_{STA} of the subtropical belt. ϕ_{STA} is given by the following relation, where r = earth's radius, h = scale height of the atmosphere, θ = potential temperature, $y(z)$ = meridional (vertical) coordinate, and STA = subtropical anticyclone:

$$\cot \phi_{STA} = \frac{r\partial\theta/\partial y}{h\partial\theta/\partial z}$$

Korff and Flohn (1969) have verified this theoretical concept* using monthly averages over many years of both the latitude ϕ_{STA} of subtropical anticyclones and the meridional temperature gradient at the 300/700 mbar layer, in both hemispheres. With correlation coefficients above 0.85, this relation describes remarkably well the seasonal variation and the actual hemispheric asymmetry of ϕ_{STA} (Figure 24).

*The Z-criterion has recently been criticized by Greenhut (1977), who has demonstrated that it leads to incorrect results if applied to tropical latitudes during northern summer, when the average meridional temperature gradient reverses. Here it is only applied to the atmospheric circulation in subtropical and temperate latitudes; the empirical verification given above leaves no doubt about its applicability in this general case.

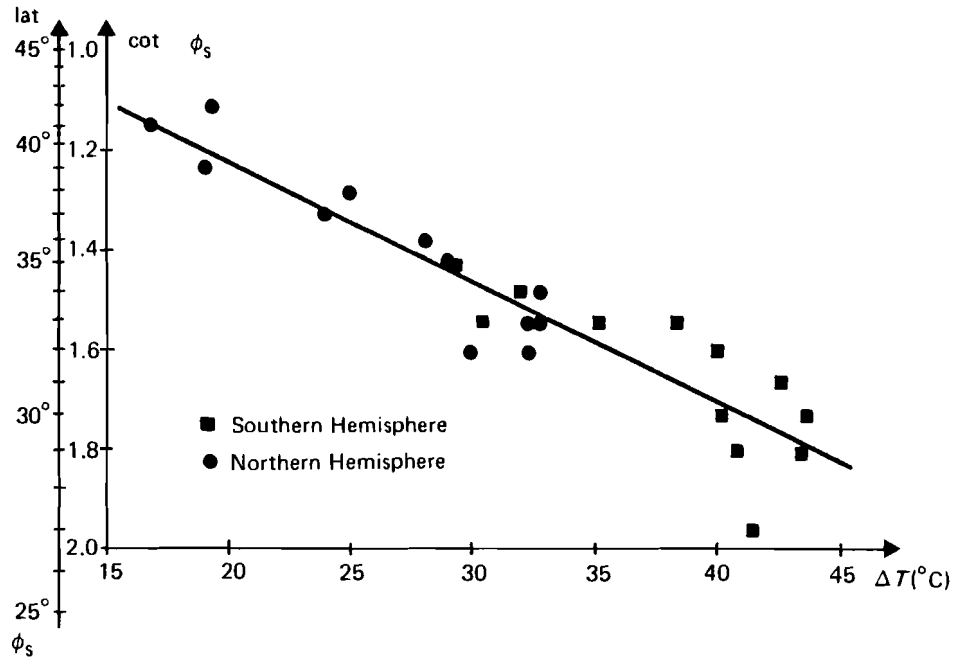

FIGURE 24 Latitude of the subtropical anticyclonic belt (ϕ_s) in each month of the year vs. the current equator–pole temperature difference. The monthly data for the 300/700 mbar layer are from Flohn (1967); data on subtropical anticyclonic belts are from Pflugbeil (1967).

The role of the lapse rate $\partial\theta/\partial z$ should be taken into account; as early as 1964 a diagram (Figure 25) was published (Flohn 1964b), which demonstrated that an increase in the lapse rate would reduce ϕ_{STA}. A quite similar diagram was published later by Bryson (see Williams 1978, p. 151).

There are two factors that impede simple quantification by means of the Manabe–Wetherald diagram (see Figure 7). First, because of theoretical considerations, it is an open question whether $\partial T/\partial y$ in Figure 25 can be taken as a linear average between the equator and the pole or as the highest value in the subtropical baroclinic zone (the latter assumption is preferred by Flohn, 1964b).

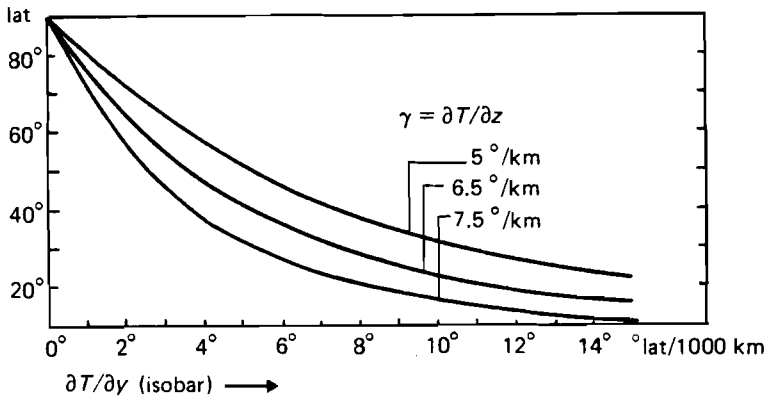

FIGURE 25 Latitudinal position of the subtropical anticyclonic belt as a function of vertical stability γ and the meridional temperature gradient $\partial T/\partial y$. y and z are the meridional and vertical coordinates, respectively. Source: Flohn (1964b).

Second, introduction of clouds into the Manabe–Wetherald (1975) model in a simplified manner yields discontinuities in the tropospheric lapse rate below 300 mbar (Figure 7), which make it difficult to use the quantitative estimate in the above formula. The combined role of meridional and vertical temperature gradients with respect to the *Z*-criterion merits further investigation.

A simple extrapolation based on the temperature distribution above an ice-free Arctic (see Figure 23), with the temperatures above the equator and the South Pole unchanged, would yield only a small northward displacement of the subtropical anticyclonic belt. However, neglecting the 700/1,000 mbar layer, in which most of the warming (+21 °C) occurs, leads to unrealistic results. The *Z*-criterion is based on the concept of baroclinic instability; the slope of the 300 mbar surface, which is representative of tropospheric baroclinicity (or the temperature gradient), depends on the temperature pattern of the troposphere as a whole. There is no way of realistically estimating the properties of the 700/1,000 mbar layer at the Antarctic (where it is completely under the surface), but one may use more realistic values, valid for the 300/1,000 mbar layer, to estimate the temperature increase above the Arctic: +11 °C in winter, +3 °C in summer, and +7 °C year-round. This would produce an annual shift of the northern subtropical high-pressure belt from the present lat 37° to lat 43–45°, with the location of the southern subtropical belt remaining unchanged (31 °S) (see Figure 24). In summer, the shift would probably extend not much farther than 100 or 200 km, but in winter the subtropical belt may be displaced to the north by some 800 km or even more. This would drastically reduce the extension of the subtropical belt of winter rains, now supplying California, the

Mediterranean, the Middle East up to Turkestan (USSR), and the Punjab region of India. The belt situated at 45–50 °N would probably be frequently affected by summer droughts.

Such an asymmetric displacement of the northern STA together with a constant southern STA would also shift the average position of the "meteorological equator" to lat 9–10 °N, from its current position at 6 °N. Because of the much higher intensity of the southern Hadley cell and the southern trade winds, this position may also be displaced further north, i.e., near lat 12 °N. In this case penetration of the equatorial rain belt across the mathematical equator into the southern hemisphere would occur probably only occasionally in northern winter; the seasonal displacement of the rain belt would be restricted to the belt between the equator and lat 20 °N. As a consequence, tropical summer rains south of the equator would decrease markedly, eventually leading to natural desertification in many countries situated within the belt between 0 and 20 °S. This would probably be aggravated by more frequent and more intense equatorial upwelling, causing a drastic reduction of oceanic evaporation in this belt, especially in northern summer/southern winter, when the meteorological equator reaches its northernmost position. In this case, strong equatorial upwelling can be expected to occur permanently (with El Niño situations no longer arising), at least in the Pacific and Atlantic oceans. For the equatorial Indian Ocean, no evidence of past (or present) upwelling is available.

In the big oceans, the position of the equatorial upwelling zone is controlled by the disappearance of the Coriolis force at the mathematical equator. Since no meridional climatic shift is possible in this case, the equatorial upwelling zone can serve as a marker for latitudinal shifts of tectonic plates (Winterer 1973). The different view expressed by Kozur (1976) results from a misunderstanding of the geophysical background of oceanic upwelling along the equator, which never coincides with the atmospheric intertropical convergence zone (see Chapter 2).

In the present Sudan–Sahel belt, between about lat 8 °N and 18 °N (or perhaps 20 °N), an increase in precipitation could be possible. However, this contention is based on only one argument, namely the northward shift of planetary climatic belts. But in Africa the actual seasonal advance of the rainfall belt in summer is remarkably small; this is most probably due to the tropical easterly jet, which, in an area of decreasing speed, forces the air beneath to subside (Flohn 1964a, 1966). This effect should also persist during an ice-free Arctic ocean phase. Another essential prerequisite for an increase in precipitation, if one follows the convincing model studies by Charney (1975) and many others, would be the conservation of vegetation that might reappear because of expanding summer rains, i.e., the protection of vegetation against overgrazing and other desertification processes triggered by man.

In the monsoon area of southern Asia, the planetary circulation patterns are largely controlled by and disturbed by the existence of the mountain area

north of the Himalayas. Here any rational attempt to predict the effects of disappearing Arctic sea ice seems to be impossible. Since the late Tertiary, the altitude of the giant mountain range in this area has increased considerably; vertical motions are still occurring, and climatological evidence from a period when the Himalayas did not exist can certainly not be assumed to resemble what could be expected under present boundary conditions. Striking evidence for uplifting is the Tibetan Plateau, whose weak rolling topography has risen from near sea level in the late Tertiary to a present altitude of 4–5 km. Being an elevated heat source, the plateau controls the tropical easterly jet (Flohn 1964a, 1968) and the entire monsoon circulation between western Africa and the Philippines. In this wide area, the influence of an ice-free Arctic could be rather weak or even negligible in summer. In winter, a northward displacement of the subtropical jet at lat 5–6° (like in other longitudes, see p. 65) could mean wintertime disturbances across the whole of southern Asia, perhaps with increasing rainfall in areas as remote as Chinese Turkestan, but with decreasing winter rain south of the Himalayas.

After a possible disappearance of the central core of the Arctic drift ice, one of the first consequences in the cold season would be the formation of a baroclinic zone along the northern coast of the continents, between the cold air continuously formed above the snow-covered land and the relatively warm air above the open Arctic ocean. It must remain an open question as to what extent coastal ice, and perhaps also a thin seasonal mid-ocean ice cover, could form. In any case, the rate of snowfall along the northern coasts of the continents and Arctic islands would be enhanced by such a development. In summer, the low-level stratus clouds now above the melting ice could probably disappear, and the thermal circulation arising between the heated continents and the relatively cool water could produce a distinct predominance of anticyclonic situations above the Arctic Ocean (which will then be characterized by subsidence and little cloudiness).

Changes in the global water budget (see Chapter 2) are difficult to estimate. While a weaker tropical circulation can be assumed for the moderate warm phases considered in the global warming scenario discussed in Chapter 5, evidence from past climates, based on signs of increasing aridity in the late Tertiary are unambiguous; the fact that the peak of Antarctic glaciation, together with the eustatic drop of the sea level, also reduced the area of ocean evaporation lends weight to this conclusion. If one assumes strong upwelling for only six months of the southern winter, the loss due to this effect is 30×10^3 km^3/yr. On the other hand, an ice-free Arctic ocean would evaporate much faster than at present; (currently the evaporation is only on the order of 5–10 cm/yr). If one assumes a rather large increase in evaporation, i.e., by +100 cm/yr, this would yield no more than 10×10^3 km^3/yr for an area of 10^7 km^2. Based on the incomplete evidence from past climates, the extension of the southern belt to lat 0–20 °S and the displacement of the northern STA to lat 35–45 °N (or even farther) would support a general increase in aridity, with a global loss of water on the order of at least 4–5%.

The prospects for a worldwide rise in the sea level as a possible consequence of global warming must be considered quantitatively. Melting of drifting sea ice does not change the sea level at all; floating ice is in static equilibrium with water, like an ice cube in a glass of whisky. Within the human time scale (~ 100 years), any worldwide rise in the sea level could only be caused by large-scale surges of continental ice caps, e.g., on the order of 10^5 km^3 or more, leading (with a density of almost 0.9) to a 25 cm sea-level rise per 10^5 km^3 of ice melted.

Only one area is prone to such a surge, the "western" part of Antarctica (between South America and long 150 °W), situated on a rock foundation largely below sea level. Surges of this order have been suggested for the 19th century (Lamb 1967), as well as for the postglacial period (Wilson 1978), and the probability of such an event may increase with global warming. There seems to be a gradual transition from one surge to another (of unknown time scale!), as well as extended calving of existing ice shelves. Possibly more interesting are surges on the order of 2×10^6 km^3, equivalent to a sea-level rise of 5 m; the last event of this kind may have occurred about 110,000 years ago (Hollin 1977) or, with more widespread evidence, about 125,000 years ago (Mercer 1978). The risk of such a global rise in the sea level – possibly produced by a mechanism of calving bays, as proposed by Hughes (1977) – has been examined by Mercer (1978). At present, the risk seems to be quite small, but certainly not negligible (see Chapter 2 of this report). Some theoretical studies have been made, but more detailed field investigations are needed, as well as monitoring of Antarctic ice shelves and coastal sea ice.*

The possibility of a significant melting of continental ice caps (e.g., in Greenland and in the Antarctic) is also rather small. The surface of the Antarctic ice cap, with temperatures between −20 °C and −70 °C and an albedo of 80–90%, can be considered stable. Even a very marked warming through greatly increased transport of warm air would not suffice to cause significant melting (or evaporation). After a possible disappearance of the Arctic sea ice, Greenland (lat 60–83 °N) would be affected by some melting during the warm season (at least at its southern part), but it would also receive much greater winter snowfall due to increased cyclone activity. It is difficult to estimate the ratio of both processes without model computations. But in the worst and rather unlikely case, an estimated annual net loss of as much as 50 cm water-equivalent would cause an additional sea-level rise of 2.5 mm/yr, as compared with the present value of 1.2 mm/yr.

As a result of these considerations, the probability of a catastrophic or even only appreciable rise in the sea level during the next 100 years seems small (estimated to be 1% or less) – much smaller than the probability of a large-scale shift of climatic belts due to a global warming – but is certainly not negligible.

*The possible time scale of such a disintegration could be on the order of 100–200 years, equivalent to an average sea-level rise on the order of 2–5 cm/yr. This is suggested by a similar event caused by the catastrophic incursion of the sea into the present Hudson Bay about 7,800 years ago (Andrews *et al.* 1972), simultaneously with an observed eustatic sea-level rise of 7–10 m over 200 years on the coasts of northwest England (Tooley 1974) and southwest Sweden (Mörner 1976).

7 CONCLUSIONS

Small changes in the global average temperature (see Table 3) are utterly misleading for the general reader. A temperature drop of 1 °C near the northern boundary of agricultural land (affecting, for instance, wheat in northern Canada, or hay in Iceland) may reduce the growing season by several weeks, with detrimental effects on harvests. Even more essential are the accompanying changes in the frequency of extremes in weather in lower and middle latitudes, i.e., long and cold springs, cool and wet summers, and so on. According to the present state of the art, a sudden cooling, similar to that which occurred during the Little Ice Age and its forerunners, cannot be excluded, since natural internal climatogenetic processes are at present still unpredictable (see Chapter 2). The most catastrophic years were 1316, 1430, 1570, and several years in the 1690s and 1780s (the latter apparently affecting Europe,* North America, as well as Japan). The European revolutions of 1789 and 1848 occurred after a succession of years with bad weather, bad harvests, and high cereal prices; some of the most severe climatic and economic conditions were reported in the years following some very heavy volcanic eruptions, e.g., after 1766, 1783, 1815, and finally, 1883.

The problem of natural climatic fluctuations due to the varying frequency and intensity of volcanic explosions merits some discussion. As far as can be seen, this effect alone could counteract, with a certain degree of probability, the evolution outlined in the admittedly one-sided scenario discussed in this paper (see the basic assumptions given on p. 5). Lamb (1970, 1977b) has demonstrated the time variability of volcanic eruptions using an estimated Dust Veil Index (see Figure 26). There is little doubt that the peaks of volcanic activity by and large coincide with series of particularly cool years (and especially cool summers); their role in climatic history, perhaps on all time scales (see

*These data have been derived from historical records including a comparison of some 25 long series of cereal prices (1200–1790) in northwest and central Europe. A detailed study is in preparation; see also the documented evidence given by Ladurie (1971) and Lamb (1977a).

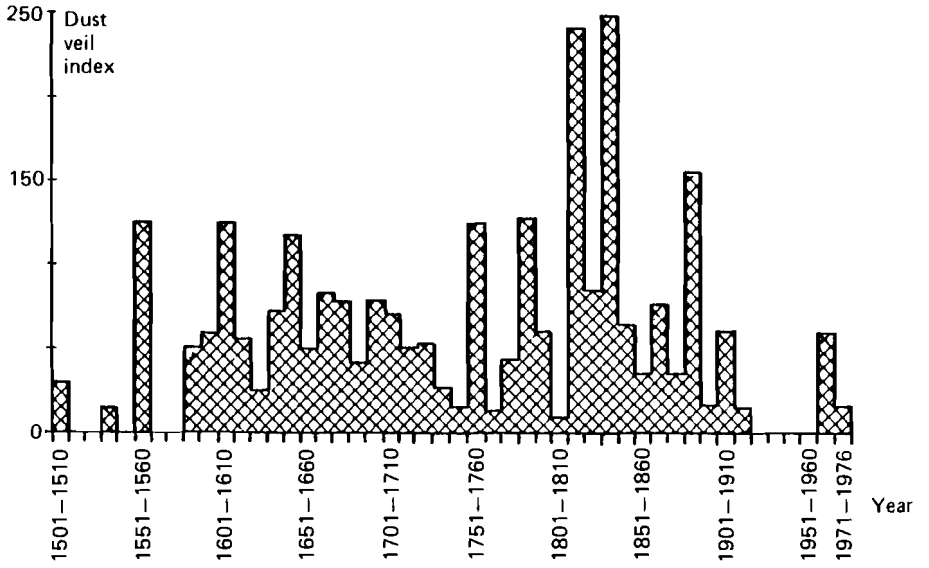

FIGURE 26 Ten-year averages of volcanic activity in the northern hemisphere since 1500, measured in terms of the Dust Veil Index. Source: Lamb (1977b).

Figure 20), can hardly be overrated. Volcanic eruptions are very difficult to forecast, as has been confirmed by recent occurrences; such forecasts are virtually impossible beyond the time scale of weeks or months. On a global scale, the geophysical concept of plate tectonics has contributed much to a better understanding of volcanic eruptions; mid-oceanic rift systems burst, hot material ascends and erupts in individual volcanoes, and plates move horizontally towards the continents, where they are subdued by heavy earthquakes. In recent years a series of unusually severe earthquakes has occurred, all of them along well-known active tectonic zones, but volcanic activity has remained moderate. Should we soon expect an increase in the frequency of really heavy volcanic explosions? There is no answer to this question, but volcanologists would be hardly surprised if this were to happen. An example of discontinuous manifestations of the slow plate motion – which is probably responsible for the observed clustering of volcanic (and possibly seismic) events – recently occurred at the mid-Atlantic rift system which crosses Iceland. In April 1977 two innocent-looking, but steaming, parallel cracks, each with a diameter of about 1 m, formed in the Myvatn area, and a geothermal power station which stood just before completion lost its resources.

Since volcanic activity has until now been unpredictable, a statistical technique can be used to estimate the probability of a cooling episode similar to the Little Ice Age occurring during the next 100 years. On the basis of Figure A 31 in the excellent report *Understanding Climatic Change*, issued by the US National Academy of Sciences (1974), one can estimate that the

probability that an event which may occur randomly once every 1,000 years will occur during the following 100 years is about 10–20%. This estimate only indicates an order of magnitude, but to disregard such a probability would be irresponsible.

In this context, our scenario leads to the following conclusions: if the atmospheric CO_2 content continues to rise, and if other man-made trace gases add another 50% (or more) to the greenhouse effect of infrared absorption, developments similar to those outlined in the global warming scenario based upon past climates in Chapter 5, must eventually be expected. The Eem period may serve as a first guide to what might happen if the real CO_2 content rises to about 500–550 ppm; if the effect of other trace gases were negligible, the relevant threshold of the virtual CO_2 content would be about 600–700 ppm (see Table 3). As the Manabe–Wetherald model (Figure 7) indicates, a doubling of the CO_2 content could be accompanied by quite serious regional consequences, some of them benign, but others deleterious. These consequences would be more profound than all climatic changes mankind has experienced during the last 10,000 years. To avoid serious risks, provision should be made to avoid exceeding about 450 ppm, as a threshold value of the real CO_2 content.

The real danger, however, is related to the possible consequences outlined in Chapter 6. Can we stop at a CO_2 content between 450 and 750 ppm? Since the necessary time of transition from one energy system to another is on the order of several decades (Häfele and Sassin 1977a, 1977b), it will soon be too late for any effective countermeasures. The report of a working group of specialists (Williams 1978, p. 315) states that "mankind needs and can afford a time window of between 5 and 10 years for vigorous research and planning . . . to justify a major change in energy politics . . . ." At first glance, the idea of a planet with one pole heavily glaciated and the other ice-free seems so fantastic and inconceivable that emotional resistance against it, especially among non-scientists, will be difficult to overcome. But there is no doubt that exactly this pattern had existed and was stable for a period of ten million years; this is established as a fact.

It goes beyond the capability of a climatologist, familiar with the historical and geophysical background of his science, to predict the time sequence of future increases in CO_2 and a rise in the temperature. This depends on economic and political decisions which occur outside his sphere of knowledge and experience. As a first guide to different CO_2 growth rates, the reader is referred to Figure 8 in this paper. Taking into account all uncertainties, especially with respect to the role of the biosphere and the oceans, specialists argue that an increase in atmospheric CO_2 by a factor of 3 to 5 could be expected over the next 100 years or so (see p. 26).

From a climatological point of view the *decisive threshold* of the real CO_2 level should be somewhere between 550 and 750 ppm; that of the virtual CO_2 level is somewhat higher, e.g., between 800 and 1,000 or 1,100 ppm. Above

this threshold, the probability of an evolution toward an ice-free Arctic increases rapidly – a development of this kind could occur quite abruptly, i.e., in a matter of few decades (or less), and would then be irreversible. Since this situation had been maintained, under purely natural conditions, over a period of no less than ten million years, it would again be stable, at least for a period well beyond a millenium, before the deep ocean has absorbed the additional input of CO_2. What has happened can happen again; after a series of catastrophic weather extremes, it would lead to a nearly inconceivable displacement of climatic zones by 400–800 km (or more), definitely affecting mankind as a whole.

The author firmly believes that this risk is unacceptable and must be avoided even at very high cost. It is at least as large as, but probably much larger than, all the risks involved in the transitional use of nuclear energy under special precautions. The risk of a global warming can be avoided if decisions regarding future energy policies and all their consequences are carefully planned and can be executed, under an international agreement, without undue delay.

REFERENCES

Monographs

Andersen, N.R., and A. Malakhov, eds. (1977) The Fate of Fossil Fuel CO_2 in the Oceans. Marine Science, Vol. 6. New York: Plenum Press.

Bach, W., J. Pankrath, and W. Kellogg, eds. (1979) Man's Impact on Climate. Developments in Atmospheric Science, Vol. 10. Amsterdam: Elsevier.

Baumgartner, A., and E. Reichel (1975) The World Water Balance. Munich: Oldenbourg.

Bryson, R.A., and Th.J. Murray (1977) Climates of Hunger. Madison: University of Wisconsin Press.

Budyko, M.I. (1974) Izmeneniia klimata. Leningrad: Gidrometeoizdat (in Russian). Translated into English by the American Geophysical Society in 1977.

Cline, R.M., and J.D. Hays, eds. (1976) Investigation of Late Quaternary Paleoceanography and Paleoclimatology. Geological Society of America Memoir 145.

Frenzel, B. (1967) Die Klimaschwankungen des Eiszeitalters. Braunschweig: Vieweg.

Frenzel, B. (1968a) Grundzüge der pleistozänen Vegetationsgeschichte Nord-Eurasiens. Wiesbaden: Franz Steiner.

Gabriel, B. (1977) Zum ökologischen Wandel im Neolithikum der Östlichen Zentralsahara. Berliner Geographische Abhandlungen 27.

GARP, in B. Bolin, ed. (1975) The physical basis of climate and climate modeling. GARP Publication Series 16. Geneva: World Meteorological Organization.

Gribbin, J., ed. (1978) Climatic Change. Cambridge: Cambridge University Press.

Hare, F.K. (1977) Climate and desertification. Pages 63–167, Desertification: its Causes and Consequences, edited by the Secretariat of the United Nations Conference on Desertification. Oxford: Pergamon.

Ives, J.D., and R.G. Barry, eds. (1974) Arctic and Alpine Environments. London: Methuen.

Labeyrie, J., ed. (1974) Variation du Climat au Cours du Pleistocène. Paris: Centre Nationale de Recherches Scientifiques.

Ladurie, E.L. (1971) Times of Feast, Times of Famine. A History of Climate Since the Year 1000. New York: Doubleday.

Lamb, H.H. (1972) Climate: Present, Past and Future, Vol. 1. London: Methuen.

Lamb, H.H. (1977a) Climate: Present, Past and Future, Vol. 2. London: Methuen.

Lvovich, M. (1969) Water Resources for the Future. Moscow: Posveshchenie (in Russian).
Mägdefrau, K. (1968) Paläobiologie der Pflanzen. 4th ed. Stuttgart: Gustav Fischer.
Nairn, A.E.M., ed. (1961) Descriptive Paleoclimatology. London: Interscience.
Nairn, A.E.M., ed. (1964) Problems in Paleoclimatology. NATO Paleoclimatology Conference at the University of Newcastle/Tyne, Jan. 7–12, 1963. London: Interscience.
National Academy of Sciences (1974) Understanding Climatic Change. A Program for Action. Washington, D.C.
National Academy of Sciences (1979) Carbon Dioxide and Climate. A Scientific Assessment. Washington, D.C.
Nicholson, S.E. (1976) A Climatic Chronology for Africa: Synthesis of Geological, Historical and Meteorological Information and Data. Ph.D. thesis, Department of Meteorology, University of Wisconsin. Madison, Wisconsin.
Olsen, J.S., H.A. Pfuderer, and Y.K. Chan (1978) Changes in the Global Carbon Cycle and the Biosphere. ORNL-1050. Oak Ridge, Tennessee: Oak Ridge National Laboratory.
Palmén, E., and C.W. Newton (1969) Atmospheric Circulation Systems. International Geophysics Series 13.
Pittock, A.B., L.A. Frakes, D. Jenssen, J.A. Peterson, and J.W. Zillman, eds. (1978) Climatic Change and Variability. A Southern Perspective. Cambridge: Cambridge University Press.
Schwarzbach, M. (1974) Klima der Vorzeit. Eine Einführung in die Paläoklimatologie. 3rd ed. Stuttgart: Enke.
Servant, M. (1973) Séquences Continentales et Variations Climatiques: Elévation du Basin du Tchad Canozoique Supérieure. Doctoral Dissertation, University of Paris.
Stumm, W., ed. (1977) Global Chemical Cycles and Their Alteration by Man. Berlin: Abakon.
Takahashi, K., and M.M. Yoshino, eds. (1978) Climatic Change and Food Production. Tokyo: University of Tokyo Press.
van Zinderen Bakker, E.M., ed. (1978) Antarctic Glacial History and World Palaeoenvironments. Rotterdam: Balkema.
Vasari, Y., H. Hyvarinen, and S. Hicks, eds. (1972) Climatic Change in Arctic Areas during the Last Ten Thousand Years. Acta Universitatis Ouluensis A3, Geologica (1).
Williams, J., ed. (1978) Carbon Dioxide, Climate and Society. IIASA Proceedings Series Environment, Vol. 1. Oxford: Pergamon Press.
Williams, M.A.J., and H. Faure, eds. (1980) The Sahara and the Nile. Rotterdam: Balkema.
World Meteorological Organization (1979) Proceedings of the World Climate Conference. Publication No. 537. Geneva: World Meteorological Organization.

Selected References on Geophysics, Modeling, and Related Topics

Aagard, K., and L.K. Coachman (1975) Eos-Transactions of the American Geophysics Union 56: 484–487.
Aagard, K., and P. Greisman (1975) Journal of Geophysical Research 80: 3821–3827.
Andreas, E.L., C.A. Paulson, R.M. Williams, R.W. Lindsay, and J.A. Businger (1979) Boundary-Layer Meteorology 17: 57–91.
Angell, J.K., and J. Korshover (1978) Monthly Weather Review 106: 755–770.
Augustsson, T., and V. Ramanathan (1977) Journal of Atmospheric Sciences 34: 448–451.
Bacastow, R. (1976) Nature 261: 116–118.
Bacastow, R. (1977) Pages 33–44, The Fate of Fossil Fuel CO_2 in the Oceans, edited by N.R. Andersen and A. Malakhov. Marine Science, Vol. 6. New York: Plenum Press.
Bach, W. (1976a) Review of Geophysics and Space Physics 14: 429–474.

Bach, W. (1976b) Bonner Meteorologische Abhandlungen 24.
Bach, W. (1978) Pages 141–168, Carbon Dioxide, Climate, and Society, edited by J. Williams, Oxford: Pergamon.
Barnett, T.P. (1977) Journal of Physical Oceanography 7: 221–236, 633–647.
Berkofsky, L. (1976) Applied Meteorology 15: 1139–1144.
Berkofsky, L. (1977) Beiträge zur Physik der Atmosphäre 50: 312–320.
Berlage, H.P. (1957) Medelingen en Verhandelingen Koninklijk Nederlandsch Meteorologisch Instituut De Bilt 69.
Berlage, H.P. (1966) Medelingen en Verhandelingen Koninklijk Nederlandsch Meteorologisch Institut De Bilt 88.
Bjerknes, J. (1969) Monthly Weather Review 97: 163–172.
Bjornsson, A., K. Saemundson, P. Einarsson, E. Tryggvassen, and K. Gronvold (1977) Nature 266: 318–322.
Borzenkova, I.I., K.Ya. Vinnikov, L.P. Spirina, D.I. Stekhnovskii (1976) Meteorologiya i Gidrologiya 7: 27–35.
Bryson, R.A., W.M. Wendland, J.D. Ives, and J.T. Andrews (1969) Arctic and Alpine Research 1: 1–14.
Budyko, M.J. (1962) Izvestiya Akademii Nauk SSR, Seriya Geograficheskaya 6: 3–10 (in Russian).
Budyko, M.J. (1969) Tellus 21: 611–619.
Budyko, M.J. (1972) Eos-Transactions of the American Geophysics Union 53: 868–874.
Budd, W.F. (1975a) Science 186: 925–927.
Budd, W.F. (1975b) Journal of Glaciology 14: 3–21.
Cess, R.D. (1976) Journal of Atmospheric Sciences 33: 1831–1843.
Cess, R.D. (1977) Journal of Atmospheric Sciences 34: 1824–1827.
Charney, J.G. (1975) Quarterly Journal of the Royal Meteorological Society 101: 193–202.
Damon, P.E., and St. M. Kunen (1976) Science 193: 447–453.
Doberitz, R. (1968) Berichte des Deutschen Wetterdienstes 112.
Doberitz, R. (1969) Bonner Meteorologische Abhandlungen 11.
Donn, W.L., and D.H. Shaw (1966) Journal of Geophysical Research 71: 1087–1093.
Dronia, H. (1974) Meteorologische Rundschau 27: 166–174.
Ellsaesser, H.W., M.C. MacCracken, G.L. Potter, and F.M. Luther (1976) Quarterly Journal of the Royal Meteorological Society 102: 655–666.
Fletcher, J.O., Y. Mintz, A. Arakawa, and T. Fox (1973) World Meteorological Organization Technical Note 129: 181–218.
Flohn, H. (1964a) Bonner Meteorologische Abhandlungen 4.
Flohn, H. (1966) Zeitschrift für Meteorologie 17: 316–320.
Flohn, H. (1967) Annalen der Meteorologie, Neue Folge 3: 76–80.
Flohn, H. (1968) Colorado State University, Department of Atmospheric Science Paper 130.
Flohn, H. (1971) Bonner Meteorologische Abhandlungen 15.
Flohn, H. (1972) Pages 93–102, Studies in Physical Oceanography, Vol. I, edited by A.L. Gordon. New York: Gordon.
Flohn, H. (1974a) Annalen der Meteorologie, Neue Folge 9: 25–31.
Flohn, H. (1975) Bonner Meteorologische Abhandlungen 21.
Flohn, H. (1977a) Applied Sciences and Development 10: 44–58.
Flohn, H., and H. Fleer (1975) Atmosphere 13: 96–109.
Gow, A.J., H.T. Ueda, and D.E. Garfield (1968) Science 161: 1011–1013.
Greenhut, G.K. (1977) Journal of Applied Meteorology 16: 727–734.
Hahn, J., and C. Junge (1977) Zeitschrift für Naturforschung 32a: 190–214.

Hahn, J. (1979) Pages 193–213, Man's Impact on Climate, edited by W. Bach, J. Pankrath and W. Kellogg. New York: Elsevier.
Hantel, M. (1972) Pages 121–136, Studies in Physical Oceanography, Vol. I, edited by A.L. Gordon. New York: Gordon.
Hastenrath, St. (1976) Rivista Italiana di Geofisisica e Science Affini 3: 255–256.
Hastenrath, St. (1977) Annalen der Meteorologie, Neue Folge 12: 84–86.
Hattersley-Smith, G. (1974) Pages 195–223, Arctic and Alpine Environments, edited by J.D. Ives and R.G. Barry. London: Methuen.
Häfele, W., and W. Sassin (1977a) The global energy system. Pages 12–25, Annual Review of Energy, Vol. 2, edited by J. Hollander. Palo Alto, California: Annual Reviews Inc.
Häfele, W., and W. Sassin (1977b) On energy demand. International Atomic Energy Agency Bulletin 19(6): 21–37.
Henning, D., and H. Flohn (1980) Beiträge zur Physik der Atmosphäre 53: 430–441.
Hibler, W.D. (1979) Journal of Physical Oceanography 9: 815–846.
Hollis, G.E. (1978) Geographical Journal 144: 62–80.
Joseph, J.H. (1977) Pages 487–492, Proceedings of a Conference on Radiation in the Atmosphere, edited by H.J. Bolle. Princeton: Science Press.
Junge, C. (1978) PROMET, Meteorologische Fortbildung 2/3: 21–32.
Keeling, C.D., and R. Bacastow (1977) Energy and Climate. US National Research Council. Washington, D.C.: National Academy of Science.
Korff, H.C., and H. Flohn (1969) Annalen der Meteorologie, Neue Folge 4: 163–164.
Klein, C. (1977) Personal communication. Jerusalem.
Kukla, G.J., J.K. Angell, J. Korshover, H. Dronia, M. Hoshiai, J. Namias, M. Rodewald, R. Yamamoto, and T. Iwashima (1977b) Nature 270: 573–580.
Lamb, H.H. (1967) World Meteorological Organization Technical Note 87: 428–453.
Lamb, H.H. (1970) Philosophical Transactions of the Royal Society of London, Series A 266: 425–533.
Lamb, H.H. (1977b) Climate Monitor 6: 57–67.
Limbert, D.W.S. (1974) Polar Record 17: 303–306.
Madden, R.A., and V. Ramanathan (1980). Paper submitted to Science for publication.
Manabe, S., and J.L. Holloway, Jr. (1975) Journal of Geophysical Research 80: 1617–1649.
Manabe, S., and R.T. Wetherald (1975) Journal of Atmospheric Sciences 32: 3–15.
Manabe, S., and R.J. Stouffer (1979) Nature 282: 491–493.
Manabe, S., and R.T. Wetherald (1980) Journal of Atmospheric Sciences 37: 99–118.
Maykut, G.A., and N. Untersteiner (1971) Journal of Geophysical Research 76: 1550–1575.
Mass, C., and S.H. Schneider (1977) Journal of Atmospheric Sciences 34: 1995–2004.
Newell, R.E., A.R. Navato, and J. Hsiung (1978) Pure and Applied Geophysics 116: 351–371.
Oliver, R.C. (1976) Journal of Applied Meteorology 15: 933–970.
Parkinson, C.L., and W.W. Kellogg (1979) Climatic Change 2: 149–163.
Parkinson, C.L., and W.M. Washington (1979) Journal of Geophysical Research 84: 311–337.
Pflugbeil, C. (1967) Berichte des Deutschen Wetterdienstes 104.
Pollack, J.B., O.B. Toon, C. Sagan, A. Summers, B. Baldwin, and W. vanCamp (1976) Journal of Geophysical Research 8: 1071–1083.
Polunin, N., ed. (1980) Growth without Disaster. Proceedings of the Second International Conference on Environmental Future, Reykjavik, June, 1977. London: Macmillen Press.
Pratt, R.F., *et al.* (1977) Climatic Change 1: 109–135.
Ramanathan, V. (1975) Science 190: 50–52.
Ramanathan, V., and J.A. Coakley (1978) Review of Geophysics and Space Physics 16: 465–489.

Ratcliffe, R.A.S., J. Weller, and P. Collison (1978) Quarterly Journal of the Royal Meteorological Society 104: 243–255.
Roads, J.O. (1978) Journal of Atmospheric Sciences 35: 753–772.
Rothrock, D.A. (1975) Journal of Geophysical Research 80: 387–397.
Rowntree, P.R. (1972) Quarterly Journal of the Royal Meteorological Society 98: 290–321.
Rowntree, P.R., and J. Walker (1978). Pages 181–192, Carbon Dioxide, Climate, and Society, edited by J. Williams. Oxford: Pergamon.
Sagan, C., O.B. Toon, and J.B. Pollack (1979) Science 206: 1363–1368.
Salinger, M.J., and J.M. Gunn (1975) Nature 256: 396–398.
Schneider, S.H. (1975) Journal of Atmospheric Sciences 32: 2060–2066.
Schwerdtfeger, W. (1956) Anales Sociedas Cientifico Argentina 161: 53–82.
Schwerdtfeger, W. (1958) Zeitschrift für Gletscherkunde und Glazialgeologie 4: 73–86.
Schwerdtfeger, W. (1970) Pages 253–355, World Survey of Climatology, Vol. 14, edited by H.E. Landsberg. Amsterdam: Elsevier.
Sellers, W.D. (1969) Journal of Applied Meteorology 8: 392–400.
Sellers, W.D. (1973) Journal of Applied Meteorology 12: 241–254.
Smagorinsky, J. (1963) Monthly Weather Review 91: 99–165.
Söderlund, R., and B.H. Svensson (1976) Pages 23–73, SCOPE Report No. 7. London: Wiley.
Thorndike, A.S., D.A. Rothrock, G.A. Maykut, and R. Colony (1975) Journal of Geophysical Research 80: 4501–4513.
Trempel, U. (1978) Diplomarbeit. Universität Bonn.
Untersteiner, N. (1975) Pages 206–224, GARP Publication Series 16. Geneva: World Meteorological Organization.
van Loon, H., and J. Williams (1976) Monthly Weather Review 104: 364–380, 1003–1011, 1591–1596.
van Loon, H., and J. Williams (1977) Monthly Weather Review 105: 636–647.
van Loon, H., and J.C. Rogers (1978) Monthly Weather Review 106: 296–310.
Vowinckel, E., and S. Orvig (1970) Pages 129–252, World Survey of Climatology, Vol. 14, edited by H.E. Landsberg. Amsterdam: Elsevier.
Vowinckel, E., and S. Orvig (1973) World Meteorological Organization Technical Note 129: 143–166.
Walsh, J.E. (1977) Monthly Weather Review 105: 1527–1535.
Walsh, J.E., and C.M. Johnson (1979) Journal of Physical Oceanography 9: 580–591.
Wang, W.C., Y.L. Yung, A.A. Lacis, T. Mo, and J.E. Hansen (1976) Science 194: 685–690.
Washington, W.M., R.M. Chervin, and G. Rao (1977) Pure and Applied Geophysics 115(5–6): 1335–1336.
Wetherald, R.T., and S. Manabe (1975) Journal of Atmospheric Sciences 32: 2044–2059.
Wright, P.B. (1975) CRU 4. University of East Anglia, Climate Research Unit.
Wright, P.B. (1977) Report 77-13. Hawaii Institute of Geophysics.
Wyrtki, K. (1977) Journal of Physical Oceanography 7: 779–787.
Yamamoto, R., T. Iwashima, and M. Hoshiai (1975) Journal of the Meteorological Society of Japan 53: 482–486.
Yamamoto, R., M. Hoshiai, and T. Iwashima (1977) Archiv für Meteorologie, Geophysik, und Bioklimatologie, Serie B 25: 105–115.
Zimen, K.E. (1977a) Global Chemical Cycles and Their Alteration by Man, edited by W. Stumm. Berlin: Abakon.
Zimen, K.E. (1977b) Zeitschrift für Naturforschung 32a: 1544–1554.

Selected References on Paleoclimatology

Adam, D.P. (1978) X. International Union for Quaternary Research (INQUA) Congress, Birmingham, UK. Abstracts. Page 3.

Alexandre, P. (1977) Annales Economies, Sociétiés, Civilisations 32: 183–197.

Andrews, J.T., A. Mears, G.H. Miller, and D.R. Pheasant (1972) Nature–Physical Science 239: 147–149.

Barry, R.G., W.H. Arundale, J.T. Andrews, R.S. Bradley, and H. Nichols (1977) Arctic and Alpine Research 9: 193–210.

Bernabo, J.C., and T. Webb III (1977) Quaternary Research 8: 64–96.

Bowler, J.M., G.S. Hope, J.N. Jennings, G. Singh, and D. Walker (1976a) Quaternary Research 6: 359–394.

Bowler, J.M. (1976b) Earth Science Reviews 12: 279–310.

Bryson, R. (1978) Pages 316–327, Climate Changes and Variability: A Southern Perspective, edited by A.B. Pittock *et al.* Cambridge, Massachusetts: Cambridge University Press.

Butzer, K.W., G.L. Isaac, J.L. Richardson, and C. Washbourn-Kamau (1972) Science 175: 1069–1076.

Butzer, K.W. (1975) Pages 389–410, Problems in Prehistory: North Africa and the Levant, edited by F. Wendorf and A.E. Marks. Dallas, Texas: Southern Methodist University Press.

Chu, C.Ch. (1973) Scientia Sinica 16: 226–256.

Cifelli, R. (1976) Nature 264: 431–342.

Dansgaard, W., *et al.* (1972) Quaternary Research 2: 396–398.

Dansgaard, W., N. Reeh, N. Gundestre, H.B. Clausen, and C.U. Hammer (1975) Nature 255: 24–28.

Dansgaard, W. (1978) Journal of Glaciology 20: 3–30.

Diester-Haas, L. (1976) Quaternary Research 6: 299–314.

Dorf, E. (1960) American Scientist 48: 341–364.

Duplessy, J.C., J. Labeyrie, C. Lalou, and H.V. Nguyen (1970) Nature 226: 631–633.

Emiliani, C., and N.J. Shackleton (1974) Science 183: 511–514.

Flohn, H. (1964b) Geologische Rundschau 54: 504–515.

Flohn, H. (1974b) Quaternary Research 4: 385–404.

Flohn, H. (1978a) Pages 3–13, Antarctic Glacial History and World Paleoenvironments, edited by van Zinderen Bakker. Rotterdam: Balkema.

Flohn, H. (1978b) Pages 124–134, Climatic Changes and Variability: A Southern Perspective, edited by A.B. Pittock *et al.* Cambridge, Massachusetts: Cambridge University Press.

Flohn, H. (1978c) Pages 227–238, Carbon Dioxide, Climate, and Society, edited by J. Williams. Oxford: Pergamon.

Flohn, H. (1979) Quaternary Research 12: 135–149.

Flohn, H., and Sh. Nicholson (1980) Paleoecology of Africa 12: 3–21.

Frakes, L.A. (1978) Pages 53–69, Climatic Changes and Variability: A Southern Perspective, edited by A.B. Pittock, *et al.* Cambridge, Massachusetts: Cambridge University Press.

Frenzel, B. (1968b) Science 161: 637–649.

Fuji, N. (1976) Pages 316–356, Paleolimnology of Lake Biwa and the Japanese Pleistocene 4, edited by S. Horie. Otsu, Japan.

Gardner, J.V., and J.D. Hays (1976) Pages 221–246, Geological Society of America Memoir 145, edited by R.M. Cline and J.D. Hays.

Gasse, F., and G. Delibrias (1976) Pages 529–575, Paleolimnology of Lake Biwa and the Japanese Pleistocene 4, edited by S. Horie. Otsu, Japan.

Hays, J.D., J. Lozano, N. Shackleton, and G. Irving (1976) Pages 337–369. Geological Society of America Memoir 145, edited by R.M. Cline and J.D. Hays.
Hays, J.D. (1978) Pages 57–71, Antarctic Glacial History and World Paleoenvironments, edited by van Zinderen Bakker. Rotterdam: Balkema.
Herman, Y. (1977) Personal communication.
Hollin, J.T. (1977) Boreas 6:33–52.
Hopkins, D.M., ed. (1967) The Bering Land Bridge. Stanford, California: Stanford University Press.
Hopkins, D.M. (1971) Palaeogeography, Palaeoclimatology, Palaeoecology 9: 211–231.
Hsü, K.J., W.B.F. Ryan, and M.B. Cita (1973) Nature 242: 240–244.
Hsü, K.J. (1974) Die Naturwissenschaften 61: 137–142.
Hsü, K.J., L. Montadert, D. Bernoulli, M.B. Cita, A. Erickson, R.E. Garrison, R.B. Kidd, F. Mélierés, C. Müller, and R. Wright (1977) Nature 267: 399–403.
Hughes, T. (1973) Journal of Geophysical Research 78: 7884–7910.
Hughes, T. (1975) Review of Geophysics and Space Physics 13: 502–526.
Hughes, T. (1977) Review of Geophysics and Space Physics 15: 1–46.
Kanno, S., and F. Masuda (1978) Pages 63–70. Climatic Change and Food Production, edited by K. Takahashi and M. Yoshino. Tokyo: University of Tokyo Press.
Kellogg, T.B. (1976) Pages 77–110, Geological Society of America Memoir 145, edited by R.M. Cline and J.D. Hays.
Kemp, E.M. (1978) Palaeogeography, Palaeoclimatology, Palaeoecology 24: 169–208.
Kempe, S. (1977) Mitteilungen des Geologisch-Paläontologischen Instituts der Universität Hamburg 47:125–228.
Kennett, J.P. (1977a) Journal of Geophysical Research 82: 3843–3860.
Kennett, J.P., and R.C. Thunell (1975) Science 187: 497–503.
Kennett, J.P., and R.C. Thunell (1977b) Science 196:1231–1234.
Kennett, J.P., A.R. McBirney, and R.C. Thunell (1977c) Journal of Volcanology and Geothermal Research 2: 145–163.
Kennett, J.P., and P. Huddlestone (1972) Quaternary Research 2: 384–395.
Kozur, H. (1976) Nova Acta Leopoldina, Neue Folge 224: 413–472.
Kukla, G.J. (1977a) Earth Science Review 13: 307–374.
Lamb, H.H. (1979) Quaternary Research 11: 1–20.
Lotze, F. (1964) Pages 491–507. Problems in Paleoclimatology, edited by A.E.M. Nairn. London: Interscience.
Maley, J. (1977a) Nature 269: 573–577.
Maley, J. (1977b) Pages 187–197. Recherches Françaises sur le Quaternaire. International Union for Quaternary Research, Brussels.
Maley, J. (1980) Pages 63–86, The Sahara and the Nile, edited by M.A.J. Williams and H. Faure. Rotterdam: Balkema.
Mercer, J.H. (1976) Quaternary Research 6: 125–166.
Mercer, J.H. (1978) Nature 271: 321–325.
Mörner, N.A. (1976) Palaeogeography, Palaeoclimatology, Palaeoecology 19: 63–85.
Nichols, H. (1975) University of Colorado, Institute of Arctic Alpine Research, Paper 15.
Nicholson, S.E. (1980) Pages 173–200, The Sahara and the Nile, edited by M.A.J. Williams and H. Faure. Rotterdam: Balkema.
Pachur, H.J. (1975) Die Erde–Zeitschrift der Gesellschaft für Erdkunde Berlin 106: 21–46.
Pastouret, L., H. Chamley, G. Delibrias, J.C. Duplessy, and J. Thiede (1978) Oceanologica Acta 1: 217–232.
Pisias, N.G. (1979) Quaternary Research 11: 373–386.

Prell, W.L., J.V. Gardner, A.W.H. Bé, and J.D. Hays (1976) Pages 247–266, Geological Society of America Memoir 145, edited by R.M. Cline and J.D. Hays.

Rognon, P., and M.A.J. Williams (1977) Palaeogeography, Palaeoclimatology, Palaeoecology 21: 285–327.

Saito, T., L.H. Burckle, and J.D. Hays (1975) Pages 226–244, Late Neogene Epoch Boundaries, edited by T. Saito and L.H. Burckle. New York: American Museum of National History.

Savin, S.M., R.G. Douglas, and F.G. Stehli (1975) Geological Society of America Bulletin 86: 1499–1510.

Sarnthein, M. (1978) Nature 272: 43–46.

Singh, G., R.D. Joshi, S.K. Chopra, and A.B. Singh (1974) Philosophical Transactions Royal Society of London, Series B 267: 467–501.

Shackleton, N.J. (1977) Pages 401–427, The Fate of Fossil Fuel CO_2 in the Oceans, edited by N.R. Andersen and A. Malakhov. Marine Science, Vol. 6. New York: Plenum Press.

Starkel, L. (1977) X. International Organization for Quaternary Research (INQUA) Congress. Birmingham, UK. Abstracts, Page 433.

Taira, K. (1975) Palaeogeography, Palaeoclimatology, Palaeoecology 17: 333–338.

Tooley, M.J. Geographical Journal 140 (Feb.): 18.

van Zinderen Bakker, E.M. (1976) Palaeoecology of Africa 9: 159–202.

Wigley, T.M.L. (1977) Interim final report to NOAA. University of East Anglia, Climate Research Unit.

Wigley, T.M.L., D. Jones, and P.M. Kelley (1980) Nature 283: 17–21.

Wijmstra, T.A. (1978) Pages 25–45, Climatic Change, edited by J. Gribbin. Cambridge: Cambridge University Press.

Wilson, A.T. (1964) Nature 201: 147–149.

Wilson, A.T. (1978) Pages 33–39, Antarctic Glacial History and World Palaeoenvironments, edited by E.M. van Zinderen Bakker. Rotterdam: Balkema.

Winterer, E.L. (1973) American Association of Petroleum Geologists-Bulletin 57: 265–282.

Woillard, G.M. (1975) Acta Geographica Lovaniensia 14: 1–168.

Woillard, G.M. (1978) Quaternary Research 9: 1–21.

Woillard, G.M. (1979) Nature 281: 558–562.

Yoshino, M.M. (1978) Pages 63–70, Climatic Change and Food Production, edited by K. Takahashi and M.M. Yoshino. Tokyo: University of Tokyo Press.

ABSTRACTS OF OTHER IIASA PUBLICATIONS

Linnerooth, J., The Value of Human Life: A Review of the Models. IIASA Research Report RR-80-25, June 1980.
Reprinted from *Economic Enquiry*, Vol. 17, 1979, pp. 52–74.

This paper reviews four consumer maximization models where the probability of premature death enters as a variable that is both known to the consumer and under his control. These models generate a number of interesting results with respect to a person's willingness to pay for an increased chance of living. The most useful to the cost–benefit analyst is the derived relationship between this willingness-to-pay value and a person's lifetime earnings, and thus the relationship between the theoretically correct willingness-to-pay approach to the valuation of life-saving programs and the widely-used human-capital approach. However, the conclusions of the reviewed models are in this regard conflicting. Two of the models establish a theoretical basis for investigating the correlation of these two measures; however, this basis is shown to follow from an unrealistic assumption concerning the person's lifetime utility function. The remaining two models, although based upon more realistic assumptions, do not claim to provide theoretical grounds for making such investigations. The conclusion of this review is that in the absence of available data on personal demand for increased survival probability it is impossible to determine the relationship between the willingness-to-pay and the human-capital approaches to placing a value on human life.

Levien, R.E., et al., The 1980 IIASA Issue of *Behavioral Science*. IIASA Research Report RR-80-39, November 1980.
Reprinted from *Behavioral Science*, Vol. 25(5), 1980, pp. 327–398.

This Research Report reprints the September 1980 issue of *Behavioral Science*, which was devoted entirely to research done under the auspices of IIASA. The Report contains the following papers:

Roger E. Levien, Systems Analysis in an International Setting: Recent Progress and Future Prospects.

Kerry Thomas, Elisabeth Swaton, Martin Fishbein, and Harry J. Otway, Nuclear Energy: The Accuracy of Policy Makers' Perceptions of Public Beliefs.

David Hughes, Evgeni Nurminski, and Geoffrey Royston, Use of Nondifferentiable Optimization in a Health Care Problem.

Åke E. Andersson and Jari Mantsinen, Mobility of Resources, Accessibility of Knowledge, and Economic Growth.

Kirit S. Parikh and T.N. Srinivasan, Food and Energy Choices for India: A Programming Model with Partial Endogenous Energy Requirements.

Fumiko Seo, An Integrated Approach for Improving Decision-Making Processes.

Andersson, Å., and H. Persson, Integration of Transportation and Location Analysis: A General Equilibrium Approach. IIASA Research Report RR-80-40, November 1980.

Reprinted from *Papers of the Regional Science Association,* Vol. 42, 1979, pp. 39–55.

This paper describes an integrated approach to the study of transportation and growth of production in different locations. The model approach is based on a non-linear dynamic input–output growth model, which is endogenously related to a spatial framework with a transportation model. Both the transportation and the dynamic location models are based on different equilibrium concepts. The model structure is developed in such a way as to permit computational possibilities.

Basile, P., The IIASA Set of Energy Models: Its Design and Application. IIASA Research Report RR-80-43, 1980, forthcoming.

A set of models for evaluating alternative energy scenarios has been developed and applied at IIASA. The model set, long in development and following the initiative and guidance of Professor Wolf Häfele, includes several models: an accounting framework type energy demand model, a dynamic linear programming energy supply and conversion system model, an input–output model for calculating the impacts of alternative energy scenarios, a macroeconomic model, and an oil trade gaming model. The models have been designed into an integrated set for long-term, global analyses. The models together are a set that makes use of a highly iterative process for energy scenario projections and analyses. Each model is quite simple and straightforward in structure; a great deal of human involvement is necessary in applying the set. A first application of the models to study two alternative energy scenarios for 50 years has been completed. Some samples of the results reveal the wealth of information common to many modeling techniques. Several of the models are documented so that details of equations, assumptions, and data can be observed.

IIASA NEWS

Report on the Task Force Meeting on Decision Support Systems, 23–25 June 1980

Göran P. Fick, *Management and Technology Area*

Managers in every type of organization face problems that require action. The process leading to action is often referred to as "decision making," although the managers involved are not always able to identify the points at which decisions are made.

During the past decade, tools provided by management science, operations research, economics, and systems analysis have proven valuable in helping managers formulate, analyze, and tackle many types of problems. However, some classes of problems are initially so underspecified that the successful application of such tools is not possible, i.e., the analysts and the managers themselves have a limited understanding of the hidden properties of the problem. If this is the case, one way of proceeding is to help the manager (or "user") develop his own "decision support system" to stimulate learning about the nature of the problem; interaction with a decision support system allows him to gain experience that leads him, in an iterative process, to develop practical problem-solving strategies. Modern information technology provides a great number of computer tools, methods, equipment, and theories to support such a process.

The Management and Technology Area at IIASA sponsored a three-day task force meeting on 23–25 June 1980 to assess the current status and possible future development of decision support systems (DSS). Thirty-four participants from ten countries listened to a variety of papers on such topics as defining DSS, the contributions of other scientific disciplines to DSS, and applications of specific decision support systems. The participants also took part in four parallel discussion sessions on issues for the future in DSS.

A FRAMEWORK FOR DSS

The first two papers delivered at the meeting were designed to establish a framework within which the participants could explore the nature and scope of DSS. The field is so new that theory and specific definitions do not exist. Recognizing this dilemma, Ralph Sprague created a framework for the field based on the roles of the three actors involved in the development of a DSS: the manager, the builder of the DSS, and the "toolsmith." Peter G.W. Keen focused his analysis on the interactions among the user, the builder, and the system. He argued that, for a system to be denoted as a decision support system, the six possible flows of influence among these three elements must have certain characteristics.

RESOURCE DISCIPLINES

The next four papers offered contributions to DSS from several important "resource" disciplines: organization theory, artificial intelligence, data base, and managerial communication and decision making.

The role alloted to a DSS in an organization will depend on the actors' view of the nature of the organization. George P. Huber stressed the importance of taking a nondogmatic view of organizations. He characterized four main conceptual models of organizational decision making as the "rational" model, the "political" model, the "garbage can" model, and the "program" model. Acceptance of a given model will lead to conclusions about the nature of the decision support system to be created – owing mainly to the differing information requirements associated with each of the conceptual models.

The discussions also focused on the importance of data and model manipulation for DSS. Daniel Sagalowicz showed how the combined application of recent advancements in data-base technology and natural language processing in the field of artificial intelligence can be used to create highly flexible personal data bases for decision support. Frank A. Manola surveyed the developments in data-base technology relevant to DSS applications.

Fernando Flores broadened the scope of the discussions in an important paper by examining the complex set of human interactions that is often referred to as "decision making." He argued that, although information is important in the decision-making process, all communication that takes place in an office in the form of directives, commissives, assertions, and declarations must be recognized and understood before effective decision support systems can be developed.

DSS APPLICATIONS

Five presentations on real experiences with DSS served to make the discussions more concrete.

Les Earnest from the Stanford Artificial Intelligence Laboratory reported on the advanced "electronic office" in operation at his home institution and drew attention to the potential links between such new technologies and DSS. The rise and fall of a decision support system in a big American firm led Ephraim R. McLean to offer several hypotheses about factors leading to success or failure with DSS. He discussed the amount of time spent on different phases of DSS design, design methodologies, prototype designs, the use of APL, the characteristics of user-friendly systems, the question of user education, organizational stability, and measures of success. Gennady Kochetkov discussed the transition to decision support systems within industry and other organizations in the USSR. Critical areas influencing this transition have been changes in the thinking of managers, the social nature of choices, behavioral factors, man–machine interaction, and group decisions. Vladimir B. Britkov described a decision support system in the USSR that provided a good example of a DSS "generator," to use Ralph Sprague's term.

Finally, Roman L. Sheinin reviewed different approaches to the design of a DSS and the structure of DSS software in the USSR.

ISSUES FOR THE FUTURE IN DSS

The participants in all four parallel discussion sessions were given the same mandate of examining issues for the future in DSS, and the results were broad-ranging. One group focused on the process of creating a decision support system, i.e., decision support engineering, and attempted to characterize this process. Another group focused on the meanings of the terms "underspecification," "adaptivity," "system behavior," and "facilitator" – producing several ideas about additional research needed in these areas. Other topics touched upon by the discussion groups included the inadequacy of current methods for measuring the performance of a DSS; the lack of understanding about the process of adult learning – a bottleneck hindering the incorporation of such learning into DSS; and the tendency for DSS to concentrate on "personal DSS," while support systems for group and organizational decision making remain relatively undeveloped. Much discussion also centered on the moral responsibilities and ethics of the DSS practitioner, qualities on which the adaptive, evolutionary development process of DSS depends. Michael A.H. Dempster, representing IIASA's System and Decision Sciences Area, provided a summary of the main points raised during the discussions for the participants at the task force meeting.

DECISION SUPPORT SYSTEMS: ISSUES AND CHALLENGES

The papers delivered during the task force meeting and summaries of the discussions have been published in the IIASA Proceedings Series: Göran Fick and Ralph H. Sprague, eds., *Decision Support Systems: Issues and Challenges, Proceedings of an International Task Force Meeting,* Pergamon Press Limited, Oxford, 1980. With the volume they emphasize that DSS challenges traditional one-shot systems analyses followed by choice, decisions, implementation, and use. They point to a class of problems for which the iterative, evolutionary process embodied by DSS is more effective. They stress, too, that moral and ethical issues are central to the design of effective solutions for real managerial problems.

BIOGRAPHIES

Hermann Flohn, FRG

Hermann Flohn received his doctorate in 1934 from the Goethe University, Frankfurt am Main, and then joined the Reichswetterdienst. In 1946 he joined the staff of the Deutscher Wetterdienst and was appointed Director of its Research Division in 1952. In his capacity as Full Professor at the University of Bonn, he founded the University's Institute of Meteorology in 1961. In 1977 he became Professor Emeritus.

Professor Flohn is a member of the Deutsche Akademie der Naturforscher und Ärtze in Halle, the Akademien der Wissenschaften in Düsseldorf and Munich, and the Koninklijke Academie voor Wetenschappen, Letteren en Schone Kunsten van België in Brussels.

Ilya Gouevsky, Bulgaria

Ilya Gouevsky was at IIASA from August 1974 to December 1977 and again in June 1978. Dr. Gouevsky studied at the Higher Institute of Engineering and Electrotechnics in Sofia, Bulgaria, where he obtained his Ph.D. in 1972 in the field of optimum control of resource systems. He is currently at the Institute for Engineering Cybernetics of the Bulgarian Academy of Sciences. Dr. Gouevsky's scientific research interests include: general systems theory; management science and operations research; management of resource and environmental systems; and decision theory.

Tsuyoshi Hashimoto, Japan

Tsuyoshi Hashimoto studied architectural engineering at the University of Tokyo, and environmental engineering at the University of Southern California and Cornell University. He received his Master's degree from the University of Southern California in 1974, and his Ph.D. in Environmental Systems Engineering from Cornell University in 1980. Dr. Hashimoto is interested in quantitative and qualitative aspects of general water resources management problems, particularly stochastic modeling, decision making under uncertainty, and coordinating water supply and demand.

David Maidment, New Zealand

David Maidment was at IIASA from September 1976 to December 1977 on a Rockefellar Fellowship in Environment Affairs. He was again at IIASA in June 1978. Dr. Maidment received his B.E. in Agricultural Engineering in 1971 from the University of Canterbury, New Zealand, and his M.Sc. in 1974 and his Ph.D. in 1976, both in Civil Engineering and both from the University of Illinois in the USA. He is interested in the application of mathematical modeling and optimization to natural resource planning and management, in particular to water resource planning. Dr. Maidment is currently in the Water and Soil Division of the Ministry of Works and Development in Christchurch, New Zealand.

Norio Okada, Japan

Norio Okada is Associate Professor of Civil Engineering at Tottori University. He graduated from Kyoto University in 1970, receiving his Master's degree in 1973 and his Ph.D. in Engineering in 1977. He was a research assistant in the Civil Engineering Department of Kyoto University before assuming his present position at Tottori University. In 1974 and 1975 he participated in surveys of the transportation infrastructure in South and Central America. Professor Okada's scientific interests include water management, regional planning, and multiple-objective planning.

Witold Sikorski, Poland

Witold Sikorski was at IIASA from June 1977 to September 1978. Mr. Sikorski studied Electronical Engineering at Warsaw Technical University, where he received his M.Sc. in 1973. In 1974 he completed his postgraduate studies in didactics and methodology of teaching. He is currently at the Institute of Environmental Engineering of Warsaw Technical University.

H. Peyton Young, USA

H. Peyton Young is Deputy Chairman of the System and Decision Sciences Area at IIASA. He received his B.A. in Mathematics in 1966 from Harvard University and his Ph.D. in Mathematics in 1970 from the University of Michigan. From 1971 to 1973 he was Assistant Professor and from 1973 to 1978 Associate Professor of Mathematics at the Graduate School of the City University of New York. He has been an economic consultant with the United States National Water Commission, the Northeastern Illinois Planning Commission, and a Research Associate at the School of Organization and Management at Yale University. His research interests are in public economics, game theory, and methods of fair division.

IIASA
REPORTS

Volume 2 Number 1 July-September 1980
Published quarterly

CONTENTS

IN FORTHCOMING ISSUES:

J. LEDENT Comparative Dynamics of Three Demographic Models of Urbanization

Z. PAWLOWSKI A Demoeconometric Model of Poland and its Application to Counterfactual Simulations

H. REMPEL Determinants of Rural-to-Urban Migration in Kenya

C.W. REYNOLDS Shift-Share Analysis of Regional and Sectoral Productivity Growth in Contemporary Mexico

U. KARLSTRÖM Urbanization and Industrialization: Modeling Swedish Demoeconomic Development from 1870 to 1914

Printed by NOVOGRAPHIC, Vienna, Austria.